The Hydrogeochemistry of Pond and Rice Field Recharge: Implications for the Arsenic Contaminated Aquifers in Bangladesh

by
Rebecca B. Neumann

B.S. Civil and Environmental Engineering and B.A. Art and Art History,
Rice University, 2002

Submitted to the Department of Civil and Environmental Engineering in
Partial Fulfillment of the Requirements for the Degree of

Doctor of Philosophy in the Field of Environmental Engineering
at the
MASSACHUSETTS INSTITUTE OF TECHNOLOGY

February 2010

Author ..……
Department of Civil and Environmental Engineering
September 17, 2009

Certified by…...……
Charles F. Harvey
Associate Professor of Civil and Environmental Engineering
Thesis Supervisor

Accepted by…...……
Daniele Veneziano
Chairman, Departmental Committee for Graduate Students

The Hydrogeochemistry of Pond and Rice Field Recharge: Implications for the Arsenic Contaminated Aquifers in Bangladesh

by
Rebecca B. Neumann

Submitted to the Department of Civil and Environmental Engineering on
September 17, 2009 in Partial Fulfillment of the Requirements
for the Degree of Doctor of Philosophy in the Field of Environmental Engineering

Abstract

The shallow aquifers in Bangladesh, which provide drinking water for millions and irrigation water for innumerable rice fields, are severely contaminated with geogenic arsenic. Water mass balance calculations show that groundwater-irrigated rice fields and man-made ponds are the primary sources of recharge to the contaminated aquifers. We studied the hydrology and chemistry of these anthropogenic recharge sources to determine the impact they have on groundwater arsenic concentrations.

Our hydrogeochemical investigation involved fieldwork, laboratory analyses, and modeling. The field research spanned three years and included the deployment of a sensor network to continually monitor soil moisture and water potential, tracer tests to visualize flow patterns, soil cores to determine soil properties, and soil and water samples to ascertain chemical characteristics. The large amount of generated data were synthesized with hydrologic, geochemical and mass-balance models.

The study showed that physical and chemical differences between rice fields and ponds explain the spatial patterns of arsenic in the Bangladeshi aquifers. Recharge from rice fields is both temporally and spatially heterogeneous. It is focused through bunds (the raised boundaries around the perimeter of fields) and depends on irrigation intervals. Flow from ponds is constant and uniform through the pond sediments. These distinct hydrologic behaviors produce different water chemistries. Ponds contribute anoxic recharge elevated in labile organic carbon, while rice fields contribute semi-oxic recharge that lacks labile organic carbon. The labile organic carbon in the pond recharge stimulates microbial respiration that mobilizes sediment-bound arsenic, contributing dissolved arsenic to the aquifers. Conversely, rice-field recharge does not mobilize arsenic. In fact, rice fields act as an arsenic sink. Irrigation moves arsenic-rich groundwater from the aquifers and deposits it on the rice fields. Most of the deposited arsenic does not return to the aquifers; it is sorbed by the field's surface soil and bunds, and is swept away in the monsoon floods. The results demonstrate how land-use changes in Bangladesh have impacted groundwater arsenic concentrations.

Thesis Supervisor: Charles F. Harvey

Title: Associate Professor of Civil and Environmental Engineering

Acknowledgments

Thank you to my advisor, Charles Harvey, who provided me with the freedom to develop and direct my thesis project. I have learned much from him, and have enjoyed his positive outlook on science and life. Thank you to other members of my thesis committee: Phil Gschwend, for constantly challenging and pushing me forward; Harry Hemond, for asking the probing questions that ultimately strengthened my thesis; and Colleen Hansel, for always finding the time to mentor me both scientifically and personally.

Thanks to the other mentors I had during the Ph.D. process: John MacFarlane, who taught me how to work in the lab and prepare for field work; Zoe Cardon, who broadened my scientific interests; Jenny Jay, Roger Beckie, Scott Fendorf, Stephan Hug, and Jack Germaine, all of whom provided me with invaluable advice and guidance at key points during the thesis project.

Thank you to the supportive Parson's community, including Sheila Frankel, Sheila Anderson, Vicki Murphy and Jim Long who keep everything running smoothly.

My project would not have been possible without the support of those in Bangladesh, especially Borhan Badruzzaman and Ashraf Ali. Both provided me with invaluable logistical support and cared for my safety and success while I was in their country. I also want to thank those that helped me in the field and welcomed me into their lives: Anis, Mitu, Sha'Alam, Sojib and Rasil.

I am indebted to: Matthew Polizzotto, who accompanied me on two different field trips, spending more than a month with me in Bangladesh; and Sarah Jane White, who traveled to the other side of the world at the last minute to help me with an intensive sampling campaign. Thanks also to Ashfaque Khandaker, Julie Shoemaker, Chris Neumann, Ben Kocar, Tiffany Lin, Linda Roberts, Jessica Dittmar, Andreas Voegelin, and Nithya Ramanathan for field assistance.

I had two undergraduate researchers, Allison St. Vincent and Farah Khan, who were a joy to mentor and whose work helped advance my thesis. I also received lab support from Chu-Ching Lin, Charu Varadharajan and Kajetan Zwieniecki.

To Peter Oates, Holly Michael, Ashfaque Khandaker, Hanan Karam, Elena Abarca, Kurt House and Bec Gianotti: It has been fun to share the joys and struggles of working for Charlie!

Supergroup has been an amazing educational experience. Thank you to Amy Mueller, Matthew Orzo, Charu Varadharajan, Sarah Jane White, Schuyler Senft-Grupp, Loretta Fernandez, Desiree Plata, Xanat Flores, Debra Hauslander, Dave Kuo, and Dave Griffith for their help and insights.

Thank you to those that kept my life balanced during the Ph.D. process: Sarah Jane White, Will Fox, Anne Thompson and Arne Bomblies. I've enjoyed our many social and outdoor adventures.

Thank you to my family: my dad, Wilbur, for teaching me how to think critically and write clearly – his painstaking editing of my school projects made this document possible; my mom, Buffy, who is my biggest cheerleader – her faith in my ability to accomplish anything propels me forward; and my sister, Janna, whose unconditional love and support buoys my confidence.

Thank you to my daughter, Abigail, who brought a new perspective to my life and provided me with motivation to finish this thesis. Finally, thank you to my husband, Chris, who has been there through the entire process, celebrating in my highs and helping me through my lows. Your unwavering support made everything possible – I dedicate this thesis to you.

Table of Contents

List of Figures

List of Tables

1. Introduction

1.1. Background

Geogenic arsenic contamination of groundwater is a global problem. Arsenic-contaminated groundwaters exist in West Bengal and Bangladesh (BGS et al. 2001), Cambodia (UNICEF 2003), Vietnam (Berg et al. 2001) and many other countries throughout the world (Smedley and Kinniburgh 2002, Manouchehr et al. 2008, Winkel et al. 2008). The situation in West Bengal and Bangladesh is especially extreme in terms of human exposure to arsenic. Contamination was first discovered in this region in the 1980's when people began presenting symptoms of arsenic poisoning (Chakraborty and Saha 1987, Mazumder et al. 1988), shortly after aid agencies had installed a number of wells with the goal of providing pathogen-free drinking water (Yu et al. 2003). Currently, groundwater serves as the region's primary drinking and irrigation source, and the consequent ingestion of arsenic results in 3000 fatalities per year (Yu et al. 2003).

In Bangladesh and other countries located in Southeast Asia, Asia, and South America, geogenic arsenic is mobilized off soils and sediments and into groundwater under reducing conditions (Manouchehr et al. 2008, Winkel et al. 2008). In the absence of oxygen, subsurface microbes can use Fe(III) or even As(V) as the electron acceptor for the oxidation of organic carbon. Since solid-phase arsenic is often associated with Fe(III) minerals, and As(III) is more mobile than As(V), the reductive dissolution of Fe(III) (Cummings et al. 1999) and reduction of As(V) (Zobrist et al. 2000) can release arsenic from solid-phases into the aqueous phase. Within Bangladesh and West Bengal, the source of the organic carbon that fuels these reductive processes remains controversial. Many researchers contend the responsible organic carbon resides in the aquifer sediments, either as sedimentary organic carbon or as buried peat, and thus is as old as the aquifer (~2000 years) (Nickson et al. 2000, BGS et al. 2001, McArthur et al. 2001). Other researchers contend the organic carbon originates on the land surface and is drawn

into the aquifer with recharging water, and thus is modern (Harvey et al. 2002, Harvey et al. 2006). Determining the source of the organic carbon that fuels arsenic mobilization is important. A full understanding of the contamination problem is required to develop a solution that can sustainably provide arsenic-free drinking water to the region.

1.2. Research Motivation

In Munshiganj Bangladesh, dissolved arsenic concentrations in the shallow aquifers have a distinct bell-shaped profile that peaks at a depth of ~30 m (see Figure 6.1). This pattern is not explained by local differences in the arsenic or organic carbon content of solid aquifer material (Harvey et al. 2002, Swartz et al. 2004), and hence appears to result from differences in upgradient groundwater chemistry promoted by chemical variations in the water entering the aquifer. A water balance for Munshiganj shows that constructed ponds and groundwater-irrigated rice fields provide most of the water that recharges the arsenic-contaminated aquifers each year (Harvey et al. 2006). Both of these anthropogenic water bodies are recent additions to the landscape. Ponds are dug in order to obtain the material needed to build villages and roads up above the levels of the monsoon floods. They have existed in Bangladesh for centuries, but their numbers have increased substantially during the past ~50 years as the population of Bangladesh has exploded. Rice fields currently blanket much of the landscape and produce enough food to feed the entire country (Hossain et al. 2003). Their growth is linked to the development of groundwater irrigation, which was introduced to Bangladesh in the 1970's (Hossain et al. 2003).

Due to the likely connection between recharge chemistry and arsenic patterns in the aquifer, we chose to study the hydrologic behavior and chemical nature of rice fields and ponds. We hypothesized that these anthropogenic water bodies could potentially provide the organic carbon that is responsible for mobilizing arsenic, due to both the large amount of water they

contribute to the shallow aquifers and their organic-rich nature. However, we also believed rice fields could potentially act as an arsenic sink. They are irrigated with arsenic-contaminated groundwater, which removes a significant amount of arsenic from the aquifers each year (Ali et al. 2003).

We pursued a two-pronged approach and studied both the hydrology and chemistry of the recharge sources. This approach is an important aspect of the thesis research. Flow patterns are required for the proper interpretation of chemical data.

1.3. Thesis Overview

Chapter 2 of this thesis, published under the title "The Hydrology of a Groundwater-Irrigated Rice Field in Bangladesh: Seasonal and Daily Mechanisms of Infiltration" in *Water Resources Research* (45: doi:10.1029/2008WR007542, 2009), presents the hydrologic investigation of a rice field in Munshiganj. The study captured the dynamic behavior of recharge through the rice field over an entire irrigation season by collecting data from a transect of tensiometers and time-domain reflectometry sensors, novel tracer tests, infiltration tests, soil core analyses, and calculated water budgets. Results of the study laid the framework for a chemical investigation undertaken on the same field. Chapter 4 presents the chemical investigation. It combines chemical knowledge gained from water and soil samples onto the understanding of rice-field flow behavior to track the arsenic that is pumped up from the aquifers and deposited onto rice fields. The study determines how mush of the irrigation arsenic is sequestered in the rice field soils, taken up by rice plants, recycled back to the aquifer, and exported from the system during the monsoon season.

The results from the rice-field investigations were synthesized with pond chemistry data and the results from a previous groundwater modeling study (Ashfaque 2007) to physically and

chemically track pond and rice field recharge in the aquifer. The synthesis is presented in chapter 6 and published under the title "Anthropogenic Influences on Groundwater Arsenic Concentrations in Bangladesh" in *Nature Geoscience* (accepted, 2009). The work confirms that rice fields and ponds play important, though opposing, roles in Bangladesh's arsenic contamination problem. Ponds act as an arsenic source to the aquifer and rice fields act as an arsenic sink. Organic carbon in the pond recharge stimulates anoxic microbial respiration that mobilizes sediment-bound arsenic, while rice fields receive more arsenic from irrigation than they contribute to the shallow aquifer.

The presented work, especially that in chapter 6, builds upon many years of previous research conducted at the Munshiganj field site, including comprehensive studies of the groundwater chemistry (Harvey et al. 2002, Swartz et al. 2004, Klump et al. 2006), sediment geochemistry (Harvey et al. 2002, Swartz et al. 2004, Polizzotto et al. 2006), and groundwater hydrology (Harvey et al. 2006, Ashfaque 2007). This strong scientific foundation allowed us to draw concrete conclusions regarding the cause of arsenic contamination in Munshiganj and to present a number of different solutions for providing the area with arsenic-free drinking water. These solutions are presented in chapter 8, which summarizes the conclusions of the thesis work. Chapter 8 also presents water management and arsenic mitigation strategies for rice fields and outlines future research directions for those that are interested in carrying this thesis research forward.

1.4. References

Ali, M. A., A. B. M. Badruzzaman, M. A. Jalil, M. D. Hossain, M. F. Ahmed, A. A. Masud, M. Kamruzzaman, and M. Rahman (2003), Fate of arsenic extracted with groundwater, Proc. Internat. Symp. on Fate of Arsenic in the Environment, BUET and UNU, Dhaka, Bangladesh.

Ashfaque, K. N. (2007), Effect of hydrological flow pattern on groundwater arsenic concentration in Bangladesh, Ph.D. Thesis, Massachusetts Institute of Technology: Cambridge, MA, pp. 286.

Berg, M., H. C. Tran, T. C. Nguyen, H. V. Pham, R. Schertenleib, and W. Giger (2001), Arsenic contamination of groundwater and drinking water in Vietnam: A human health threat, *Environ. Sci. Technol., 35*, 2621-2626.

BGS, DFID, and DPHE (2001), Arsenic contamination of groundwater in Bangladesh, *BGS Technical Report WC/00/19, Volume 1 & 2*, British Geological Survey, Keyworth.

Chakraborty, A. K., and K. C. Saha (1987), Arsenical dermatosis from tubewell water in West Bengal, *Indian J. Med. Res., 85*, 326-334.

Cummings, D. E., F. Caccavo, S. Fendorf, and R. F. Rosenzweig (1999), Arsenic mobilization by the dissimilatory Fe(III)-reducing bacterium Shewanella alga BrY, *Environ. Sci. Technol., 33*, 723-729.

Harvey, C. F., C. H. Swartz, A. B. M. Badruzzaman, N. Keon-Blute, W. Yu, M. A. Ali, J. Jay, R. Beckie, V. Niedan, D. Brabander, P. M. Oates, K. N. Ashfaque, S. Islam, H. F. Hemond, and M. F. Ahmed (2002), Arsenic mobility and groundwater extraction in Bangladesh, *Science, 298*, 1602-1606.

Harvey, C. F., K. N. Ashfaque, W. Yu, A. B. M. Badruzzaman, M. A. Ali, P. M. Oates, H. A. Michael, R. B. Neumann, R. Beckie, S. Islam, and M. F. Ahmed (2006), Groundwater dynamics and arsenic contamination in Bangladesh, *Chem. Geol., 228*, 112-136.

Hossain, M. D., D. Lewis, M. L. Bose, and A. Chowdhury (2003), Rice Research, Technological Progress, and Impact on the Poor: The Bangladesh Case (Summary Report), *EPTD Discussion Papers*, International Food Policy Research Institute, Washington, D.C.

Klump, S., R. Kipfer, O. A. Cirpka, C. F. Harvey, M. S. Brennwald, K. N. Ashfaque, A. B. M. Badruzzaman, S. J. Hug, and D. M. Imboden (2006), Groundwater dynamics and arsenic mobilization in Bangladesh assessed using noble gases and tritium, *Environ. Sci. Technol., 40*, 243-250.

Manouchehr, Amini, A. C, Karim, Michael, Berg, Lenny, Winkel, H. J, Stephan, Eduard, Hoehn, Hong, Yang, and J. Annette, C. (2008), Statistical modeling of global geogenic arsenic contamination in groundwater, *Environ. Sci. Technol., 42*, 3669-3675.

Mazumder, D. N. G., A. K. Chakraborty, A. Ghose, J. D. Gupta, D. P. Chakraborty, S. B. Dey, and N. Chattopadhyay (1988), Chronic arsenic toxicity from drinking tubewell water in rural West Bengal, *Bull. World Health Organiz., 66*, 499-506.

Nickson, R., J. McArthur, W. Burgess, K. M. Ahmed, P. Ravenscroft, and M. Rahman (1998), Arsenic poisoning of Bangladesh groundwater, *Nature, 395*, 338-338.

Polizzotto, M. L., C. F. Harvey, G. Li, B. Badruzzman, A. Ali, M. Newville, S. Sutton, and S. Fendorf (2006), Solid-phases and desorption processes of arsenic within Bangladesh sediments, *Chem. Geol., 228*, 97-111.

Smedley, P. L., and D. G. Kinniburgh (2002), A review of the source, behaviour and distribution of arsenic in natural waters, *Appl. Geochem., 17*, 517-568.

Swartz, C. H., N. K. Blute, B. Badruzzman, A. Ali, D. Brabander, J. Jay, J. Besancon, S. Islam, H. F. Hemond, and C. F. Harvey (2004), Mobility of arsenic in a Bangladesh aquifer: Inferences from geochemical profiles, leaching data, and mineralogical characterization, *Geochim. Cosmochim. Acta, 68*, 4539-4557.

UNICEF (2003), Situation analysis: Arsenic contamination of groundwater in Cambodia, Phenom Phen.

Winkel, L., M. Berg, M. Amini, S. J. Hug, and J. Annette, C. (2008), Predicting groundwater arsenic contamination in Southeast Asia from surface parameters, *Nature Geosci., 1*, 536-542.

Yu, W. H., C. M. Harvey, and C. F. Harvey (2003), Arsenic in groundwater in Bangladesh: A geostatistical and epidemiological framework for evaluating health effects and potential remedies, *Water Resour. Res., 39*, 1146, doi:10.1029/2002WR001327.

Zobrist, J., P. R. Dowdle, J. A. Davis, and R. S. Oremland (2000), Mobilization of arsenite by dissimilatory reduction of adsorbed arsenate, *Environ. Sci. Technol., 34*, 4747-4753.

2. The Hydrology of a Groundwater-Irrigated Rice Field in Bangladesh: Seasonal and Daily Mechanisms of Infiltration

Neumann, R. B., M. L. Polizzotto, A. B. M. Badruzzaman, M. A. Ali, Z. Zhang, and C. F. Harvey (2009), The Hydrology of a Groundwater-Irrigated Rice Field in Bangladesh: Seasonal and Daily Mechanisms of Infiltration, *Water Resour. Res., 45*, W09412, doi:10.1029/2008WR007542.

2.1. Abstract

Flow through a groundwater-irrigated rice field in Bangladesh was characterized with data collected from a transect of tensiometers and time-domain reflectometry sensors, novel tracer tests, infiltration tests, soil core analyses, and calculated water budgets. The combined data captured the dynamic hydrologic behavior of the rice field over an entire growing season, which included many irrigation events. Recharge to the aquifer flowed from the surface of the rice field through preferential flow paths located in the subsoil beneath the plowed surface of the field and in the bunds, the raised boundaries around the perimeter of the field. Water that remained within the soil matrix did not recharge the aquifer. Bund flow was the dominant loss for the field because the bulk hydraulic conductivity of the soil beneath the bunds was greater than that in the plowed and planted region of the rice field. Each year, farmers plow the rice fields, destroying cracks and decreasing the conductivity of the shallow soil, but leave the bunds unplowed because they follow property boundaries. We determined bund flow with a daily water balance, and confirmed its importance by comparing irrigation losses among fields of different sizes and geometries, and hence different ratios of perimeter to area. The perimeter-to-area ratio predicted the fraction of water lost down the bunds for these and other fields located throughout Southeast Asia. Finally, we determined the economic and environmental benefits of reducing bund flow.

2.2. Introduction

Groundwater-irrigated rice agriculture has greatly expanded since it was introduced to Bangladesh in the 1980s, and the country is now self sufficient in food production (Hossain et al. 2003). In 2002, groundwater-irrigated land covered roughly 21% of Bangladesh's landscape (Hossain et al. 2003), and in our study area, groundwater-irrigated rice fields currently cover

40% of the land surface (Harvey et al. 2006). The introduction of groundwater-irrigated agriculture in Bangladesh has not only had a profound impact on the landscape, it has also dramatically altered aquifer recharge behavior and groundwater flow patterns, decreasing the residence time of water in the shallow aquifer by more than a factor of two (Harvey et al. 2006).

Groundwater extracted from the shallow aquifer of Bangladesh is often severely contaminated with naturally occurring arsenic (BGS et al. 2001). Irrigation of rice moves arsenic-rich groundwater from the aquifer and deposits it on the rice fields, lifting approximately 1400 metric tons of arsenic a year to the surface (Ali et al. 2003). Much of the irrigation water then returns to aquifer. At our study site, water balance calculations show that rice fields contribute roughly half of the water that recharges the arsenic-contaminated aquifer every year (Harvey et al. 2006). This cycling of groundwater through rice fields raises the question of what role the fields play in the arsenic-contamination problem. The first step in understanding their role is to determine the spatial pattern and timing of rice-field recharge. Knowledge of the physical system is required for the interpretation of chemical data and the estimation of chemical fluxes.

Previous agricultural studies describe three features of rice fields that are important for their hydrology: the plow pan, which is a layer of low hydraulic conductivity that forms when the field is plowed in water-saturated conditions, termed puddling; the bund, or raised property boundary around the perimeter of the field that keeps irrigation water contained; and cracks that form preferential flow channels. The plow pan acts as a barrier to water flow. Studies have shown that excavating through the plow pan significantly increases water loss from the field (Wopereis et al. 1992, Tuong et al. 1994, Chen and Liu 2002). Plow pan formation occurs because working the fields in water-saturated conditions destroys soil aggregates, thereby

producing smaller soil particles that fill pore space and seal cracks and macro-pores as they settle (Moormann and van Breeman 1978, Sharma and De Datta 1986). The difference in effective conductivity between the plow pan and the subsoil allows for the development of an unsaturated zone directly underneath the pan, even while the field surface is flooded (Takagi 1960, Zaslavsky 1964, Wopereis et al. 1994b, Chen and Liu 2002).

Bunds and preferential flow channels act like drains for the field. Although bunds serve as dikes that contain surface water within the field, they also allow for water loss via downward infiltration. Because bunds follow property boundaries, they are usually not removed when the field is puddled. Therefore the hydraulic conductivity of the soil underneath the bund is significantly greater than that in the planted portion of the field. In rice fields with established plow pans, the horizontal and then vertical movement of surface water into and then down through bunds often provides the largest loss of water from the fields (Walker and Rushton 1984, Tuong et al. 1994, Walker 1999, Huang et al. 2003, Janssen and Lennartz 2009). Rice fields also lose water through cracks in the subsoil. Tracer tests conducted in China by Sander and Gerke (2007) and Janssen and Lennartz (2008) on dry and harvested rice fields showed that within one day, dye reached a depth of 120 cm and 90 cm, respectively, by flowing through channels in the field and in the bund. In both experiments, the tracer spread horizontally above the plow pan, which allowed it to reach the bund or to access cracks in the pan, and then penetrated through macropores in the subsoil to reach deeper depths.

In our study we examined a number of different fields and used a variety of methods including season-long tracer tests, laboratory analyses on collected soil cores, and a network of field-deployed pressure transducers, tensiometers, and water-content probes to (1) map the transient patterns of flow in an individual field for a complete agricultural season, (2) determine

water-loss rates and irrigation requirements for fields of various sizes and geometries, (3) characterize macropores and preferential flow, and (4) estimate a seasonal water balance that differentiates evapotranspiration, infiltration through the bunds, infiltration through the soil matrix, and flow through preferential channels. We conclude by considering how the determined rice field flow behavior can inform arsenic investigations and water conservation efforts. Our field study extends previous research by describing the spatial and temporal patterns of flow under a rice-field on a hourly time scale for an entire irrigation season, by quantifying the relationship between field water loss and field geometry, expressed as the field's perimeter-to-area ratio, by demonstrating the importance of the perimeter-to-area ratio in rice-field water budgets, and by showing that preferential flow through the bunds and field macropores occurs during the irrigation season, enabling rice-field water to reach and recharge the shallow aquifer.

2.3. Methods

2.3.1. Field Site

The studied rice field is located in Bashailbhog village in the Munshiganj district of Bangladesh, which is roughly 30 km south of Dhaka and 7 km north of the Ganges River (Figure 2.1). Irrigation water is pumped up from the aquifer with a diesel engine, flows through the irrigation canal denoted in Figure 2.1b, and enters the rice field at its southwestern corner.

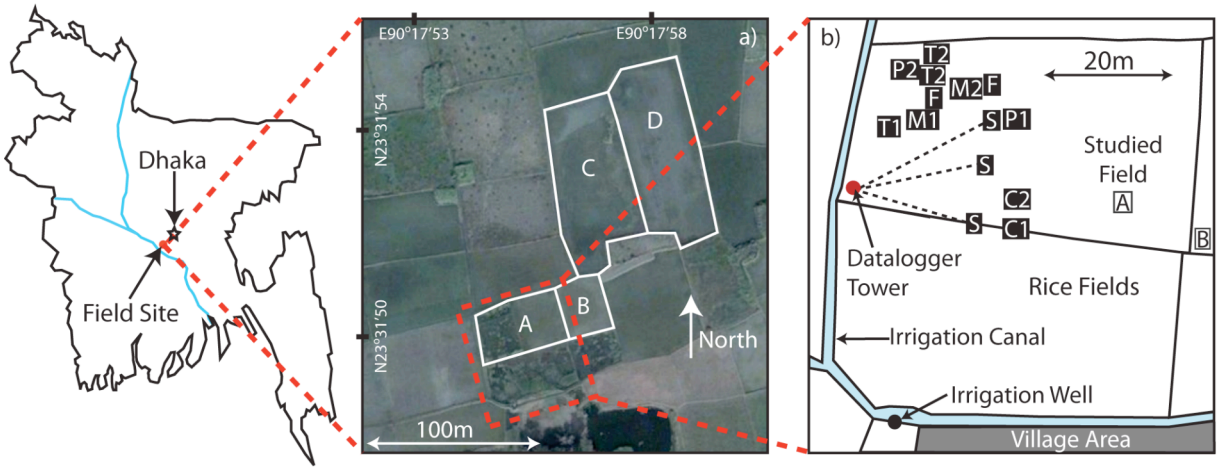

Figure 2.1 Plan view of site for hydrologic study.

a) Google Earth image of the rice fields in our study area. Field A was the intensively studied rice field with a perimeter to area ratio of 0.098 m/m^2. Water level changes were monitored in fields B, C and D , which have a perimeter to area ratios of 0.133 m/m^2, 0.068 m/m^2 and 0.066 m/m^2, respectively.

b) The intensively studied field with the locations of instrumentation and tracer tests marked: S: Sensor station installed 2006 (tensiometer and TDR probes), P1: 2006 and 2007 pressure transducer, P2: 2007 pressure transducer, T1: 2006 tracer test, T2: 2007 tracer tests, F: 2008 infiltrometer tests, M1: 2007 Marriott bottle evapotranspiration system, M2: 2008 Marriott bottle evapotranspiration system, C1: 2007 bund soil core, C2: 2007 field soil core.

2.3.2. Tensiometers and Time-Domain Reflectometry (TDR) Probes

A transect of three bundles of three vertically distributed pairs of time domain reflectometry (TDR) probes (Campbell Scientific CS616) and tensiometers (UMS T4E) were installed to monitor water content and both positive and negative water pressure. Figure 2.1b shows the plan view of the sensor transect and Figure 2.2 shows the profile view. The probes were connected to a multiplexer (Campbell Scientific AM16/32) and datalogger (Campbell Scientific CR10X) and were powered by a 12 V deep-cycle marine battery. They were installed after the field was puddled and planted with rice. Because the field site is submerged by approximately 4.5 meters of monsoon flood waters every year, the datalogger, multiplexer and battery were stored in a 9 m tall tower that was installed at the southwestern corner of the field (Figure 2.1b). Wires from the sensors were run along the top of the field to the tower. They were not buried for fear of breaking the plow pan.

The sensors were installed by augering a hole in the field to the desired depth. The TDR probes were positioned vertically with the steel rods pointing downwards, pushed through the bottom of the augered hole. Their water content measurements represented the average condition of an approximately 30 cm vertical segment of soil centered at the depth of the corresponding tensiometer (Figure 2.2). The sensor holes were backfilled with soil and bentonite. Since the standard equations used to convert raw TDR measurements into water content values are not accurate for the silty clayey loam at our site (Jones et al. 2002), we calibrated the TDR probes using undisturbed soil cores. The details and results of the calibration are presented in the supporting information, chapter 3.

The elevations of the installed tensiometers were determined relative to a nearby, surveyed well using a clear, flexible, water-filled tube. The tensiometers measure the pressure

difference from atmospheric by use of a porous diaphragm located at the top of the sensor. After the first irrigation season ended, we attempted to protect the porous diaphragm from the 4.5 m-high monsoon floodwaters by running air tubes down from the tower and sealing them around the diaphragm. However, since the sensors' calibration was lost during the monsoon season (see supporting information, chapter 3), it appears that floodwater leaked into the protective tubes and that the 4.5 m of pressure ruptured the porous diaphragm. Therefore, our tensiometer data are restricted to the 2006 irrigation season.

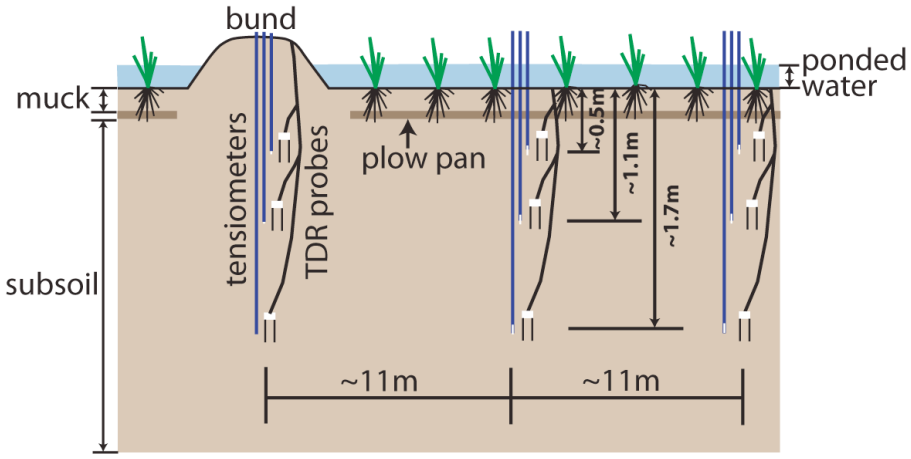

Figure 2.2 Profile view of sensor transect and field features.

2.3.3. Tracer Tests

Three season-long tracer tests were conducted on the studied field, one in 2006 and two in 2007. For all three tests, at the start of the irrigation season, an approximately 76-cm-diameter concrete ring was pushed into the top of the plow pan. The seal between the ring and the plow pan was tested by irrigating the field and ensuring that the soil inside the ring remained dry. During a subsequent irrigation event, a concentrated sodium bromide solution (~40 g/L or ~0.4 M) was poured into the ring to the same height as the surrounding irrigation water and was allowed to infiltrate into the rice field as the surrounding irrigation water infiltrated. During the experiment, water levels both inside and outside of the concrete ring were monitored. After incorporating evaporative losses, the rate of water loss inside of the tracer ring provided data on the vertical infiltration rate of water into the rice field. The ring was removed from the field once the bromide solution had completely infiltrated. At this point, the soil inside the ring and in the rest of the field was dry, so the farmer irrigated. The field was then left to the regular irrigation management of the farmer.

At the end of the irrigation season, after the rice crop was harvested, a trench was dug through the location of the bromide release. The face of the trench was sprayed with a silver ferrous cyanide solution, which reacted with the bromide tracer to form a Prussian blue color (Lu and Wu 2003), revealing the location of water from the start of the four-month long irrigation season. In 2006, the monsoon rains came earlier than expected and flooded the trench. Since the visualization experiment could not be completed, a series of soil cores were collected from the tracer test location and brought back to MIT for visualization. Both tests in 2007 were successful. After the on-site visualization was complete, all the soil contaminated by the silver ferrous cyanide solution was collected and transported back to Dhaka for disposal. The trenches

were filled with soil and left to consolidate during the monsoon season, and they were thoroughly puddled before the next irrigation season.

Most studies of water flow in surface soils utilize dye tracers that are visualized within a few days of the tracer release (Flury et al. 1994, Forrer et al. 1999, Yasuda et al. 2001, Kulli et al. 2003, Ohrstrom et al. 2004, Sander and Gerke 2007, Janssen and Lennartz 2008). Dyes allow for easy visualization of flow paths, but they degrade over time and sorb to the soil surface (Flury and Wai 2003). The use of bromide, a nearly conservative tracer, permitted us to carry out the tracer test for the entire four-month long irrigation season without concern of tracer degradation, while the spray method developed by Lu and Wu (2003) allowed us to visualize the bromide tracer as if it were a dye.

2.3.4. Infiltration Tests

The vertical infiltration rate of water into the rice field was measured three different ways. The first approach monitored the rate of water loss inside of the tracer ring, as explained above in section 2.3.3. The second approach used the calculated travel time for the bromide infiltration front from the tracer tests (see *Flow Behavior: Tracer Tests* in Results, section 2.4.2). The third approach employed a double-ring infiltrometer with a sealed-inner ring. We followed the ASTM standard (ASTM 2002) for this final measurement method, except: 1) the outer ring of the infiltrometer was an approximately 76-cm-diameter concrete ring, which was pushed into the top of the plow pan, 2) the inner ring was a 10-cm-diameter plastic bucket with a bulkhead fitting on the bottom of the bucket, and 3) a Marriott bottle constructed from a 15 L Nalgene carboy and a rubber stopper with an air tube was placed next to the concrete ring to maintain a constant water level in the outer ring.

2.3.5. Water Level Measurements

The water level above the plow pan was measured with a pressure transducer (Solinst 3001 Levelogger Gold). The transducer was placed inside a small piece of PVC well screen that was capped on both ends. The PVC well screen was covered with a fabric sock to ensure that the fine-grained soil in the rice field did not enter and clog the screen. The transducer system was then pushed to the top of the plow pan through the surface muck, which, when the field is flooded, is an unconsolidated slurry of soil particles that does not maintain a hydraulic head gradient. The entire transducer system was surrounded by sand to ensure rapid equilibration of the water inside the PVC pipe with the water in the field. Transducers were also placed in four fields of varying area (Figure 2.1a). Measurements from these fields helped us understand the relationship between water loss and the field perimeter-to-area ratio.

The Solinst pressure transducers measure absolute pressure, which is affected by changes in atmospheric pressure. Therefore, a transducer was also placed in the tower to monitor atmospheric pressure. The error associated with the water level measurements was estimated as ±0.6 cm. This value represents two standard deviations of data collected in the laboratory for a static water level, treating the atmospheric transducer and water-level-measurement transducer as a single instrument.

2.3.6. Meteorological Data

Meteorological data, including rain and pan evaporation, were collected from a meteorological station located 4 km southwest of the field site and run by the Bangladesh Water Development Board (BWDB). Rain measurements were made with a totaling rain gauge that was emptied daily. We estimated the error associated with this measurement as ±0.05 cm based on the precision of the rain gauge, as reported by the BWDB. At the meteorological station, pan

evaporation was determined by adding or removing water everyday with a cup of a known volume so that the water level in the pan was always at a specified height. Evaporation was determined from the volume of water added divided by the area of the pan. On days when water was removed from the pan, the rain gauge data were used to determine net evaporation. Based on the error involved in determining the area of the pan, the volume of the cup, and the fractional amounts of water removed or added with the cup, the uncertainty in the pan evaporation measurement was estimated as ±0.1 cm.

Pan evaporation measurements from the meteorological station were compared to evapotranspiration measurements taken in the rice field using a large-scale Marriott bottle, following the protocol outlined in Tomar and O'Toole (1980) (see supporting information, chapter 3). The pan evaporation measurements approximated field evapotranspiration measurements well at the beginning of the irrigation season (January) and slightly underestimated field evapotranspiration at the end of the irrigation season (April) (see supporting information, chapter 3). Due to the relatively good agreement, pan evaporation measurements from the meteorological station were used for field evapotranspiration estimates.

2.3.7. Irrigation Input

The application of irrigation water to our rice field was monitored primarily with changes in the measured water level. Increases in the water level were attributed to irrigation input if the nearby meteorological station did not detect rain. This method was verified two different ways. The first approach involved the farmer recording when he started and when he completed irrigating the rice field. The second approach involved placing a weather-proof camera (Cuddeback Expert) in the tower that was programmed to take a picture of the field's irrigation inlet every hour during the day. Irrigation events generally lasted from one to two hours. The

farmer's log and the photographs were used, along with the irrigation well's average pump rate (Harvey et al. 2006), to calculate the amount of water added to the field. It should be noted that the pump rate of a given irrigation well can vary depending on its maintenance, and thus these verification methods provide only a rough estimate of the amount of irrigation water added to the field.

The transducer method for determining irrigation input assumes that losses during an irrigation event are small compared to the amount of water applied to the field. Data show that an irrigation event adds roughly 6 cm of water to the field, while 0.3 cm is lost to evapotranspiration and different infiltration pathways (see supporting information, chapter 3). The amount of water lost is smaller than the error associated with the irrigation input measurement, which was determined by propagating the uncertainty of the pressure transducer measurements for the initial and final field water levels: $\pm\sqrt{0.6\text{cm}^2 + 0.6\text{cm}^2} = \pm 0.85$ cm.

2.3.8. Soil Cores

Soil cores used for laboratory measurements of soil properties were collected from the bund and from the puddled portion of the rice field (Figure 2.1) in 3" by 30" (7.6 cm by 76.2 cm) Shelby tubes. The tubes were pushed into the field as far as possible by hand. Once they stopped advancing, they were gently hammered down into the soil until the top of the tubes corresponded with the top of the soil. The ends of the retrieved, soil-filled tubes were capped with plastic caps for shipment back to MIT.

The collected cores were x-rayed to non-destructively determine the quality of the core and the structure of the sampled soil profile. The radiograph can detect density differences within the soil core due to compaction or cracks. Using the radiograph as a guide, multiple three-inch (7.6 cm) sections of the rice field core were chosen for hydraulic conductivity, bulk density, and

porosity measurements. The constant rate of strain test (CRS), which works well for clayey and cohesive soil, was utilized to determine all three of these parameters (Wissa et al. 1971, ASTM 2006). The bund core was not analyzed because the CRS test requires a cohesive soil section, and the bund core was full of cracks and macropores (see *Physical Characteristics: Soil Cores* in the Results, section 2.4.4). Processed data and calculations from the CRS tests are in the supporting information, chapter 3. The error in the hydraulic conductivity measurement was estimated at 50% due to data fitting that is required in the CRS methodology (see supporting information, chapter 3). The error associated with the porosity and bulk density measurements were estimated at 15% and 1%, respectively, and were determined by propagating the uncertainty associated with the data needed to calculate these values. The relatively large porosity error is due to the fact that we did not measure specific gravity (a value needed for the calculation), but instead used an average value of 2.78 based on results from mineralogical studies of groundwater-irrigated paddy soils in the region (Norra et al. 2005) (see supporting information, chapter 3).

2.4. Results

2.4.1. Water Loss and the Field Perimeter-to-Area Ratio

Water level data collected from four different fields show that the initial rate of water loss in the fields was dependent on the size and geometry of the fields (Figure 2.3a). Both the mean and median rate of water loss for the first 5 cm of water after an irrigation event, which roughly corresponded with the depth of ponded water (Figure 2.2), was linearly related to the perimeter-to-area ratio of the fields. The relationship held over a factor of two difference in the perimeter-to-area ratio, with an r^2 value of 0.96 to 0.99. The relationship for the mean rate of water loss passed the F-distribution test, which determines if the relationship occurs by chance (see

LINEST function in Microsoft Excel), at the 2.5% confidence level, and the relationship for the median rate of water loss passed at the 1% confidence level.

The significant relationship between the perimeter-to-area ratio and the initial rate of water loss did not correspond with an equally strong relationship between the perimeter-to-area ratio and the amount of irrigation water applied to the fields. In general, smaller fields (larger perimeter-to-area ratio) required proportionally more water than larger fields (smaller perimeter-to-area ratio), but the linear fit of the data was neither extremely strong (r^2=0.76) nor statistically significant (Figure 2.3b).

The strength of the relationship in Figure 2.3a implies that the size and geometry of the field, characterized as the perimeter-to-area ratio, determined the initial rate of water loss and therefore played an integral role in the loss mechanism for ponded water. However, the weaker relationship between the perimeter-to-area ratio and the amount of applied irrigation water per unit area demonstrates that field size and geometry did not dictate total water use. The two different relationships suggest that after an irrigation event, initial flow behavior did not match later flow behavior; the loss mechanisms for the first 5 cm of water were different than the loss mechanisms for the remaining irrigation water. The discrepancy indicates that rice field flow behavior is dynamic, motivating the use of continuously recording sensors and season-long tracer tests.

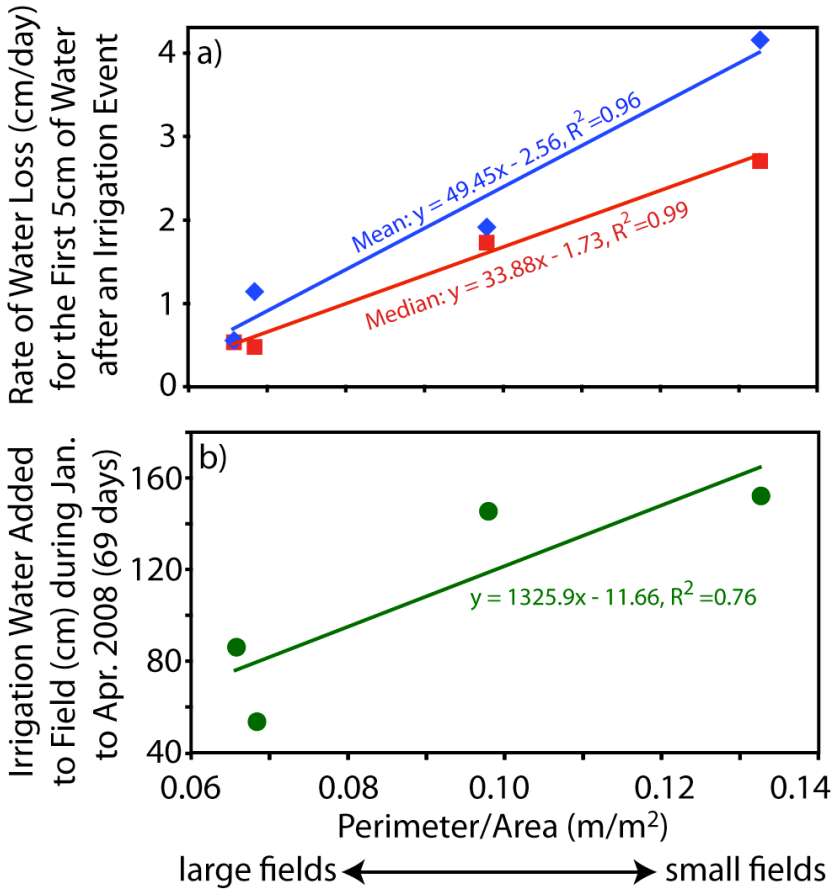

Figure 2.3 Water loss and the perimeter-to-area ratio.

Data are for a 69-day period starting in January and ending April 2008.
a) The mean and median rate of water loss for the first 5 cm of water after an irrigation event versus the perimeter-to-area ratio. On average, the first 5 cm of water represented the depth of puddled water sitting on top of the surface muck, in contact with the bund.
b) Amount of irrigation water added per unit area to a field versus the perimeter-to-area ratio. The relationship shows that the perimeter-to-area ratio was a decent indicator of total water use per unit area of field. However, the relationship in panel b), is weaker than the one in panel a). The discrepancy indicates that the loss mechanisms for the first 5 cm of water were different than the loss mechanisms for the remaining irrigation water.

2.4.2. Field Flow Behavior: Sensor Transect

Data collected by the tensiometers and TDR probes demonstrate that our rice field developed an unsaturated zone beneath standing water during the irrigation season, and that recharge was focused through the bunds. From February to April 2006, when the field was continuously flooded with water (Figure 2.4a), the shallowest sensors both within the bund and beneath the plow pan detected unsaturated conditions, as indicated by negative pressures (Figure 2.4b) and decreased water content (Figure 2.4c). According to the TDR calibration (supporting information, chapter 3), the bund experienced a 5 to 7% decrease in water content, while the soil underneath the plow pan experienced a 0.5 to 1% decrease in water content, a small, but detectable decrease. The plow pan dampened pressure changes due to fluctuations in the ponded water level, allowing the soil underneath it to remain unsaturated for almost an entire month during the irrigation season (Figure 2.4b). In contrast, the pressures in the bund were sensitive to changes in the height of water in the rice field; they oscillated up and down with the field water level, alternating between saturated and unsaturated conditions (Figure 2.4b).

Figure 2.5 shows linearly interpolated hydraulic head contours in the subsurface of the rice field both during (Figure 2.5a) and after (Figure 2.5b) an irrigation event. In both situations, horizontal contours developed through and directly beneath the plow pan, signifying that flow from the surface of the field through the plow pan was vertically downwards. During the irrigation event (Figure 2.5a) near vertical contours developed underneath the bund, indicating horizontal flow of water from the bund towards the middle of the field's subsurface. The unsaturated zone, denoted as the region where the interpolated head value was less than the corresponding elevation, was contained within the middle of the field. As the ponded surface water receded (Figure 2.5b), the subsurface head contours underneath the bund widened and lost

their near-vertical nature, indicating slower bund flow with a downward component. The unsaturated zone grew to occupy the entire field. The volume of the unsaturated zone could change due to gas solution and dissolution or by direct exchange with the atmosphere either through the bund or through the rice plants. A movie of the continuously recorded data, created by Neumann et al. (2009), shows the hydraulic head contours and the extent of the unsaturated zone for the 2006 irrigation season. The interpolated contours both in Figure 2.5 and in the movie imply that flow converged on the bottom two tensiometers located approximately 11 m from the bund, rather than on the middle of the field (~21 m from the bund), as expected. One explanation for this anomalous behavior is that the head gradient in the middle of the field was extremely flat (~0.1 cm/cm), so centimeter errors in the tensiometer calibration would have a noticeable effect on the shape of the contours. In addition, our chemical samples, to be published in a subsequent paper and presented in chapter 4, suggest that the deepest tensiometer in the middle of the field was located within a preferential flow region. This tensiometer likely had a stronger hydraulic link to the surface of the field, which led to higher head values and the convergence of flow on the middle set of tensiometers.

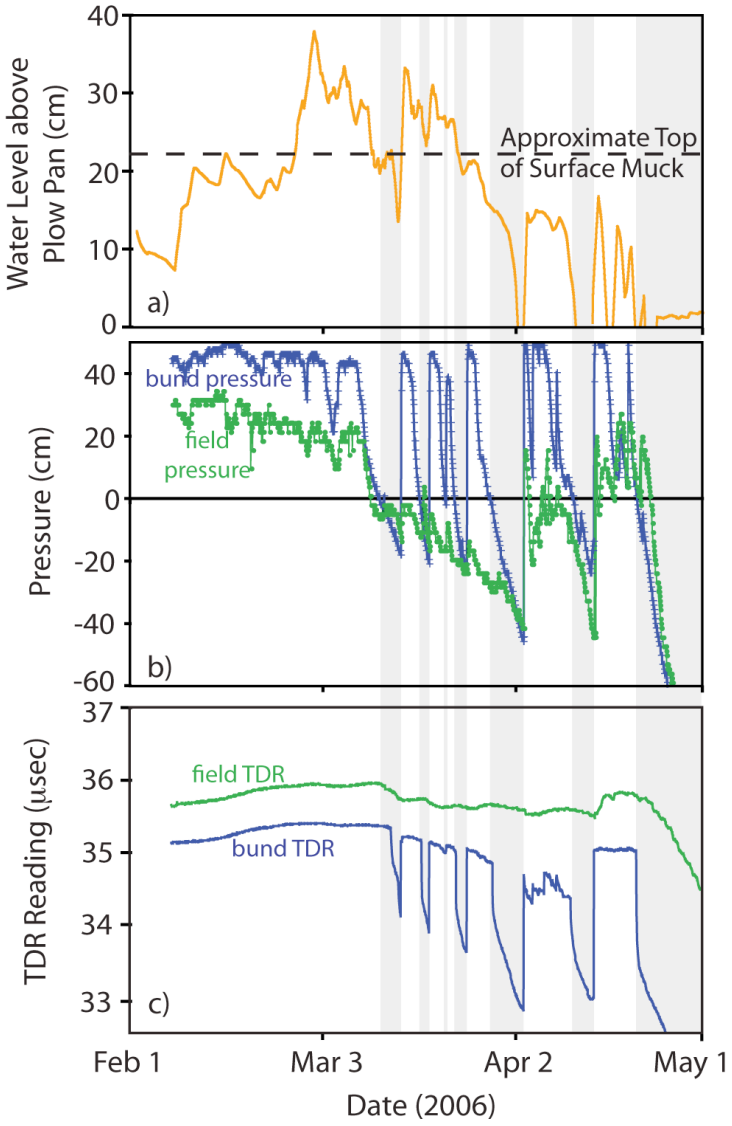

Figure 2.4 Sensor data for the 2006 irrigation season.

a) Water level in the rice field.

b) Pressures measured by the shallowest tensiometers installed in the bund and in the middle of the field underneath the plow pan. The vertical grey bars mark the time periods during which the tensiometer in the bund measured negative pressures, signifying unsaturated conditions.

c) TDR readings for the shallowest sensors in the bund and in the middle of the rice field underneath the plow pan. Dips in the TDR readings indicate unsaturated conditions and correspond with negative pressures. The bund soil experienced 5 to 7% desaturation while the field soil experienced only 0.5 to 1% desaturation, a small but detectable amount of desaturation. See section 3.5 for error associated with the TDR calibration.

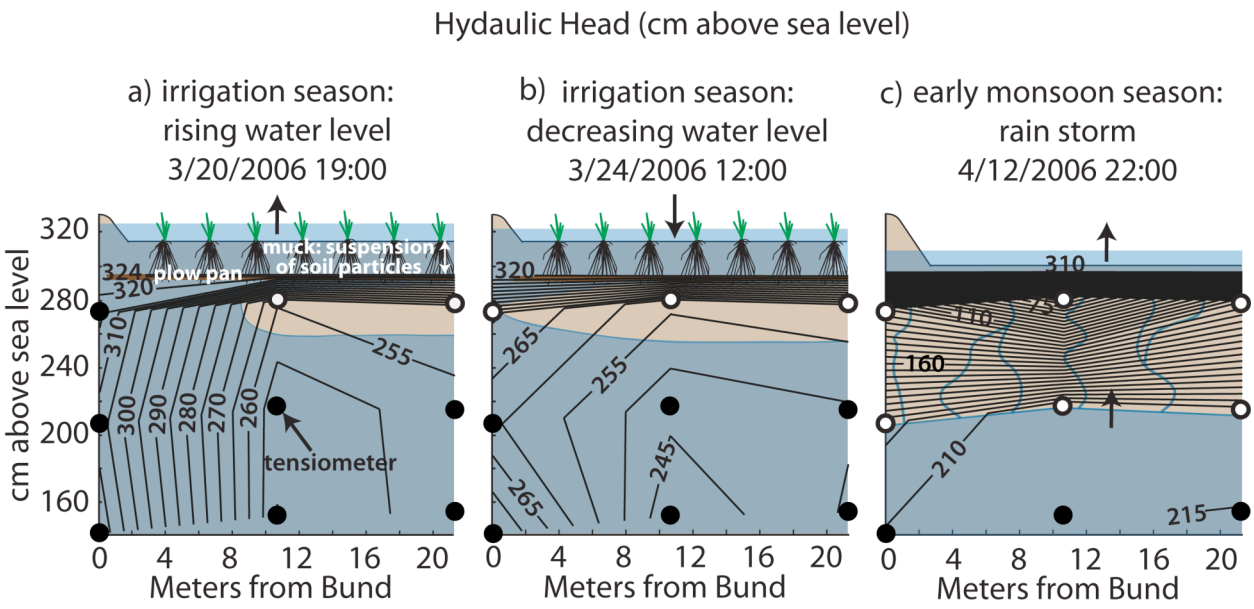

Figure 2.5 Linearly interpolated hydraulic head contours.

Contours are in cm of water above sea level at 5 cm intervals. The unsaturated zone, represented as the light brown region, is the area where the interpolated head values are less than the corresponding elevation, meaning that the pressure head component of hydraulic head was less than atmospheric. The nine circles mark the location of the tensiometer measurements. A black circle signifies that the tensiometer measured positive pressures while a white circle signifies that the tensiometer measured negative or less than atmospheric pressures. With standing water on the field, the surface muck is an unconsolidated suspension of soil particles that does not maintain a hydraulic gradient.

a) Hydraulic head in the subsurface of the rice field during an irrigation event. The horizontal contours through and directly beneath the plow pan signify that flow from the surface of the rice field through the plow pan was vertically downwards, while the vertical contours underneath the bund signify that flow was horizontal from bund towards the middle of the field's subsurface. The unsaturated zone was contained within the middle of the field.

b) Hydraulic head in the subsurface as the water in the rice field receded. The more widely spaced and less vertical contours underneath the bund signify slower flow rates with a downward component. The unsaturated zone occupied the entire field.

c) Hydraulic head in the subsurface after the rice season but before inundation by monsoon floods. Cracks that formed when the surface of the field dried out provided channels for the flow of rain water down through the unsaturated subsoil into the deeper soil layers, which raised the water table from below without altering the upwards direction of the head gradient within the soil matrix.

2.4.2. Flow Behavior: Tracer Tests

The tracer tests revealed the flow paths of water four months after entering the rice field. The tracer uniformly infiltrated the soil to a depth of roughly 40 cm below the field surface (Figure 2.6a–c), which is just below the depth of plow pan at 20 to 25 cm (Dittmar et al. 2007). In addition, tracer reached a depth of at least 150 cm, the bottom of the trench, by flowing through cracks and macropores in the subsoil (Figure 2.6b and 2.6c). It is likely that during the four-month long test, tracer reached depths greater than 150 cm by flowing through these preferential flow channels. Previous tracer tests conducted on dry fields showed preferential flow reaching depths of 90 cm to 120 cm within a single day (Sander and Gerke 2007, Janssen and Lennartz 2008). The tracer visualizations demonstrate that although preferential flow channels were not everywhere in the rice field (Figure 2.6a and 2.6c), they did exist in multiple locations and actively transported water during the irrigation season (Figure 2.6b and 2.6c). Underneath the plow pan, preferential flow, not matrix flow, had the potential to recharge the shallow aquifer.

Measured water levels from the 2006 tracer test are presented in Figure 2.7. The rate of water loss inside the tracer ring was relatively constant during the eight days the test was conducted, and it was greater than that due to evapotranspiration. The difference represents vertical infiltration into the rice field. Due to bund flow, the rate of water loss outside the tracer ring was initially greater than that inside the ring. However, once the water level outside of the ring reached the top of the surface muck, its loss rate decreased to match that inside the tracer ring. Without ponded water in the field, bund flow was minimal to absent, causing the water outside of the tracer ring to experience the same loss mechanisms as the water inside the tracer ring, namely vertical infiltration and evapotranspiration. These data support the dynamic

behavior of bund flow detected by the sensor transect, with bund flow dominating during and immediately after irrigation (Figure 2.5a) and decreasing in importance as the ponded water receded (Figure 2.5b). In addition, our results match those of Walker and Rushton (1986), which showed for a West Sumatran rice field, that the vertical infiltration rate through the plow pan was constant, and that bund flow ceased when the water level in the field dropped below a certain threshold. Their modeling work (Walker and Rushton 1984) indicates that bund flow cessation occurs because the shallow water depth cannot maintain saturated flow through the bund, and desaturation of the bund decreases its conductivity. Our data support this mechanism. Figure 2.4 shows that in our field, the bund desaturated when the water level in the rice field dropped to the top of the surface muck, which is the water level at which bund flow ceased (Figure 2.7). These data and Walker and Rushton's (1984) mechanism further imply that the horizontal movement of water through the surface muck towards the bund did not occur.

The results of the tracer test were not an artifact of density driven flow. The concentration of the sodium bromide tracer (~40 g/L) resulted in a density gradient of ~0.04, while, according to the contours in Figure 2.5, the head gradient across the studied cross section was an order of magnitude larger, ~0.5 (see supporting information, chapter 3, for details of the calculation).

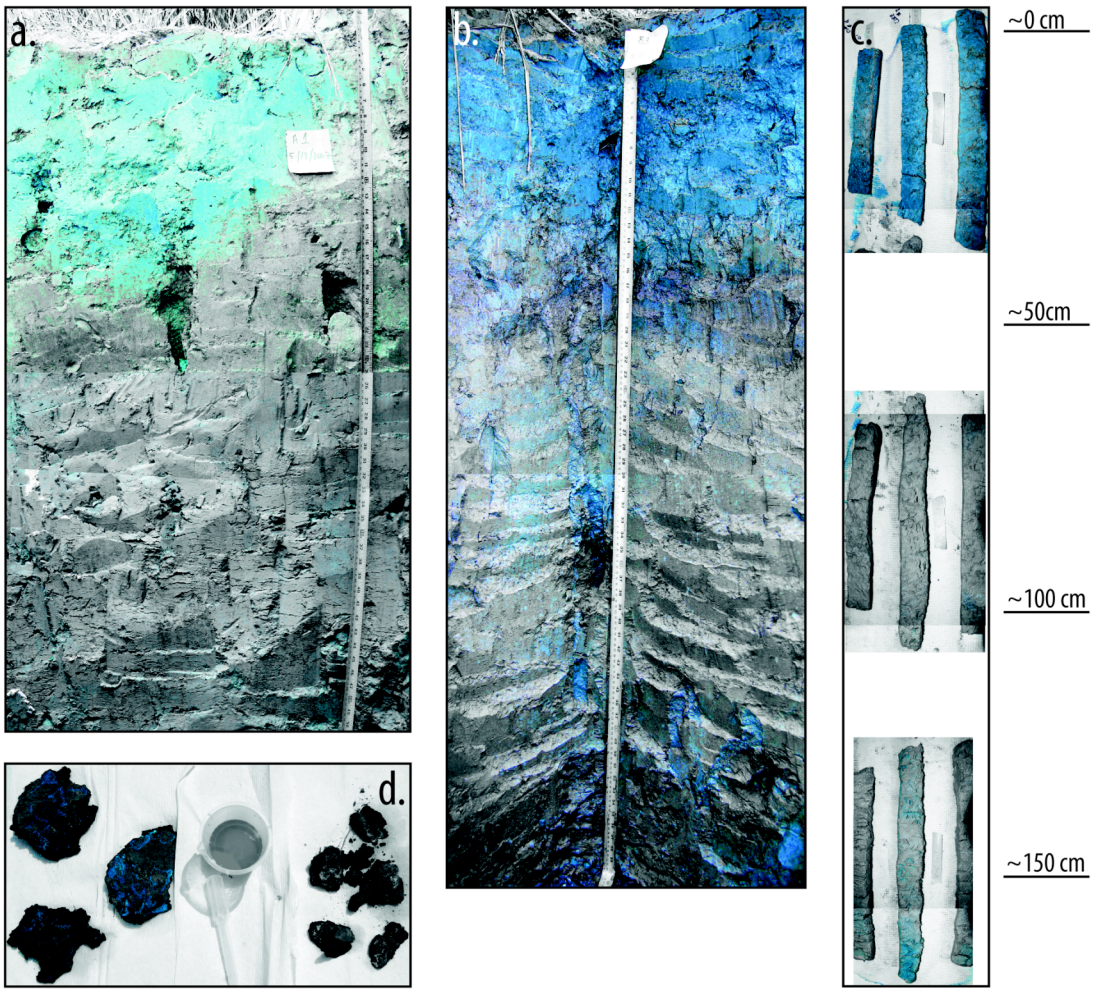

Figure 2.6 Tracer tests results.

Panels a, b and c are approximately aligned with the depths noted on the right hand side of the figure.
a) 2007 tracer test, location 1. Few preferential flow paths.

b) 2007 tracer test, location 2. Many preferential flow paths.

c) Cores from 2006 tracer test location. The middle core intersected a preferential flow path at a depth of 150 cm. The other cores did not intersect a flow path.

d) Control experiment for the tracer test visualization. The soil on the left is from a location exposed to bromide. The soil on the right was from a location not exposed to bromide.

Rice field water that stayed in the soil matrix only managed to reach a depth of ~40 cm while rice field water that entered a preferential flow path managed to reach depths of at least 150 cm over the course of the irrigation season.

2.4.3. Flux Determination: Infiltration Tests

The Infiltration rate of water through the plow pan was measured three different ways.

1) Monitoring the rate of water loss inside the tracer rings:

   After accounting for losses due to evapotranspiration, water level data from the inside of all three tracer rings (see Figure 2.1 for tracer ring locations) indicate that the vertical infiltration rate into the field was 0.35±0.1 cm/day (see Figure 2.7 for water level data from the 2006 tracer test).

2) Calculating travel time through the soil matrix for the bromide tracer infiltration front:

   In all three tracer tests, the bromide infiltration front reached a depth of 40 cm by flowing through the soil matrix (Figure 2.6). Using a porosity of 0.5 (see Figure 2.8) and a 120-day irrigation season, this infiltration depth corresponds with an infiltration rate of 0.17 cm/day, which is roughly half the rate determined by monitoring the rate of water loss inside the tracer rings.

3) Employing a double-ring infiltrometer with a sealed-inner ring (ASTM 2002):

   The rate measured at two different locations with the double-ring infiltrometer (see Figure 2.1 for infiltrometer locations) was 0.15±0.03 cm/day, which matches the rate determined with the bromide infiltration front.

The tracer test visualization (Figure 2.6) shows that bromide in the infiltration front traveled through the soil matrix, not through preferential flow channels. Therefore, the rate of 0.15±0.03 cm/day determined with this method and with the double-ring infiltrometer method is taken as the infiltration rate through the soil matrix. The difference between this soil-matrix infiltration rate and the rate determined with the tracer rings (0.35±0.1 cm/day) is attributed to preferential flow. The footprint of the tracer ring was roughly 8x larger than the footprint of the

inner infiltrometer ring. Therefore, the area covered by the tracer ring was more likely to include preferential flow paths, which as the tracer visualizations show were active but spatially distinct (Figure 2.6). The infiltration rate measured by the rate of water loss inside the tracer ring was taken as the sum of preferential flow losses and soil-matrix infiltration.

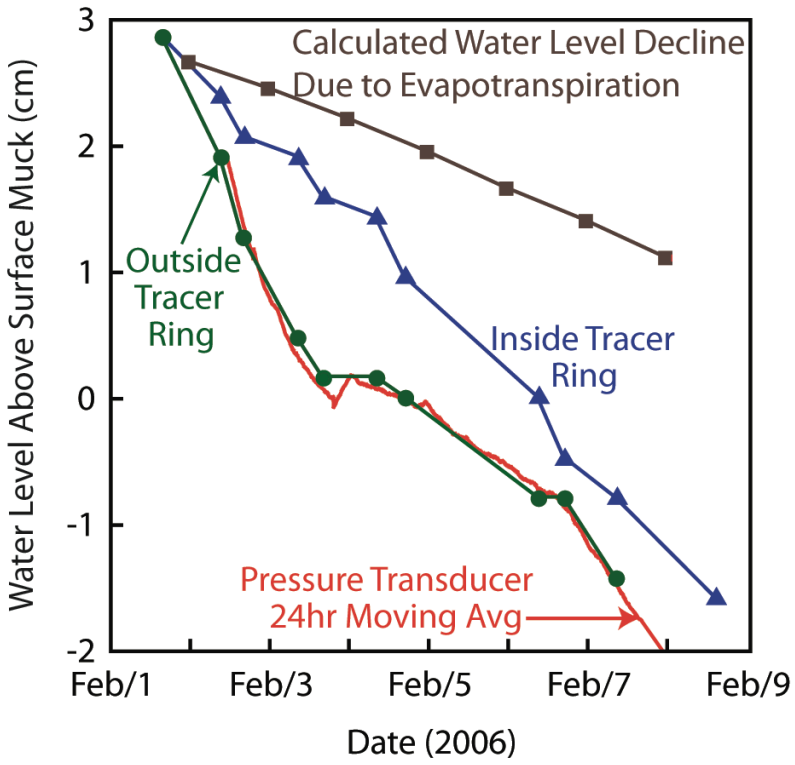

Figure 2.7 Water levels measured both inside and outside of the tracer ring.

Data are from the 2006 tracer test. The rate of water loss both inside and outside the tracer ring was greater than that due to evapotranspiration. Loss of water from inside the tracer ring is due to evapotranspiration and vertical infiltration through the plow pan. Water that infiltrates through the plow pan travels either through the soil matrix or preferential flow channels. Loss of water outside the tracer ring is due to evapotranspiration, vertical infiltration through the plow pan, and bund flow.

2.4.4. Physical Characteristics: Soil Cores

Radiographs of the two collected soil cores are presented in Figure 2.8. The rice field core had root remnants in its top section and relatively homogenous subsoil, while the bund core was full of cracks and void spaces. The radiographs provide a good indication of why bund flow occurs.

The constant rate of strain (CRS) tests showed that the saturated hydraulic conductivity of the soil in the rice field was fairly homogeneous. The hydraulic conductivity of the field soil sections varied by a factor of two, which was within our measurement error (Figure 2.8c). An extremely low conductivity layer representing the plow pan was not present in any of the tested soil sections. Based on a soil study performed in an adjacent rice field, the plow pan was expected at a depth of 20 to 25 cm (Dittmar et al. 2007). Unfortunately, the CRS test on the soil from this depth failed due to operator error and a conductivity measurement was not obtained. However, bulk density and porosity data collected during the CRS tests (Figure 2.8d and 2.8e) suggest that the entire profile was relatively homogeneous. These two measurements varied by less than a factor of 1.5 throughout the tested profile.

Tuong et al. (1994) in the Philippines and Chen and Liu (2002) in Taiwan determined that the puddled soil in their respective fields had an order of magnitude lower conductivity than the non-puddled soil (0.15 versus 2.3 cm/day and 0.05 versus 1.5 cm/day, respectively), even though the bulk density (Tuong et al. 1994, Chen and Liu 2002) and porosity (Chen and Liu 2002) of the two soils varied by less than a factor of two. Based on these results, it is possible that the conductivity of our missing 20–25 cm soil section was lower than the rest of the soil profile, despite the uniformity in our porosity and bulk density measurements. However, it is also possible that the conductivity of this soil section matched the rest of the profile. Hundal and

De Datta (1984) in the Philippines found that the saturated hydraulic conductivity of the soil beneath the surface muck was uniform at 0.25 cm/day. Appropriately, a review by Sharma and De Datta (1986) states that plowing fields in water-saturated conditions can increase, decrease or leave unchanged the soil's bulk density, porosity and conductivity values. The impact depends on the soil type, its aggregation status, and the orientation of the soil particles

As a comparison to the CRS-determined conductivity values, we calculated effective conductivity values from field measurements of infiltration rates and hydraulic gradients. Figure 2.5 demonstrates that on average, the head gradient across the plow pan was 3.8, while the head gradient across the entire depth of the studied transect was 0.5. Since the matrix infiltration rate of 0.15 cm/day (see *Flux Determination: Infiltration Tests* in Results, section 2.4.3) corresponded with flow through the soil matrix, we used this rate with the 3.8 head gradient to calculate an effective plow pan conductivity value of 0.04 cm/day. This conductivity value is within the range of values measured by the CRS test (Figure 2.8). Since the joint matrix infiltration and preferential flow rate of 0.35 cm/day (see section 2.4.3) corresponded with flow through the entire studied cross section, we used this rate with the 0.5 head gradient to calculate an effective subsurface conductivity value of 0.7 cm/day. This effective conductivity value is an order of magnitude larger than the values measured by the CRS tests. Other researchers (Lauren et al. 1988) found that field and laboratory methods produced dissimilar conductivity values, and attributed the discrepancy to differences in macropore continuity. At our site, the higher field-determined conductivity value (0.7 cm/day) suggests that cracks and macropores, not intrinsic matrix permeability, controlled the field-scale infiltration rates.

Based on these results, we hypothesize that the matrix material in the 20 to 25 cm soil section, which represents the location of the plow pan, did not have a significantly lower

hydraulic conductivity than the matrix material in the surrounding soil. Instead, we believe the effective conductivity of the plow pan was reduced relative to the rest of the field because it lacked the cracks and macropores that existed in the bund (Figure 2.8a) and subsoil (Figure 2.6); the process of puddling the field destroyed a majority of the macropores to the depth of the plow pan, mitigating irrigation loss through the pan.

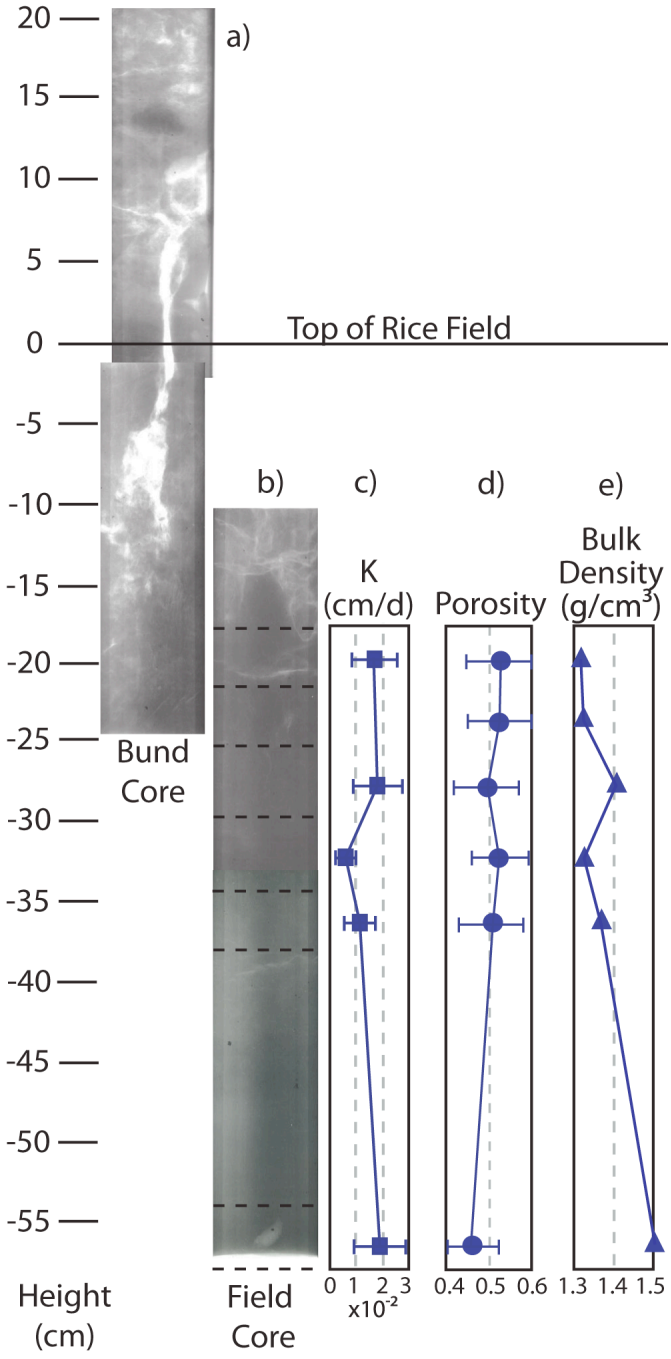

Figure 2.8 Soil core data.

a) Radiograph of bund core (C1 in Figure 2.1). White color corresponds with cracks in the bund.
b) Radiograph of rice field core (C2 in Figure 2.1).
c) Hydraulic conductivity of soil sections from the field core.
d) Porosity of soil sections from the field core.
e) Bulk density of soil sections from the field core.

2.5. Discussion

2.5.1. Mechanisms and Dynamic Patterns of Recharge

Flow beneath our studied rice field was controlled by differences in the field-scale effective hydraulic conductivity of the bund, the plow pan, and the subsoil; and, we believe the effective hydraulic conductivities of these different features were controlled by the presence or lack of cracks. Beneath the plow pan, the cracks that allowed for preferential flow were likely due to animals or ancient tree roots. In the surface soil and bund, cracks were caused by soil drying after the rice was harvested and before the monsoon season began (see supporting information, chapter 3, for photograph). Other researchers documented that soil drying resulted in cracks that persisted even after resubmergence of the field (Moormann and van Breeman 1978, Wopereis et al. 1994a, Cabangon and Tuong 2000, Islam et al. 2004). However, on our and other fields (Moormann and van Breeman 1978, Wopereis et al. 1994a, Cabangon and Tuong 2000), puddling largely sealed the surface cracks. The extremely tight contour lines that correspond with the plow pan in Figure 2.5 demonstrate that in our field, this surface layer of soil had a lower effective conductivity than the subsoil.

Flow through the bunds was greatest during and immediately after irrigation events when standing water in the rice field was deepest, covering a larger surface area of the bund. The water potentials within the subsoil measured by the tensiometer network show that bund flow increased after irrigation (Figure 2.5a and animation in Neumann et al. (2009)). The interpolated iso-potential lines indicate that flow paths originated from the bund and then spread laterally into the subsoil. Over an irrigation cycle, as the water level receded, the sequence of measured potentials shifted such that less flow entered through the bunds; bund flow ceased altogether when the ponded water reached the top of the surface muck and the bund desaturated (Figure 2.4 and

Figure 2.7). Prior to our season-long sensor-based data set, bund flow dynamics were inferred from steady-state numerical models (Walker and Rushton 1984, Walker and Rushton 1986, Walker 1999) or from the rate of water loss in fields with normal and sealed bunds (Tuong et al. 1994, Wopereis et al. 1994b). Our continuous and explicit measurements support the findings from these previous studies that bund flow depends on the depth of ponded water and is a dominant water loss for rice fields.

The time sequence of sensor data also shows that an unsaturated zone developed underneath the flooded field. This observation confirms earlier theoretical work (Takagi 1960, Zaslavsky 1964) that predicted an unsaturated zone beneath the plow pan if the difference in effective conductivity between the pan and the subsoil was great enough. The continuous sensor data show that the size of the unsaturated-zone varied as the water level in the rice field went up and down with irrigation (Figure 2.5 and animation in Neumann et al. (2009)). When the water level in the field was high and bund flow was large, the unsaturated zone was contained with the middle of the field. As the ponded water in the rice field receded and bund flow decreased, the unsaturated zone grew to occupy the entire field. Previous rice-field investigations detected the presence of an unsaturated zone underneath a flooded field surface using vertical profiles of water pressure or water content measurements (Wopereis et al. 1992, Tuong et al. 1994, Wopereis et al. 1994b, Chen and Liu 2002). However, neither these nor numerical modeling studies (Walker and Rushton 1984, Walker and Rushton 1986, Walker 1999) determined that the unsaturated zone changes its shape and size during an irrigation cycle. Our findings raise several questions for future research: What is the composition of the gas in the unsaturated zone, and does the volume of this zone change by gas solution and dissolution, or by direct exchange with the atmosphere?

The tracer test results show that macropores and cracks beneath the puddled soil layer actively transported water to deeper depths during the irrigation season (Figure 2.6). Previous tracer tests on dry and harvested rice fields (Sander and Gerke 2007, Janssen and Lennartz 2008) illustrated that fields have an extensive network of subsurface preferential flow channels, but could not confirm that these networks persisted during the growing season. On our field, recharge to the underlying aquifer was composed of water that traveled through preferential flow channels located either in the subsoil or underneath the bund. Rice field water that infiltrated through the plow pan, but did not enter a preferential flow path reached a depth of only ~ 40 cm as a nearly uniform, plug-flow, front (Figure 2.6).

Water within the soil matrix below the 40 cm plug-flow front (the un-dyed portion of the soil matrix in Figure 2.6) was likely a mixture of residual aquifer water, rainwater and rice field water. Soil moisture measurements taken after the end of the rice season and before the start of the monsoon season demonstrate that desaturation of the soil down to ~2 m depth created roughly 10 cm of void space or capacity for monsoonal rainwater or ground water (see supporting information, chapter 3, for data and calculation). Hydraulic head contours from after the irrigation season (see animation in Neumann et al. (2009)) show that on May 1st 2006, when the entire subsurface soil was desaturated, the head gradient switched from pointing downwards to pointing upwards. After this point in time, water from rainstorms did not appreciably change the saturation state in the soil nor infiltrate very deeply through the soil matrix. The hydraulic gradient was upward when the soil re-saturated (Figure 2.5c), so flow into the lower void spaces must have come from below, even through rain had fallen on the surface. The water table rise could have been caused by increasing river water levels pushing the regional groundwater table upwards (Harvey et al. 2006) and/or rainwater traveling to deeper depths through preferential

flow channels that bypass the soil matrix. In either case, a maximum of 10 cm of rainwater could have infiltrated the soil matrix. These calculations do not consider compressive storage of the soil matrix.

The hydraulic head contours in the subsoil cross section during the post-irrigation and pre-monsoon season also support our conceptual model of flow through the bund, plow pan, and preferential channels. Unlike the head contours during the irrigation season, the measured patterns of water potential after the irrigation season (see animation in Neumann et al. (2009)) are not influenced by the bund. It appears that cracks observed on the surface of the field (see supporting information, chapter 3) removed the plow pan as a barrier to flow such that standing water on the field was no longer channeled into the bund.

2.5.2. The Importance of the Field's Perimeter-to-Area Ratio

The results of the field study enable us to develop a water-balance equation for the rice field. Inputs include irrigation and rain, while losses include evapotranspiration, preferential flow, matrix infiltration, and bund flow. These fluxes, along with the system boundary, are illustrated in Figure 2.9. The bund-flow term is a function of the field's perimeter, and based on our field data, it also is a function of the height of puddled water (h_p in Figure 2.9). Over any time increment, the change in the volume of water in the field must be balanced by the inflows and outflows:

$$A\frac{\Delta h}{\Delta t} = I + \left(R - E - PF - MI\right)A - \psi P h_p \qquad (1a)$$

where, h = height of water in the field above the plow pan [L], t = time [T], I = irrigation input [L^3/T], R = rainfall [L/T], E = evapotranspiration [L/T], PF= preferential field flow [L/T], MI = matrix infiltration [L/T], A = area of field [L^2], Ψ = bund flow per unit cross-section of the bund

covered by water [L/T], P = field perimeter [L], and h_p= height of ponded water [L]. Mathematically, $h_p=(h-h_m)$ when $h>h_m$, and $h_p=0$ when $h\leq h_m$, where h_m is the height of the surface muck above the plow pan. The flow per unit area is:

$$\frac{\Delta h}{\Delta t} = \frac{I}{A} + R - E - PF - MI - \frac{\psi P h_p}{A} \quad (1b)$$

Equation 1b quantifies the dependence of bund flow on the field's perimeter-to-area ratio and explains the strong relationship presented in Figure 2.3a between this ratio and the rate of water loss for the first 5 cm of water. On average, the height of puddled water (h_p) after an irrigation event was 5 to 6 cm (see Figure 2.11), and thus this loss rate represents the period of time for which $h_p \geq 0$. The equation also explains the weaker relationship between the perimeter-to-area ratio and the total amount of irrigation water applied to the field (Figure 2.3b). Once $h_p = 0$, the field's water balance no longer depends on the perimeter-to-area ratio. In addition, our observations of the local farming practice suggest that the weakness of this relationship may be due to different irrigation behaviors of the farmers. Some farmers allow the field to sit dry for long periods of time, while other farmers never let the field dry out. This discrepancy is likely caused by the farmer's understanding of what type of water regimes produce the highest yields, or his financial situation and ability to buy diesel fuel for the irrigation well pump.

Equation 1b and Figure 2.3 emphasize the importance of the field's perimeter-to-area ratio. Because perimeter and area are not independent, the ratio is needed to understand the significance of bund flow in a field's water budget. In 1978, Wickham and Sen (1978) and Wickham and Singh (1978) reported on studies in which the smaller fields lost significantly more water due to perimeter seepage. A similar trend is highlighted in Figure 2.10, which shows the calculated fraction of water lost down the bunds as a function of the perimeter-to-area ratio (see figure caption for details on the bund loss calculation). The smaller the field or larger the

perimeter-to-area ratio, the greater the proportion of water lost down the bunds. The calculated relationship nicely matches results from the few water balance studies, including ours (see below), for which we could determine a perimeter-to-area ratio. The fit between the calculated relationship and data from three different rice fields, one in Bangladesh and two in the Philippines (Tuong et al. 1994, Wopereis et al. 1994b), stresses the importance of the perimeter-to-area ratio and suggests that this ratio can provide a first order estimate of the fraction of water lost down the bunds of a given field.

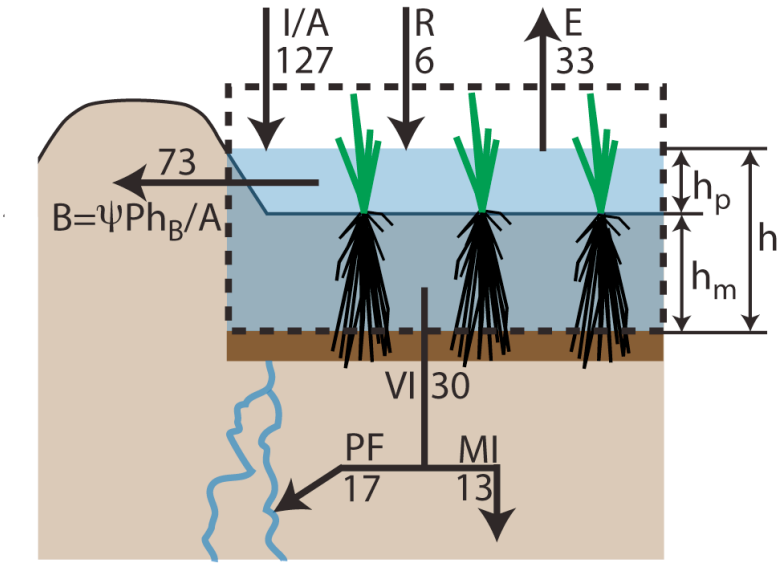

Figure 2.9 Water balance cartoon.

The system boundary for the water balance is marked with the dashed line. The fluxes across this boundary are designated by the large black arrows. The numbers on the arrows denote the average seasonal magnitude of each flux from Figure 2.12 in units of cm/season.

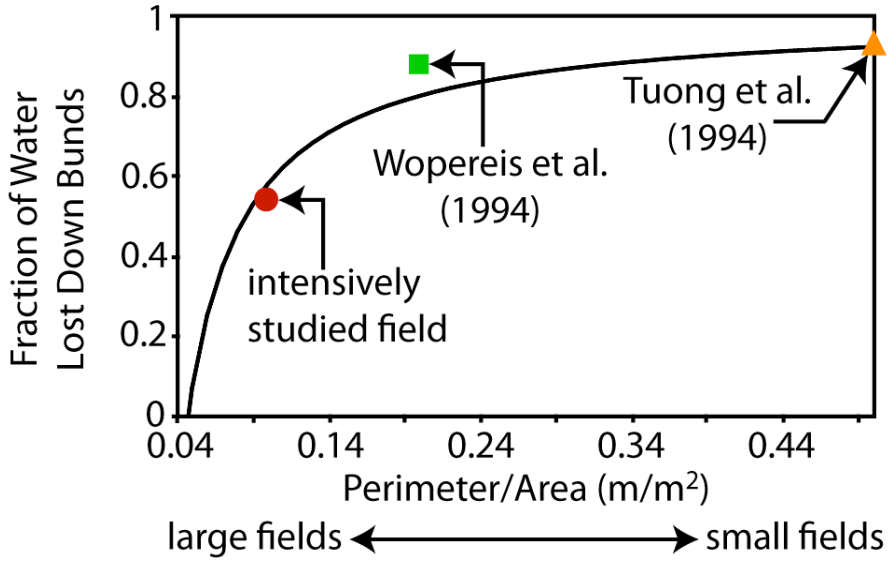

Figure 2.10 Fraction of water lost down the bunds versus the perimeter-to-area ratio.

The data points are water balance results from three different field studies and the black line represents the calculated bund-loss fraction. Bund loss was calculated by first estimating the total amount of water added to a field using the linear fit in Figure 2.3b, and then subtracting losses due to evapotranspiration, matrix infiltration, and preferential field flow. Evapotranspiration was assumed constant at 0.39 cm/day, which was the average rate during the 2006 and 2007 irrigation seasons, and the sum of matrix infiltration and preferential field flow was assumed constant at 0.35 cm/day (see *Flux Determination: Infiltration Tests* in Results, section 2.4.3).

2.5.3. Irrigation Season Water Balance

Of the different fluxes into or out of the rice field, flow into bunds is the most difficult to measure directly because of its transience. Here we estimate the flow into bunds by constructing a complete water balance for the rice field. Although the time sequences of water potentials and water content clearly show recharge entering the bund and diverging into the subsoil, these spatial patterns can not be directly translated into accurate estimates of flux because of the uncertainties of modeling unsaturated flow. The water balance approach attributes changes in the rate of water level decline, not explained by changes in the evapotranspiration rate, to bund flow. We have direct measurements, or independent estimates, of all the fluxes in Equation 1b other than bund flow (see Methods, section 2.3). The meteorological data (rain and pan evaporation) were collected on a daily time scale, so this was the finest resolution at which bund loss could be calculated. Bund flow was calculated by solving Equation 1b for $\Psi Ph_p/A$ as a lumped quantity, and the error was estimated by propagating the uncertainty associated with other fluxes (see Methods and Results, sections 2.3 and 2.4) through Equation 1b, assuming that each uncertainty was normally distributed around the determined flux value. The daily and seasonal fluxes are shown in Figures 2.11 and 2.12.

The seasonal model results (Figure 2.12) indicate that half of the water lost from the surface of the rice field flowed through the bund, a fourth of the water was lost to evapotranspiration, an eighth was lost to preferential flow through the subsoil and an final eighth infiltrated through the soil matrix. In both years, roughly the same amount of irrigation water was added to the field and roughly the same amount was lost down the bund. The magnitude of these seasonal fluxes is denoted on the water balance cartoon in Figure 2.9.

The estimated bund flow approaches zero as the water level in the field approaches the soil surface (Figure 2.11). These model results support the accuracy of our estimates for matrix infiltration (MI) and preferential field flow (PF), which were both specified as constants with time (see *Flux Determination: Infiltration Tests* in Results, section 2.4.3). Bund flow must cease when the height of water above the field surface (h_p) goes to zero (Equation 1b). The model can only reproduce this behavior if the sum of the specified flows is correct.

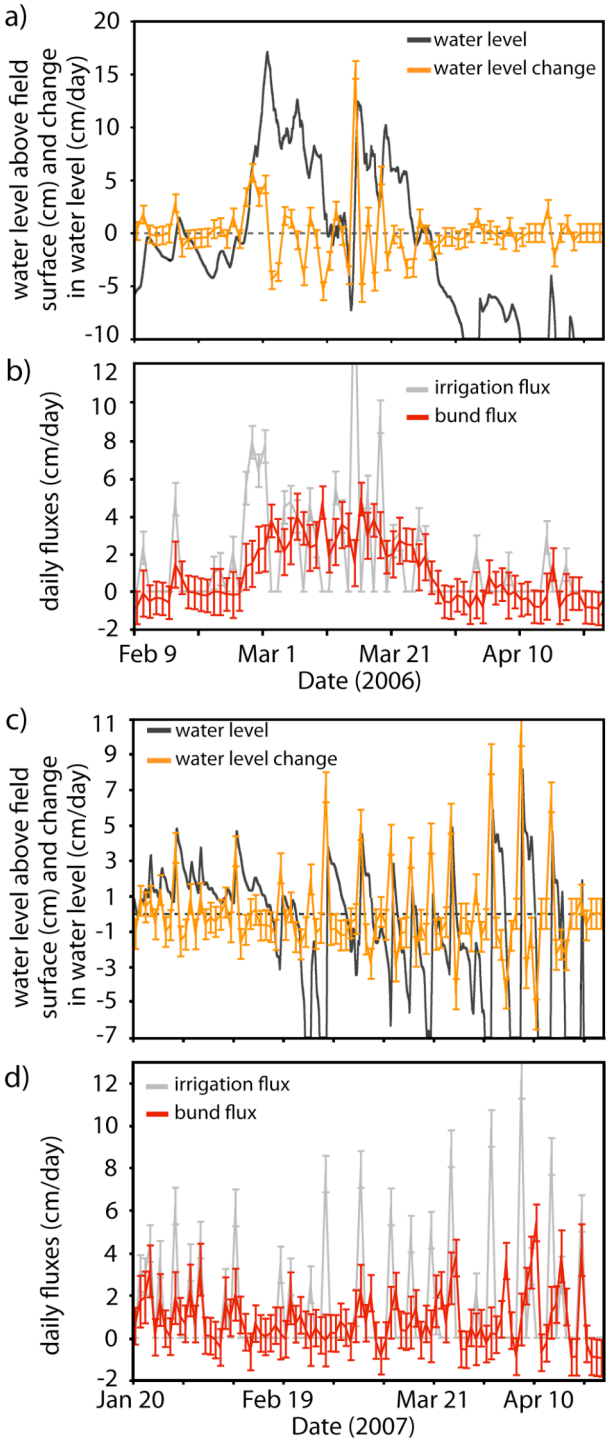

Figure 2.11 Water balance results.

a & c) Water level above the surface muck and daily change in water level. A negative water level means that the water is within the surface muck but above the plow pan.
b & d) Daily irrigation and bund fluxes. Bund flow occurs immediately after irrigation when the water of the field is above the surface muck

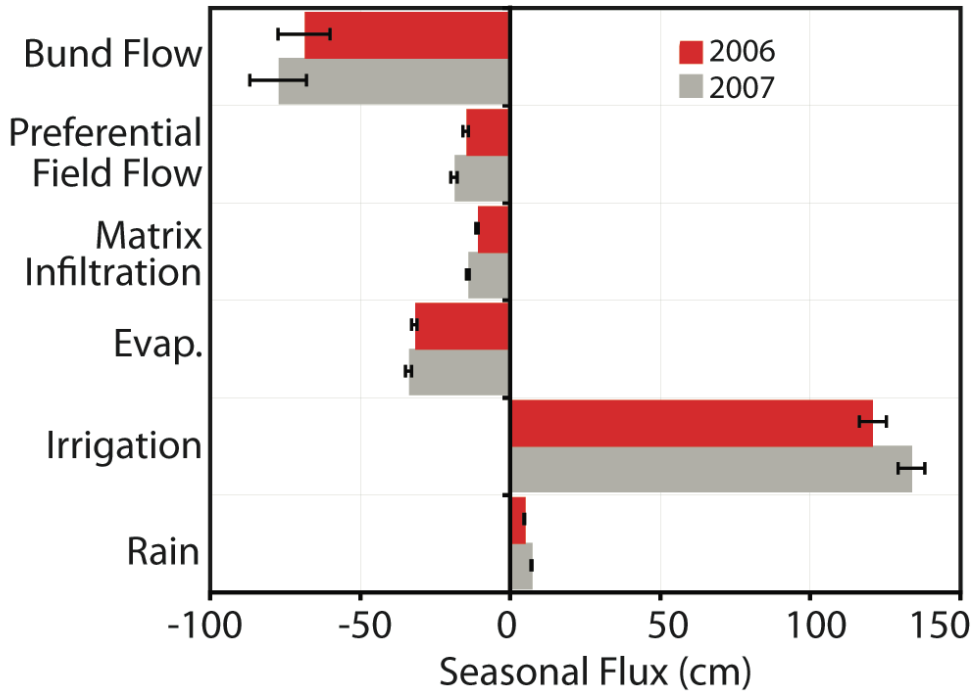

Figure 2.12 Seasonal water balance for the 2006 and 2007 irrigation seasons.

Roughly 50% of all the irrigation water applied to the field is lost down the bund. However, bund flow makes up 80% of the water that recharges the aquifer, which includes only preferential-flow water and bund water.

2.5.4. Broader Impacts

Our field data illustrate that to determine the impact that recharge through rice fields has on Bangladesh's groundwater chemistry, and hence arsenic contamination problem, one must characterize the chemical composition of bund and macropore water, not matrix water. It is the water passing through these preferential pathways that recharges the underlying aquifer and affects groundwater chemistry and the biogeochemical processes that mobilize arsenic from sediments. Furthermore, the chemical properties of subsoil matrix water and preferential-flow water are likely different. The matrix is oxygenated when the soil dries after irrigation and refills with rainwater or groundwater, while the preferential flow paths in the bund and subsoil actively receive irrigation water. At least initially, the chemical signature of the water passing through bunds and macropores may be similar to that of the standing water in the rice field, as described by Roberts et al. (2007). However, preferential flow paths are known to have high microbial biomass (Bundt et al. 2001), and may mobilize sediment-bound arsenic and transport it to depth (Corwin et al. 1999).

In addition, our results suggest that plowing the soil underneath the bunds, and rebuilding the bunds each year, would significantly reduce the amount of irrigation water applied to rice fields, especially in smaller fields. In Bangladesh, where the rice fields are irrigated with methane-rich groundwater (Dowling et al. 2002, Harvey et al. 2002), this reduction in water use would correspond with a decrease in carbon dioxide emissions from the diesel irrigation pumps and a potential decrease in methane emissions from the irrigation water itself. Using the relationships from Figure 2.3b and Figure 2.10, we estimate that 41 km^3 of water is unnecessarily lost down the bunds each year in Bangladesh (see supporting information, chapter 3, for calculations). Using information about diesel prices, pump efficiencies, and groundwater

methane concentrations we approximate that: 1) bund loss costs Bangladesh 79.8 to 101 million dollars each year, which is 0.04 to 0.05% of its GDP, 2) combustion of diesel fuel for pumping the irrigation water associated with bund loss releases 0.26 Tg of CO_2, which is 1.7% of Bangladesh's 1990 carbon dioxide emissions (Ahmed et al. 1996), and 3) if the methane in the irrigation water degasses to the atmosphere before it is oxidized by methanotrophs in the rice field, then the methane released from bund loss is 0.41 Tg, or 36% of Bangladesh's 1990 methane emissions (Ahmed et al. 1996). Although our estimation methods are crude, they suggest that Bangladesh could benefit economically and reduce greenhouse gas emissions by controlling bund loss.

2.6. Acknowledgments

This work was supported by NSF EAR 0651678 and 0605515, and The Center for Environmental Sensing and Modeling at the Singapore MIT Alliance for Research and Technology. The authors would like to thank Jack Germaine for his help with the CRS tests and soil-core X-rays, and for allowing us to use his equipment. We would also like to thank Ashfaque Khandaker, Ben Kocar, Linda Roberts, Jessica Dittmar, Andreas Voegelin, Stephan Hug, Nithya Ramanathan and Tiffany Lin for help in the field; Allison St. Vincent, Farah Khan and Kajetan Zwieniecki for help in the laboratory; the research groups of Phil Gschwend and Harry Hemond for intellectual support; and our associate editor Andrew J. Guswa and three anonymous reviewers for their constructive feedback on our manuscript. Finally, we would like to thank Anis and Mitu at B.U.E.T. and the people of Bashailbhog village, especially Ripon Chowdhury, Sojib Chowdhury, Sha'alam and Rasil, for their instrumental support of our project.

2.7. References

Ahmed, A. U., K. Islam, and M. Reazuddin (1996), An inventory of greenhouse gas emissions in Bangladesh: initial results, *Ambio, 25*, 300-303.

Ali, M. A., A. B. M. Badruzzaman, M. A. Jalil, M. D. Hossain, M. F. Ahmed, A. A. Masud, M. Kamruzzaman, and M. Rahman (2003), Fate of Arsenic Extracted with Groundwater, Proc. Internat. Symp. on Fate of Arsenic in the Environment, BUET and UNU, Dhaka, Bangladesh.

ASTM (2006) D 4186-06: Standard test method for one-dimensional consolidation properties of saturated cohesive soils using controlled-strain loading.

ASTM (2002) D 5093-02: Standard test method for field measurement of infiltration rate using a double-ring infiltrometer with a sealed-inner ring.

BGS, DFID, and DPHE (2001), Arsenic contamination of groundwater in Bangladesh, *BGS Technical Report WC/00/19, Volume 1*, British Geological Survey, Keyworth.

Bundt, M., F. Widmer, M. Pesaro, J. Zeyer, and P. Blaser (2001), Preferential flow paths: biological hot spots in soils, *Soil Biol. Biochem., 33*, 729-738.

Cabangon, R. J., and T. P. Tuong (2000), Management of cracked soils for water saving during land preparation for rice cultivation, *Soil Tillage Res., 56*, 105-116.

Chen, S. K., and C. W. I. Liu (2002), Analysis of water movement in paddy rice fields (I) experimental studies, *J. Hydrol., 260*, 206-215.

Corwin, D. L., A. David, and S. Goldberg (1999), Mobility of arsenic in soil from the Rocky Mountain Arsenal area, *J. Contam. Hydrol., 39*, 35-58.

Dittmar, J., A. Voegelin, L. Roberts, S. J. Hug, G. C. Saha, M. A. Ali, A. B. M. Badruzzaman, and R. Kretzschmar (2007), Spatial distribution and temporal variability of arsenic in irrigated rice field in Bangladesh: 2. Paddy soil, *Environ. Sci. Technol., 41*, 5967-5972.

Dowling, C. B., R. J. Poreda, A. R. Basu, S. L. Peters, and P. K. Aggarwal (2002), Geochemical study of arsenic release mechanisms in the Bengal Basin groundwater, *Water Resour. Res., 38*,

Flury, M., H. Fluhler, W. A. Jury, and J. Leuenberger (1994), Susceptibility of soils to preferential flow of water: A field-study, *Water Resour. Res., 30*, 1945-1954.

Flury, M., and N. N. Wai (2003), Dyes as tracers for vadose zone hydrology, *Rev. Geophys., 41*, 1002, doi: 10.1029/2001RG000109.

Forrer, I., R. Kasteel, M. Flury, and H. Fluhler (1999), Longitudinal and lateral dispersion in an unsaturated field soil, *Water Resour. Res., 35*, 3049-3060.

Harvey, C. F., C. H. Swartz, A. B. M. Badruzzaman, N. Keon-Blute, W. Yu, M. A. Ali, J. Jay, R. Beckie, V. Niedan, D. Brabander, P. M. Oates, K. N. Ashfaque, S. Islam, H. F. Hemond, and M. F. Ahmed (2002), Arsenic mobility and groundwater extraction in Bangladesh, *Science, 298*, 1602-1606.

Harvey, C. F., K. N. Ashfaque, W. Yu, A. B. M. Badruzzaman, M. A. Ali, P. M. Oates, H. A. Michael, R. B. Neumann, R. Beckie, S. Islam, and M. F. Ahmed (2006), Groundwater dynamics and arsenic contamination in Bangladesh, *Chem. Geol., 228*, 112-136.

Hossain, M. D., D. Lewis, M. L. Bose, and A. Chowdhury (2003), Rice Research, Technological Progress, and Impact on the Poor: The Bangladesh Case (Summary Report), *EPTD Discussion Papers*, International Food Policy Research Institute, Washington, D.C.

Huang, H. C., C. W. Liu, S. K. Chen, and J. S. Chen (2003), Analysis of percolation and seepage through paddy bunds, *J. Hydrol., 284*, 13-25.

Hundal, S. S., and S. K. De Datta (1984), In situ water transmission characteristics of a tropical soil under rice-based cropping systems, *Agric. Water Manage., 8*, 387-396.

Islam, M. J., S. S. Parul, A. B. M. B. U. Pathan, M. A. Quasem, and M. S. Islam (2004), Influence of cracking on rice seasons and irrigation in Bangladesh, *J. Biol. Sci., 4*, 11-14.

Janssen, M., and B. Lennartz (2008), Characterization of Preferential Flow Pathways through Paddy Bunds with Dye Tracer Tests, *Soil Sci. Soc. Am. J., 72*, 1756-1766.

Janssen, M., and B. Lennartz (2009), Water losses through paddy bunds: Methods, experimental data, and simulation studies, *J. Hydrol.*, doi: 10.1016/j.jhdrol.2009.02.038.

Jones, S. B., J. M. Wraith, and D. Or (2002), Time domain reflectometry measurement principles and applications, *Hydrol. Processes, 16*, 141-153.

Kulli, B., M. Gysi, and H. Fluhler (2003), Visualizing soil compaction based on flow pattern analysis, *Soil Tillage Res., 70*, 29-40.

Lauren, J. G., R. J. Wagenet, J. Bouma, and J. H. M. Wosten (1988), Variability of saturated hydraulic conductivity in a glossaquic Hapludalf with macropores, *Soil Sci., 145*, 20-28.

Lu, J., and L. Wu (2003), Visualizing bromide and iodide water tracer in soil profiles by spray methods, *J. Environ. Qual., 32*, 363-367.

Moormann, F. R., and N. van Breeman (1978), *Rice: Soil, Water, Land,* International Rice Research Institute, Los Banos, Laguna, Philippines.

Neumann, R.B., M.L. Polizzotto, A.B.M. Badruzzaman, M.A. Ali, Z. Zhang, C.F. Harvey (2009), The hydrology of a groundwater-irrigated rice field in Bangladesh: Seasonal and daily mechanisms of infiltration, *Water Resour. Res.,* 45, doi:10.1029/2008WR007542.

Norra, S., Z. A. Berner, P. K. Agarwala, F. Wagner, D. Chandrasekharam, and D. Stuben (2005), Impact of irrigation with As rich groundwater on soil and crops: A geochemical case study in West Bengal Delta Plain, India, *Appl. Geochem., 20*, 1890-1906.

Ohrstrom, P., Y. Hamed, M. Persson, and R. Berndtsson (2004), Characterizing unsaturated solute transport by simultaneous use of dye and bromide, *J. Hydrol., 289*, 23-35.

Roberts, L., S. J. Hug, J. Dittmar, A. Voegelin, G. C. Saha, M. A. Ali, A. B. M. Badruzzaman, and R. Kretzschmar (2007), Spatial distribution and temporal variability of arsenic in irrigated rice fields in Bangladesh: 1. Irrigation water, *Environ. Sci. Technol., 41*, 5960-5966.

Sander, T., and H. H. Gerke (2007), Preferential flow patterns in paddy fields using a dye tracer, *Vadose Zone J., 6*, 105-115.

Sharma, P. K., and S. K. De Datta (1986), Physical properties and processes of puddled rice soils, *Adv. Soil Sci., 5*, 139-168.

Takagi, S. (1960), Analysis of the vertical downward flow of water through a two-layered soil, *Soil Sci., 90*, 98-103.

Tomar, V. S., and J. C. O'Toole (1980), Measurement of evapotranspiration in rice, Symposium on the Agrometerology of the Rice Crop, International Rice Research Institute, Los Benos, Laguna, Philippines.

Tuong, T. P., M. C. S. Wopereis, J. A. Marquez, and M. J. Kropff (1994), Mechanisms and control of percolation losses in irrigated puddled rice fields, *Soil Sci. Soc. Am. J., 58*, 1794-1803.

Walker, S. H. (1999), Causes of high water losses from irrigated rice fields: field measurements and results from analogue and digital models, *Agric. Water Manage., 40*, 123-127.

Walker, S. H., and K. R. Rushton (1984), Verification of lateral percolation losses from irrigated rice fields by a numerical-model, *J. Hydrol., 71*, 335-351.

Walker, S. H., and K. R. Rushton (1986), Water losses through the bunds of irrigated rice fields interpreted through an analog model, *Agric. Water Manage., 11*, 59-73.

Wickham, T. H., and C. N. Sen (1978), Water management for lowland rice: water requirements and yield response, in *Soils and Rice*, edited by The International Rice Research Institute, Los Banos, Philippines.

Wickham, T. H., and V. P. Singh (1978), Water movement through wet soils, in *Soil and Rice*, edited by The International Rice Research Institute, Los Banos, Philippines.

Wissa, A. E. Z., J. T. Christian, E. H. Davis, and S. Heiberg (1971), Consolidation at constant rate of strain, *J. Soil Mech. Found. Div., ASCE, 97*, 1393-1413.

Wopereis, M. C. S., J. Bouma, M. J. Kropff, and W. Sanidad (1994a), Reducing bypass flow-through a dry, cracked and previously puddled rice soil, *Soil & Tillage Research, 29*, 1-11.

Wopereis, M. C. S., B. A. M. Bouman, M. J. Kropff, H. F. M. Tenberge, and A. R. Maligaya (1994b), Water-use efficiency of flooded rice fields.1. Validation of the soil-water balance model Sawah, *Agric. Water Manage., 26*, 277-289.

Wopereis, M. C. S., J. H. M. Wosten, J. Bouma, and T. Woodhead (1992), Hydraulic resistance in puddled rice soils - measurement and effects on water-movement, *Soil Tillage Res., 24*, 199-209.

Yasuda, H., R. Berndtsson, H. Persson, A. Bahri, and K. Takuma (2001), Characterizing preferential transport during flood irrigation of a heavy clay soil using the dye Vitasyn Blau, *Geoderma, 100*, 49-66.

Zaslavsky, D. (1964), Theory of unsaturated flow into a non-uniform soil profile, *Soil Sci., 97*, 400-410.

3. Supporting Information for Chapter 2

3.1. TDR Calibration

The soil in the rice field is a silt loam to silty clayey loam (Dittmar et al. 2007). In this media, the standard equations used to convert raw TDR measurements into water content values are not always accurate (Jones et al. 2002). Therefore, the TDR probes were calibrated in the laboratory at MIT using undisturbed soil cores collected in 4-inch-diameter liners during the tower excavation. The rice field soil was completely saturated when the cores were collected. However, the open ends of the cores were covered in cheesecloth and the cores were soaked in water for a few weeks to counter act any drying that may have occurred during transport of the cores back to MIT. The TDR probes were then inserted into the center of the cores, ensuring that the probe ends were surrounded by soil and that the core liner did not interfere with the measurements. The probes were hooked up to a datalogger that was programmed to record readings every hour. The cores with the inserted probes were weighted to get the mass of the saturated system. The open ends of the cores were then covered in Saran wrap and the cores and probes were left for approximately a week until the TDR reading stabilized. The Saran wrap was then removed and the cores were re-weighed. They were then left with the Saran wrap off for a few days to dry. The cores were then re-weighed to determine the loss of water, the open ends of the cores were covered with Saran wrap, and the cores were left for a week to achieve stable TDR readings. The procedure was repeated multiple times.

Figure 3.1a shows that each probe provides slightly different reading in air, so an absolute calibration could not be obtained. Instead, the relative change in the TDR reading from saturated conditions is used to determine the water content (Figure 3.1b). Thus, a field measurement in saturated conditions is required to determine absolute water content. A linear least squares fit was applied to the first five calibration points of the two probes and the errors on

the slope and intercept of the fit were used to estimate the precision of the calibration (Figure 3.2). Calibration shows that a decrease of 1.5 μsec in the TDR reading from saturated conditions corresponds with a 4 to 5% decrease in water content (Figure 3.1b and Figure 3.2). The horizontal error bars in Figure 3.1b represent the maximum and minimum values measured by the TDR probe for that given calibration point once the probe reading had leveled off. Therefore, these error bars account for drift in the measurements. On average, 160 data points were used for each calibration point. The vertical error bars represent the uncertainty propagated through the water content calculation, and include uncertainty about the core volume and its measured mass.

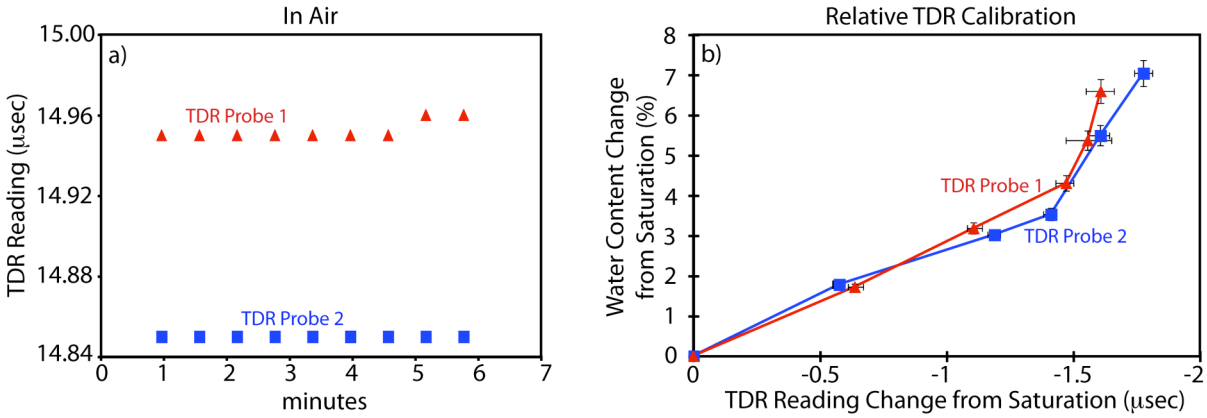

Figure 3.1 Calibration of the TDR probes.

a) TDR readings in air for two different probes. The difference between the probes suggests that an absolute calibration is not possible.

b) Relative TDR calibration for the two different probes. The water content change is determined from the change in the TDR reading from saturated conditions.

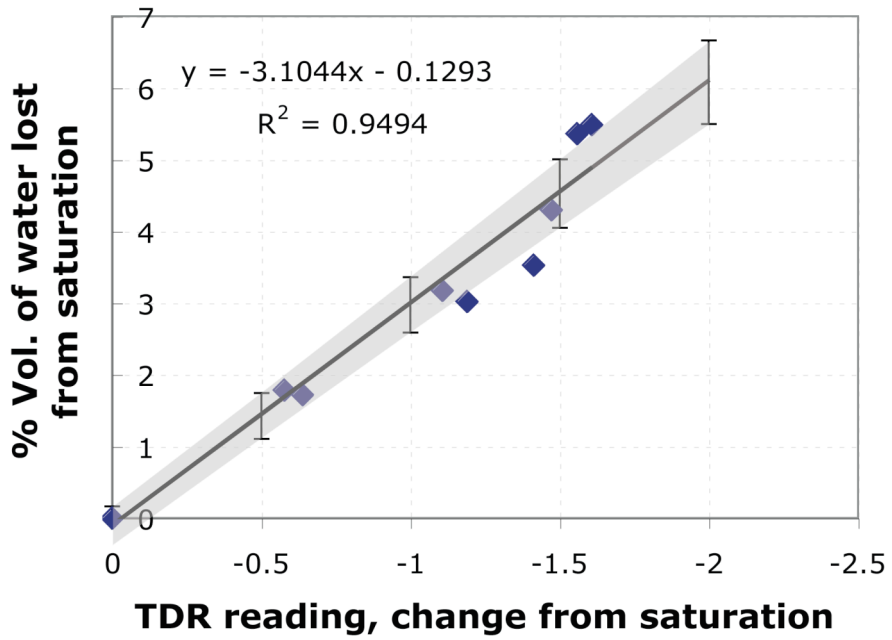

Figure 3.2 Linear least squares fit of TDR calibration data

The black line represents the linear least squares fit to the data. The error bars and gray area represent the uncertainty in the fit based on the standard error of the slope and intercept estimates. The uncertainty in the fit is greater than that due to experimental error or sensor drift, as shown in Figure 3.1.

3.2. Pressure and Head Data for the 2006 Irrigation and Monsoon Season

Data from all nine of the tensiometers installed in the field are shown below. The pressure data (Figure 3.3) show that at the end of the irrigation season (~May), all of the tensiometers measured negative pressures, signifying unsaturated conditions. The head data (Figure 3.4) show that the calibration of the tensiometers was lost during the monsoon season. During the monsoon season the entire land surface is flooded and there is no vertical or horizontal hydraulic gradient, so all of the tensiometers should be measuring the same head. Therefore, only the sensor data from the first field season were used for the hydrologic study.

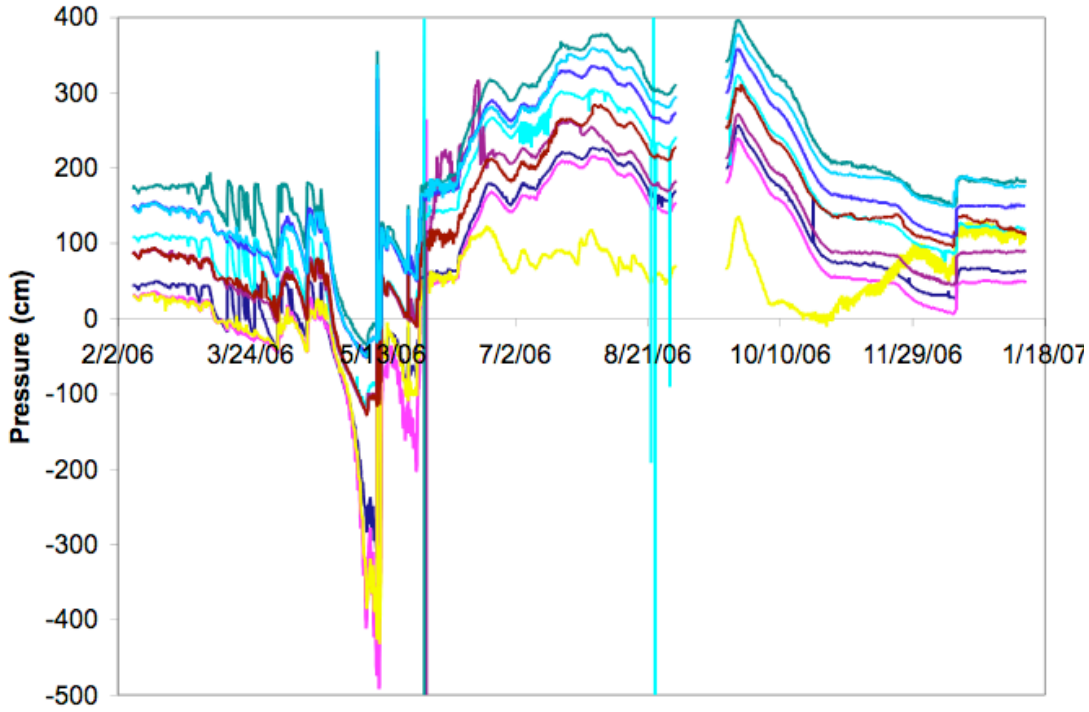

Figure 3.3 Pressure data from the 2006 irrigation and monsoon season.
At the end of the irrigation season (May) all of the tensiometers measured negative pressures, signifying unsaturated conditions. During the monsoon season (June to December), the entire soil profile is saturated.

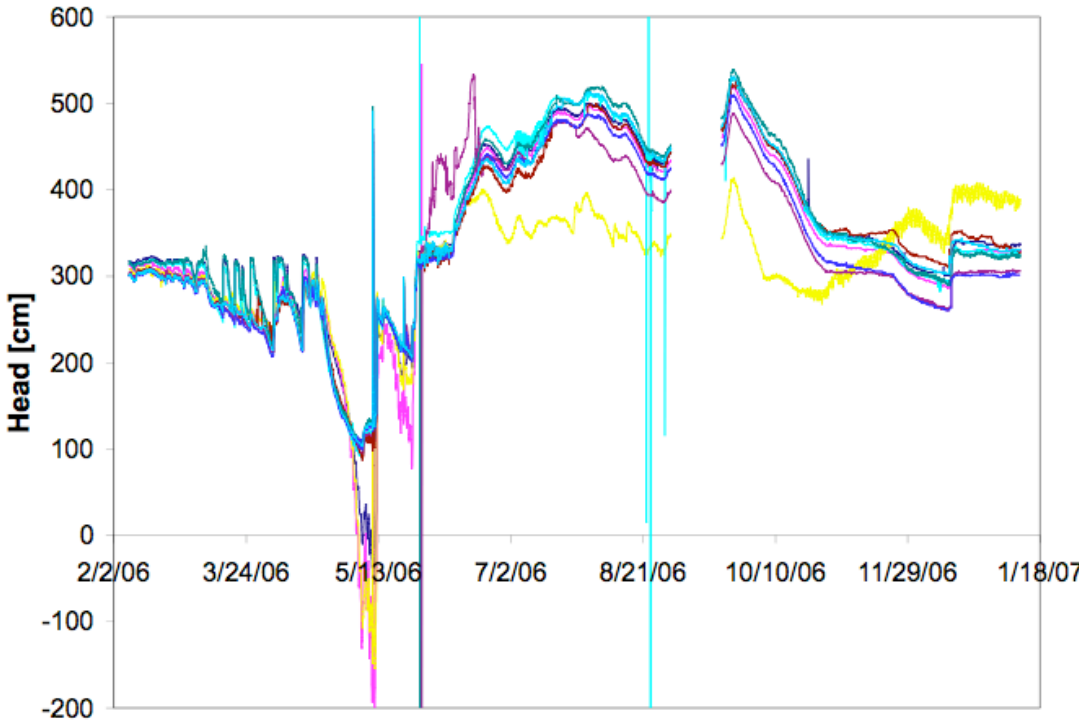

Figure 3.4 Head data from the 2006 irrigation and monsoon season.

During the monsoon season (June to December), all of the head value should equal each other since the entire land surface is flooded with water and there are no hydraulic gradients to drive flow. The fact that the head data does not match during this time implies that the sensor calibration was lost during the monsoon season.

3.3. On-site Evapotranspiration Measurements

On-site evapotranspiration measurements were taken with a large-scale Marriott bottle, following the protocol outlined in Tomar and O'Toole (1980). A 33 cm diameter bucket was partially buried in the rice field and filled with the displaced soil and rice plants. The top of the bucket was placed just slightly above the location corresponding with the maximum height of water in the field, to ensure that irrigation water did not enter the bucket. The bucket was then connected with a flexible tube and a valve to a 1.2-m-tall vertical section of 10-cm-diameter PVC pipe. The bottom of the PVC pipe was capped with a PVC cap and the top of the pipe was sealed with a removable black rubber stopper. With the stopper in place and properly greased, the vertical PVC pipe was completely air tight, except for an air tube that ran through the middle of the stopper into the PVC pipe. When the PVC pipe was filled with water, water flowed from the PVC pipe into the soil-filled bucket until the water level inside the bucket reached the same height as the bottom of the air tube inside the PVC pipe. This setup always kept the water in the bucket at the same height. When the bucket lost water due to evapotranspiration, water from the PVC pipe would immediately flow into the bucket. Since the diameter of the bucket was roughly 10x larger than the PVC pipe, evapotranspiration losses from the bucket were amplified by this amount in the PVC pipe.

In 2007, the utilized PVC pipe was the standard opaque white color, and changes in water level inside the pipe were detected with a pressure transducer that recorded measurements every 15 minutes. The pressure transducer was not placed in the water column, which due to the setup of the system actually does not undergo pressure changes, but was instead placed in the gas phase. The gas phase inside the PVC pipe begins at less than atmospheric pressure and approaches atmospheric pressure as water is lost from the pipe. The recorded changes in pressure

were translated into corresponding changes in water level. The error associated with this evapotranspiration measurement was estimated at ±0.08 cm/day, which is the propagated error of the pressure transducer measurements multiplied by the ratio of the PVC pipe area to the evaporation bucket area. In 2008, the utilized PVC pipe was clear. Water level changes were manually measured twice a day. In both years, the volume of the gas phase inside of the PVC pipe was kept small compared to the volume of the water phase to minimize the impact of temperature fluctuations on the measurement method. In addition, the PVC pipes were covered with a silver reflective tarp.

Figure 3.5 Marriott bottle setups.
Left-hand picture is the 2007 setup and the right-hand picture is the 2008 setup; both pictures taken without the silver reflective tarp. The vertical pipes are the 10-cm-diameter PVC pipes which are connected to the sliver bucket placed within the rice field soil.

The weakness of this measurement method is that data collection cannot occur remotely because the PVC pipe has to be periodically filled with water. Therefore, data collected during field visits were compared to the continuously collected pan evaporation measurements from the

nearby meteorological station. Figure 3.6 shows the data comparison and illustrates that the pan evaporation measurements closely approximate field evapotranspiration at the beginning of the irrigation season (January), when 9 out of 10 data points fall on the 1:1 line. Towards the end of the irrigation season (April), only 3 of 6 data points fall on the 1:1 line. In general, during this period of time, the evapotranspiration rate determined with the Marriott system is greater than that determined with the evaporation pan. At the end of the season the rice plants are taller, which both increases the leaf area available for transpiration and shades the ponded water in the field. Increased leaf area would act to increase transpiration while shading would act to decrease evaporation. The comparison in Figure 3.6 suggests that increased transpiration from increased leaf area slightly offsets the decreased evaporation from shading.

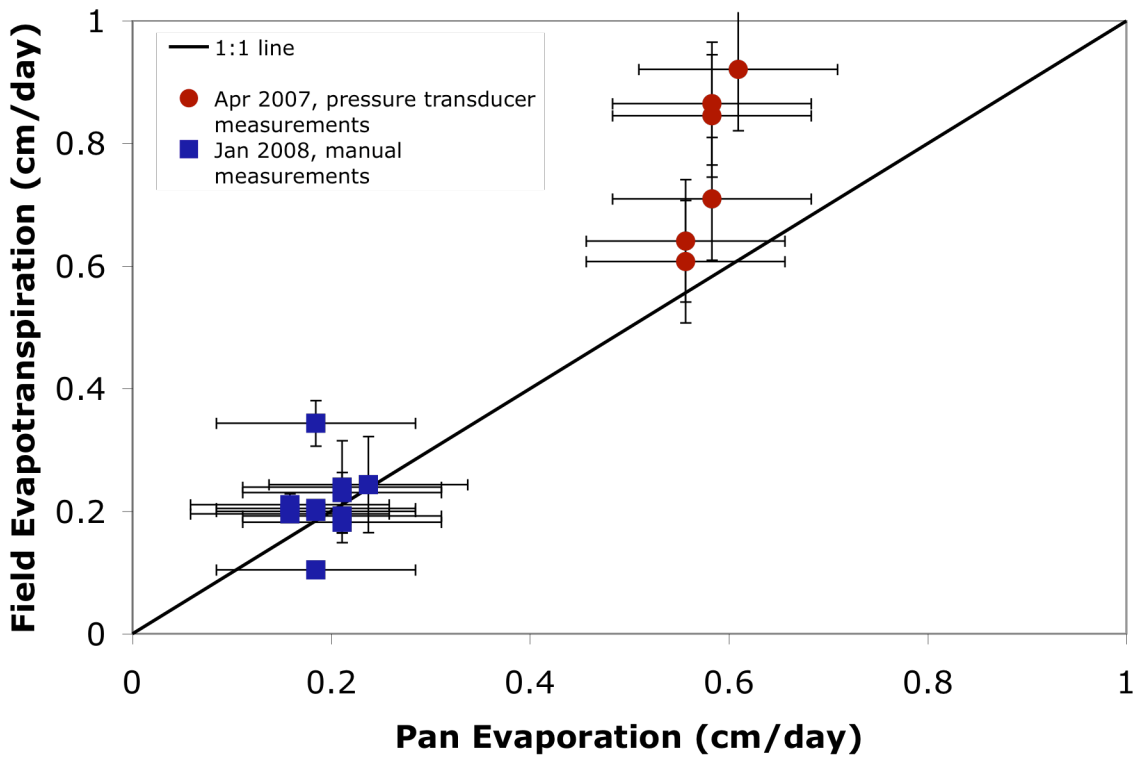

Figure 3.6 Evapotranspiration method comparison.

Direct Comparison between the meteorological station's pan evaporation measurements and the on-site Marriott-bottle evapotranspiration measurements.

3.4. Calculation of Irrigation Input and Losses

Figure 2.11 shows that the irrigation flux is roughly 6 cm/day, or 6 cm per irrigation event, and the bund flux is roughly 3 cm/day. Data show that infiltration through the plow pan averages 0.35 cm/day (see section 2.4.3), and the average rate of evaporation from the meteorological station's evaporation pan for the entire season is 0.39 cm/day. Therefore, 3.7 cm/day of water is lost to evaporation, bund flow and plow pan infiltration. Since irrigation events last approximately 2 hours, ~0.3 cm of water is lost during an irrigation event due to these three processes, which is much less than the 6 cm of water applied to the field during irrigation.

3.5. CRS Test Results

Hydraulic conductivity, void ratio and bulk density of sections of the collected rice field core were determined following the protocol outlined in the ASTM standard for the constant rate of strain test (ASTM 2006). Data from the tests are below. The depths of the tested core section correspond to the depths designated in Figure 2.8.

Table 3.1 CRS Test 872, Core Section at -20 cm

Measurement	Value	Uncertainty
Wet soil, cutter & Recess mass (g)	437.75	0.05
Cutter Mass (g)	273.49	0.05
Recess tool Mass (g)	49.84	0.05
Initial Wet Mass (g)	114.4	0.9
Initial Height (cm)	2.350	0.001
Area (cm^2)	27.80	0.01
Final Dry Mass and Tare (g)	108.18	0.05
Final Tare mass (g)	22.13	0.05
Dry Mass (g)	86.1	0.9
Specific Gravity	2.78	0.20
Initial Water Content (%)	32.97	
Initial Void Ratio	1.11	0.17
Porosity	0.53	0.08
Initial Saturation (%)	82.53	
Wet Density (g/cm^3)	1.751	
Dry Density (g/cm^3)	1.317	0.013
Height of solids (cm)	1.1134	

Lines shaded gray represent measured values, the un-shaded lines represent calculated values, and the lines shaded yellow represent assumed values. The assumed, specific gravity value was determined from the mineralogy of a groundwater-irrigated rice soil in West Bengal (Norra et al. 2005). The soil contained: 33% quartz (specific gravity 2.65), 8% calcite (specific gravity 2.71), 2% dolomite (specific gravity 2.85), 14% feldspar (specific gravity 2.76), 15% illite (specific

gravity 2.9), 10% kaolinite (specific gravity 2.7), 18% other phylosillicates, which based on the work of Polizzotto et al. (2006) for our field site, are likely biotite or hornblede (specific gravity 3). This mineral composition results in a bulk specific gravity of 2.78. The uncertainty is due to the fact that many of the minerals, including illite, feldspar, kaolinite and biotite, actuall have a range of specific gravities due to natural mineral variations and mineralogical composition of our Munshiganj rice field may be different than that in the studied West Bengal field (Norra et al. 2005).

During the test, the soil section is strained at a slow and continuous rate. Processed data from the tests are plotted below. The hydraulic conductivity and void ratio relationship was determined for the specimen from the stabilized portion of the test (shown in pink). The in-situ hydraulic conductivity was calculated from this relationship using the initial void ratio of the specimen.

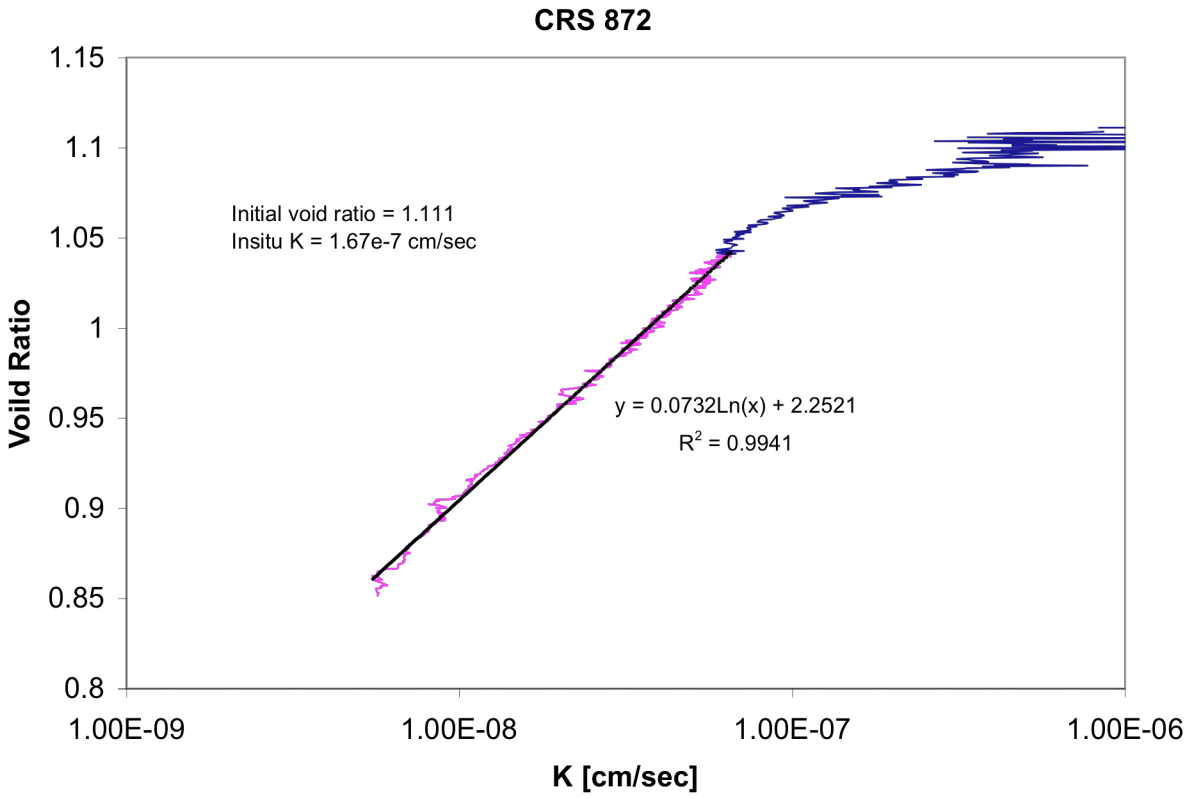

Figure 3.7 Void ratio vs. conductivity for CRS test 872 with core section from -20 cm.

Table 3.2 CRS Test 873, Core Section at -24 cm

Measurement	Value	Uncertainty
Wet soil, cutter & recess mass (g)	442.13	0.05
Cutter Mass (g)	275	0.05
Recess tool Mass (g)	49.84	0.05
Initial Wet Mass (g)	117.3	0.9
Initial Height (cm)	2.350	0.001
Area (cm^2)	28.04	0.01
Final Dry Mass and Tare (g)	109.85	0.05
Final Tare mass (g)	22.42	0.05
Dry Mass (g)	87.4	0.9
Specific Gravity	2.78	0.20
Initial Water Content (%)	34.15	
Initial Void Ratio	1.095	0.164
Porosity	0.52	0.08
Initial Saturation (%)	86.69	
Wet Density (g/cm^3)	1.780	
Dry Density (g/cm^3)	1.327	0.013
Height of solids (cm)	1.1216	

The CRS test failed for this specimen so we could not determine its hydraulic conductivity.

Table 3.3 CRS Test 881, Core Section at -28 cm

Measurement	Value	Uncertainty
Wet soil, cutter & recess mass (g)	444.04	0.05
Cutter Mass (g)	273.5	0.05
Recess tool Mass (g)	49.84	0.05
Initial Wet Mass (g)	120.7	0.9
Initial Height (cm)	2.3500	0.001
Area (cm^2)	27.80	0.01
Final Dry Mass and Tare (g)	114.8	0.05
Final Tare mass (g)	23.09	0.05
Dry Mass (g)	91.7	0.9
Specific Gravity	2.78	0.20
Initial Water Content (%)	31.61	
Initial Void Ratio	0.980	0.147
Porosity	0.50	0.07
Initial Saturation (%)	89.64	
Wet Density (g/cm^3)	1.848	
Dry Density (g/cm^3)	1.404	0.014
Height of solids (cm)	1.1867	

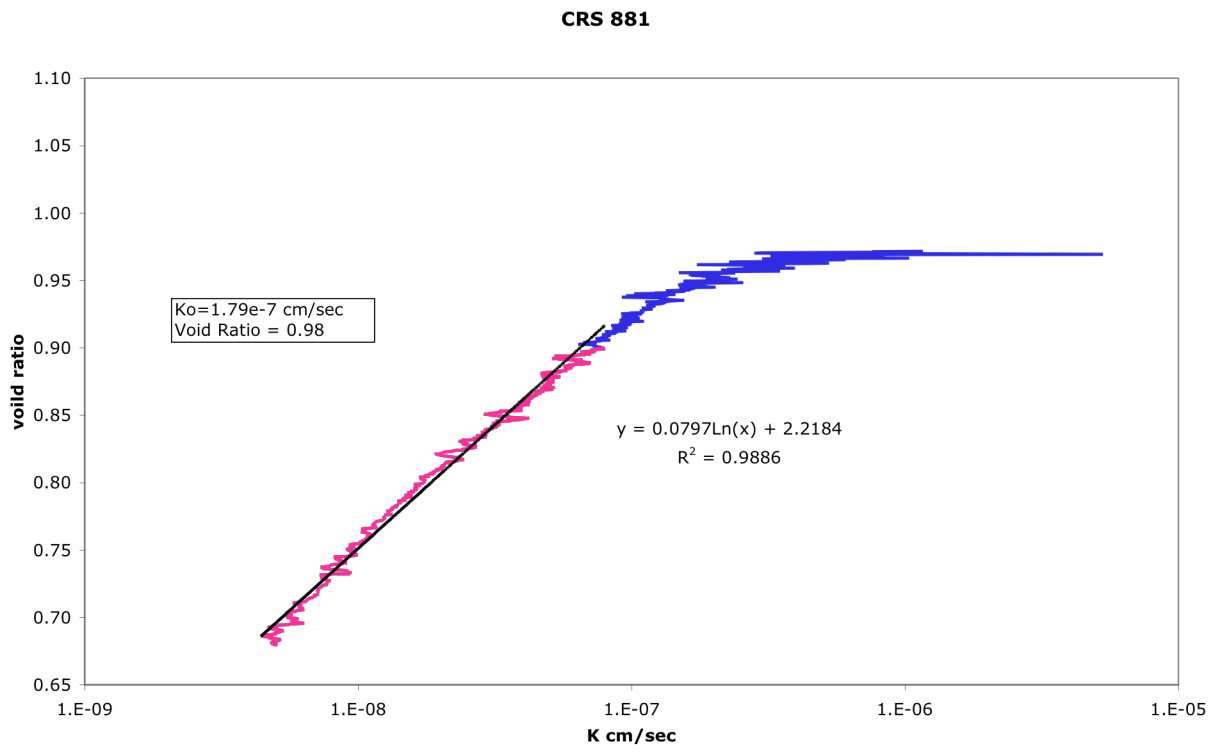

Figure 3.8 Void ratio vs. conductivity for CRS test 881 with core section from -28 cm.

Table 3.4 CRS Test 880, Core Section at -33 cm

Measurement	Value	Uncertainty
Wet soil, cutter & recess mass (g)	441.24	0.05
Cutter Mass (g)	273.55	0.05
Recess tool Mass (g)	49.84	0.05
Initial Wet Mass (g)	117.9	0.9
Initial Height (cm)	2.3500	0.001
Area (cm^2)	27.80	0.01
Final Dry Mass and Tare (g)	110.05	0.05
Final Tare mass (g)	23.26	0.05
Dry Mass (g)	86.8	0.9
Specific Gravity	2.78	0.20
Initial Water Content (%)	35.79	
Initial Void Ratio	1.093	0.164
Porosity	0.52	0.08
Initial Saturation (%)	91.06	
Wet Density (g/cm^3)	1.804	
Dry Density (g/cm^3)	1.328	0.013
Height of solids (cm)	1.1230	

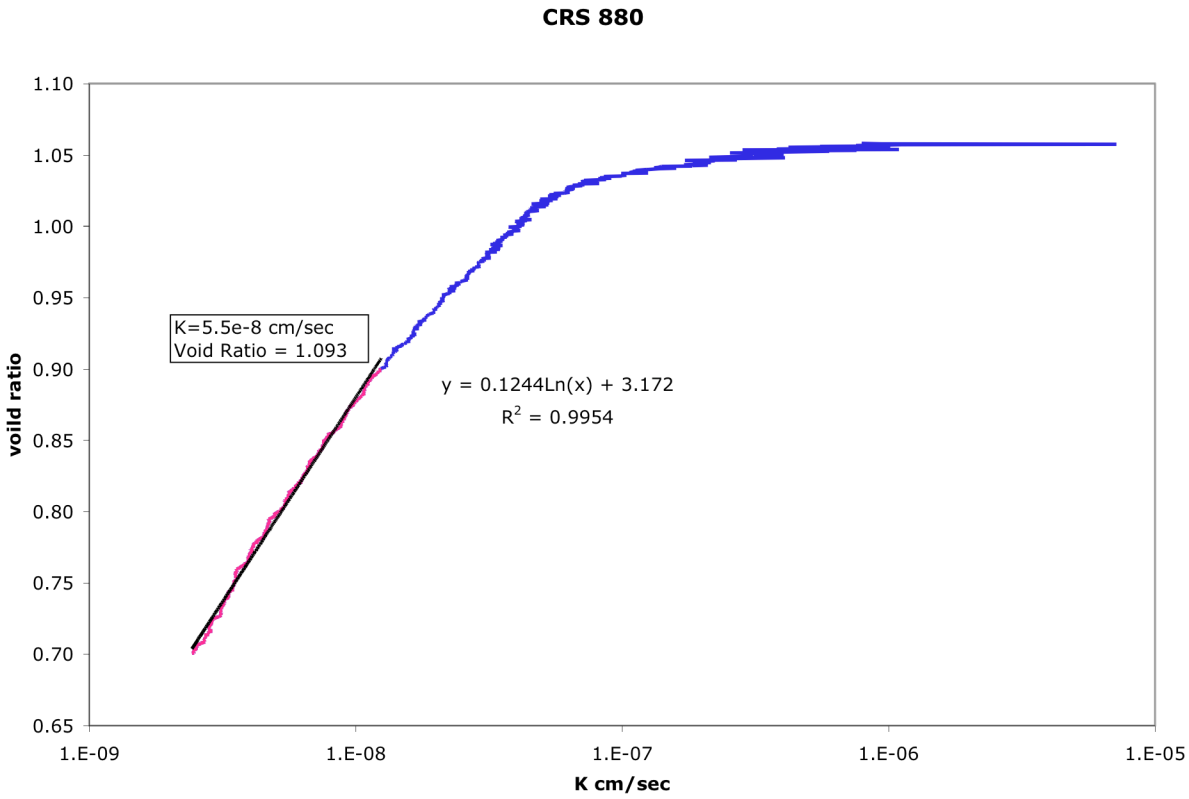

Figure 3.9 Void ratio vs. conductivity for CRS test 880 with core section from -33 cm.

Table 3.5 CRS Test 879, Core Section at -36 cm

Measurement	Value	Uncertainty
Wet soil, cutter & recess mass (g)	443.71	0.05
Cutter Mass (g)	273.51	0.05
Recess tool Mass (g)	49.84	0.05
Initial Wet Mass (g)	120.4	0.9
Initial Height (cm)	2.3500	0.001
Area (cm^2)	27.80	0.01
Final Dry Mass and Tare (g)	112.11	0.05
Final Tare mass (g)	22.53	0.05
Dry Mass (g)	89.6	0.9
Specific Gravity	2.78	0.20
Initial Water Content (%)	34.36	
Initial Void Ratio	1.027	0.154
Porosity	0.51	0.08
Initial Saturation (%)	92.97	
Wet Density (g/cm^3)	1.842	
Dry Density (g/cm^3)	1.371	0.014
Height of solids (cm)	1.1591	

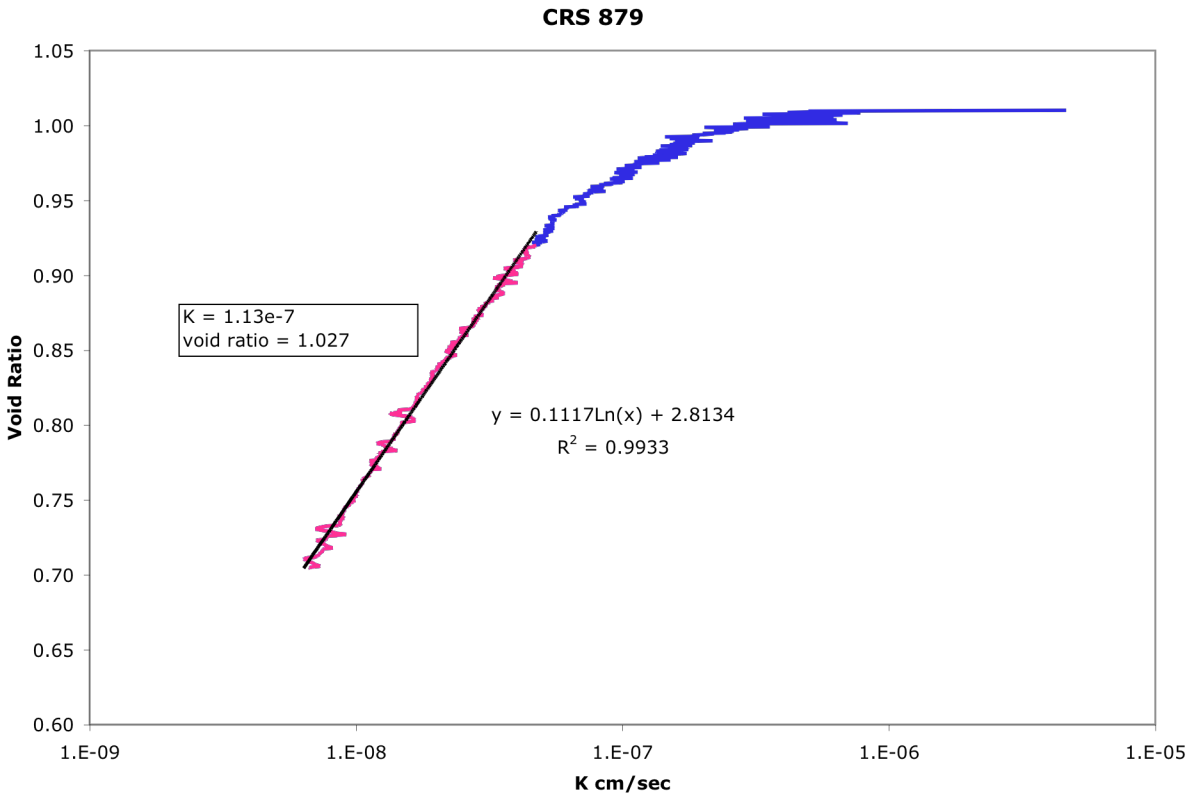

Figure 3.10 Void ratio vs. conductivity for CRS test 879 with core section from -36 cm.

Table 3.6 CRS Test 864, Core Section at -55 cm

Measurement	Value	Uncertainty
Wet soil, cutter & recess mass (g)	450.94	0.05
Cutter Mass (g)	273.49	0.05
Recess tool Mass (g)	49.84	0.05
Initial Wet Mass (g)	127.6	0.9
Initial Height (cm)	2.3500	0.001
Area (cm^2)	27.80	0.01
Final Dry Mass and Tare (g)	120.42	0.05
Final Tare mass (g)	22.09	0.05
Dry Mass (g)	98.3	0.9
Specific Gravity	2.78	0.20
Initial Water Content (%)	29.78	
Initial Void Ratio	0.847	0.127
Porosity	0.46	.07
Initial Saturation (%)	97.73	
Wet Density (g/cm^3)	1.953	
Dry Density (g/cm^3)	1.505	0.015
Height of solids (cm)	1.2723	

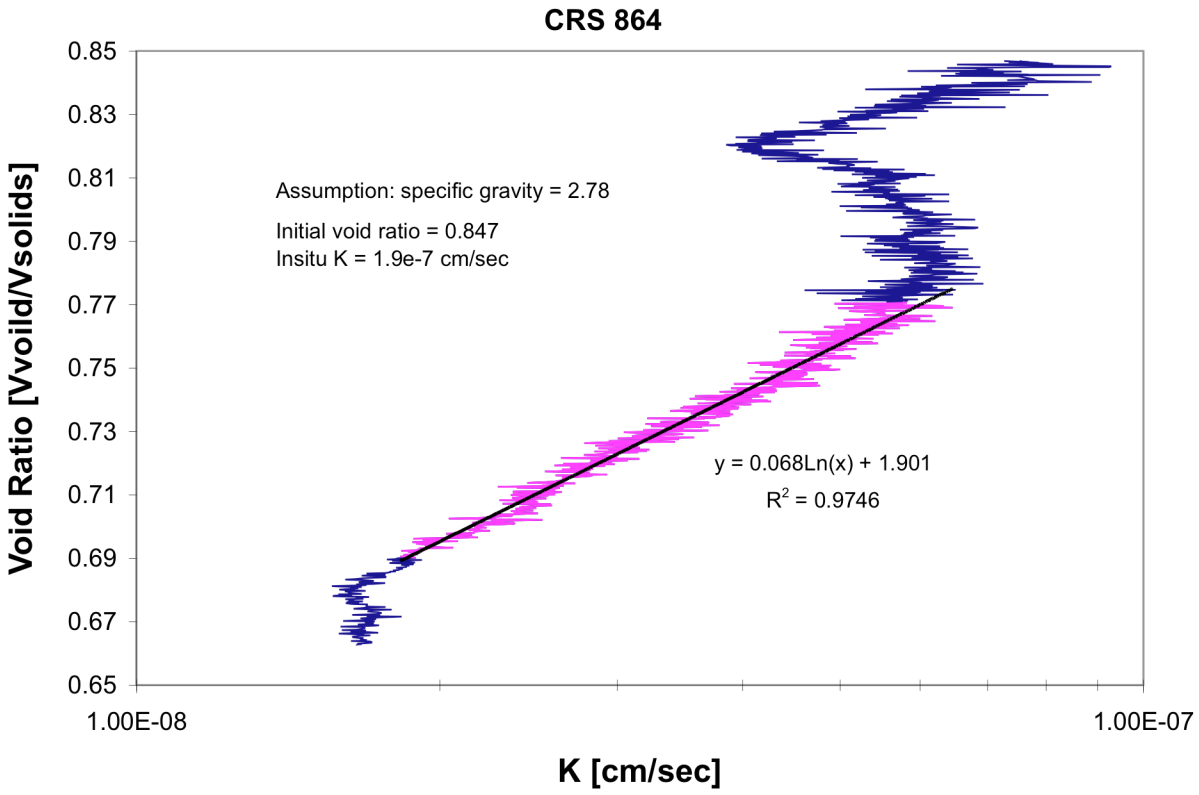

Figure 3.11 Void ratio vs. conductivity for CRS test 864 with core section from -55 cm.

3.6. Calculation of Density Effects for Bromide Tracer Tests

The variable density form of Darcy's equation is (Frind 1982):

$$q_z = K_f \left(\frac{\partial h_f}{\partial z} + \frac{\rho - \rho_f}{\rho_f} \right)$$

where q_z is flow in the vertical direction, K_f is the fresh water hydraulic conductivity, h_f is the fresh water head, z is depth, ρ is density of the solution and ρ_f is density of fresh water. Figure 2.5 shows that the vertical hydraulic gradient from the top of the rice field to the bottom of the sensor transect in the middle of the field was roughly 75 cm/144 cm = 0.5 during an entire irrigation cycle. The concentration of the sodium bromide tracer applied to the field was ~40 g/L, resulting in ρ=1040 g/L, while ρ_f=1000 g/L. These density values lead to a density gradient of 0.04, which is an order of magnitude smaller than the head gradient, and therefore has a negligible impact on vertical flow behavior.

3.7. Surface Cracks in Rice Field

Figure 3.12 Cracks in the surface soil

This picture was taken May 2006, after the rice was harvested and before the monsoon season began. The cracks remain open and active even after the field is resubmerged with water. Therefore, the farmers must plow the fields each year to seal the cracks.

3.8. Available Dry Season Void Space Calculation

Data from the driest point of the 2006 dry season (May 11th) were used to determine the total amount of rainwater that could enter the rice field soil. TDR data from this day are plotted versus depth in Figure 3.13. An exponential function was fit to the three data points, assuming the shallow soil layers were significantly more dry than the deeper soil layers due to evaporation during the dry season. This fit was used, along with a porosity value of 0.5, to calculate that the soil profile had 10 cm per unit area of available void space on this day. It was assumed that these 10 cm per unit area were filled with rain that fell on the landscape after May 11th.

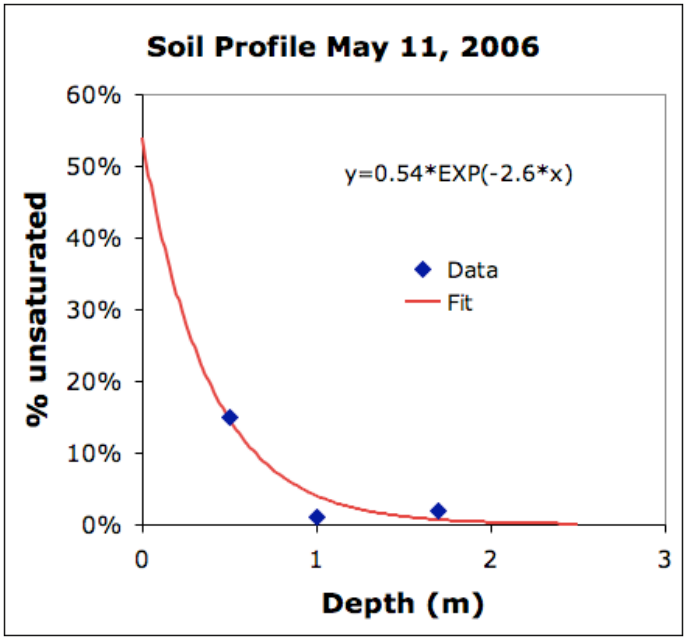

Figure 3.13 Water content data from driest point of 2006.
TDR data from May 11, 2006, the driest point before the monsoon season began, in % unsaturated along with an exponential fit to the three data points. The equation for the fit is shown on the graph. The data and fit provide information about void space in the soil available to fill with rainwater or floodwater during the onset of the monsoon season.

3.9. Bund Loss Calculations for Bangladesh

We present a simple analysis of the potential economic benefits and reduction in greenhouse gas emissions from reducing irrigation loss down bunds. Using the relationships from Figure 2.3b and Figure 2.10, we estimated the amount of water lost down bunds each year for a 1 km^2 area (473 fields) centered on our studied rice field by determining the dimensions of the fields within that region through Google Earth. The resulting estimate of seasonal bund loss for each field, in units of length, was multiplied by the area of the field to determine the total volume of water lost down the bund. The estimated loss for all 473 fields was summed to find a total loss for the 1 km^2 area of 7.7e8 liters (Table 3.8). Results obtained for the 1 km^2 area were scaled-up to the entire country by simply multiplying by the total area of land currently under groundwater-irrigated rice agriculture in Bangladesh. Finally, we used information about diesel prices, pump efficiencies, and groundwater methane concentrations to approximate the money and greenhouse gas emissions associated with this lost water. The constants used in the calculations are in Table 3.7, while the results of the calculations are in Table 3.8.

Table 3.7 Constants used for bund loss calculations.

Constants used in Calculations	Value	Source
Area of rice fields in chosen 1km^2 area	0.76 km^2	Google Earth
Area of groundwater-irrigated rice fields in Bangladesh	40,000 km^2	(Hossain et al. 2003)
Average irrigation pump speed	24 L/sec	(Harvey et al. 2006)
Gross power required by irrigation pump for a head of 2m	0.84 kW	(Robinson 2002)
Fuel use by pump	0.25 L·kW^{-1}·hr^{-1}	(Robinson 2002)
Wholesale cost of diesel fuel (July 2008)	1.02 $/L	(EIA 2008)
Subsidized cost of diesel fuel in Bangladesh (July 2008)	0.81 $/L	(BangladeshNews.com.bd 2008)
CO_2 emitted by diesel fuel	2664 g/L	(EPA 2005)
CH_4 concentration in irrigation water	0.010 g/L	(Dowling et al. 2002, Harvey et al. 2002) and unpublished data in Figure 3.14
Bangladesh GDP	$206.7 billion	(CIA 2008)
Bangladesh CO_2 emissions (1990 estimate)	10e12 g/yr	(Ahmed et al. 1996)
Bangladesh CH_4 emissions (1990 estimate)	1.15e12 g/yr	(Ahmed et al. 1996)
Global warming potential for CH_4 on a 100yr time horizon	25	(IPCC 2007)

Table 3.8 Resulting values from bund loss calculations.

Calculated Quantity for Water Lost Down Bund Every Year	1km2 Studied Area	Scaled to all of Bangladesh	Perspective when Scaled to all of Bangladesh
Water lost down bund (L)	7.7e8	4.1e13	
Pump time needed (hr)	9e3	4.7e8	
Fuel used (L)	1.9e3	9.9e7	
Wholesale cost of fuel ($)	1.9e3	1.0e8	0.05% of GDP
Subsidized cost of fuel ($)	1.1e3	8.0e7	0.04% of GDP
CO2 emitted by pumping (g)	5.0e6	0.26e12	1.7% of Bangladesh's 1990 CO_2 emissions
CH4 contained in pumped water (g)	7.7e6	0.41e12	36% of Bangladesh's 1990 CH_4 emissions if CH_4 degasses before being oxidized by methanotrophs
Total global warming potential on 100yr time horizon (g CO_2eq)	2.0e8	11e12	27% of Bangladesh's 1990 global warming potential

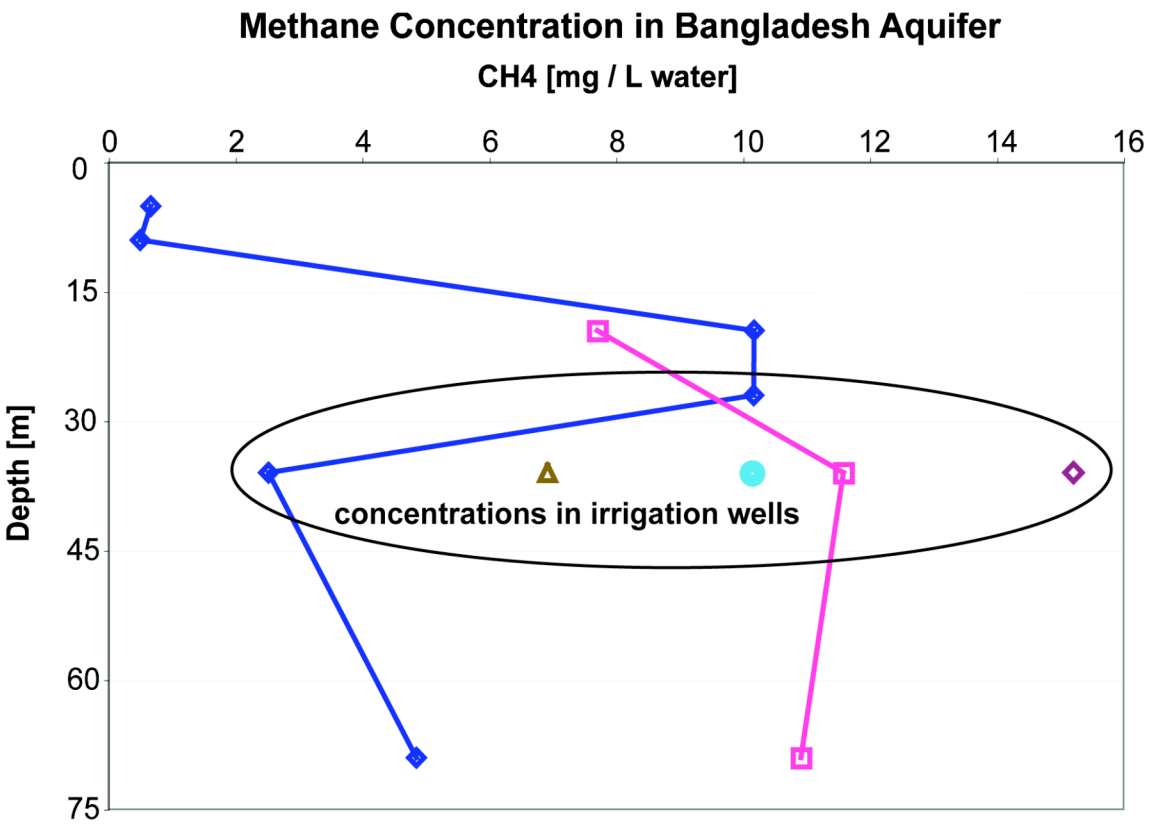

Figure 3.14 Methane concentrations in Bangladesh's shallow aquifer.

Data collected from five different well nests within a 16km^2 area surrounding the studied rice field. Data used in Table 3.7. See section 7.1.4 for details on sample collection and analysis.

3.10. References

Ahmed, A. U., K. Islam, and M. Reazuddin (1996), An inventory of greenhouse gas emissions in Bangladesh: initial results, *Ambio, 25*, 300-303.

ASTM (2006) D 4186-06: Standard test method for one-dimensional consolidation properties of saturated cohesive soils using controlled-strain loading.

BangladeshNews.com.bd (2008) Octane now Tk90, diesel Tk 55. *http://www.bangladeshnews.com.bd/2008/07/01/octane-now-tk-90-diesel-tk-55/*.

CIA (2008) Bangladesh. *The World Factbook. https://www.cia.gov/library/publications/the-world-factbook/print/bg.html*.

Dittmar, J., A. Voegelin, L. Roberts, S. J. Hug, G. C. Saha, M. A. Ali, A. B. M. Badruzzaman, and R. Kretzschmar (2007), Spatial distribution and temporal variability of arsenic in irrigated rice field in Bangladesh: 2. Paddy soil, *Environ. Sci. Technol., 41*, 5967-5972.

Dowling, C. B., R. J. Poreda, A. R. Basu, S. L. Peters, and P. K. Aggarwal (2002), Geochemical study of arsenic release mechanisms in the Bengal Basin groundwater, *Water Resour. Res., 38*,

EIA (2008) Monthly US NO.2 Diesel Wholesale/Resale Price by Refiners. *http://tonto.eia.doe.gov/dnav/pet/hist/a223700002m.htm*.

EPA (2005), Emission Facts: Average carbon dioxide emissions resulting from gasoline and diesel fuel, *EPA420-F-001*, Office of Transportation and Air Quality, Washington, DC.

Frind, E. O. (1982), Simulation of long-term transient density-dependent transport in groundwater, *Adv. Water Resour., 5*, 73 - 88.

Harvey, C. F., C. H. Swartz, A. B. M. Badruzzaman, N. Keon-Blute, W. Yu, M. A. Ali, J. Jay, R. Beckie, V. Niedan, D. Brabander, P. M. Oates, K. N. Ashfaque, S. Islam, H. F. Hemond, and M. F. Ahmed (2002), Arsenic mobility and groundwater extraction in Bangladesh, *Science, 298*, 1602-1606.

Harvey, C. F., K. N. Ashfaque, W. Yu, A. B. M. Badruzzaman, M. A. Ali, P. M. Oates, H. A. Michael, R. B. Neumann, R. Beckie, S. Islam, and M. F. Ahmed (2006), Groundwater dynamics and arsenic contamination in Bangladesh, *Chem. Geol., 228*, 112-136.

Hossain, M. D., D. Lewis, M. L. Bose, and A. Chowdhury (2003), Rice Research, Technological Progress, and Impact on the Poor: The Bangladesh Case (Summary Report), *EPTD Discussion Papers*, International Food Policy Research Institute, Washington, D.C.

IPCC (2007), *Climate Change 2007: The Physical Science Basis,* Cambridge University Press, New York.

Jones, S. B., J. M. Wraith, and D. Or (2002), Time domain reflectometry measurement principles and applications, *Hydrol. Processes, 16*, 141-153.

Norra, S., Z. A. Berner, P. K. Agarwala, F. Wagner, D. Chandrasekharam, and D. Stuben (2005), Impact of irrigation with As rich groundwater on soil and crops: A geochemical case study in West Bengal Delta Plain, India, *Appl. Geochem., 20*, 1890-1906.

Polizzotto, M. L., C. F. Harvey, G. Li, B. Badruzzman, A. Ali, M. Newville, S. Sutton, and S. Fendorf (2006), Solid-phases and desorption processes of arsenic within Bangladesh sediments, *Chem. Geol., 228*, 97-111.

Robinson, D. W. (2002), Construction and Operation of Groundwater Pumps for Irrigation in the Riverine Plain, *Technical Report 20/02*, CSIRO Land and Water, Clayton South, Australia.

Tomar, V. S., and J. C. O'Toole (1980), Measurement of evapotranspiration in rice, Symposium on the Agrometerology of the Rice Crop, International Rice Research Institute, Los Benos, Laguna, Philippines.

4. The Fate of Arsenic in Two Groundwater-Irrigated Rice Fields in Bangladesh

4.1. Abstract

Approximately 1400 tons of arsenic are withdrawn from the shallow aquifers of Bangladesh each year and deposited onto groundwater-irrigated rice fields. We combine knowledge of rice field flow behavior with chemical measurements collected by ourselves and others to determine how much of this irrigation arsenic is sorbed by the rice field soils, taken up by the rice plants, recycled back to the aquifer, and exported from the system during the monsoon season. A significant fraction of the irrigation arsenic enters the rice field bunds, the raised boundaries around the perimeter of fields, where it is sequestered by the bund soil and neither impacts the rice crop nor recycles back to the shallow aquifer. The ultimate fate of the bund arsenic is unclear. It is hypothesized that a portion of it is lost during the monsoon season when the bunds are eroded by the floodwaters. The amount of arsenic that enters the bund depends on the perimeter-to-area ratio of the field. Fields with larger perimeter-to-area ratios lose more water out their bunds, and thus assume more arsenic into their bunds. However, these fields also require more irrigation water due to the increased bund loss, which increases the total amount of arsenic deposited onto the field. The net result is that the surface soils of most fields receive roughly equivalent arsenic loads, while the bunds receive different arsenic loads. These results, combined with those from previous studies, demonstrate that irrigation pumping and monsoon flooding act together as an unintentional pump-and-treat system for the arsenic-contaminated aquifers of Bangladesh. Irrigation pumping removes arsenic from the shallow aquifer and deposits it onto the rice fields. Most of the irrigation arsenic is retained within either the surface soils or bunds of the fields. A majority of this retained arsenic is then lost to the floodwaters, via diffusion or erosion, during the monsoon season and eventually flushed out to the Bay of Bengal when the floodwaters recede.

4.2. Introduction

Rice fields blanket the landscape in Bangladesh, covering up to 40% of the land area in some parts of the country (Ashfaque 2007). The dry-season, groundwater-irrigated rice crop cultivated in these fields has allowed the country to become self-sustainable with respect to food production (Hossain et al. 2003). However, the groundwater used to irrigate most of these fields is severely contaminated with geogenic arsenic (BGS et al. 2001). It is estimated that, nationwide, groundwater irrigation removes ~1400 tons of arsenic from the shallow aquifer each year and deposits this arsenic onto rice fields (Ali et al. 2003). The fate of this irrigation arsenic has human-health implications since the arsenic can enter the rice field soil (Meharg and Rahman 2003, Norra et al. 2005, van Geen et al. 2006, Dittmar et al. 2007, Saha and Ali 2007, Hossain et al. 2008, Panaullah et al. 2009) and impact the yield (Abedin et al. 2002a, Abedin et al. 2002b, Williams et al. 2005, Panaullah et al. 2009) and arsenic content of the rice crop (Duxbury et al. 2003, Meharg and Rahman 2003, Williams et al. 2006, Adomake et al. 2008, Hossain et al. 2008, Pal et al. 2009), or it can cycle back to the shallow aquifer, which serves as the primary drinking and irrigation water supply for the country.

Previous water-balance studies for Munshiganj, Bangladesh showed that irrigation return-flow from rice fields provides roughly half of the water that recharges the arsenic contaminated aquifer each year (Harvey et al. 2006), and that a majority of this recharge flows through the bunds, the raised boundaries around the perimeter of the rice field (Neumann et al. 2009b and chapter 2). In fact, only rice-field water that flows through bunds or through preferential flow channels in the subsoil of the field recharges the aquifer (Neumann et al. 2009b and chapter 2). Bund flow dominates recharge because the soil beneath bunds has a higher conductivity than the soil in the planted and plowed portion of the field (Tuong et al. 1994, Walker 1999). The bunds

follow property boundaries and are not removed when the field is plowed; therefore cracks and void spaces in the bund soil are not sealed like they are in the plow pan that underlies the remainder of the field (Janssen and Lennartz 2008, Neumann et al. 2009b).

Bund flow is a function of the perimeter-to-area ratio of the field (Wickham and Sen 1978, Wickham and Singh 1978, Wopereis et al. 1994, Neumann et al. 2009b) and the height of water in the field (Walker and Rushton 1984, Walker and Rushton 1986, Neumann et al. 2009b). Fields with larger perimeter-to-area ratios and therefore more bund exposure per unit area (e.g., smaller fields), lose proportionately more water out their bunds and therefore require more irrigation water per unit area (Figure 2.3). A relatively strong relationship exists between the fraction of water lost down the bunds and the perimeter-to-area ratio for fields located throughout Southeast Asia (Figure 2.10). For fields of all sizes and geometries, bund flow is greatest immediately after irrigation when the height of water in the field is maximum and a larger cross-sectional area of the bund is covered by water (Walker and Rushton 1984, Walker and Rushton 1986, Neumann et al. 2009b).

These bund dynamics are particularly relevant for the rice fields in Bangladesh that are irrigated with arsenic-contaminated water. First, since fields with larger perimeter-to-area ratios (e.g., smaller fields) require proportionately more irrigation water, they receive a proportionately larger arsenic load. Second, work by Roberts et al. (2007) showed that arsenic concentrations in the surface water of the rice field are greatest immediately after irrigation, when bund flow occurs, and then decrease with time due to the formation of As-bearing iron aggregates and arsenic sorption to soil minerals. The correspondence between peak bund flow and maximum arsenic concentrations suggests that a significant fraction of the arsenic applied to the field in the irrigation water may enter the bund where it avoids impacting the rice crop and has the potential

to re-enter the aquifer. An interesting relationship exists between the perimeter-to-area ratio and the amount of arsenic entering the field's surface soil and rice crop; fields with larger perimeter-to-area ratios receive more irrigation arsenic per unit area, but also lose more water through their bunds. This situation raises the possibility that proportionately more arsenic is transported out their bunds.

In order to understand the fate of irrigation arsenic and the larger role that groundwater-irrigated rice fields play in Bangladesh's arsenic contamination problem, we conducted an intensive, three-year-long field study on a rice field located in Munshiganj, Bangladesh. We combined chemical knowledge gained from previous studies (Dittmar et al. 2007, Roberts et al. 2007, Adomake et al. 2008, Lu et al. 2009, Roberts et al. 2009) and from soil samples, surface water samples and soil pore water samples that we collected onto our understanding of the field's hydrology to track arsenic as it is pumped up from the aquifers, deposited onto rice fields, transported into the bunds, sequestered by the surface and bund soils, recycled back to the aquifer, and exported from the system during the monsoon season. In addition, by using perimeter-to-area relationships and published data for another field in our study area (Dittmar et al. 2007, Roberts et al. 2007), we determined the fate of arsenic in a second field with a smaller perimeter-to-area ratio.

4.3. Methods

4.3.1. Field Site

The studied rice fields are located in Bashailbhog village in the Munshiganj district of Bangladesh, which is roughly 30 km south of Dhaka and 7 km north of the Ganges River (Figure 4.1). The area experiences two distinct seasons, a monsoon season (June to November) and a dry season (December to May). The landscape is covered by ~4 m of floodwater during the

monsoon season and blanketed with groundwater irrigated rice fields during the dry season (Harvey et al. 2006). Rice is generally planted in late February or early January and harvested in May. Irrigation water with ~400 μg/L As (Roberts et al. 2007) is pumped up from a 30-60 m depth in the aquifer with a diesel engine at a rate of roughly 19 L/s (Roberts et al. 2007), although the pump rate can vary substantially depending on the mechanical maintenance of the pump. Pumped water flows through the irrigation canal and enters Field 1 at its southwestern corner and Field 2 at its southeastern corner (Figure 4.1). Irrigation events generally last a few hours, during which time 2 to 10 cm of water are applied to the field (Roberts et al. 2007, Neumann et al. 2009b) (Figure 2.11). Based on both observations (Roberts et al. 2007) and water level data (see supporting information, chapter 5), it takes 2-3 hours for the irrigation water to spread across the entire field area. The total amount of irrigation water applied to a field during the season depends on the perimeter-to-area ratio of the field (Neumann et al. 2009b) (Figure 2.3). Field 1, with a perimeter-to-area ratio of 0.1 m/m^2, requires 127±10 cm of water, while Field 2, with a perimeter-to-area ratio of 0.07 m/m^2, requires 85±26 cm of water (see supporting information, chapter 5). Based on these perimeter-to-area ratios, Field 1 loses 57±1% of its water out the bund while Field 2 loses 37±5% of its water out the bund (see supporting information, chapter 5).

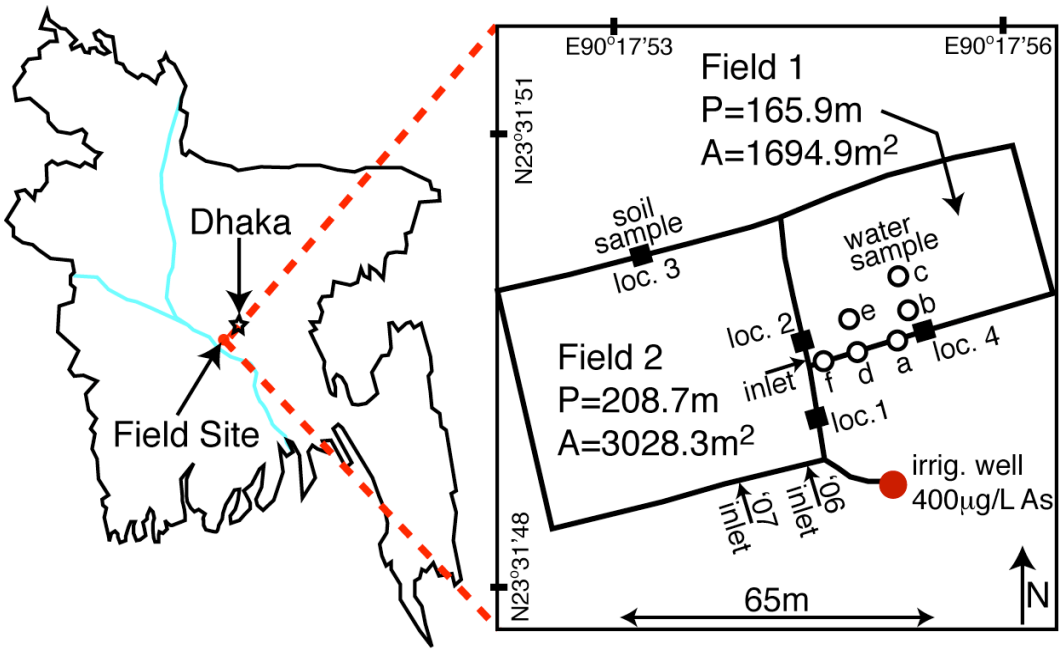

Figure 4.1 Site overview for chemical study.

Field 1 is the field on which Neumann et al. (2009b) conducted their hydrologic investigation (see Chapter 2). Field 2 is the field on which Roberts et al. (2007) and Dittmar et al. (2007) conducted their surface water and soil sampling campaigns. For this study, the locations from which water samples, both surface and pore water samples, were collected are marked with open circles. The locations from which soil samples, both surface samples and soil cores, were collected are marked with filled squares.

4.3.2. Field Campaigns

Water samples were collected from the surface and subsurface of Field 1 during the 2007 and 2008 irrigation seasons. In 2007, single sampling events were conducted in January, March and May. In 2008, multi-day sampling events that extended across an entire irrigation cycle were conducted both in January and April. Due to the intensive sampling schedule in 2008, at the start of the season a bamboo structure was built, which allowed access to the sampling locations without disturbing the rice field surface (see supporting information, chapter 5, for picture).

4.3.3. Soil Pore Water Samples.

Soil pore water samples were collected with Prenart Super Quartz Lysimeters installed both in the bund and in the subsoil of Field 1 (Figures 4.1 and 4.2). The lysimeters were installed by augering a hole to the desired depth, pushing the lysimeter tip into the bottom of the hole and backfilling with natural material. Once the lysimeter was covered with ~30 cm of natural material, the hole was sealed with ~15 cm of locally obtained bentonite. The remainder of the hole was then backfilled with natural material. The lysimeters were left to equilibrate with the surrounding soil for eight months before they were sampled.

Due to the slow nature of water flow through the field's silty-clay loam (Dittmar et al. 2007), samples were collected in foil bags that were lined on the inside with polypropylene (SKC Flex Foil bags). Laboratory tests indicated that oxygen permeated the bags at a rate of 0.03 $mg \cdot L^{-1} \cdot hr^{-1}$ (see supporting information, chapter 5). The bags were purged three times with argon immediately before they were attached to the end of the lysimeter tubing and placed in a glass vacuum chamber (see supporting information, chapter 5, for picture). A ~0.8 bar vacuum was applied to the chamber, causing water to flow into the bags. Collection generally lasted 12 hours,

during which time the system was covered with a black plastic bag to deter photochemical oxidation of the water (Hug et al. 2001). All lysimeters were purged for a minimum of 12 hours before sample collection.

After >100 ml of water were collected, it was immediately processed. A flow-through probe system that contained pH, ORP, conductivity, temperature, and dissolved oxygen electrodes (Microelectrodes Inc.) was attached to the nozzle of the foil bag. All probes were calibrated at the site prior to use. Water was slowly drawn from the bag through the probes directly into a plastic syringe (see supporting information, chapter 5, for picture). This system ensured that the water was not exposed to the atmosphere. The water in the syringe was then distributed into different bottles for preservation purposes. Both filtered and unfiltered samples were collected. A 0.2 μm polyethersulfone membrane syringe filter was used for sample filtration. Acidification with nitric acid down to pH 1 was used for metals and cation measurements. Acidification with sulfuric acid down to pH 1 was used for nitrogen and organic carbon measurements. The sulfuric acid did not oxidize the organic carbon in the collected samples (see supporting information, chapter 5). Unacidified samples were used for anion measurements and alkalinity titrations. All samples were kept in an ice-filled cooler during sampling and transport back to the USA.

Arsenic was measured on a collision cell ICP-MS at the Dartmouth Trace Elements Analysis Laboratory by monitoring mass 75 (^{75}As). Cations were measured on an ICP-AES in the Environmental Measurement 1: Gas-Solution Analytical Center at Stanford University by monitoring 317.9 nm for calcium, 259.9 nm for iron, 766.4 nm for potassium, 285.2 nm for magnesium, 257.6 nm for manganese, 589.5 nm for sodium, 213.6 nm for phosphorus, and 180.7 nm and 182.0 nm for sulfur. NH4-N, NO3-N and NO2-N were measured on a WestCo

SmartChem Discrete Analyzer (DA) in the Environmental Measurement 1: Gas-Solution Analytical Center at Stanford University. In the DA, nitrate was reduced to nitrite by a cadmium column. The nitrite formed, in addition to any nitrite originally present in the sample, was reacted with sulfanilamide and N-(1-naphthyl)ethylenediamine dihydrochloride to form azo dye, which is colorimetrically detected at 550 nm. Nitrite was separately determined using the same processes without the cadmium column. Ammonium was reacted with salicylate and hypochlorite in a buffered alkaline solution in the presence of sodium nitroferricyanide to form indophenol blue, which is colorimetrically detected at 660 nm. Non-purgable organic carbon was measured on a Shimadzu TOC Analyzer after 10 ml of sample were purged with gas for 10 minutes. Anions were measured in a bicarbonate eluent on a Dionex IC with a conductivity detector. Linear calibration curves with $r^2 \geq 0.98$ were obtained for all of the different analyses. Field and laboratory blanks set detection limits for the different measured solutes and ensured that the sampling and processing protocols did not contaminate the samples. Duplicates and known standards, treated as unknown samples, were run throughout all of the analyses to establish analytical error.

Alkalinity titrations were conducted on 10 ml sample volumes with 0.2 ml additions of ~10 mM sulfuric acid down to pH 2. Alkalinity was determined from the x-intercept of the data plotted as (volume acid added) versus (volume of sample + volume acid added)$*10^{-pH}$. Dissolved inorganic carbon was calculated from alkalinity and pH data assuming bicarbonate was equal to alkalinity.

4.3.4. Surface Water Samples

Surface water samples were collected from the same locations as the soil pore water samples (Figure 4.1). The surface water was pulled directly into a plastic syringe and immediately processed following the same protocol outlined above for the pore water samples.

During the multi-day sampling campaigns in 2008, dissolved oxygen, ORP and pH were continuously monitored in the field's surface water at location (c) (Figure 4.1) using electrodes hooked up to a HOBO datalogger. The probes were calibrated in the field before and after deployment. The calibration drifted during the deployment, so data were plotted and analyzed using both the initial and final calibration curves.

4.3.5. Soil Samples

Soil cores and surface soil samples were collected from the bunds of Field 1 and Field 2 (Figure 4.1). Cores were collected as ~60 cm sections down to a depth of ~1.2 m using an AMS Multi-Stage Soil Core Sampler lined with a plastic tube. The Multi-Stage Sampler was hammered into the ground down to the desired depth and then manually pulled out of the ground. The ends of the retrieved, soil-filled plastic tube were capped with plastic caps for shipment back to MIT. The resulting hole in the bund was augered to both widen and clean it before the next, deeper core was collected.

In Field 1, soil samples were collected off the face of the bund where it intersected with the field surface by scrapping the top 2 cm of soil into plastic collection bags. The surface sample locations corresponded with core locations (Figure 4.1). Three surface samples were collected at each location.

At MIT, the soil samples were oven dried at 80 ^{o}C, roughly ground with a mortar and pestle, and then ground into a fine powder using a ball mill. Four grams of the fine powder were combined with 1 g of Chemplex X-Ray Mix Powder and compressed into flat pellets using a Graseby Specac press. The pellets were sent to the University of British Columbia where they were analyzed for arsenic using XRF.

4.4. Results and Discussion

4.4.1. Chemical Nature of Rice Field Waters

Our hydrologic study (see chapter 2) demonstrated that Bangladeshi rice fields contain four different water types, each with a different recharge behavior: bund water, preferential-flow water, vertical-infiltration water, and subsoil-matrix water. Bund water originates as surface water that flows laterally into and then vertically downwards through the bund, eventually recharging the aquifer (Figure 4.2a). Preferential-flow and vertical-infiltration water also originate as surface water. However, for these water types, the surface water flows vertically downwards, through the plow pan into the subsurface of the field (Figure 4.2a). The preferential-flow water then enters cracks and channels in the subsoil of the field where it rapidly flows to deeper depths and likely recharges the aquifer. The vertical-infiltration water remains in the soil matrix and only reaches a depth of ~40 cm by the end of a four-month long irrigation season (Figure 2.6). After the irrigation season much of this matrix water evaporates as the soil dries. In contrast, the subsoil-matrix water does not originate as surface water in the field. It is a mixture of residual aquifer water, rainwater, and rice field water from previous seasons. The subsoil is exposed to oxygen when the rice field dries out at the end of the irrigation season, and it is then inundated with rainwater or aquifer water during the monsoon season (Neumann et al. 2009b and chapter 2).

Recharge distinctions between the different waters are chemically noteworthy because of the redox difference between the surface water and surface soil that resides above the plow pan (Figure 4.2). In the early part of the irrigation season, when rice plants are small, the surface water alternates between sub- and super-saturated in oxygen over the course of a day due to photosynthetic and respiratory activity of algae (e.g., oxygen varies from 1 mg/L to 18 mg/L),

while the surface soil remains anoxic enough to generate methane (Kirk 2004) (see supporting information, chapter 5, for oxygen and δ^{13}C-DIC/methane data). Arsenic concentrations in the pore water of rice-field surface soils routinely exceed concentrations in the irrigation water applied to the fields (Takahashi et al. 2004, Panaullah et al. 2009). In one Bangladeshi field irrigated with water containing 100 μg/L As, surface-soil pore water concentrations reached 1500 μg/L (van Geen et al. 2006). Thus, it was expected that the chemical composition of the bund water would differ from that of the waters that travel through the anoxic soil layer and infiltrate the plow pan. However, Figure 4.2 demonstrates that a clear distinction between the bund water, vertical-infiltration water and preferential-flow water does not exist. Instead, these three waters appear chemically similar to each other and distinctly different from the subsoil matrix water; they are more reduced and contain higher concentrations of dissolved organic carbon, arsenic and iron than the matrix water (Figure 4.2). The unexpected, chemical similarity between the bund water and the two water types that infiltrate through the plow pan (vertical-infiltration water and preferential-flow water), suggests that the elevated concentrations of DOC (≥13 mg/L, Figure 4.2d) and arsenic (van Geen et al. 2006) within the pore water of reduced surface soil layer are attenuated by sorption onto the plow pan soil (Jardine et al. 1989, Manning and Goldberg 1997, Lin and Puls 2000) and/or by the potential movement of air into the unsaturated soil beneath the plow pan (Figure 4.2a and Neumann et al., 2009b).

Although it appears that a majority of the organic carbon in the rice field remains in the surface soils, it is hypothesized that the chemical difference between the three field-derived water types and the subsoil-matrix water is controlled by the presence of some biologically available organic carbon (BDOC) from the surface that penetrates the subsurface. A previous experiment showed that water sampled from the deepest lysimeter in the bund contained 4.7

mg/L of dissolved organic carbon (DOC) (Figure 4.2d), and that most of this carbon was not biologically degradable (Neumann et al. 2009a and chapter 6). This result suggests that lysimeter locations with more elevated DOC concentrations (>5 mg/L) contain BDOC, while locations with lower DOC concentrations (≤5 mg/L) have lost BDOC due to oxidation. The BDOC, by definition, promotes microbial respiration, which, based on the measured ORP values and iron concentrations (Figure 4.2c,f), uses Fe(III) as the electron acceptor (Hemond and Fechner-Levy 2000). Concurrently, dissolved inorganic carbon concentrations increase with depth in the bund (see supporting information, chapter 5). It appears that this carbon mineralization process is largely constrained to the top ~1 m of the bund and the sampled preferential flow channel (Figure 4.2d and BDOC experiment in chapter 6), and that it does not mobilize arsenic off of the soil. Dissolved arsenic concentrations in the bund and underneath the plow pan are an order of magnitude less than those in the irrigation water (Figure 4.2e and 4.3a). This lack of mobilization is likely due to a large Kd value (~1000 L/kg for the bund from the data in Figure 4.3: (10 mg/kg)/(10e-3 mg/L)) that is sustained over time by the rice field soil de-saturating between irrigation events and oxidizing down to a depth of at least 2 m each year after the rice is harvested (Neumann et al. 2009b and chapter 2).

Most significantly, the data presented in Figure 4.2 demonstrate that an understanding of the field's hydrology is required to accurately assess the chemical nature of the water that ultimately recharges the arsenic-contaminated aquifer. The recharge water (bund and preferential-flow water) is chemically different than the standing water in the surface of the rice field, the pore water in the surface soil, or the pore water within the soil matrix beneath most of the field.

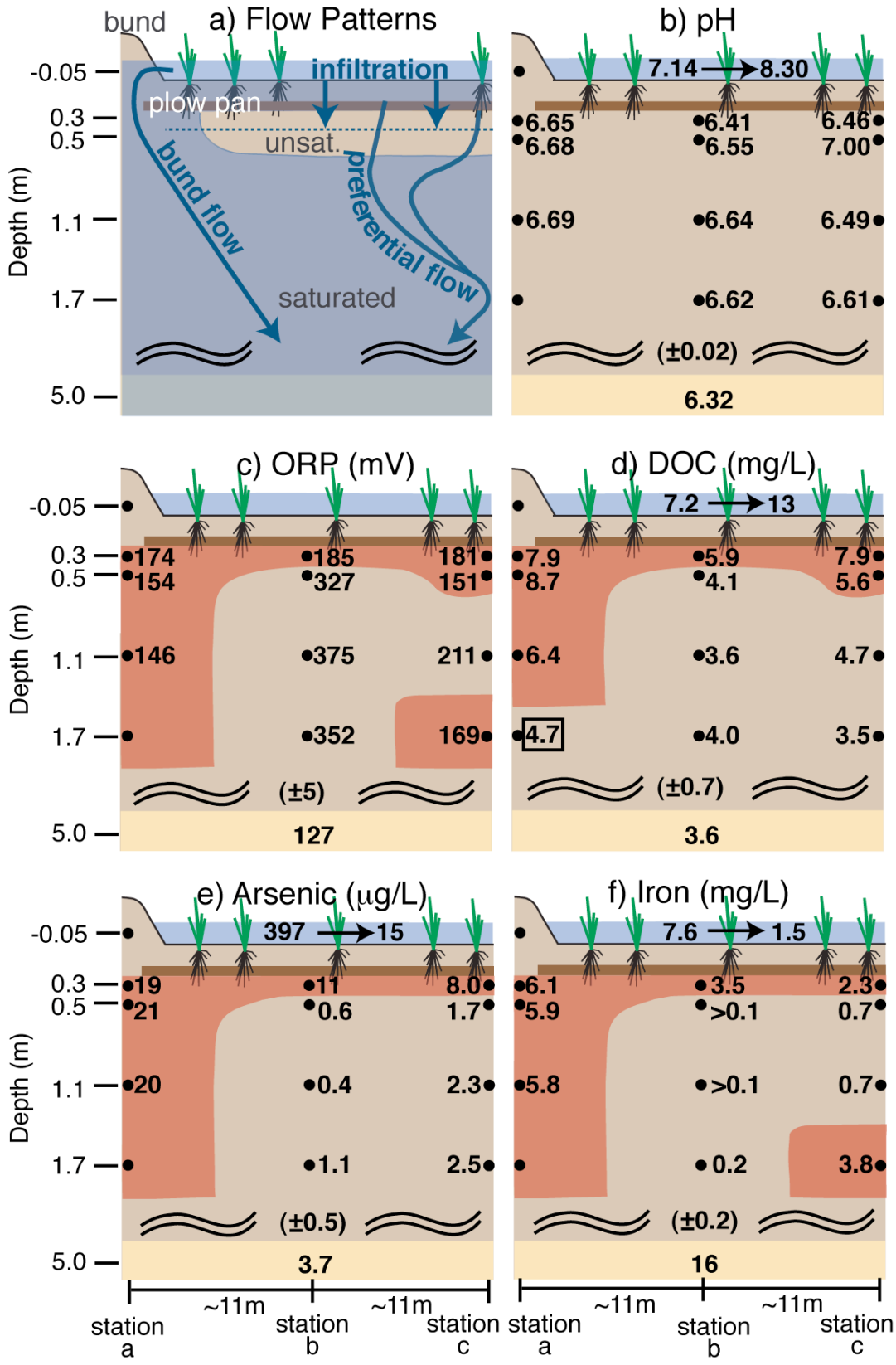
bund
a) Flow Patterns
infiltration
plow pan
unsat.
bund flow
preferential flow
saturated
b) pH
7.14 → 8.30
6.65
6.68
6.41
6.55
6.46
7.00
6.69
6.64
6.49
6.62
6.61
(±0.02)
6.32
c) ORP (mV)
174
154
185
327
181
151
146
375
211
352
169
(±5)
127
d) DOC (mg/L)
7.2 → 13
7.9
8.7
5.9
4.1
7.9
5.6
6.4
3.6
4.7
4.7
4.0
3.5
(±0.7)
3.6
e) Arsenic (μg/L)
397 → 15
19
21
11
0.6
8.0
1.7
20
0.4
2.3
1.1
2.5
(±0.5)
3.7
f) Iron (mg/L)
7.6 → 1.5
6.1
5.9
3.5
>0.1
2.3
0.7
5.8
>0.1
0.7
0.2
3.8
(±0.2)
16
Depth (m)
-0.05
0.3
0.5
1.1
1.7
5.0
~11m
~11m
station a
station b
station c

Figure 4.2 Chemical data along transect extending from location (a) to location (c).

The black dots mark the locations of the lysimeters used to sample pore water. Most of the presented lysimeter data was collected March 9, 2007. The DOC concentration presented for the deepest bund lysimeter was from a sample collected April 2008 for an experiment in which we determined the lability of the organic carbon in the bund water (Neumann et al. 2009a and chapter 6). The color contouring across the lysimeter data highlights noteworthy concentration differences. The two numbers in the surface water of the cartoon show the concentration measured in the surface water of Field 1 immediately and two days after the January 23, 2008 irrigation event. The aquifer concentration number, located at the 5-m-depth in the cartoon, represents the average concentration measured January 20, 2008 in the 4.8-m- and 5.3-m-deep wells installed in Field 1. The number in parentheses shows the average analytical error associated with the measured concentrations.

a) Flow patterns in Field 1 determined by Neumann et al. (2009b) and presented in chapter 2. A majority of the surface water flows laterally into and then vertically downwards through the bund into the subsurface of the field, eventually recharging the aquifer. Some surface water infiltrates vertically through the plow pan. Any of this water that does not enter a preferential flow channel only reaches a depth of ~40 cm by the end of the irrigation season. Thus, pore water beneath the plow pan and deeper than ~40 cm did not originate in the surface of the rice field. Plow pan water that does manage to enter a preferential flow channel travels to deeper depths in the rice field and has the potential to recharge the aquifer. Chemical data in panels (c) and (f) suggest that the deepest lysimeter located ~22 m from the bund was installed in a preferential flow channel. This determination is further supported by the fact that water was collected more quickly from this lysimeter than from the other non-bund lysimeters (see supporting information, chapter 5).

b–f) Chemical data from the surface and subsurface of the rice field. In the surface water, pH and dissolved organic carbon increase after irrigation while arsenic and iron decrease. The organic carbon concentrations immediately after irrigation match that measured in the aquifer well (Roberts et al. 2009), and almost double two days later. Surface-water ORP data were not included due to their dynamic nature. When the rice plants are small, the redox potential of the surface water oscillates up and down on a diel cycle as floating algae photosynthesize and respire, and when the rice plants are large enough the shade the water, the redox potential remains suboxic (1-2 mg/L oxygen) (see supporting information, chapter 5). The subsurface lysimeter data emphasize the chemical difference between the waters that originated in the surface of the rice field (bund water, preferential-flow water, and vertical-infiltration water) and the subsoil-matrix water. In panels (c), (e) and (f), the red contour highlights that the rice-field waters, in general, are more reduced (the ORP data were corrected to the standard hydrogen electrode) and have higher arsenic and iron concentrations than the subsoil-matrix water. In panel (d), the red contour suggests that these rice-field waters initially contain biologically available organic carbon that is oxidized as the water travels to deeper depths. With the exception of iron, the parameters measured in the shallow aquifer match those measured in the bund. This correspondence is expected since most of the rice-field recharge water flows through the bund.

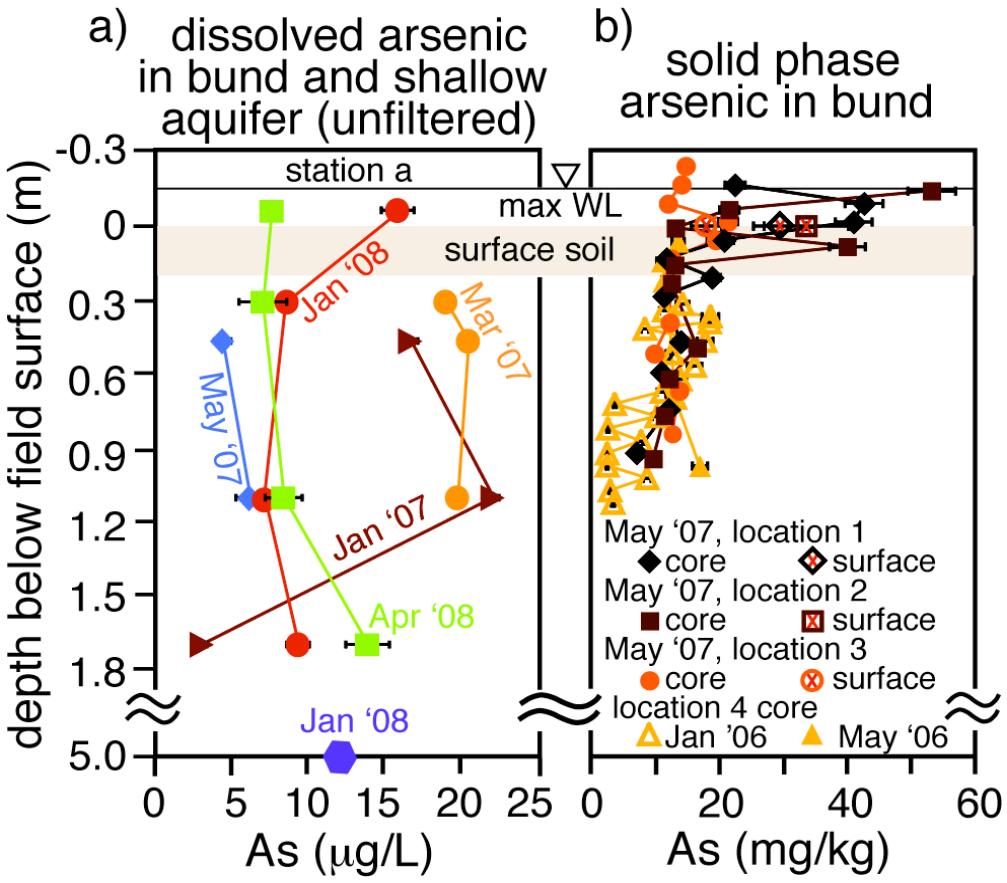

Figure 4.3 Dissolved and solid-phase arsenic in the bund and the shallow aquifer.

Aqueous data are from two consecutive irrigation seasons. The average height of the surface water and surface soil above the plow pan are marked for reference. Over two field seasons, pore water concentrations in the bund at station (a) never exceed 25 µg/L As, which is over an order of magnitude less than As in the irrigation water. Solid phase arsenic concentrations are elevated in the top portion of the bund, suggesting that most of the arsenic that enters the bund is retained by the top ~30 cm of bund soil.

4.4.2. Arsenic in the Rice Field Surface Water

Work by Roberts et al.(2007) showed that irrigation water enters Field 2 with an arsenic concentration of 390±10 μg/L and that this concentration drops to ~120 μg/L by the time the water travels across the field, approximately two hours later. The result is an arsenic gradient in the field's surface water with higher concentrations near the irrigation inlet and lower concentrations at the far corner. Dissolved arsenic continues to decrease with time, and within three days of irrigation, concentrations drop below 25 μg/L throughout the field. Roberts et al. (2007) attribute the arsenic loss to sorption onto soil particles and the formation of arsenic-bearing iron aggregates that settle out of the water column (Roberts et al. 2007). This behavior occurs at both the beginning (January) and end (April) of the irrigation season.

According to Roberts et al. (2007), Field 2 is routinely irrigated after the water level in the field drops below the soil surface, subjecting the field to periodic flooding and drying. The irrigation regime for Field 1 is not as consistent. During the January 2008 sampling campaign, irrigation water was applied to an already flooded field (Figure 4.4a), while during the April campaign, irrigation water was applied to a dry field (Figure 4.4b). Water level data from Field 1 show that between January and April 2008, water was applied 9±2 times to a flooded field and 14±2 times to a dry field (see supporting information, chapter 5). The uncertainty is due to centimeter variations in the location of the soil surface.

The different irrigation regimes for Field 1 produce different arsenic behaviors. When irrigation water is added to a flooded field (January event), the decreasing concentration trend with increasing distance from the irrigation inlet reported by Roberts et al. (2007) does not clearly develop; but when irrigation water is added to a dry field, the concentration trend does develop (Figure 4.5a). These data suggest that when irrigation water is added to a flooded field,

arsenic is not sequestered as quickly out of the water column. Within a 25 m distance from the irrigation inlet, a few hours after the January irrigation event, 9±3% of the irrigation arsenic was lost from the water column (see supporting information, chapter 5). This calculation accounts for the fact that the ~4 cm of irrigation water was diluted by ~2 cm of existing, low arsenic water (Figure 4.4a). In contrast, during the April irrigation event, 19±3% of the arsenic was lost from the water column within a 25 m distance of the irrigation inlet (see supporting information, chapter 5). However, for both events, 80 to 90% of the arsenic was lost from the water column within three days of irrigation (Figures 4.4g–h and supporting information, chapter 5).

It appears that the immediate loss of irrigation arsenic from water column, which produces the strong spatial arsenic gradient reported by Roberts et al. (2007) and seen in Field 1 during the April sampling campaign (Figure 4.5a), depends on the irrigation water interacting with an oxidized soil surface. In April, the soil surface in Field 1 was exposed to the atmosphere for three days before the irrigation event (see supporting information, chapter 5). Prolonged drying results in soil cracks (Roberts et al. 2007) (see supporting information, chapter 5, for picture) that allow oxygen to penetrate into the top few centimeters of the soil matrix. (The deeper portion of the surface-soil matrix remains saturated and anoxic between irrigation events (see supporting information, chapter 5).) Such exposure to the atmosphere likely allows for the formation of reactive iron (hydr)oxides that increase the sorption capacity of the soil matrix (McGeehan et al. 1998, Reynolds et al. 1999). In contrast, when the field is flooded, only the very top of the surface soil would be oxidized if the standing water contains a sufficient amount of oxygen. Data collected during the January and April sampling events show that when the rice plants are small (January) oxygen levels in the surface water oscillate between super- and sub-saturated over the course of a day in response to the photosynthetic (1 to 18 mg/L oxygen) and

respiratory activity of floating algae. However, when the rice plants are large (April), they shade the water, resulting in lower algal activity; oxygen levels remain sub-saturated (1 to 3 mg/L oxygen) and show no diel pattern.

The subsequent, slower loss of arsenic from the water column does not appear to depend on the state of the soil matrix since it occurs under both irrigation regimes. This loss is likely due in part to the aggregation and settling of arsenic-bearing iron (hydr)oxides formed during irrigation (Roberts et al. 2007). However, the difference between unfiltered and filtered (0.2 μm) arsenic in the surface water disappears after 24-hours in Field 2 (Roberts et al. 2007), suggesting a lack of arsenic-bearing particles larger than 0.2 μm. A similar trend was detected in January 2008 in Field 1 (see supporting information, chapter 5). Yet, arsenic loss continues after 24-hours, even though it would take ~50 years for a 0.2 μm particle to settle out of a 5 cm-deep water column (see supporting information, chapter 5). Another loss pathway may involve arsenic sorption onto plant material (e.g., rice stems and weeds) (Sundberg-Jones and Hassan 2007).

Regardless of the loss mechanisms, the different initial behavior under the two irrigation regimes has implications for arsenic fate. When irrigation water is added to a flooded field, less arsenic immediately enters the surface soil, and thus, more arsenic is available to flow into the bund.

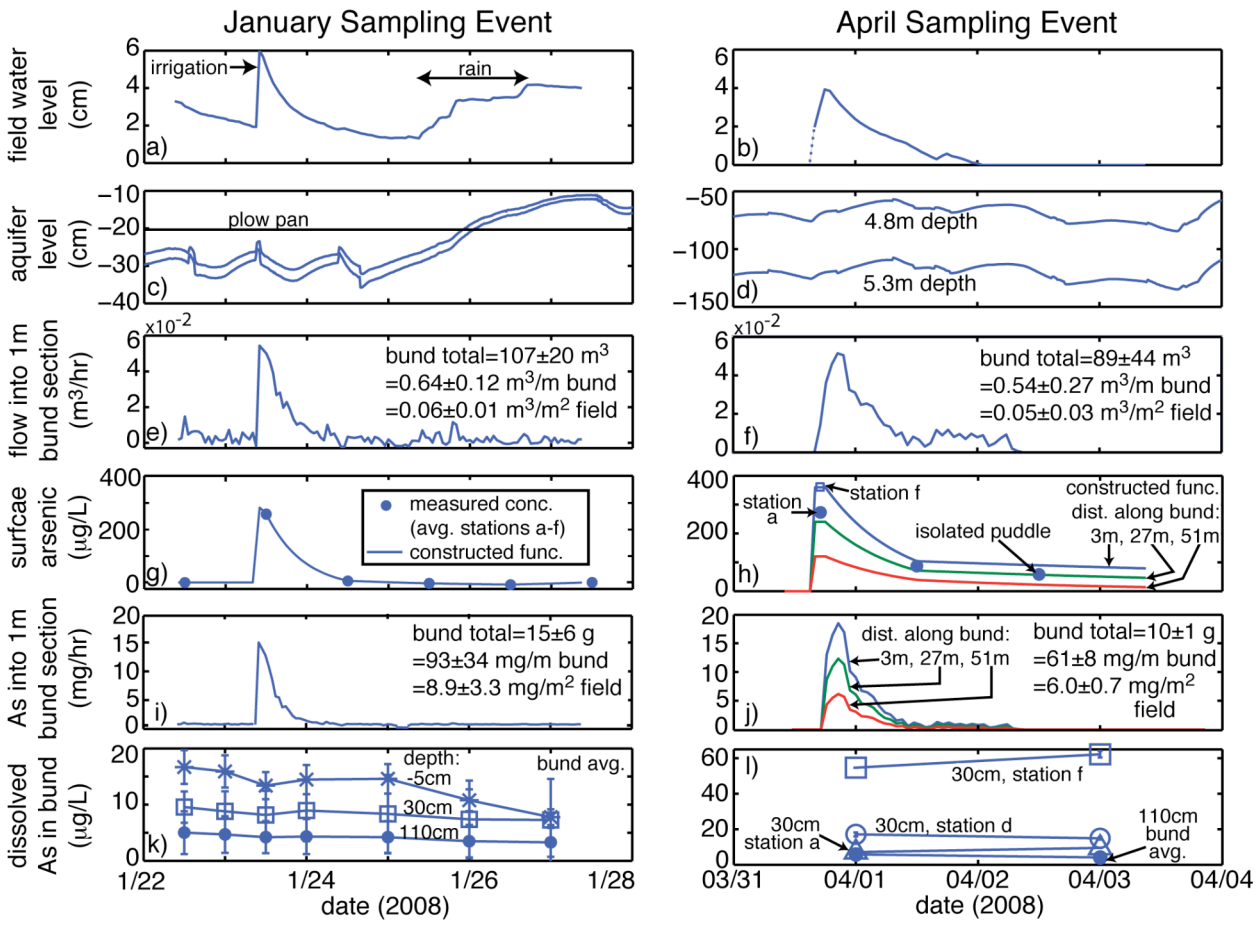

Figure 4.4 Surface water, bund flux and bund pore water data for Field 1 versus time for the January and April 2008 sampling campaigns.

(a,b) Water level in the surface of the field.
(c,d) Water level in the shallow aquifer, referenced to the surface of the rice field.
(e,f) Flow of surface water into a 1 m section of bund.
(g,h) Measured and constructed arsenic concentrations for the surface water in the rice field.
(i,j) Arsenic flux into a 1 m section of bund.
(k,l) Unfiltered arsenic concentrations in the bund pore water. The -5 cm-deep concentration in panel (k) is from location (a) while the 30 cm- and 110 cm-deep concentrations represent the average from locations (f), (d) and (a). The error bars on the -5 cm-deep concentrations represent analytical uncertainty, and the error bars on the deeper concentrations represent the standard deviation for the three different samples. In panel (l), the 110 cm-deep concentrations represent the average from locations (f), (d) and (a).

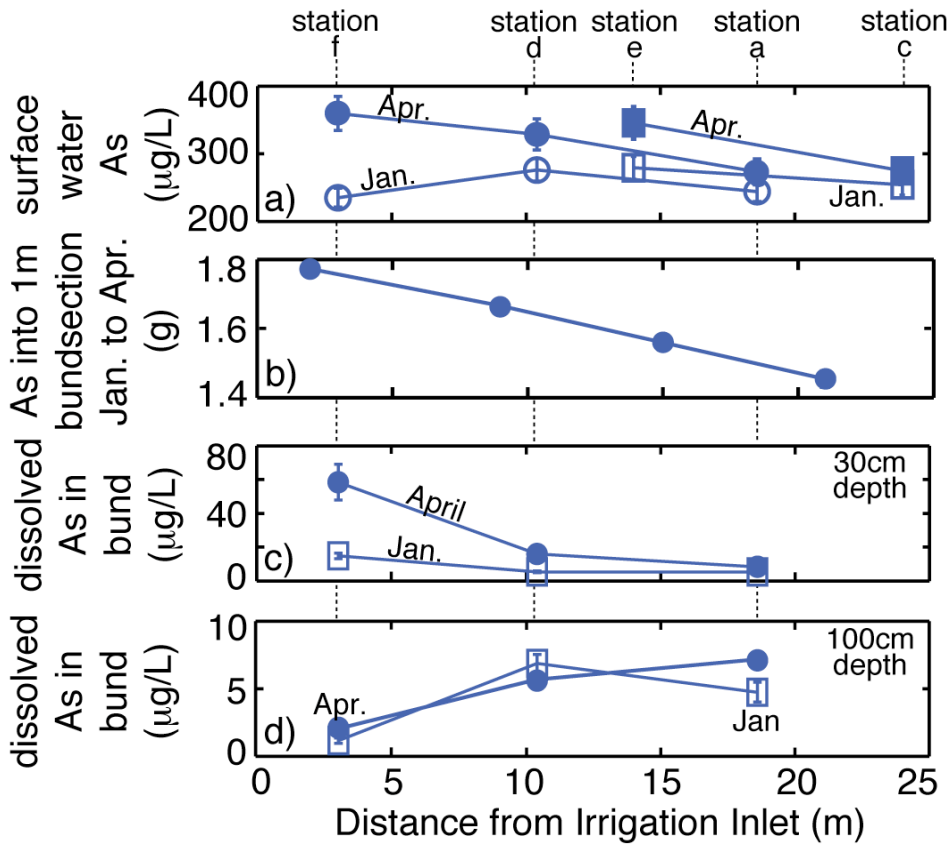

Figure 4.5 Surface water, bund flux and bund pore water data for Field 1 versus distance from the irrigation inlet for the January and April 2008 sampling campaigns.

All error bars represent analytical uncertainty.
(a) Unfiltered arsenic concentrations in the surface water.
(b) Mass of arsenic that entered a 1 m section of bund between the January and April sampling events (see supporting information, chapter 5, for calculation).
(c) Unfiltered arsenic concentrations in the bund pore water at a 30 cm depth.
(d) Unfiltered arsenic concentrations in the bund pore water at a 100 cm depth.

4.4.3. Arsenic Flux into the Bund

Knowledge of the bund water flow and surface water arsenic concentrations is required to determine the flux of arsenic entering the bund. Hourly fluxes of water into the bund for the January and April sampling events are presented in Figures 4.4e–f, and were calculated from water level data (Figure 4.4a–b), meteorological data, and knowledge of other water inputs and outputs (Neumann et al. 2009b) (see supporting information, chapter 5, for calculation). Except during the January rainstorm, the determined bund fluxes increased and decreased along with the water level in the field (Figures 4.4a–b, e–f), supporting the understanding of bund flow developed in chapter 2. The lack of bund flow during the rainstorm is explained by the fact that the aquifer water level topped the plow pan (Figure 4.4c), eliminating the hydraulic head gradient that drives flow. Above the plow pan, the soil surface is a suspension of soil particles and it dos not maintain a head gradient.

The data in Figures 4.4c–d show the water level in the shallow part of the aquifer (4.8 m and 5.3 m depths) decreases during the day from irrigation pumping and rebounds during the night after pumping ceases. The pronounced water level spikes in January represent a rise in head for a brief period after pumping starts, and are attributed to the compression of the aquifer matrix caused by reduced pressures near the pumping well (Hsieh 1996). The January rainstorm and irrigation event each contributed approximately that same amount of water to the rice field, but the aquifer water level responded more dramatically to the rainstorm than to the irrigation event. This apparent inconsistency is explained by the fact that the rainstorm was a regional phenomenon, blanketing the landscape with water and increasing pressures throughout the aquifer, while irrigation pumping was a local event in which aquifer pressures quickly dissipated.

The bund water fluxes (Figures 4.4e–f) were combined with surface water data (Figures

4.4g–h) to determine the hourly arsenic bund flux (Figures 4.4i–j). Arsenic concentrations in the surface water were assumed uniform for the January event and spatially distinct for the April event. An hourly surface water concentration function was constructed from daily measurements by assuming an exponential decay between data points (Figures 4.4g–h), and, for the April event, by assuming that the spatial trend in the five sampling locations extended across the entire field (see supporting information, chapter 5, for details). The determined arsenic fluxes (Figures 4.4i–j) illustrate that the bund receives a pulse of arsenic with each irrigation event. Proportionately less arsenic entered the bund during April sampling event (Figure 4.4j) than during the January sampling event (Figure 4.4i) due to a smaller water flux and to more arsenic sequestration by the surface soil. The January bund flux represented 48±16% of the irrigation input into Field 1, while the April bund flux represented 26±3% of the irrigation input (see supporting information, chapter 5). Seasonally, Field 1 loses 35±8% of its irrigation arsenic into the bund (Figure 4.6), assuming that the percentage lost for the January sampling event is representative of when irrigation water is applied to a flooded field (9±2 events) and that the percentage lost for the April sampling event is representative of when irrigation water is applied to a dry field (14±2 events) (see supporting information, chapter 5).

The pulsing nature of the arsenic bund flux suggests that most of the arsenic that enters the bund does so immediately after irrigation, and thus it is the concentration of arsenic in the surface water immediately after irrigation that matters. Calculations show that combining the total bund water flux, which is a function of the perimeter-to-area ratio (Neumann et al. 2009b), with the spatially-averaged arsenic concentration in the surface water immediately after irrigation accounts for 84±24% of the arsenic lost into the bund (see supporting information, chapter 5). Therefore, the arsenic bund flux for any field can be determined from initial arsenic

concentrations and the perimeter-to-area ratio. This method predicts that Field 2 loses 25±16% of its irrigation arsenic into the bund (Figure 4.6), assuming that the average arsenic concentration measured in Field 2 immediately after irrigation by Roberts et al. (2007) is representative of the entire season (see supporting information, chapter 5).

Field 1, with a larger perimeter-to-area ratio, requires more irrigation water and therefore receives more arsenic than Field 2 (Figure 4.6); but it also loses more arsenic into the bund. This dynamic causes the surface soils of both fields to receive roughly same amount of arsenic, 250–320 mg/m^2 (Figure 4.6). Calculations show that similar surface-soil arsenic loadings are expected for a wide range of perimeter-to-area ratios when the irrigation water contains ~390 μg/L As (see supporting information, chapter 5). If all of the arsenic remains in the top 10 cm of the rice field soil (Dittmar et al. 2007, Hossain et al. 2008), then this arsenic loading (~300 mg/m^2) will increase the concentration of arsenic in the soil by ~3 mg/kg (assuming a bulk density of 1 g/cm3 (Dittmar et al. 2007)). Studies have shown that a 3 mg/kg increase in soil with an arsenic concentration already at or above 10 mg/kg can increase the arsenic content of rice grains by 0.02 μg/g (Adomake et al. 2008, Hossain et al. 2008, Lu et al. 2009) to 0.05 μg/g (Pal et al. 2009). This increase represents 25 to 65% of the mean arsenic content (0.08 μg/g) of polished white rice in Bangladesh (Meharg et al. 2009). However, from a mass-balance perspective, very little of the irrigation arsenic is lost to rice plants (Figure 4.6, supporting information, chapter 5).

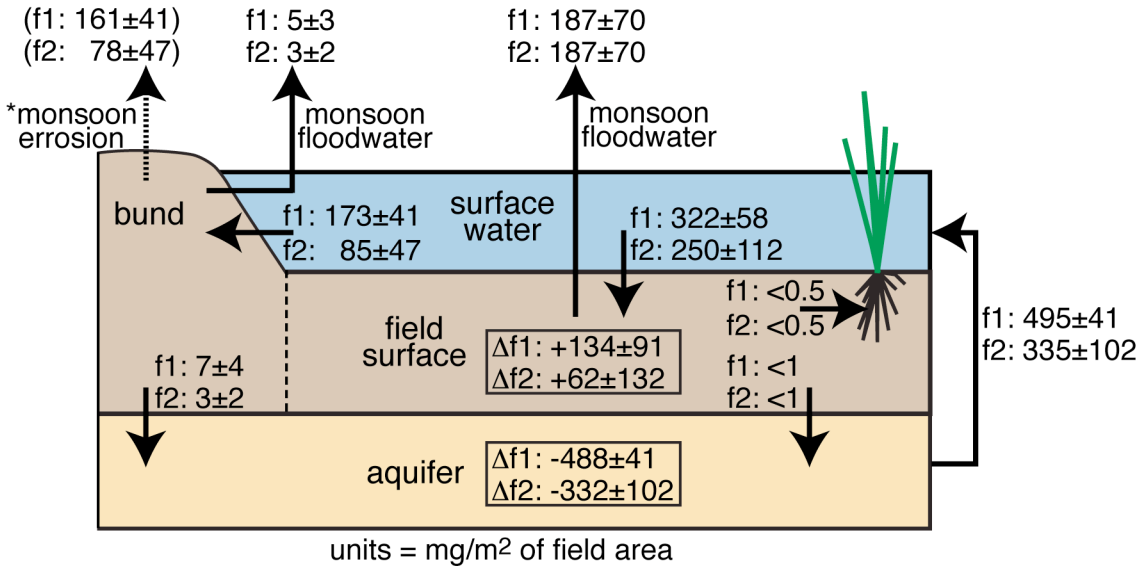

Figure 4.6 Arsenic mass balance for Field 1 and Field 2.

The numbers represent mg of arsenic per m^2 of field surface area, not bund area. All of the calculations involved in constructing this mass balance are presented in the supporting information, chapter 5. The monsoon erosion flux represents a hypothesized loss based on the fact that arsenic does not appear to accumulate from one year to the next within the bund (see main text for details).

4.4.4. Arsenic in the Bund Pore Water

Immediately following an irrigation event, surface-water arsenic pulses into the bund. However, pore water samples collected from multiple depths within the bund during both the January and April sampling campaigns showed no response to the transient arsenic flux (Figures 4.4k–l). Concentrations throughout the bund remained relatively steady over both irrigation cycles. Bund water from a single irrigation event can reach a depth of 0.4 m to 3 m, depending on how widely it spreads in the subsurface after entering the bund (see supporting information, chapter 5). These depth estimates imply that at a minimum, the two shallowest lysimeters receive fresh bund water with every irrigation event. Thus, the non-transient behavior of the pore water arsenic within these shallow lysimeters is not explained by a slow travel time for the irrigation water.

In addition to varying temporally, the arsenic bund flux varies spatially, with more arsenic entering the bund closer to the irrigation inlet (Figure 4.5b). Between the January and April sampling campaign, pore water concentrations in the shallow (30 cm) lysimeter located closest to the irrigation inlet increased by ~40 μg/L while the shallow lysimeter located furthest from the inlet increased by an insignificant amount (Figure 4.5d). However, concentrations in all of the deeper lysimeters (100 cm), regardless of their proximity to the irrigation inlet, either did not increase or increased by only ~2 μg/L between the two sampling events (Figure 4.5e). These data demonstrate that on a seasonal time scale, the arsenic flux does impact shallow pore water concentrations, but that it has a negligible impact on deeper pore water concentrations. In fact, the arsenic concentration trend in the deeper lysimeters is opposite to the loading trend; concentrations decrease closer to the irrigation inlet (Figure 4.5d).

The lack of a strong response by pore water concentrations to the spatial and temporal

nature of the arsenic bund flux suggests that most of the arsenic entering the bund is sorbed by the bund soil. This process keeps pore water concentrations low, especially within the deeper depths of the bund. Over two field seasons, all bund pore water samples collected beneath a depth of 1m had an arsenic concentration below 25 μg/L, an order of magnitude less than that in the irrigation water (Figures 4.2e, 4.3a, 4.4k–l, 4.5c–d). In addition, since BDOC in the bund water is completely oxidized by a depth of 1.7 m (Neumann et al. 2009a and chapter 6), there is no possibility for reductive dissolution and arsenic mobilization at deeper depths. These data confirm that rice fields contribute little arsenic to the shallow aquifer (Figure 4.6 and supporting information, chapter 5) since most rice field recharge flows through the bunds (see chapter 2).

4.4.5. Solid Phase Arsenic in the Bund

Flux and pore water data suggest the bund soil sorbs a majority of the arsenic that enters the bund, which is roughly 35% and 25% of all the arsenic deposited onto Field 1 and Field 2, respectively. Consequentially, solid-phase arsenic concentrations in the bund soils are elevated (Figures 4.3b and 4.7). Cores taken through the center of the bund illustrate that most of the arsenic is retained within the top 30 cm (Figure 4.3b). This retention pattern agrees with the low arsenic concentrations measured in shallow bund pore water (Figures 4.3a, 4.4k–l and 4.5c), and the apparent disconnect between arsenic loadings and deeper bund pore water concentrations (Figure 4.5b and 4.5d). On average, solid-phase concentrations decrease with increasing distance from the irrigation inlet (Figure 4.7), in agreement with the spatially heterogeneous nature of the arsenic bund flux.

Figure 4.7 shows the expected solid-phase arsenic concentrations at the end of the irrigation season in the bund of Field 2, assuming that 90% of the arsenic entering the 40 cm-wide bund is retained within the top 30 cm, and that concentrations in the bund at the start of the

irrigation season match that measured in the surface soil of the field at the start of the irrigation season (Dittmar et al. 2007). The modeled post-irrigation concentrations match those measured at three different locations along the bund at the end of the irrigation season (May 2007). Although the match between modeled and measured concentrations supports our understanding of arsenic behavior in the bund, it highlights a puzzling feature of the dataset. The modeled solid-phase increase in Figure 4.7 is due to one irrigation season and groundwater irrigated rice fields have existed for ~17 years in this area of Bangladesh (Chowdhury 2006). Thus, a majority of the arsenic that enters and sorbs to the bund soil each irrigation season must disappear before the next irrigation season.

A similar loss of solid phase arsenic occurs in the surface soils of Field 2 between the end of one irrigation season and the start of another (Dittmar et al. 2007). A recent study determined that the surface-soil arsenic loss occurs during the ~140 days that the rice fields are covered by monsoon floodwaters (Roberts et al. 2009). Anoxic conditions develop at the field-floodwater interface, promoting reductive dissolution of the arsenic-bearing iron solids that formed and settled onto the field surface during the irrigation season. The released arsenic then diffuses up into the floodwaters and is swept out to the Bay of Bengal when the floodwaters recede (Roberts et al. 2009). This process removes 187±70 mg/m^2 (Roberts et al. 2009) of arsenic off the surface of both Field 1 and Field 2 (see supporting information, chapter 5). This diffusional loss of arsenic into the floodwater accounts for significant fraction of the arsenic deposited onto the field surface (Figure 4.6). The mass balance suggests that Field 1 gains only ~134 mg/m^2 of arsenic each year, which is equivalent to a spatially-averaged concentration of 1.4 mg/kg if all of the arsenic is retained within the top 10 cm of soil. The uncertainty in the mass balance is too large to draw a conclusion regarding the retention of arsenic is the surface soil of Field 2. However,

five years worth of data from Field 2 suggest that surface soil concentrations are actually increasing at a rate of roughly 0.7 mg/kg/year (Dittmar et al. 2009), which is equivalent to 70 $mg \cdot m^{-2} \cdot year^{-1}$ if the arsenic is retained within the top 10 cm of soil. This accumulation is equal to the uncertainty in the mass balance calculations (Figure 4.6) and small enough that it would be difficult to detect without a multi-year dataset.

Compared to the field surface, the bund area exposed to the floodwater is extremely small. Thus, it is unlikely that much of the accumulated arsenic in the bund is lost via diffusion into the floodwaters (Figure 4.6, supporting information, chapter 5). We hypothesize that instead a portion of the bunds are eroded each monsoon season as the floodwaters flow into and out of our study area (Figure 4.6). Erosion is most likely when the floodwaters initially enter the field area and the bunds act as weirs. An interview with a field owner in our study area supports this hypothesis. The farmer reports that both the bunds and the irrigation channel get partially washed away during the monsoon season, and that these features are rebuilt each year using soil from the surface of the rice fields (Chowdhury 2009).

Calculations suggest that the measured bund concentrations (Figure 4.7) can be maintained over decades if 2/3 of the bund soil is eroded each monsoon season and replaced with pre-irrigation/post-monsoon soil from the surface of the rice field (see supporting information, chapter 5). Under this scenario, a steady-state situation is reached within five years, at which point the arsenic concentrations in the bund are elevated enough that a 2/3 loss of bund soil accounts for the influx of irrigation arsenic. However, due to yearly variations in both the arsenic flux and the erosional loss, it is likely that a steady-state situation is never achieved. The bunds could be gaining a small amount of arsenic each year, just like the rice field surface soil.

The fate of the eroded bund arsenic is unclear. It is possible that it is redistributed across

the study area and never completely leaves the rice-field system. The Bengal Basin currently accrues sediment, ~1 billion t/year (Goodbred et al. 2003), and thus it is unlikely that much particulate-bound arsenic is ultimately removed from the Basin. However, it is also possible that once the bund soil is redistributed and exposed to the floodwater it behaves like the soil in the rice field surface, releasing dissolved arsenic into the floodwaters (Roberts et al. 2009).

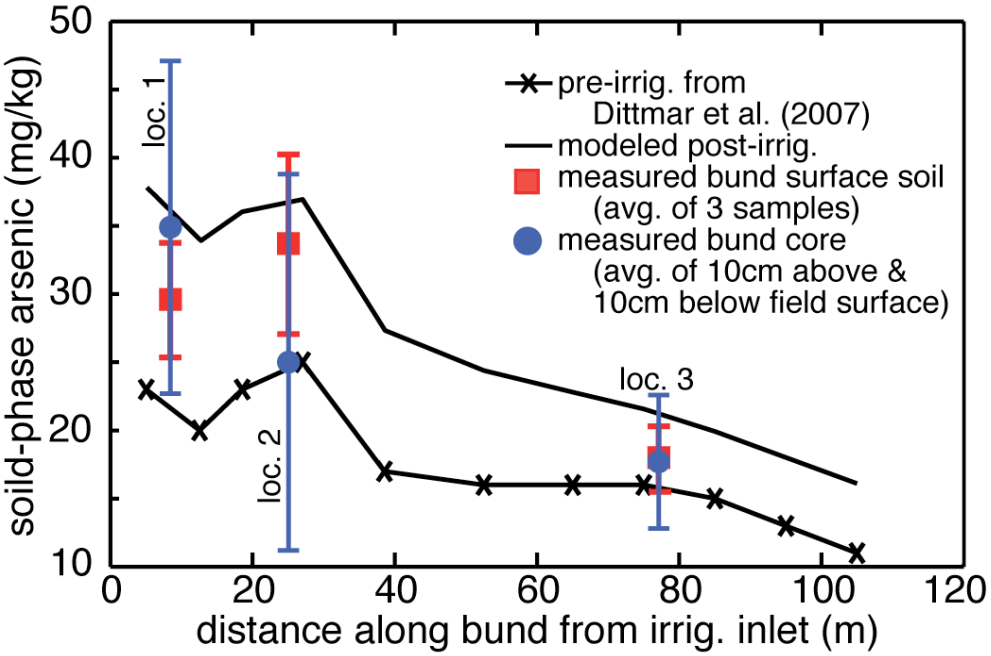

Figure 4.7 Measured and modeled solid-phase arsenic in the bund of Field 2.

Surface soil samples and soil cores were collected from the bund of Field 2 at the three locations marked in Figure 4.1. The presented concentrations for the surface samples represent the average of three duplicate samples taken from the same location, and the presented concentrations for the soil cores represent the average concentration within a 20 cm core segment centered on the elevation of the field surface. Error bars represent one standard deviation. The pre-irrigation concentration of the bund was assumed to match the December 2004 concentrations measured by Dittmar et al. (2007) in surface soil samples located the same distance from the irrigation inlet and adjacent to the bund. The modeled post-irrigation concentration was determined from the seasonal arsenic bund flux for Field 2 (see supporting information, chapter 5), assuming that 90% of the arsenic remains in the top 30 cm of the 40-cm-wide bund.

4.4.6. Arsenic in the Aquifer

The mass balance calculations presented in Figure 4.6 demonstrate that the rice fields in our study area act as an unintentional pump-and-treat system for the arsenic contaminated aquifer. During the irrigation season, a large amount of arsenic is pumped up from the aquifer (Ali et al. 2003), and essentially none of it returns to the aquifer. A large portion of this irrigation arsenic eventually leaves the rice-field system when it is flushed out to the Bay of Bengal with the receding floodwaters (Roberts et al. 2009). Calculations (see supporting information, chapter 5) suggest that for our study area, with the current rate of irrigation, it will take ~150 years to remove all of the arsenic residing in the top 30 m of the aquifer that is weakly adsorbed or co-precipitated with carbonates, acid volatile sulfides, amorphous metal oxides and magnetite (Swartz et al. 2004). Irrigation wells in our study are screened at a 30 m depth (Harvey et al. 2006), and as they pump water up from this depth they also pull pond recharge down to this depth, which promotes the dissolution of solid-phase arsenic (Neumann et al. 2009a and chapter 6). If the hydrologic system is not perturbed in the future, such that flow paths extending from ponds to the irrigation wells do not shift, it may be possible for the irrigation wells in our study area to pump low arsenic groundwater sooner than 150 years. Such cleansing of irrigation flow paths may already be occurring. Harvey et al. (2003) note that irrigation wells, which withdraw a large amount of water from the aquifer, have lower arsenic concentrations than drinking wells, which draw proportionately less water from the aquifer.

The pump-and-treat nature of the groundwater-irrigated fields in our study area depends on annual monsoon flooding to remediate both the surface soil and the bund. In other parts of Bangladesh or West Bengal where flooding does not occur, we expect there is a significant buildup of arsenic in the soils and bunds of groundwater-irrigated rice fields.

4.5. References

Abedin, M. J., M. S. Cresser, A. A. Meharg, J. Feldmann, and J. Cotter-Howells (2002a), Arsenic accumulation and metabolism in rice (Oryza sativa L.), *Environ. Sci. Technol., 36*, 962-968.

Abedin, M. J., J. Cotter-Howells, and A. A. Meharg (2002b), Arsenic uptake and accumulation in rice (Oryza sativa L.) irrigated with contaminated water, *Plant Soil, 240*, 311-319.

Adomake, A. R. M. Solaiman, P. N. Williams, C. Deacon, G. K. M. M. Rahman, and A. A. Meharg (2008), Enhanced transfer of arsenic to grain for Bangladesh grown rice compared to US and EU, *Environ. Int.,* doi 10.1016/j.envint.2008.07.010.

Ali, M. A., A. B. M. Badruzzaman, M. A. Jalil, M. D. Hossain, M. F. Ahmed, A. A. Masud, M. Kamruzzaman, and M. Rahman (2003), Fate of Arsenic Extracted with Groundwater, Proc. Internat. Symp. on Fate of Arsenic in the Environment, BUET and UNU, Dhaka, Bangladesh.

Ashfaque, K. N. (2007), Effect of hydrological flow pattern on groundwater arsenic concentration in Bangladesh, Ph.D. Thesis, Massachusetts Institute of Technology: Cambridge, MA, pp. 286.

BGS, DFID, and DPHE (2001), Arsenic contamination of groundwater in Bangladesh, *BGS Technical Report WC/00/19, Volume 1 & 2*, British Geological Survey, Keyworth.

Chowdhury, R. (2009), Owner of Field 1, *Personal communication,* January 20.

Chowdhury, R. (2006), Owner of Field 1, *Personal communication*, August 15.

Dittmar, J., A. Voegelin, L. Roberts, S. J. Hug, G. C. Saha, M. A. Ali, A. B. M. Badruzzaman, and R. Kretzschmar (2007), Spatial distribution and temporal variability of arsenic in irrigated rice fields in Bangladesh: 2. Paddy soil, *Environ. Sci. Technol., 41*, 5967-5972.

Dittmar, J., A. Voegelin, L. C. Roberts, S. J. Hug, G. C. Saha, M. A. Ali, A. B. M. Badruzzaman, and R. Kretzschmar (2009), Estimating long-term trends of arsenic accumulation in irrigated paddy soil in Bangladesh: A mass balance approach, AGU Chapman Arsenic Conference, Siem Reip, Cambodia.

Duxbury, J. M., A. B. Mayer, J. G. Lauren, and N. Hassan (2003), Food chain aspects of arsenic contamination in Bangladesh: Effects on quality and productivity of rice, *J. Environ. Sci. Health Part A, 38*, 61-69.

Goodbred, S. L., S. A. Kuehl, M. S. Steckler, and M. H. Sarker (2003), Controls on facies distribution and stratigraphic preservation in the Ganges-Brahmaputra delta sequence, *Sediment. Geol., 155*, 301-316.

Harvey, C. F., C. Swartz, A. B. M. Badruzzaman, N. Keon-Blute, W. Yu, M. A. Ali, J. Jay, R. Beckie, V. Niedan, D. Brabander, P. Oates, K. Ashfaque, S. Islam, H. Hemond, and M. F. Ahmed (2003), Response to Comments on "Arsenic Mobility and Groundwater Extraction in Bangladesh", *Science, 300*, 584d.

Harvey, C. F., C. H. Swartz, A. B. M. Badruzzaman, N. Keon-Blute, W. Yu, M. A. Ali, J. Jay, R. Beckie, V. Niedan, D. Brabander, P. M. Oates, K. N. Ashfaque, S. Islam, H. F. Hemond, and M. F. Ahmed (2002), Arsenic mobility and groundwater extraction in Bangladesh, *Science, 298*, 1602-1606.

Harvey, C. F., K. N. Ashfaque, W. Yu, A. B. M. Badruzzaman, M. A. Ali, P. M. Oates, H. A. Michael, R. B. Neumann, R. Beckie, S. Islam, and M. F. Ahmed (2006), Groundwater dynamics and arsenic contamination in Bangladesh, *Chem. Geol., 228*, 112-136.

Hemond, H., and E. J. Fechner-Levy (2000), *Chemical Fate and Transport in the Environment,* Academic Press, San Diego.

Hossain, M. D., D. Lewis, M. L. Bose, and A. Chowdhury (2003), Rice Research, Technological Progress, and Impact on the Poor: The Bangladesh Case (Summary Report), *EPTD Discussion Papers*, International Food Policy Research Institute, Washington, D.C.

Hossain, M. B., M. Jahiruddin, G. M. Panaullah, R. H. Loeppert, M. R. Islam, and J. M. Duxbury (2008), Spatial variability of arsenic concentration in soils and plants, and its relationship with iron, manganese and phosphorus, *Environ. Pollut., 156*, 739-744.

Hsieh, P. A. (1996), Deformation-induced changes in hydraulic head during ground-water withdrawal, *Ground Water, 34*, 1082-1089.

Hug, S. J., L. Canonica, M. Wegelin, D. Gechter, and G. von, Urs (2001), Solar oxidation and removal of arsenic at circumneutral pH in iron containing waters, *Environ. Sci. Technol., 35*, 2114-2121.

Janssen, M., and B. Lennartz (2008), Characterization of preferential flow pathways through paddy bunds with dye tracer tests, *Soil Sci. Soc. Am. J., 72*, 1756-1766.

Jardine, P. M., J. F. McCarthy, and N. L. Weber (1989), Mechanisms of dissolved organic carbon adsorption on soil, *Soil Sci. Soc. Am. J., 53*, 1378-1385.

Kirk, G. (2004), *The Biogeochemistry of Submerged Soils,* John Wiley & Sons, New Jersey.

Lin, Z., and R. W. Puls (2000), Adsorption, desorption and oxidation of arsenic affected by clay minerals and aging process, *Environ, Geol., 39*, 753-759.

Manning, B. A., and S. Goldberg (1997), Arsenic(III) and arsenic(V) absorption on three California soils, *Soil Sci., 162*, 886-895.

McGeehan, S. L., S. E. Fendorf, and D. V. Naylor (1998), Alteration of arsenic sorption in flooded-dried soils, *Soil Sci. Soc. Am. J., 62*, 828-833.

Meharg, A. A., and M. Rahman (2003), Arsenic contamination of Bangladesh paddy field soils: Implications for rice contribution to arsenic consumption, *Environ. Sci. Technol., 37*, 229-234.

Meharg, A. A., P. N. Williams, A. Eureka, Y. Y. Lawgali, D. Claire, V. Antia, R. C. J. Cambell, S. Guoxin, Z. Yong-Guan, F. Joerg, R. Andrea, Z. Fang-Jie, I. Rafiqul, H. Shahid, and Y. Junta (2009), Geographical variation in total and inorganic arsenic content of polished (white) rice, *Environ. Sci. Technol., 43*, 1612-1617.

Neumann, R. B., K. N. Ashfaque, A. B. M. Badruzzaman, M. A. Ali, J. Shoemaker, and C. F. Harvey (2009a), Anthropogenic influences on groundwater arsenic concentrations in Bangladesh, *Nature Geosci.,* accepted.

Neumann, R. B., M. L. Polizzotto, A. B. M. Badruzzaman, M. A. Ali, Z. Zhang, and C. F. Harvey (2009b), The hydrology of a groundwater-irrigated rice field in Bangladesh: Seasonal and daily mechanisms of infiltration, *Water Resour. Res., 45*, doi:10.1029/2008WR007542.

Norra, S., Z. A. Berner, P. K. Agarwala, F. Wagner, D. Chandrasekharam, and D. Stuben (2005), Impact of irrigation with As rich groundwater on soil and crops: A geochemical case study in West Bengal Delta Plain, India, *Applied Geochemistry, 20*, 1890-1906.

Pal, A., U. K. Chowdhury, D. Mondal, B. Das, B. Nayak, A. Ghosh, S. Maity, and D. Chakraborti (2009), Arsenic burden from cooked rice in the populations of arsenic affected and nonaffected areas and Kolkata City in West-Bengal, India, *Environ. Sci. Technol., 43*, 3349-3355.

Panaullah, G., T. Alam, M. Hossain, R. Loeppert, J. Lauren, C. Meisner, Z. Ahmed, and J. Duxbury (2009), Arsenic toxicity to rice (Oryza sativa L.) in Bangladesh, *Plant Soil, 317*, 31-39.

Reynolds, J. G., D. V. Naylor, and S. E. Fendorf (1999), Arsenic sorption in phosphate-amended soils during flooding and subsequent aeration, *Soil Sci. Soc. Am. J., 63*, 1149-1156.

Roberts, L., S. J. Hug, J. Dittmar, A. Voegelin, R. Kretzschmar, B. Wehrli, O. A. Cirpka, G. C. Saha, M. A. Ali, and A. B. M. Badruzzaman (2009), Arsenic mobilization from paddy soils during monsoon flooding, *Nature Geosci.,* accepted.

Roberts, L., S. J. Hug, J. Dittmar, A. Voegelin, G. C. Saha, M. A. Ali, A. B. M. Badruzzaman, and R. Kretzschmar (2007), Spatial distribution and temporal variability of arsenic in irrigated rice fields in Bangladesh: 1. Irrigation water, *Environ. Sci. Technol., 41*, 5960-5966.

Saha, G. C., and M. A. Ali (2007), Dynamics of arsenic in agricultural soils irrigated with arsenic contaminated groundwater in Bangladesh, *Sci. Total Environ., 379*, 180-189.

Sundberg-Jones, S., and S. Hassan (2007), Macrophyte sorption and bioconcentration of elements in a pilot constructed wetland for flue gas desulfurization wastewater treatment, *Water Air Soil Pollut., 183*, 187-200.

Swartz, C. H., N. K. Blute, B. Badruzzman, A. Ali, D. Brabander, J. Jay, J. Besancon, S. Islam, H. F. Hemond, and C. F. Harvey (2004), Mobility of arsenic in a Bangladesh aquifer: Inferences from geochemical profiles, leaching data, and mineralogical characterization, *Geochim. Cosmochim. Acta, 68*, 4539-4557.

Takahashi, Y., R. Minamikawa, K. H. Hattori, K. Kurishima, N. Kihou, and K. Yuita (2004), Arsenic behavior in paddy fields during the cycle of flooded and non-flooded periods, *Environ. Sci. Technol., 38*, 1038-1044.

Tuong, T. P., M. C. S. Wopereis, J. A. Marquez, and M. J. Kropff (1994), Mechanisms and control of percolation losses in irrigated puddled rice fields, *Soil Sci. Soc. Am. J., 58*, 1794-1803.

van Geen, A., Y. Zheng, Z. Cheng, Y. He, R. K. Dhar, J. M. Garnier, J. Rose, A. Seddique, M. A. Hoque, and K. M. Ahmed (2006), Impact of irrigating rice paddies with groundwater containing arsenic in Bangladesh, *Sci. Total Environ., 367*, 769-777.

Walker, S. H. (1999), Causes of high water losses from irrigated rice fields: field measurements and results from analogue and digital models, *Agric. Water Manage., 40*, 123-127.

Walker, S. H., and K. R. Rushton (1984), Verification of lateral percolation losses from irrigated rice fields by a numerical-model, *J. Hydrol., 71*, 335-351.

Walker, S. H., and K. R. Rushton (1986), Water losses through the bunds of irrigated rice fields interpreted through an analog model, *Agric. Water Manage., 11*, 59-73.

Wickham, T. H., and C. N. Sen (1978), Water management for lowland rice: water requirements and yield response, in *Soils and Rice*, edited by The International Rice Research Institute, Los Banos, Phillipines.

Wickham, T. H., and V. P. Singh (1978), Water movement through wet soils, in *Soil and Rice*, edited by The International Rice Research Institute, Los Banos, Philippines.

Williams, P. N., A. H. Price, A. Raab, S. A. Hossain, J. Feldmann, and A. A. Meharg (2005), Variation in arsenic speciation and concentration in paddy rice related to dietary exposure, *Environ. Sci. Technol., 39*, 5531-5540.

Williams, P. N., M. R. Islam, E. E. Adomako, A. Raab, S. A. Hossain, Y. G. Zhu, J. Feldmann, and A. A. Meharg (2006), Increase in rice grain arsenic for regions of Bangladesh irrigating paddies with elevated arsenic in groundwaters, *Environ. Sci. Technol., 40*, 4903-4908.

Wopereis, M. C. S., B. A. M. Bouman, M. J. Kropff, H. F. M. Tenberge, and A. R. Maligaya (1994), Water-use efficiency of flooded rice fields .1. validation of the soil-water balance model Sawah, *Agric. Water Manage., 26*, 277-289.

Lu, Y., E. E. Adomako, A. R. M. Solaiman, M. R. Islam, C. Deacon, P. N. Williams, G. K. M. M. Rahman, and A. A. Meharg (2009), Baseline soil variation Is a major factor in arsenic accumulation in Bengal Delta paddy rice, *Environ. Sci. Technol., 43*, 1724-1729.

5. Supporting Information for Chapter 4

5.1. 2008 Water Level Data for Field 1

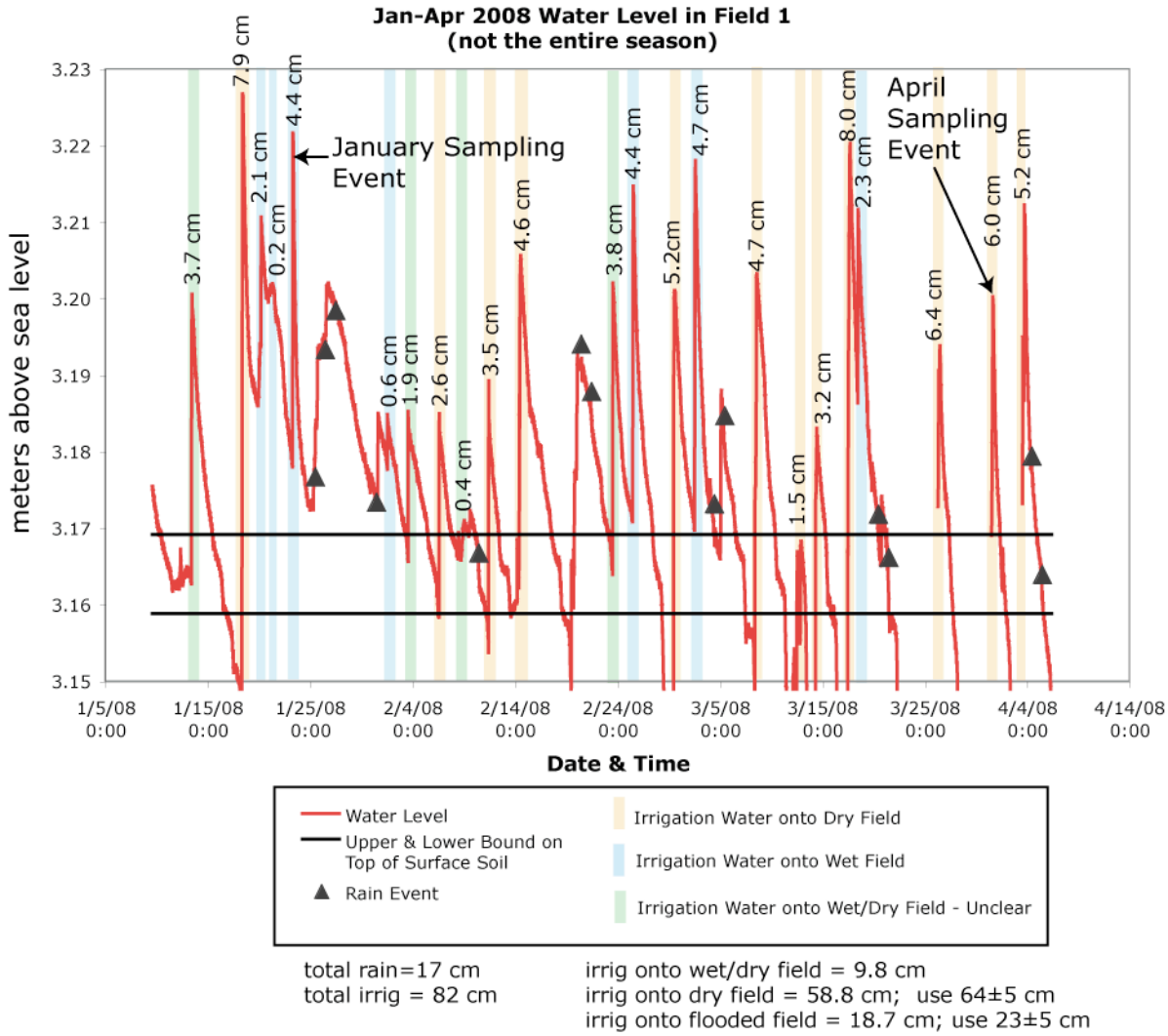

Figure 5.1 2008 water level data from Field 1.

The data are for a portion of the irrigation season (January to April) , not the entire irrigation season which lasts until May. Each irrigation event is coded with a color depending on if water was added to a flooded (blue color) or dry (brown color) field. The surface of the rice field fluctuates, so the status of the field is unclear for some events (green color). The numbers that correspond with each irrigation event designate the amount of irrigation added to the field per unit area. Water level increases marked with a triangle are due to rain events. The data demonstrate the irrigation regime for Field 1 during and between the two intensive sampling campaigns.

Water level data in Field 1 were collected at a 15 min interval with a pressure transducer placed above the plow pan. See chapter 2 for more details on water level measurements.

The top horizontal line in the water level figure represents the average upper bound for the top of the surface soil in the field while the bottom horizontal line represents the average lower bound. Using these bounds, 14±2 times irrigation water was applied to a dry field (i.e., the initial water level was below the bottom horizontal line) and 9±2 times irrigation water was added to a wet field (i.e., the initial water level was above the top horizontal line).

The rate of change in the water level during an irrigation event was used in conjunction with the average pump speed of the irrigation well, 19 L/s (Roberts et al., 2007), to determine the time it takes for irrigation water to spread across the field. The unknown area covered by the irrigation water was calculated from the known volume of water that flowed into the field from the irrigation well (via the pump rate) and the height of water in the field.

Table 5.1 Time for water to cover Field 1

Irrigation Event	Time for Water to Cover Field Area
Jan 18	2.8 hr
Jan 23	3.4 hr
Feb 11	0.7 hr
Feb 14	1.6 hr
Feb 29	2.4 hr
Average	**2.2 hr**

The calculations agree with observation (Roberts et al., 2007). It takes 2 to 3 hours for irrigation water to travel across the field.

5.2. Irrigation Requirements and Bund Loss for Field 1 and Field 2

The perimeter-to-area relationship developed in a previous study for a 69-day period (Neumann et al., 2009b and chapter 2) suggests that Field 1, with a perimeter to area ratio of 0.1 m/m^2 requires: 1325.8*P/A-11.66 = 121 cm of water. The scatter of data around the determined perimeter-to-area relationship (see Figure 2.3) suggests that the error in this estimate is ±20 cm. Data collected from **Field 1** for the entire 2006 and 2007 irrigation season showed that the field actually received **127±10 cm** of water (Neumann et al., 2009b and chapter 2). Thus, the actual amount is 1.05±0.19 larger than the value determined from the perimeter-to-area relationship. With this scaling for the entire season, **Field 2**, with a perimeter-to-area ratio of 0.07 m/m^2 requires [(1325.8*P/A-11.66) ±20 cm]*1.05±0.19 = **85±26 cm** of water.

These irrigation amounts mean that, seasonally, **Field 1** receives

(127±10 cm)(390±10 μg/L)(L/1000 cm^3)(100 cm/m)^2(mg/1000 μg)=**495±41mg As/m^2**

while **Field 2** receives

(86±26 cm)(390±10 μg/L)(L/1000 cm^3)(100 cm/m)^2(mg/1000 μg)=**335±102 mg As /m^2.**

The previous hydrologic study (Neumann et al., 2009b and chapter 2) also demonstrated that during the 2006 and 2007 irrigation season, **Field 1** lost **57±1%** of its irrigation water down the bund. This percentage matches the fraction of water lost out the bund predicted with the perimeter-to-area ratio (see Figure 2.10). This perimeter-to-area relationship predicts that **Field 2** loses **37%** of its water out the bund. Based on data from three different field studies that were compared to this relationship, the error in the relationship appears to be **±5%**.

5.3. Field Site Pictures

Figure 5.2 Bamboo scaffolding in Field 1.

The scaffolding extends from the bund out to locations (e) and (c) in the middle of the field.

Figure 5.3 Close up view of bamboo scaffolding at location (e).

Figure 5.4 Purging foil bags with argon gas.

Figure 5.5 Lysimeter vacuum chambers at location (a).

The lysimeter tubing extended out of the bund and connected to the chambers through a stopcock. Inside the vacuum chambers, the nozzle of the foil bag connected to tubing that penetrated through the rubber stopper of the vacuum chamber. A vacuum was applied to the chambers using the pump shown in the picture, which allowed water to flow through the lysimeter tubing into the foil bag.

Figure 5.6 Flow through probe system.

The system contained pH, ORP, DO, conductivity, temperature and reference probes. The probes connected to the nozzle of the foil bag on one end and a plastic syringe on the other. Water from the bag was pulled through the probe system direction into the syringe.

Figure 5.7 Cracks in rice field due to prolonged drying between irrigation events.

5.4. Dissolved Oxygen Test on SKC Flex Foil Bags

A SKC flex foil bag was filled with de-oxygenated water and left sitting in the open atmosphere for roughly two days. Periodically, the bag was transferred into a nitrogen-purged glove box to test the water's dissolved oxygen (DO) content. Dissolved oxygen was tested with both a DO probe and a DO Hach Kit. The two measurement methods disagreed on the total oxygen content of the water, but reported the same rate of oxygen increase, $0.03 mg \cdot L^{-1} \cdot hour^{-1}$.

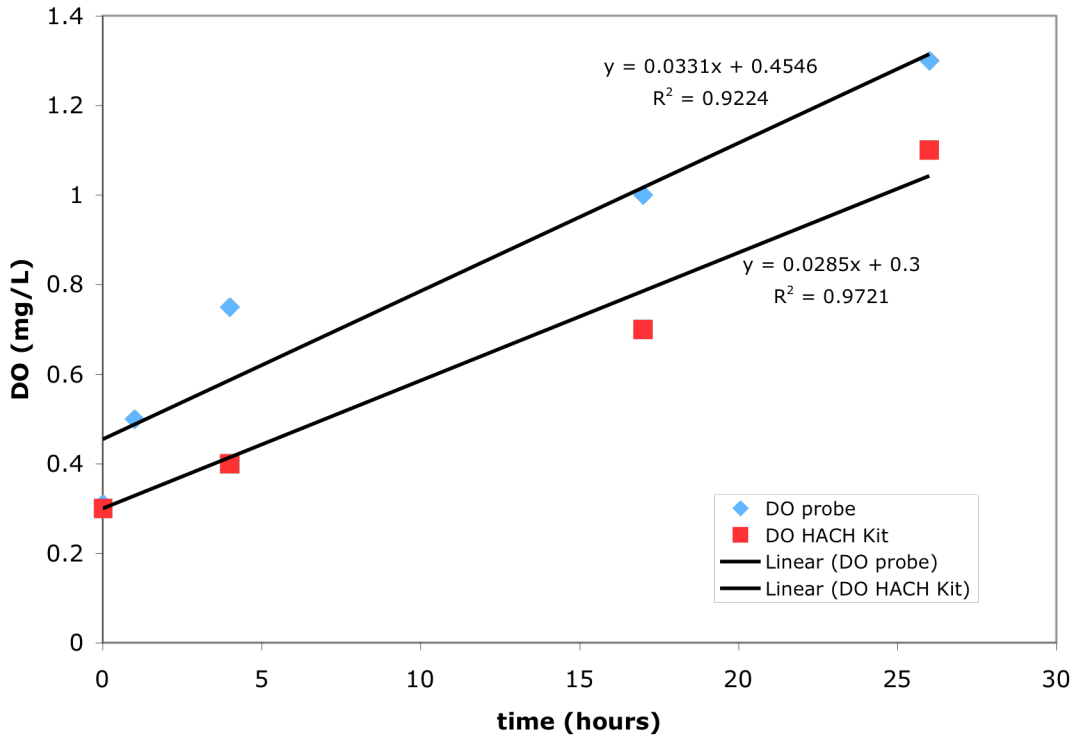

Figure 5.8 Dissolved oxygen test for SKC Flex Foil bags.
The data demonstrate the rate at which oxygen permeates the sample collection bags. Water collection and processing generally occurred within an 18-hour time frame.

Theoretically, the oxygen concentration inside the bag should not linearly increase since diffusion is a function of the concentration gradient. However, the linear increase in Figure 5.8 is due to the fact that the oxygen concentrations within the bag are much less than saturation.

5.5. Preservation Acid and Organic Carbon Experiment

Rice field water samples for nutrient and organic carbon analysis were preserved with sulfuric acid. Sulfuric acid was used since analytical methods already existed to analyze these constituents within small-volume water samples preserved with this acid. However, sulfuric acid is an oxidant. An experiment was conducted to test if the acid impacted organic carbon concentrations. Water samples from the bund and from the sediments of two different ponds were collected into the SKC flex-foil bags, immediately transferred to an argon glove bag, filtered and sealed in a glass BOD bottles. The field samples were then placed on ice and transported back to MIT. At MIT, aliquots of water from the BOD bottles were preserved with different acids (H_3PO_4, H_2SO_4, and HCl) and placed in the fridge for three months. The aliquots were then analyzed for organic carbon. The results (Figure 5.9) show that the different acids did not impact the carbon measurements in the three collected water samples.

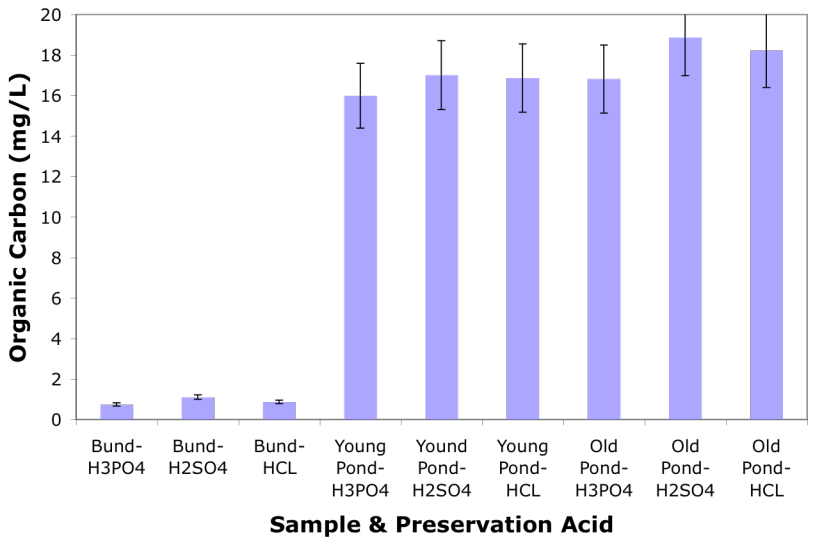

Figure 5.9 Organic carbon concentrations using different preservation acids.
The two oxidizing acids, sulfuric and hydrochloric acid, did not oxidize the organic carbon in the water samples.

5.6. Oxygen Data for Surface Water in Field 1

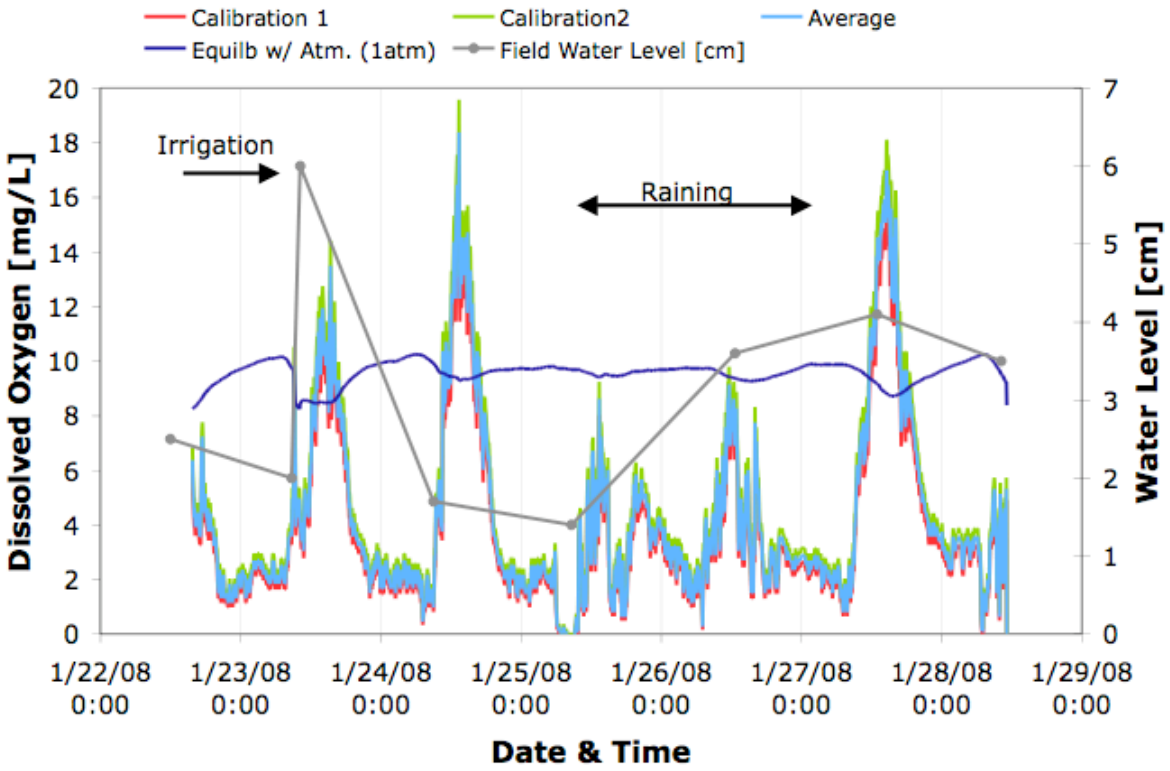

Figure 5.10 Dissolved oxygen and water level in Field 1, January 2008 sampling campaign.

Dissolved oxygen was continuously measured in the rice field surface water with a DO probe hooked up to a HOBO logger. The dark blue line shows the concentration that would exist in the water if it were in equilibration with the atmosphere. The measured concentration exceeds saturation during the day, except when it was raining, and then drops close to zero during the night. In January, the rice plants in the field are small, roughly 20 cm tall.

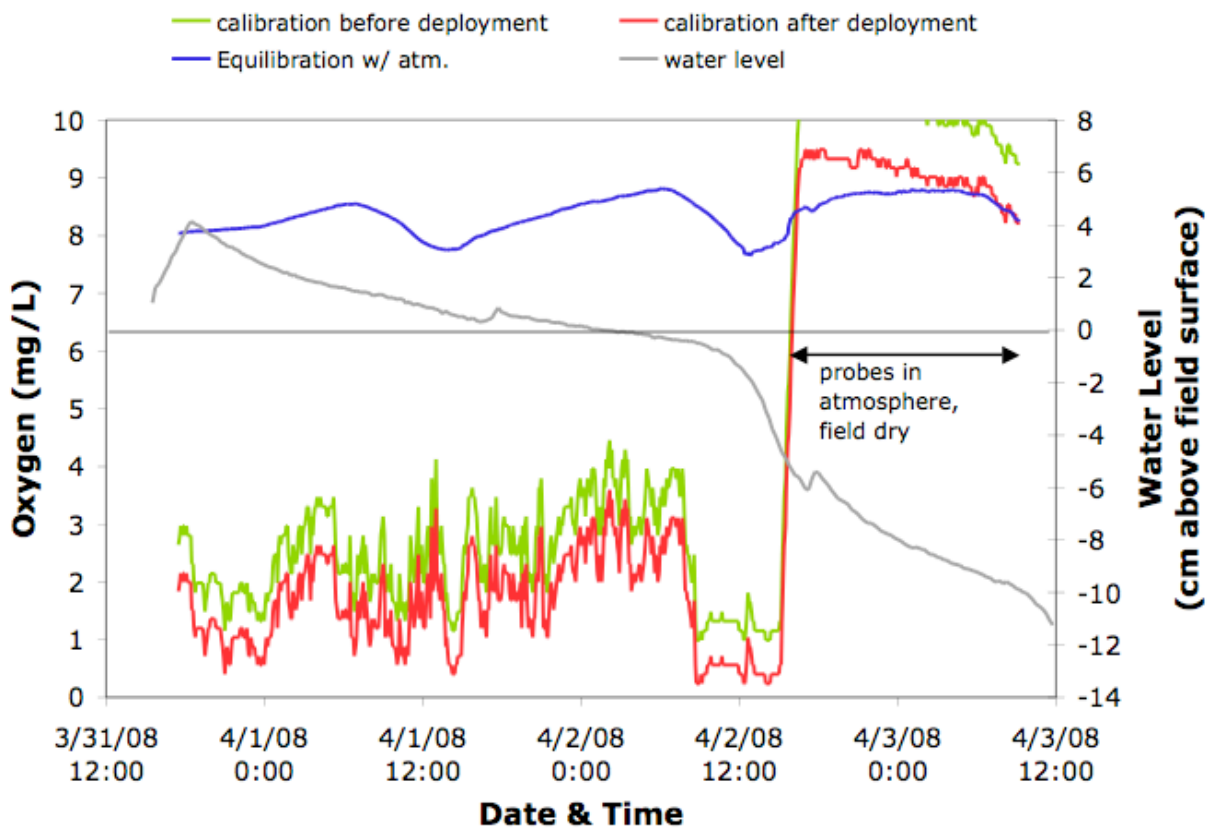

Figure 5.11 Dissolved oxygen and water level in Field 1, April 2008 sampling campaign.

Dissolved oxygen was continuously measured in the rice field surface water with a DO probe hooked up to a HOBO logger. The dark blue line shows the concentration that would exist in the water if it were in equilibration with the atmosphere. The measured concentration is below saturation for the entire sampling period. In April, the tall rice plants shade the water in the field, so photosynthesis cannot occur at a very high rate, and the water column remains suboxic.

5.7. δ^{13}C-DIC Data for Field 1

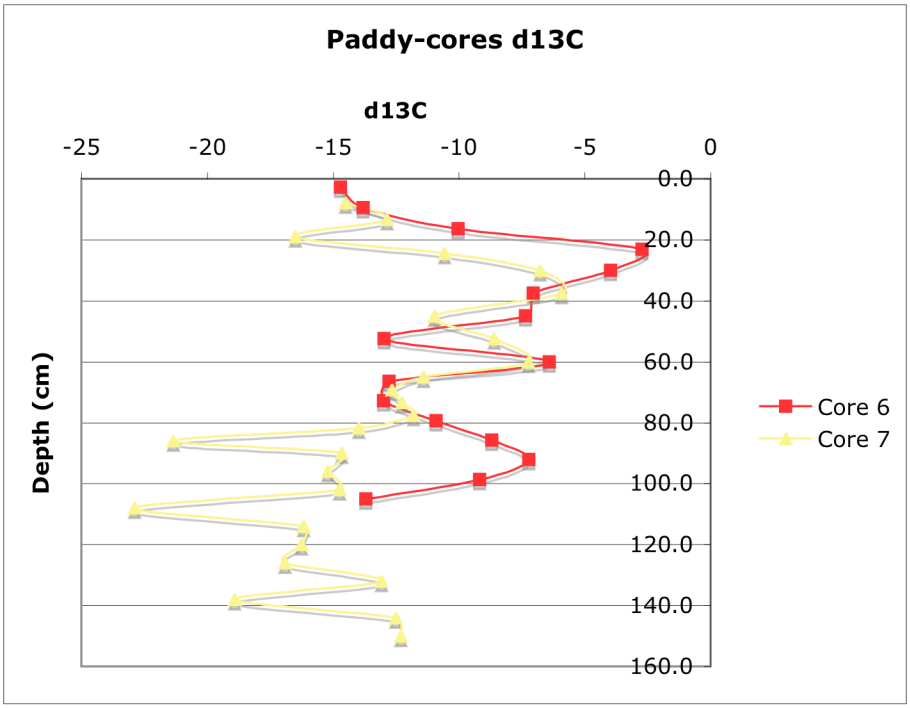

Figure 5.12 δ^{13}C of DIC of pore water in Field 1 soil cores.

Core 6 corresponds with location (b) and core 7 corresponds with location (c) in Figure 4.1. Data collected by Julie Shoemaker, March 2007. See section 7.1.7 for details on sample collection and analysis. Methane production corresponds with a shift towards heavier isotopic values.

The δ^{13}C of DIC increases when it is subjected to the microbial production of methane (Whiticar, 1999). δ^{13}C-DIC measurements above show that the δ^{13}C-DIC is heaviest at a depth of ~20 cm, which corresponds with the approximate location of the plow pan. The data demonstrate that most, if not all, of the methane in the field is generated in the surface soil layer, just above or within the plow pan. See chapter 7 and Neumann et al. (2009a) for details on the methods used to collect these data.

5.8. Dissolved Inorganic Carbon Data for Field 1

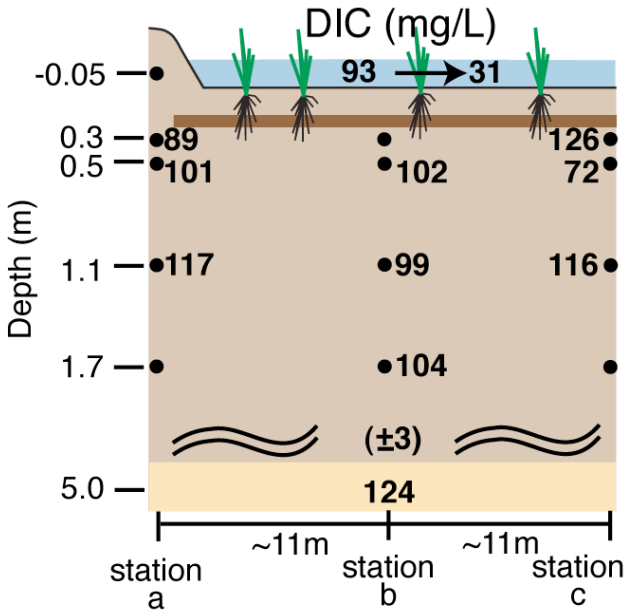

Figure 5.13 Dissolved inorganic carbon in Field 1.

Lysimeter data were collected March 2007, while surface water and aquifer data were collected January 2008. For more information see caption for Figure 4.2.

Dissolved inorganic carbon (DIC) increases with depth in the bund. This increase is attributed, in part, to the oxidation of BDOC; although the increase is larger than the measured loss in organic carbon with depth. DIC decreases in the surface water with time. This is due to the irrigation water degassing carbon dioxide to the atmosphere.

5.9. Amount of Water Collected from Each Lysimeter in Field 1

We believe the deepest lysimeter at location (c) in the middle of the rice field (see Figure 4.1) is installed within a preferential flow path. This determination was made based on chemical data (see Figure 4.2) and on the fact that water was consistently collected more quickly from this lysimeter than from the other non-bund lysimeters. All of the lysimeters were placed under roughly the same vacuum and were left to collect water for approximately the same length of time. Therefore the amount of water collected from each lysimeter was indicative of the ease with which water was collected. The data below show that the full sampling bag from the deepest lysimeter at location (c) consistently weighed more than the full sampling bags from the other non-bund lysimeters.

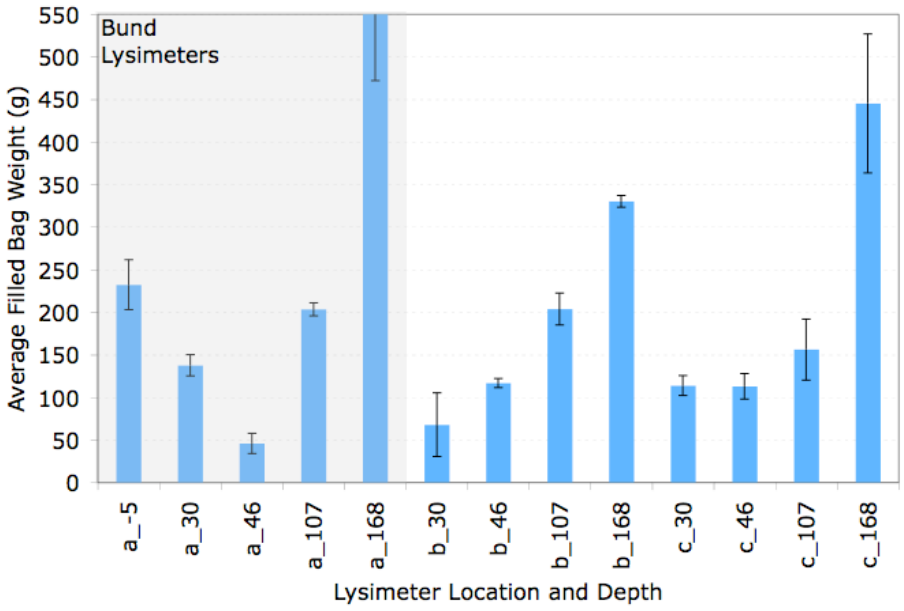

Figure 5.14 Weight of full lysimeter sampling bags.
Depth designations are in cm below the field surface. The deepest lysimeter in the middle of the field (C_168), consistently collected more water than all of the other non-bund lysimeters, suggesting that it is sampling a preferential flow channel.

5.10. Surface-Water Arsenic Loss During Irrigation Events

The loss of arsenic immediately after the April irrigation event was calculated from data collected from the five sampling locations at the end of the irrigation event and compared to the expected concentration of 390±10 μg/L (Roberts et al., 2007) in the irrigation water. The error in the measured concentrations represents analytical uncertainty.

April Loss Fraction = 1- [360±25 μg/L + 329±23 μg/L + 273±19 μg/L + 346±24 μg/L + 275±19 μg/L]/[(390±10 μg/L)*5] = **0.19±0.03**

The loss of arsenic immediately after the January irrigation takes into account the dilution of the 4.4 cm to 4.8 cm of 390±10 μg/L irrigation water with the 1.9 cm of existing, low arsenic water. The 4.4 cm of irrigation water was determined from the measured change in the surface water level due to irrigation (see section 5.1). However, in section 5.14 (see IrrigDay variable), it was determined that 4.8 cm of irrigation was actually applied to the field. It is possible that the extra 0.2 cm of water immediately entered the bund and did not thoroughly mix with the existing water. It takes 2-3 hours for irrigation water to travel across the field, and the 4.4 cm change occurred within 1.25 hours. This uncertainty in the irrigation water amount is accounted for with two different calculations, one using the 4.4 cm number and one using the 4.8 cm number. Error for the measured concentrations represents analytical uncertainty.

Jan Dilution Correction w/ 4.4 cm
= {[(244±15 μg/L) + (254±15 μg/L) + (235±14 μg/L) + (276±17 μg/L) + (279±17 μg/L)](6.3 cm) – [(22±1 μg/L) + (18±1 μg/L) + (23±1 μg/L) + (26±2 μg/L) + (27±2 μg/L)]*1.9 cm}/(4.4 cm)
= [(1288±35 μg/L)(6.3 cm) – (116±3 μg/L)(1.9 cm)]/(4.4 cm)
= 1794±50 μg/L
Jan Loss w/ 4.4m = 1 – (1794±50 μg/L)/[(390±1 0μg/L)*5] = 0.08±0.03

Jan Dilution Correction w/ 4.8 cm

= [(1288±35 μg/L)(6.7 cm) – (116±3 μg/L)(1.9 cm)]/(4.8 cm) = 1752±49 μg/L

Jan Loss w/ 4.8 cm = 1 – (1752±49 μg/L)/[(390±10 μg/L)*5] = 0.10±0.03

If we assume that reality falls somewhere between these two estimates, then we can calculate the January loss as the average of the two estimates.

Estimated Jan Loss Fraction = (0.08±0.03 + 0.10±0.03)/2 = **0.09±0.03**

The loss of arsenic over a longer time period is determined using data from location (c), which is in the middle of the rice field:

Table 5.2 Arsenic in the surface water over time

mg/L	January, location (c), unfiltered	April, location (c), unfiltered
Immediately after irrigation	254±15	274±6
24-hrs after irrigation	26.9±1.6	76.8±1.9
48-hrs after irrigation	16.7±1.0	52.8±0.8
% Loss over 48-hrs	93±8 %	81±3 %

5.11. Water-Level Drop in Surface Soil Between Irrigation Events

The previous hydrologic study, presented in chapter 2, showed that once the water level in the field reaches the top of the surface soil, bund flow no longer occurs. In this situation, water loss is due to evapotranspiration, vertical infiltration, and preferential flow. Vertical infiltration and preferential flow are relatively constant and summed together, equal to 0.35 cm/day (Neumann et al., 2009b and chapter 2). The average evapotranspiration rate for the dry season is 0.39 cm/day (Neumann et al., 2009b and chapter 2). Thus, the water level in the soil surface decreases at a rate of 0.74 cm/day divided by porosity. The porosity of the soil beneath the plow pan is ~0.5 (Figure 2.8). However, the surface soil above the plow pan has a higher porosity. This fact is clear from water content measurements taken on two different soil cores (the plow pan is located at ~20 cm depth).

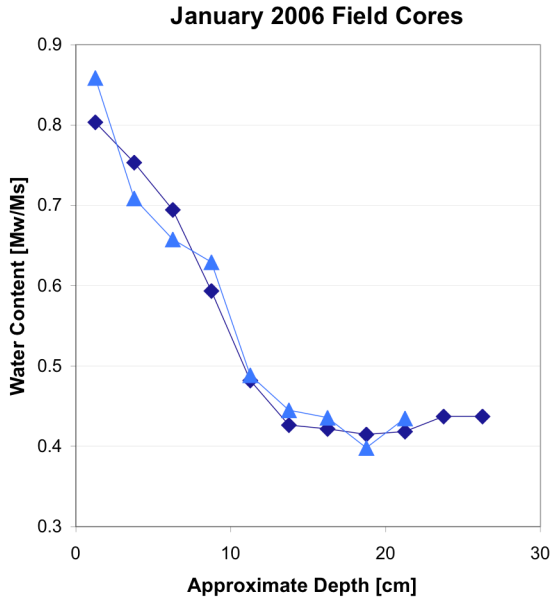

Figure 5.15 Water content data for the surface soil of Field 1.
The surface soil in the field has a larger porosity than the soil beneath the plow pan, and thus, when the soil is saturated, it also has a greater water content.

Assuming the cores were completely saturated, the water content data suggest that the porosity (n) of the surface soil is:

$n/(1-n) = (M_w/M_s)(\rho_s/\rho_w) = (.8)(2.65) = 2.12$

$n = 0.7$

Therefore, between irrigation events (max of 5 days), the water level in the surface soil can drop: (0.74 cm/day)/(.7)*5 days = 5 cm. This drop is enough to expose the top portion of the soil surface, but not enough to expose the entire surface soil profile. The surface soil directly above the plow pan remains saturated and anoxic between irrigation events.

5.12. Difference Between Filtered and Unfiltered Arsenic Concentrations in Field 1

Table 5.3 Unfiltered minus filtered (0.2 μm) concentrations for Field 1 surface water.

Day	Location	Unfiltered – Filtered As μg/L
Day 1 1/22/08	a	3.9±1.6
	c	3.1±1.3
	f	5.8±1.6
	d	4.7±1.7
	e	2.0±1.9
Day 2 1/23/08 **Irrigation Event**	a	80±10
	c	74±10
	f	73±10
	d	87±11
	e	81±11
Day 3 1/24/08	a	7.7±1.9
	c	5.8±1.8
	f	3.6±1.9
	d	2.7±1.8
	e	N/A
Day 4 1/25/08	a	2.5±1.3
	c	3.3±1.2
	f	11.7±1.3
	d	5.6±1.6
	e	N/A
Day 5 1/26/08	a	4.6±1.0
	c	0.3±1.2
	f	4.9±1.3
	d	0.1±1.3
	e	N/A
Day 6 1/27/08	a	3.3±0.8
	c	1.4±1.4
	f	6.3±1.8
	d	1.4±2.1
	e	5.3±2.1

5.13. Settling Velocity for 0.2 μm Particle

The lack of a significant difference between filtered and unfiltered concentrations in the surface water of the field within ~24 hours of irrigation (Table 5.3) suggests that arsenic solids larger than 0.2 μm do not exist at this point in time. However, arsenic concentrations continue to decrease in the surface water of the field. Stoke's law provides a way to calculate if this loss could be due to settling of particles smaller than 0.2 μm.

Stoke's Law:

$$v = \frac{2}{9}\frac{\left(\rho_p - \rho_w\right)gr^2}{\mu},$$

where v is the settling velocity, ρ_p density of the particle in kg/m^3, ρ_w density of water in kg/m^3, g gravity in m/s^2, r radius of the particle in m, and μ the dynamic viscosity in Pas.

If we assume that the 0.2 μm particle has a density of 2.65 g/cm^3, we calculate that the settling velocity is:

$$v = \frac{2}{9}\frac{\left(1650 kg/m^3\right)\left(9.81 m/s^2\right)\left(1x10^{-7} m\right)^2}{1 Pas} = 4x10^{-11} m/s$$

Therefore, it would take ~44 years for a 0.2 μm particle to travel 5 cm, which means that other loss mechanisms must exist for arsenic in the surface water of the field.

5.14. Bund-Water Flux Calculations for Field 1

January Sampling Campaign – 9am 1/22/2008 to 9am 1/27/2008

```
%Daily Values
RainDay = [0  0  0.15  2.98  0.87];    %cm, from met station
EvapDay = [0.21  0.18  0.12  0  0.11]; %cm, pan from met station
InfDay = 0.35;5        %cm/day, vertical infiltration through plow pan into soil matrix
                        % and preferential flow channels, see chapter 2
IrrigDay = 4.8;        %cm, calc. from pump rate and irrig. length

%Hourly Values
inddh = [37:4:517];    %Water level data were collected at a 15min interval for the entire
                       %irrigation season. "inddh" is an index that pulls out data on an
                       %hourly time step for 1/22/08 to 1/27/08
dh = WL(:,inddh(2:end))-WL(:,inddh(1:end-1));
%Change in water level in the field over a 1-hour time period.
dherror = 0.4*ones(1,length(dh));
% propagated error for 1 stdev of WL data measurements, see section 2.3.5

Esin = sin(0:pi/24:pi);
% sin function used to transform the daily evaporation value into hourly values.
Evaphr(1:15) =EvapDay(1)*Esin(11:end)/sum(Esin);
Evaphr(16:24 ) =EvapDay(1)*Esin(2:10)/sum(Esin);
Evaphr(1+24:15+24) =EvapDay(2)*Esin(11:end)/sum(Esin);
Evaphr(16+24:24+24) =EvapDay(2)*Esin(2:10)/sum(Esin);
Evaphr(1+48:15+48) =EvapDay(3)*Esin(11:end)/sum(Esin);
Evaphr(16+48:24+48) =EvapDay(3)*Esin(2:10)/sum(Esin);
Evaphr(1+72:15+72) =EvapDay(4)*Esin(11:end)/sum(Esin);
Evaphr(16+72:24+72) =EvapDay(4)*Esin(2:10)/sum(Esin);
Evaphr(1+96:15+96) =EvapDay(5)*Esin(11:end)/sum(Esin);
Evaphr(16+96:24+96) =EvapDay(5)*Esin(2:10)/sum(Esin);
% daily evaporation error (see section 2.3.6) distributed evenly across hours in the day
Evaphrerror = 0.1/24*ones(1,length(Evaphr));

%Irrigation water distributed across two hours
Irrighr = zeros(1,120);
Irrighr(25)=.955*IrrigDay;
Irrighr(26)=.045*IrrigDay;
%Irrigation error (see section 2.3.7) distributed across two hours
Irrighrerror = zeros(1,length(inddh)-1);
Irrighrerror(25) = .955*0.4;
Irrighrerror(26) = 0.045*0.4;

% Infiltration assumed constant during day, see chapter 2
Infhr = InfDay/24*ones(1,120);
```

```
Infhr(84:end)=0; % rain storm keeps infiltration from happening
%Infiltration error (see section 2.4.3)
Vinfhrerror = 0.1/24*ones(1,length(Vinfhr));
Vinfhrerror(84:end) = 0;

% Daily rain distributed in proportion to increase in water level in the
% field on the days that it rains.
Rainhr = zeros(1,120);
D3inc = find(dh(49:72)>0); %WL increase on Day 3
Rainhr(D3inc+48)=RainDay(3)*dh(D3inc+48)/sum(dh(D3inc+48));
D4inc = find(dh(73:96)>0); %WL increase on Day 4
Rainhr(D4inc+72)=RainDay(4)*dh(D4inc+72)/sum(dh(D4inc+72));
D5inc = find(dh(97:120)>0);
Rainhr(D5inc+96)=RainDay(5)*dh(D5inc+96)/sum(dh(D5inc+96));
%Rain error (see section 2.3.6) distributed like rain value
Rainhrerror = zeros(1,length(inddh)-1);
Rainhrerror(D3inc+24*2)= 0.05*dh(D3inc+24*2)/sum(dh(D3inc+24*2));
Rainhrerror(D4inc+24*3)= 0.05*dh(D4inc+24*3)/sum(dh(D4inc+24*3));
Rainhrerror(D5inc+24*4)= 0.05*dh(D5inc+24*4)/sum(dh(D5inc+24*4));

%Bund flux calculated from hourly water balance
Bundhr = Irrighr + Rainhr - Evaphr - Infhr - dh; %cm/hr
Bundhrerror = (Irrighrerror.^2 + Rainhrerror.^2 + Evaphrerror.^2 + Vinfhr.^2 + dherror.^2).^.5;
% Error in bund flux = propagated error from its components

% Bund flow per 1m bund section = bund flux*field area/perimeter
QBund = Bundhr*(1694.8*100^2)/(165.9); %cm3/hr lost to 1m long bund section
QBundError = BundhrErr*(1694.8*100^2)/(165.9); %cm3/hr

sum(QBund)/100^3 = 0.64; % m3/m bund
(sum(QBundError.^2))^.5/100^3 = 0.12; % m3/m bund
```

April Sampling Campaign – 9am 3/31/2008 to 9am 4/3/2008

```
% Daily Values
ARainDay = [0 0 0];   % cm, from met station
AEvapDay = [.53 .5 .43]; % cm, from met station
AInfDay = 0.35;       % cm/day, vertical infiltration through plow pan into soil matrix and
                      preferential flow channels, see chapter 2
AIrrigDay = 5.99;     % cm, calc. from pump rate and irrig. length

% Hourly Values
AEsin = sin(0:pi/24:pi);
% sin function used to transform the daily evaporation value into hourly values.
AEvaphr(1:15) =AEvapDay(1)*AEsin(11:end)/sum(AEsin);
AEvaphr(16:24) =AEvapDay(1)*AEsin(2:10)/sum(AEsin);
AEvaphr(1+24:15+24) =AEvapDay(2)*AEsin(11:end)/sum(AEsin);
AEvaphr(16+24:24+24) =AEvapDay(2)*AEsin(2:10)/sum(AEsin);
AEvaphr(1+48:15+48) =AEvapDay(3)*AEsin(11:end)/sum(AEsin);
AEvaphr(16+48:24+48) =AEvapDay(3)*AEsin(2:10)/sum(AEsin);
% daily evaporation error (see section 2.3.6) distributed evenly across hours in the day
AEvaphrerror = 0.1/24*ones(1,length(AEvaphr));

% Irrigation water distributed across 5 time nodes, based on field notes
AIrrighr= zeros(1,72);
AIrrighr(6)=AIrrigDay*(.175);
AIrrighr(7)=AIrrigDay*(.25);
AIrrighr(8)= AIrrigDay*(.25);
AIrrighr(9)= AIrrigDay*(.25);
AIrrighr(10)= AIrrigDay*(.075);
% Irrigation error (see section 2.3.7) distributed like irrigation values
AIrrighrerror = zeros(1,72);
AIrrighrerror(6) = 0.85*.175;
AIrrighrerror(7) = 0.85*.25;
AIrrighrerror(8) = 0.85*.25;
AIrrighrerror(9) = 0.85*.25;
AIrrighrerror(10) = 0.85*.075;
% Farmer siphoned off small amount of water from the irrigation canal when water
% was flowing through it to irrigated another field in the study area.
AIrrighr(32)=.3; % cm
AIrrighr(33)=.23;
% Irrigation error (see section 2.3.7) split across two hours
AIrrighrerror(32) = 0.85/2;
AIrrighrerror(33) = 0.85/2;

% Infiltration assumed constant
AInfhr = AInfDay/24*ones(1,72);
% Infiltration error (see section 2.4.3)
AVinfhrerror = 0.1/24*ones(1,72);
```

```
% No Rain during sampling event
ARainhr=zeros(1,72);
ARainhrerror=zeros(1,72);

Ainddh = [5:4:268];
%Water level data were collected at a 15min interval for the entire irrigation season. "inddh" is
% an index that pulls out data on an hourly time step. Before the sampling event in April, the
% water level dropped below the field surface. Thus we do not have Water Level data until
% hour 5

% change in water level in the field on an hourly time step.
Adh=zeros(1,72);
Adh(6)=AWL(Ainddh(1))*.44;
Adh(7)=AWL(Ainddh(1))*.56
% initial water level change is equal to the first water level measurement because before
% this point, water level is below pressure transducer.
Adh(8:end)= AWL(Ainddh(2:end))-AWL(Ainddh(1:end-1));
Adherror(6:end) = 0.4;
% propagated error for 1 stdev of WL data measurements, see section 2.3.5
Adhzero = find(Adh==0); % index that finds where water level change is zero
Adh(Adhzero) = -AEvaphr(Adhzero)-AInfhr(Adhzero);
% since we lack data when water level drops below pressure transducer, we calculate no
% change in water level. But this is not realistic. Still losing water to evaporation
% and infiltration.
Adherror(Adhzero) = .14; % propagated error for evaporation and infiltration measurements.

% April bund flux calculated via water mass balance
ABundhr = AIrrighr + ARainhr - AEvaphr - AInfhr - Adh;
ABundhr(40)=ABundhr(39)/3;
% artifically set b/c water level dropped below sensor & sharp change in WL that model
% fit as bund flow. But in reality it isn't bund flow
ABundhrerror = (AIrrighrerror.^2 + ARainhrerror.^2 + AEvaphrerror.^2 + AVinfhrerror.^2 +
Adherror.^2).^.5;
 % Error in bund flux = propagated error from its components

% Bund flow through 1m section of bund = bund flux*area/perimeter
AQBund = ABundhr*(1694.8*100^2)/165.9; % cm3/hr per 1m bund section
AQBundError = ABundhrerror*(1694.8*100^2)/(165.9);

sum(AQBund)/100^3 = 0.54; % m3/m bund
(sum(AQBundError.^2))^.5/100^3 = 0.27; % m3/m bund
```

5.15. Hourly Surface Water Arsenic Concentrations for Field 1

During both the January and April sampling campaigns, surface water data were collected once a day, usually in the middle of the day. These daily values were transformed into the needed hourly values by assuming an exponential decay in concentration between sampling events.

In January, arsenic concentrations in the surface water of the field were assumed uniform. Therefore, for each day, the average concentration from the five sample locations was calculated. These values were connected together with exponential functions, as shown below (D2= Day 2, the day of irrigation, D3=Day 3, etc.):

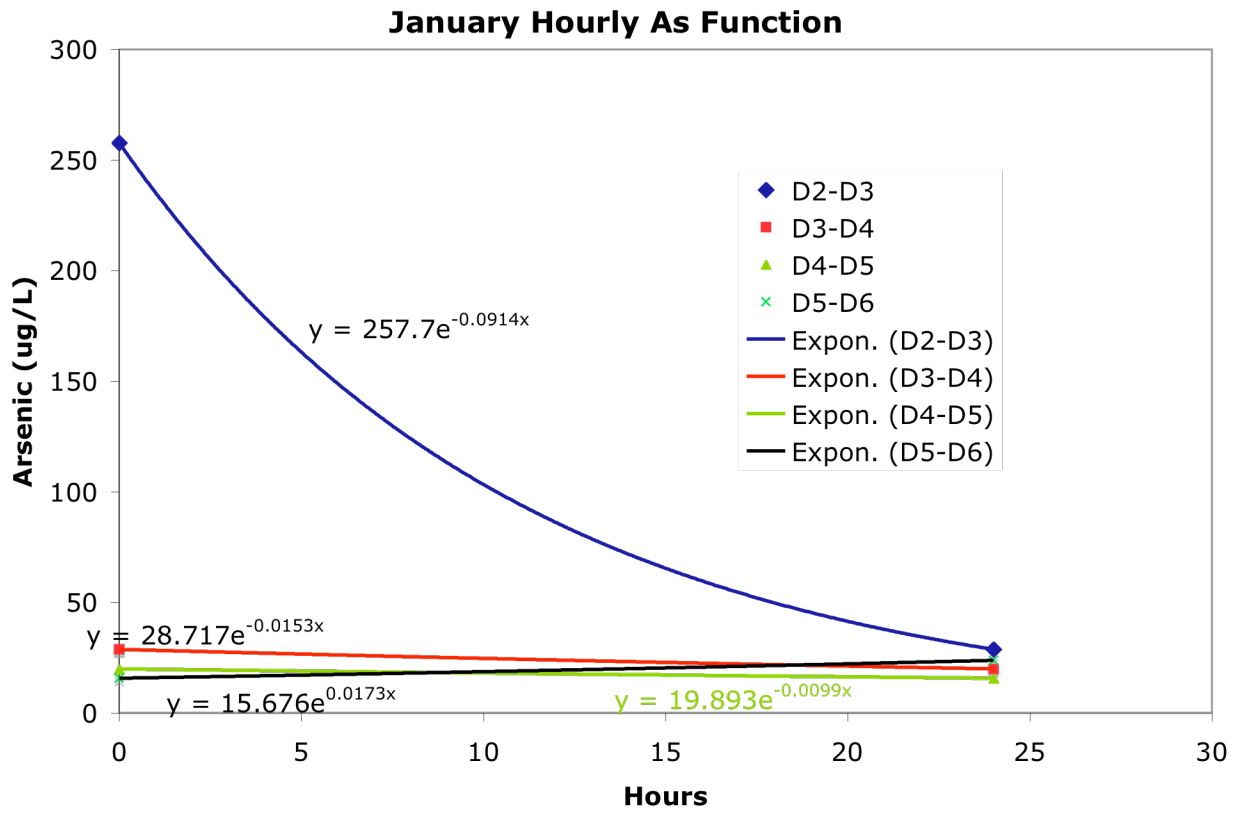

Figure 5.16 Hourly arsenic function for Field 1 surface water.

The January arsenic flux into the bund was thus calculated:

```
hr24 = [0:1:23];
AsSurfConc = [23.18*ones(1,23) 150 280 270 ...
  257.7*exp(-.0914*hr24) 28.7*exp(-.0153*hr24) ...
  19.9*exp(-.0099*hr24) 15.7*exp(.0173*hr24(1:end-2))]/1000;
        % ug/cm3, arsenic concentration in field on Day 1 was 23.2 ug/L. A step increase
        % was assumed during irrigation between this value and the sampled value of 257.7 ug/L
        % immediately after irrigation ended.
AsFlux = QBund.*AsSurfConc/1000; %mg/hr into 1 m bund section.
        % Calculation of QBund shown in section 5.14.
AsFluxError = (QBund.^2*(10/1000)^2 + (AsSurfConc).^2.*QBundError.^2).^.5/1000;
%mg/hr into 1 m bund section, assuming error on surface water concentrations is 10 ug/L
        % Calculation of QBundError shown in section 5.14.
```

sum(AsFlux) = 93 *% mg into 1m bund section*
(sum(AsFluxError.^2))^.5 = 34 *% mg into 1m bund section*

In April, arsenic concentrations in the surface water of the field were spatially distinct. The concentration trend detected in the sampled locations was assumed to extend across the entire field. The estimated spatially varying concentrations for each day are shown below along with the measured data. The estimated, spatially-averaged concentration for Day 1 is 168 μg/L.

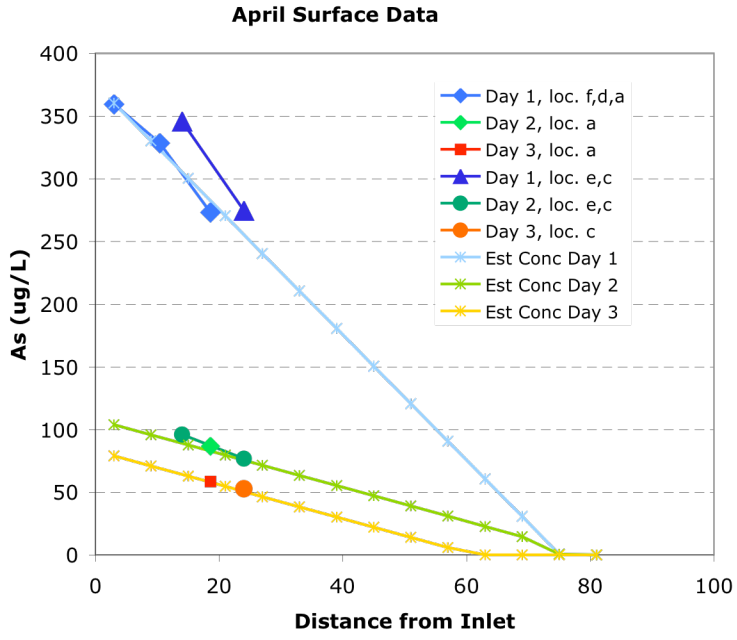

Figure 5.17 Field 1 surface-water arsenic versus distance from inlet.

To construct the hourly arsenic function, the spatially-varying daily concentrations at each location were connected together with an exponential function of the form $C=b*m^t$, where C is concentration, t is time on an hourly interval, and b and m were fitted parameters based on the concentrations of the two daily concentration values. The result was a concentration matrix (ApAsSurf) that contained a 72 hourly values for each of the 14 locations.

The April flux into the bund was thus calculated:

```
AQBundm = AQBund'*ones(1,14);
        % cm3/hr per 1m bund section for 14 bund locations evenly space along entire bund,
        % convert bund flux vector into a matrix. See section 5.14 for the development of the
        % bund flux vector AQBund.
ApAsFlux = (AQBundm).*(ApAsSurf/1000)/1000;
        % (cm3/hr)*(ug/L/1000)/1000 = mg/hr per 1m bund section for 14 bund locations
ApAsFluxError = (AQBundm.^2*(10/1000)^2 +
(ApAsSurf/1000).^2.*AQBundmError.^2).^.5/1000;
% mg/hr per 1m bund section for 14 bund locations,  assuming error on surface water
% concentrations is 10 ug/L
        %Calculation of QBundError shown in section 5.14.
sum(sum(ApAsFlux))/14 = 61 % mg into 1m bund section for the entire field
sum(sum(ApAsFluxError.^2))^.5/14 = 8 % mg into 1m bund section for the entire field
```

5.16. Arsenic Lost Down the Bund of Field 1

During the January sampling campaign, 4.8 cm of 390±10 μg/L arsenic irrigation water was added to the field (see section 5.14, IrrigDay variable), and 8.9±3.3 mg of arsenic per m^2 of field area entered the bund (see Figure 4.4i):

Jan% = (8.9±3.3 mg/m2)/[(4.8 cm)(390±10 μg/L)(.01)]*100= **48±16 %**

During the April sampling campaign, 6.0 cm of irrigation water was added to the field (see section 5.14, AIrrigDay variable), and 6.0±0.7 mg of arsenic per m^2 of field area entered the bund (see Figure 4.4j):

Apr% = (6.0±0.7 mg/m2)/[(6.0 cm)(390±10 μg/L)(.01)]*100= **26±3 %**

We can use these percentages to predict the seasonal amount of arsenic lost down the bund for Field 1 if we assume that when irrigation water is added to a flooded field (January event), 48±16% of the arsenic enters down the bund, and that when water is added to a dry field (April event), 26±3% of the arsenic enters the bund. We combine these percentage losses with the total amount of irrigation arsenic applied to Field 1 (495±41 mg/m2, section 5.2) and weight them by the number of times during the season that water was added to a flooded field (10±2 times) and to a dry field (9±2 times) (see section 5.1):

Field 1 Seasonal As Bund Loss =
[(0.48±0.16)*(9±2) + (0.26±0.03)*(14±2)]/23*(495±41 mg/m^2)
=(4.4±1.7 + 3.6±0.7)/23*(495±41 mg/m^2)=(8.0±1.8)/23*(495±41 mg/m^2)=**173±41 mg/m^2**

This loss represents 35±8 % of the all the arsenic applied to Field 1, and is in mg As per m^2 of field area, not bund area.

We can determine the spatially varying mass of arsenic that entered the bund of Field 1 between the January and April sampling campaigns, if we assume that the spatially distinct bund

fluxes determined for January and April represent the flux behavior for when water is added to a flooded and dry field, respectively. We can scale the magnitude of the January and April fluxes with water level data presented in section 5.1. The water level data show that between the January and April events, 18 to 28 cm of water was added to the field when it was flooded and 54 to 64 cm of water were applied to the field when it was dry. These differences were used to bracket the estimate:

```
% Jan type water if use 3.159 m above sea level (m.a.s.l.) as top of soil
Jwater1= 18; % cm
JAsFluxevent1=(sum(AsFlux))*Jwater1/4.4; %mg into 1 m long bund section,
        % 4.4 = cm of water for Jan event as measured by water level difference, Figure 5.1.
% Jan type water if use 3.17 m.a.s.l. as top of soil (+-1cm error in top of field)
Jwater2= 28;
JAsFluxevent2=(sum(AsFlux))*Jwater2/4.4; % mg into 1 m long bund section
% April type water if use 3.159 m.a.s.l. as top of soil
 Awater1= 64;
% April type water if 3.169 m.a.s.l. as top of soil
Awater2= 54;
AAsFluxevent1 = zeros(length(Adwater1),14);
for i=1:14
   AAsFluxevent1(:,i)=sum(ApAsFlux(:,i))*Awater1/6;
   % 6 = cm of water for Apr event
end
AAsFluxevent2 = zeros(length(Awater2),14);
for i=1:14
   AAsFluxevent2(:,i)=sum(ApAsFlux(:,i))*Awater2/6;
end
TotAsBundSec1 = (AAsFluxevent1 + JAsFluxevent1)/1000; % g into 1 m bund section
TotAsBundSec2 = (AAsFluxevent2 + JAsFluxevent2)/1000; % g into   m bund section
```

The results of this calculation are presented in Figure 4.5b in the manuscript. This water-level approach for scaling the January and April fluxes could not be used for the seasonal estimate because the water level data were not collected for the entire season.

5.17. Calculated As Bund Flux Using P/A Ratio and Initial As Concentrations

Since most of the arsenic that flows into the bund does so immediately after irrigation, it is likely that the As bund flux can be estimated from the fraction of water that is lost down the bund, which depends on the perimeter-to-area ratio, and from surface water concentration data collected immediately after irrigation. This calculation method is verified below using data from Field 1.

Field 1 loses 57±1% of its irrigation water down the bund (see section 5.2). We can use this fractional loss along with the average concentration measured in the surface water immediately after irrigation to predict the seasonal arsenic bund flux. For Field 1 we also need to consider the number of times irrigation water was applied to a wet or to a dry field (see section 5.1). Thus, we assume that the average surface water concentration measured in January (258 μg/L, section 5.15) represents the concentration when irrigation water is added to a flooded field, and that the average surface water concentration measured in April (168 μg/L, section 5.15) represents the concentration when irrigation water is added to a dry field:

P/A estimate for Field 1 As Bund Loss =
[(258 mg/m3)*(9±2)+(168 mg/m3)(14±2)]/23*(0.57±0.01)*(127±10 cm)/100
=(203±27 mg/m3)(.72±.06 cm) = 146±23 mg/m^2

The more accurate As bund loss calculated above in section 5.16 for Field 1, which depended on the fraction loss of arsenic down the bund under each irrigation regime, rather than on initial concentrations, was 173±41 mg/m^2. Thus this concentration and perimeter-to-area method captures (146±23 mg/m2)/(173±41 mg/m^2) = 0.84±0.24 of the As bund flux.

If we assuming that this concentration and perimeter-to-area method always captures 0.84±0.24 of the As bund flux, we can use it to estimate the amount of arsenic lost down the bund of Field 2. Based on its perimeter-to-area ratio, Field 2 loses 37±5% of its 85±26cm of irrigation water down the bund (see section 5.2). The spatially-averaged arsenic concentrations in Field 2 measured by Roberts et al. (2007) in February 2006 immediately after irrigation was 226±77 μg/L (the error represents one standard deviation of the data). Thus:

Field 2 As Bund Loss =
[(226±77 mg/m^3)*(0.37±0.05)*(85±26 cm)/100/(0.84±0.24) =
=(84±31 mg/m2) *(0.85±0.26 cm)/(0.84±0.24)
=(71±34)/(0.84±0.24)= **85±47 mg/m^2**

In section 5.2 we determined that Field 2 receives 335±102 mg/m^2 of irrigation arsenic each season. Thus, it loses (85±47 mg/m^2)/(335±102 mg/m^2)*100 = 25±16% of its arsenic down the bund.

This same method was used to calculate the spatially varying arsenic bund flux for Field 2, using the actual concentration measured next to the bund immediately after irrigation (Roberts et al., 2007). The resulting, spatially variable flux was used to create Figure 4.7.

5.18. Arsenic Load to the Surface Soil

The arsenic load to the surface soil of Field 1 and Field 2 can be calculated from the As irrigation input determined in section 5.2 and from the As bund flux determined in section 5.16/5.17:

Field 1 As into Surface Soil = (495±41 mg/m^2) - (173±41 mg/m^2) = **322±58 mg/m^2**

Field 2 As into Surface Soil = (335±102 mg/m^2) - (85±47 mg/m^2) = **250±112 mg/m^2**

These loadings are fairly similar. Field 1 receives more arsenic but also loses more arsenic out the bund.

Using the As bund flux calculation method developed in section 5.17 we can estimate the arsenic load to the surface soil of any field using its perimeter-to-area ratio, given that a certain fraction of the irrigation arsenic remains dissolved in the water column immediately after irrigation. The perimeter-to-area ratio determines both the total amount of irrigation water and As applied to the field (see Figure 2.3) and the total fraction of water lost down the bund (see Figure 2.10). The predicted surface soil arsenic loads for irrigation water with 390 μg/L As are plotted below as a function of the perimeter-to-area ratio and the fraction of irrigation water that remains dissolved in the water column immediately after irrigation. On the same plot are data points marking the location of Field 1 and Field 2 within the contoured space. Using surface water concentration data introduced in section 5.17, we calculate that the average fraction of irrigation arsenic that remains in Field 1 (P/A=0.1) is (203±27 μg/L)/(390±10 μg/L) = 0.52±0.07, while the fraction that remains in Field 2 (P/A=0.07) is (226±77 μg/L)/(390±10 μg/L) =0.58±0.20.

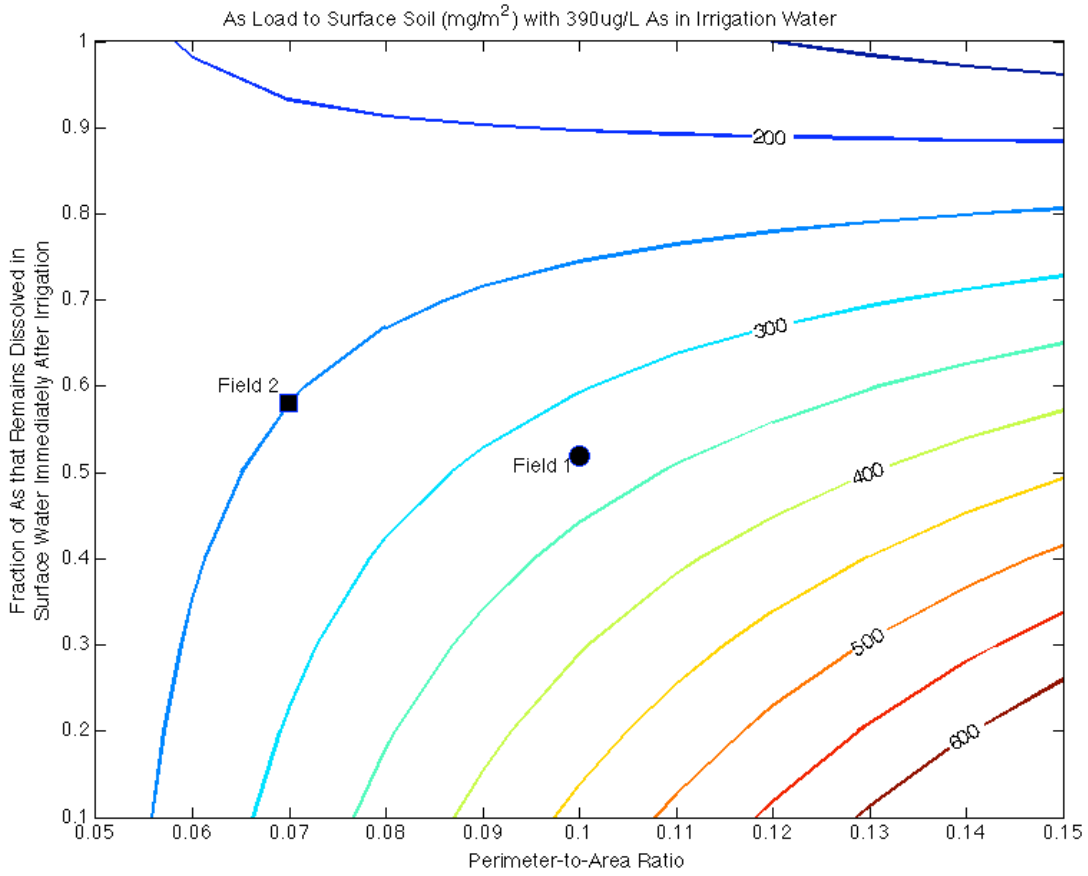

Figure 5.18 Calculated arsenic load to the surface soil with 300 µg/L As in irrigation water.

The plot shows that if roughly half of the irrigation arsenic remains dissolved in the water column immediately after irrigation, which is the case for both Field 1 and Field 2, then the surface soil of all the fields in our study area, regardless of their geometry, receive 200 to 400 mg/m^2 of As each season.

5.19. Amount of Arsenic Taken up by Rice Plants

Complied data from Lu et al. (2009) and Adomake et al. (2008) show that in a soil with 20 mg/kg As, rice grain contains 0.4±0.2 mg/kg As and the rice shoot contains 0.45±0.2 mg/kg. In a greenhouse experiment, Abedin et al. (2002) reported that on average, a pot with ~30 mg/kg As soil resulted in 6.5±0.5 g of grain and 10±0.5 g of straw. Each pot contained three rice plants. In Field 1, plants were spaced approximately 10 cm apart. Thus, a 1 m^2 area contained ~100 plants. If we assume this is also the density of plants in Field 2, then we can calculate the amount of arsenic taken up by rice plants in both **Field 1 and Field 2**:

(100 plants/m^2)[(0.4±0.2 mg As/kg grain)(6.5±0.5 g grain/3 plants) +

(0.45±0.2 mg/kg shoot)(10±0.5 g straw/3 plants)](1 kg/1000 g) = (0.1)[0.9±0.4 + 1.5±0.7]

= **0.24±0.08 mg/m^2**

5.20. Depth to which Bund Water Travels in a Single Irrigation Event

During the January and April sampling campaigns, 0.64 m^3 and 0.54 m^3 of water flowed into a 1 m section of bund in Field 1 (see Figures 4.4e–f). The bunds in our study area are roughly 40 cm wide and the porosity of the subsoil is 0.5 (Figure 2.8). If water does not spread any wider than the width of the bund once it enters the subsurface, then water from the January and April irrigation events could have reached a depth of (0.64 m^3)/(1 m*0.4 m*0.5) = 3.2 m and (0.54 m^3)/(1 m*0.4 m*0.5)=2.7 m, respectively. These depths likely over-estimate the depth that water from a single irrigation event can reach within the bund since the head gradients that develop underneath the bund immediately after irrigation show that water actually flows horizontally away from the bund into the subsoil of the field rather than just vertically downwards (see Figure 2.5).

Chemical data presented in Figure 4.2 show that bund flow does not reach the middle set of lysimeters installed in the planted portion of the rice field, ~11 m away from the bund. Thus, bund flow does not spread any wider than 11 m as it travels downwards through the bund. We can use this fact to slightly constrain our depth estimate. Using the January and April bund water fluxes, and the geometry presented in the figure below, we can calculate the minimum depth that bund water must reach.

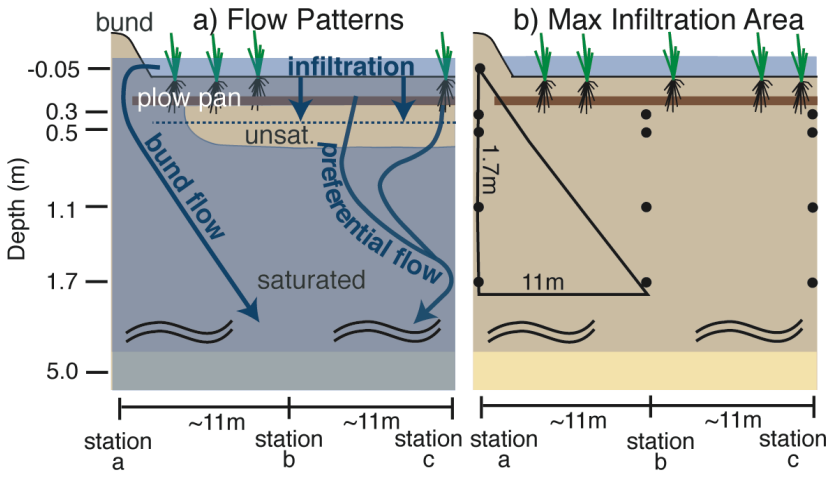

Figure 5.19 Plow patterns and geometry for maximum infiltration area.

January Event: $(0.64\ m^3)=2*(1\ m*0.5*d^2*11\ m/1.7\ m*0.5)$; $d = 0.44$ m

April Event: $(0.54\ m^3)=2*(1\ m*0.5*d^2*11\ m/1.7\ m*0.5)$; $d = 0.41$ m

Therefore, water from a single irrigation event can reach depths of 0.4 to 3 m within the bund. The actual depth to which bund water flows in a single irrigation event is likely closer to the 0.4 m estimate than the 3 m estimate. Even though the calculation resulted in a wide depth range, it shows that our top two sets of lysimeters (-0.05 m and 0.3 m depths) receive fresh bund water with every irrigation event.

5.21. Contribution of Rice-Field Arsenic to the Shallow Aquifer

The only types of rice field water that recharge the shallow aquifer are bund water and preferential flow water (Neumann et al., 2009b and chapter 2). Bund pore water data presented in the manuscript show that arsenic concentrations in the deepest lysimeters (1.7 m depth) in Field 1 are 10±5 μg/L. If we assume that bund water in Field 2 has the same concentration, we can calculate the amount of arsenic entering the aquifer from the bunds of each of these fields. In section 5.2 we determined that Field 1 loses 57±1% of its 127±10 cm of irrigation water down the bund and the Field 2 loses 37±5% of its 85±26 cm of irrigation water down the bund.

Field 1 Bund: (10±5 mg/m^3)(.57±.01)(1.27±0.1 m) = (10±5 mg/m^3)(0.72±0.06 m)

= **7.2±3.6 mg/m^2**

Field 2 Bund: (10±5 mg/m^3)(.37±.05)(0.85±0.26 m) = (10±5 mg/m^3)(0.31±0.11 m)

= **3.1±1.9 mg/m^2**

The hydrologic study of Field 1 showed that roughly 0.2 cm/day is lost to preferential flow and that this loss is relatively constant. We will assume that Field 2 experiences the same preferential flow water loss as Field 1. Figure 4.2 illustrates that the concentration of arsenic in the sampled preferential flow channel is an order of magnitude less than that in the bund water. If we assume that this is the case for all preferential flow water, then we can calculate the arsenic input into the aquifer from **preferential flow**:

(0.002 m/day)(120 days irrigation season)(2.5 mg/m^3) = **0.6 mg/m^2**

5.22. Diffusional Loss of Arsenic During the Monsoon Season

Roberts et al. (2009) estimated the flux of arsenic off of the soil in Field 2 into the overlying monsoon floodwater using three different approaches. The first approach involved calculating an arsenic flux using a temperature-adjusted diffusion coefficient for As (weighted based on measured As(III) and As(V) concentrations), tortuosity and porosity estimates, and the arsenic gradient at the field-floodwater interface determined with data collected from pore water samplers. This approach resulted in a seasonal flux of 53 mg/m^2. The other two approaches involved concentration changes measured in the floodwater. During periods of negligible mixing the arsenic flux was determined from the buildup of a vertical arsenic gradient within the bottom 80 cm of the floodwater, assuming negligible lateral flow and mixing with bulk floodwater. This approach resulted in a seasonal flux of 256 mg/m^2, assuming a 139-day monsoon season. During periods of receding floodwater level, when the entire water column was well mixed, the flux was determined from an increase in floodwater concentration after accounting for the arsenic lost via lateral flow. This approach resulted in a seasonal flux of 117 g/m^2, assuming a 139-day monsoon season. We believe the second two approaches, which actually measured a build up of arsenic in the floodwater, provide a more realistic estimate of the arsenic flux off of the field surface during the monsoon season. Therefore, for **Field 2**, we assume that **187±70 mg/m^2** is lost from the surface soil during the monsoon season.

If we assume that the arsenic flux off of the field is proportional to the concentration of arsenic in the surface soil, we can determine a flux for Field 1. Soil data collected by Dittmar et al. from the start of the irrigation season show that arsenic concentrations in top 10 cm of Field 2 ranged from 11 to 25 mg/kg (18±7 mg/kg). If we assume that this range is also representative of

the initial arsenic concentrations in Field 1, we can determine a post-irrigation concentration range based on the calculated input of arsenic into the surface soil.

Field 1 post-irrigation concentration: (18±7 mg/kg)+(3.22±0.58 mg/kg) = 21±7 mg/kg

Field 2 post-irrigation concentration: (18±7 mg/kg)+(2.50±1.12 mg/kg) = 21±7 mg/kg

The calculation shows that the spatially-averaged input of arsenic into the field during the irrigation season is small compared to the initial soil concentration and therefore does not have a large impact. We assume that the arsenic flux leaving **Field 1 equals that leaving Field 2**.

A similar approach is used to estimate the diffusive flux of arsenic out of the bund. The 187±70 mg/m^2 flux off of the fields is adjusted by the concentration of arsenic in the bund and the surface area of the bund exposed to the floodwater. It was assumed that the pre-irrigation concentration of the bund was 18±7 mg/kg and that 90% of the arsenic that entered the bund 40 cm wide bund during the irrigation season remained in the top 30 cm, which is an area of 0.12 m^2.

Field 1 post irrigation bund concentration: (18±7 mg/kg) + (.9)(173±41 mg/m^2)(1694.9 m^2) /(0.12 m^2*165.9 m)(1 m^3/100^3 cm^3)(1 cm^3/g)(1000 g/kg)

= (18±7 mg/kg) + (13±3 mg/kg) = 31±8 mg/kg

Field 1 bund flux, per m^2 of bund area: (187±70 mg/m^2)(31±8 mg/kg)/(21±7 mg/kg)

= (187±70 mg/m^2)(1.48±0.62) = 277±155 mg/m^2 bund

Field 1 bund flux, per m^2 field area, assuming 10 cm height on either side of bund is concentrated in arsenic and exposed to floodwater (A=0.2 m*perimeter of field):

(277±155 mg/m^2 bund)*(0.2 m*165.9 m)/1694.9 m^2 = **5±3 mg/m^2**

Field 2 post irrigation bund concentration: (18±7 mg/kg) + (.9)(85±47 mg/m^2)(3028.3 m^2)

/(0.12 m^2*208.7 m)(1 m^3/100^3 cm^3)(1 cm^3/g)(1000 g/kg)

= (18±7 mg/kg) + (9±5 mg/kg) = 27±9 mg/kg

Field 2 bund flux, per m^2 of bund area exposed to floodwater:

(187±70 mg/m^2)(27±9 mg/kg)/(21±7 mg/kg) = (187±70 mg/m^2)(1.29±0.60)

= 241±144 mg/m^2 bund

Field 2 bund flux, per m^2 field area, assuming 10 cm height on either side of bund is concentrated in arsenic and exposed to floodwater (A=0.2 m*perimeter of field):

(241±144 mg/m^2 bund)*(0.2 m*208.7 m)/3028.3 m^2 = **3±2 mg/m^2**

5.23. Build-up of Solid-Phase Arsenic in the Bund of Field 2

The mass balance presented in Figure 4.6 suggests that the hypothesized erosional loss of arsenic from the bund needs to equal the flux of arsenic that enters the bund during the irrigation season. Since only a portion of the bund is eroded, and not the entire bund (see chapter 4), to reach this steady-state situation, arsenic concentrations in the bund soil must be high enough that this partial erosion accounts for the seasonal flux of irrigation arsenic.

If we use the spatially-distinct arsenic bund flux for Field 2 (see section 5.17), and assume that 2/3 of the bund is eroded each year and replaced with pre-irrigation/post-monsoon soil from the surface of Field 2 (Dittmar et al. 2007), we see that a steady-state situation is quickly reached and that the steady-state concentrations roughly match those measured in the bund of Field 2 (see Figure 5.20).

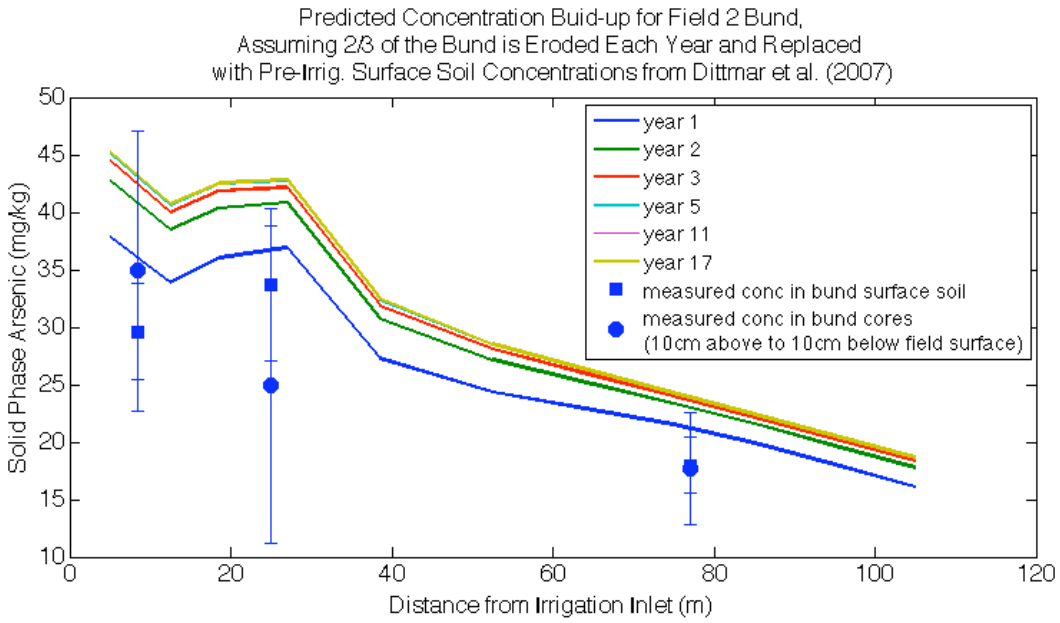

Figure 5.20 Predicted arsenic build-up in the bund of Field 2.

If we assume that less of the bund is eroded each year, then it takes longer to reach steady state and the steady-state concentrations are higher. This calculation implicitly assumes that the residual and replacement soil are perfectly mixed together in the bund, which is likely not the case. However, the exercise demonstrates that partial erosion of the bund can account for the determined arsenic fluxes and the measured solid-phase arsenic concentrations.

5.24. Time Needed for Irrigation to Remediate the Shallow Aquifer

The aquifer sediments in our 9 km^2 study area contain, on average, 629 ng/g of non-crystalline arsenic (Swartz et al., 2004). This number represents the cumulative amount of arsenic removed from the aquifer sediments with a magnesium chloride, phosphate, HCl and oxalic acid sequential extraction (Swartz et al., 2004). If we assume an aquifer porosity of 0.3 and grain density of 2.65 g/cm^3, we calculate that the top 30 m of the aquifer contains:

(629ng As/g sed.)(9 km^2)(1000 m/km)^2(30 m)(0.7)(2.65 g/cm^3)(100 cm/m)^3(10^{-12} kg/ng)

= 315,035 kg As.

In our 9 km^2 study area, rice fields cover 38% of the landscape (Ashfaque, 2007). Assuming that on average, the rice fields receive 1.2 m of irrigation water each season (Figure 2.3) and that the water contains 550 μg/L As (Neumann et al., 2009a and chapter 6), then irrigation removes:

(.38)(9 km^2)(1000 m/km)^2(1.2 m)(550 mg/m^3)(10^{-6} kg/mg) = 2,257 kg As/year.

Thus, it will take (315,035 kg)/(2,257 kg/year) = 140 years to depleted the non-crystalline arsenic reservoir within the top 30 m of the aquifer in our study area.

5.25. References

Abedin, M. J., M. S. Cresser, A. A. Meharg, J. Feldmann, and J. Cotter-Howells (2002), Arsenic accumulation and metabolism in rice (Oryza sativa L.), *Environ. Sci. Technol., 36*, 962-968.

Adomake, A. R. M. Solaiman, P. N. Williams, C. Deacon, G. K. M. M. Rahman, and A. A. Meharg (2008), Enhanced transfer of arsenic to grain for Bangladesh grown rice compared to US and EU, *Environ. Int.,* doi 10.1016/j.envint.2008.07.010.

Ashfaque, K. N. (2007), Effect of hydrological flow pattern on groundwater arsenic concentration in Bangladesh, Ph.D. Thesis, Massachusetts Institute of Technology: Cambridge, MA, pp. 286.

Dittmar, J., A. Voegelin, L. Roberts, S.J. Hug, G.C. Saha, M.A. Ali, A.B.M. Badruzzaman, R. Kretzschmar (2007) Spatial distribution and temporal variability of arsenic in irrigated rice fields in Bangladesh: 2. Paddy soil, *Environ. Sci. Technol.*, 41, 5967-5972.

Hsieh, P. A. (1996), Deformation-induced changes in hydraulic head during ground-water withdrawal, *Ground Water, 34*, 1082-1089.

Neumann, R. B., K. N. Ashfaque, A. B. M. Badruzzaman, M. A. Ali, J. Shoemaker, and C. F. Harvey (2009a), Anthropogenic influences on groundwater arsenic concentrations in Bangladesh, *Nature Geosci.,* accepted.

Neumann, R. B., M. L. Polizzotto, A. B. M. Badruzzaman, M. A. Ali, Z. Zhang, and C. F. Harvey (2009b), The hydrology of a groundwater-irrigated rice field in Bangladesh: Seasonal and daily mechanisms of infiltration, *Water Resour. Res., 45*, doi:10.1029/2008WR007542.

Roberts, L., S. J. Hug, J. Dittmar, A. Voegelin, R. Kretzschmar, B. Wehrli, O. A. Cirpka, G. C. Saha, M. A. Ali, and A. B. M. Badruzzaman (2009), Arsenic mobilization from paddy soils during monsoon flooding, *Nature Geosci.,* Accepted.

Roberts, L., S. J. Hug, J. Dittmar, A. Voegelin, G. C. Saha, M. A. Ali, A. B. M. Badruzzaman, and R. Kretzschmar (2007), Spatial distribution and temporal variability of arsenic in irrigated rice fields in Bangladesh: 1. Irrigation water, *Environ. Sci. Technol., 41*, 5960-5966.

Swartz, C. H., N. K. Blute, B. Badruzzman, A. Ali, D. Brabander, J. Jay, J. Besancon, S. Islam, H. F. Hemond, and C. F. Harvey (2004), Mobility of arsenic in a Bangladesh aquifer: Inferences from geochemical profiles, leaching data, and mineralogical characterization, *Geochim. Cosmochim. Acta, 68*, 4539-4557.

Whiticar, M. J. (1999), Carbon and hydrogen isotope systematics of bacterial formation and oxidation of methane, *Chem. Geol., 161*, 291-314.

Lu, Y., E. E. Adomako, A. R. M. Solaiman, M. R. Islam, C. Deacon, P. N. Williams, G. K. M. M. Rahman, and A. A. Meharg (2009), Baseline soil variation is a major factor in arsenic accumulation in Bengal Delta paddy rice, *Environ. Sci. Technol., 43*, 1724-1729.

6. Anthropogenic Influences on Groundwater Arsenic Concentrations in Bangladesh

Neumann, R. B., K. N. Ashfaque, A. B. M. Badruzzaman, M. A. Ali, J. Shoemaker, and C. F. Harvey (2009), Anthropogenic influences on groundwater arsenic concentrations in Bangladesh, *Nature Geosci.,* accepted.

6.1. Abstract

Researchers have puzzled over the origin of dissolved arsenic in the aquifers of the Ganges Delta since widespread arsenic poisoning from groundwater was publicized two decades ago. Previous work has concluded that biological oxidation of organic carbon drives geochemical transformations that mobilize arsenic from sediments; however, the source of the organic carbon that fuels these processes remains controversial. Here we present a combined hydrologic and biogeochemical analysis of a typical site in Bangladesh where constructed ponds and groundwater-irrigated rice fields are the main recharge sources. We show that only recharge through pond sediments provides the biologically degradable organic carbon that can drive arsenic mobilization. Numerical groundwater simulations as well as chemical and isotopic indicators suggest that contaminated groundwater originates from excavated ponds and that water originating from rice fields is low in arsenic. Furthermore, geochemical modeling shows that likely reactions between pond recharge and aquifer sediments are consistent with the solute composition in arsenic-contaminated water. Our findings indicate that land-use changes have influenced aquifer biogeochemistry, and that patterns of arsenic contamination in the shallow aquifer are due to recharge-source variation and complex three-dimensional flow.

6.2. Introduction

In the shallow (<100 m) aquifers of the Ganges Delta, dissolved arsenic varies between 0.01 to 10 μM over vertical and horizontal distances of tens of meters (BGS et al. 2001). The patterns of dissolved arsenic observed at a variety of sites have not been explained by local differences in the composition of solid aquifer material collected from cores (Dowling et al. 2002, Harvey et al. 2002, Swartz et al. 2004, Zheng et al. 2005, Stollenwerk et al. 2007), and

hence appear to result from upstream differences in groundwater chemistry. At our field site in the Munshiganj district of Bangladesh, groundwater arsenic concentrations measured below rice fields and village peripheries have a distinct bell-shaped profile that peaks at approximately 30 m (Figure 6.1a), the depth at which most wells extract water (Harvey et al. 2006). A similar arsenic pattern has been observed at other sites (BGS et al. 2001, Dowling et al. 2002, Anawar et al. 2003, Van Geen et al. 2003, Stollenwerk et al. 2007, Mitamura et al. 2008) and regionally (BGS et al. 2001) (see supporting information, chapter 7).

Previous research at our site provides some insight into the source of the contaminated water. Tritium–helium-3 analysis has shown that the water at the depth of the arsenic peak is roughly 50 years old (Klump et al. 2006), and analysis of the carbon-14 dates of methane and dissolved inorganic carbon has shown that the carbon source for microbial respiration was recently (<700 years) transported from the surface (Harvey et al. 2002). A water balance shows that groundwater-irrigated rice fields and constructed ponds contribute most of the recharge to the aquifer, while river discharge and irrigation pumping drain the aquifer (Harvey et al. 2006). However, two key questions remain: what is the recharge source for the contaminated groundwater and what is the source of the organic carbon responsible for arsenic mobilization?

Here we present hydrogeologic and biogeochemical data that indicate recharge entering through organic-rich and permanently anoxic pond sediments contains biologically available organic carbon and is likely responsible for arsenic-contaminated groundwater, whereas recharge from irrigated rice fields lacks biologically available organic carbon and remains low in arsenic. The finding that recharge through anoxic pond sediments drives arsenic mobilization is consistent with a recent study in Cambodia (Benner et al. 2008, Polizzotto et al. 2008) that found arsenic was mobilized into recharge entering the aquifer through the anoxic sediments of

wetlands. However, due to human intervention, the groundwater system in Bangladesh differs from that in Cambodia. Many ponds in Bangladesh have been excavated in the last fifty years (see supporting information, chapter 7) and groundwater irrigation has greatly altered subsurface flow paths (Harvey et al. 2006).

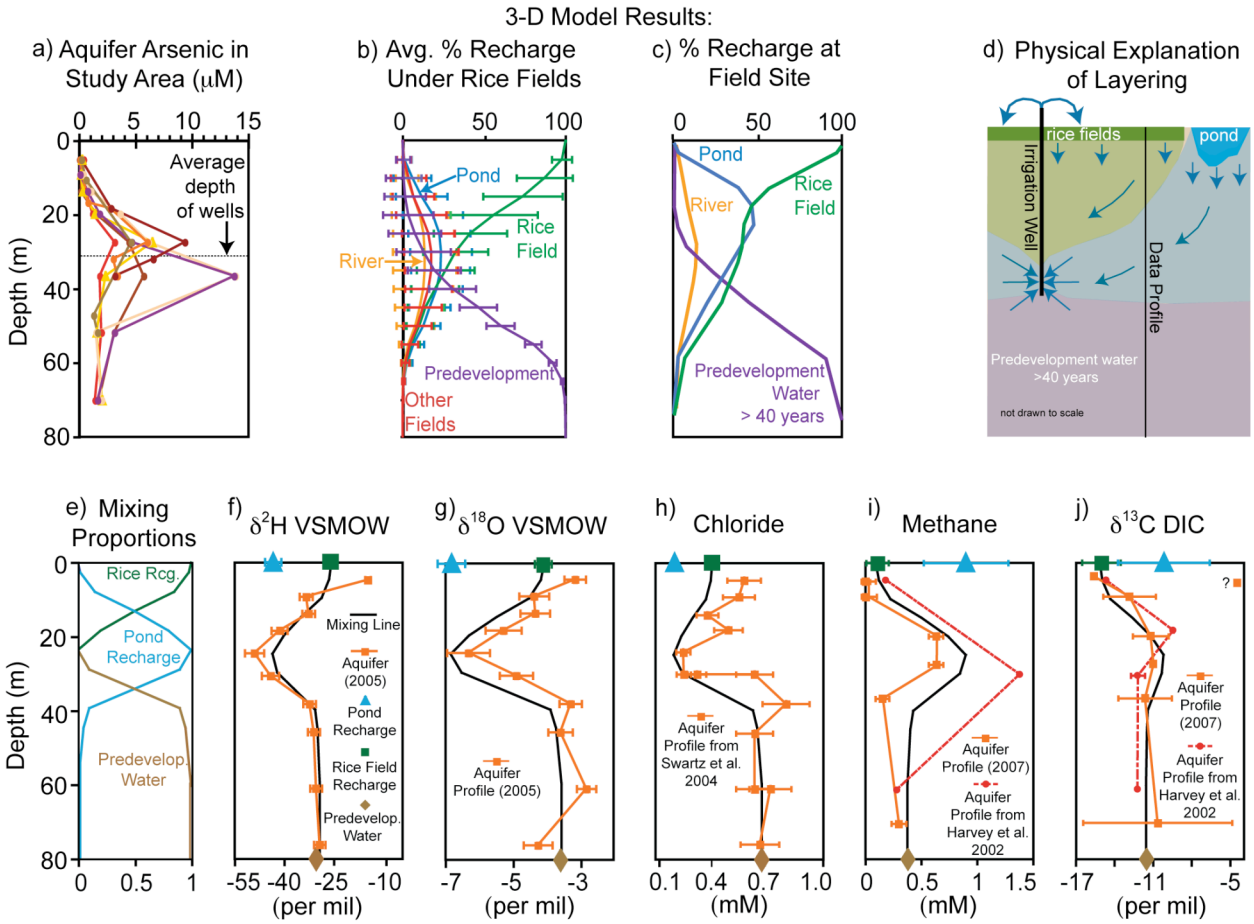

Figure 6.1 Concentration and recharge profiles in Munshiganj, Bangladesh
a) Arsenic concentrations in seven well clusters within a 0.03 km^2 area.

b&c) Layering of recharge predicted by the three-dimensional groundwater flow model 40 years after the development of ponds and groundwater-irrigated rice agriculture.
(b) Average percent of groundwater beneath rice fields derived from different recharge sources. The error bars represent one standard deviation. The average values were calculated from model data at grid points (5 m spacing) located beneath areas where rice fields contribute 100% of the recharge in the shallowest aquifer layer (see Methods, section 6.8). Figure 6.2b presents the amount of pond recharge at these grid-point locations. (c) Recharge at the location of the observation wells from which we collected detailed geochemical data (Swartz et al. 2004). This

local recharge profile is consistent with the understanding of regional groundwater flow and the average recharge profile in panel (b).

d) Physical description of recharge layering in the aquifer.

e) Recharge mixing proportions used to predict the aquifer concentrations shown in black within panels (f-j). The profile was developed with output from the numerical model for the location of our observation wells (Figure 6.1c) (see Methods, section 6.8).

f–j) Measured (orange and red data points) and predicted (black) concentrations of (f) deuterium, (g) oxygen-18, (h) chloride, (i) methane, and (j) carbon-13 in dissolved inorganic carbon in the aquifer. Unless specified, error bars represent analytical uncertainty. Aquifer concentrations were predicted by combining measured recharge concentrations in the proportions shown in panel (e). The pond (blue triangle) and rice-field (green square) recharge concentrations were measured and the predevelopment water concentration (brown diamond) was set to match the deepest aquifer samples.

Panels (f–h): The pond value is the average concentration of samples collected throughout the surface-water columns of a young and old pond and the rice field value is the average concentration of pore water samples collected from depths of 0.5 to 1.7 m in the bund. Error bars represent one standard deviation. Panels (i–j): Concentrations represent pore water samples collected (i) 2.7 m below the young pond's bottom and 1.7 m within the rice field bund and (j) 20 cm below the old pond's bottom and 1.2 m within the rice field bund.

6.3. The Groundwater Flow System and Tracers of Recharge

To investigate the origin of contaminated water we numerically simulated transient three-dimensional groundwater flow, tracking recharge from different surface sources through the modeled groundwater system. The model domain (Figure 6.2a) was chosen as a 9 km^2 area bounded on one side by a zero gradient condition and on the other three sides by rivers represented in the model by prescribed heads along the river bed and zero flux conditions extending from the centre line of the river to the base of the underlying aquifer, 90 m deep. Within this domain, ponds (~11% of the area), villages (~22% of the area), irrigated rice fields (~38% of the area), non-irrigated fields (~27% of the area) and 35 irrigation wells are distributed approximately uniformly. Pump tests provided drawdown data for characterizing model parameters, hydraulic conductivity and specific storage (see supporting information, chapter 7). The simulation was initiated with a steady-state solution for average annual river stages and

recharge fluxes under predevelopment conditions, without constructed ponds or irrigated rice fields. Then ponds, rice fields and irrigation pumping were added to the model, and the system was simulated on weekly time steps, with seasonally varying river heads and recharge, for forty years. Inflow from the ponds, irrigated rice fields, non-irrigated fields, and the river was tracked through the system by simulating advection and dispersion of conservative tracers.

The simulation shows that beneath rice fields, where our clusters of observation wells collect data, pond recharge is focused at the depth of the arsenic peak (Figure 6.1b–c and Figure 6.2b). Following monsoon flooding in November and December, stream tubes emanating from ponds extend towards the rivers below a layer of rice-field recharge. Then in January, when irrigation begins, the flow pattern shifts to local flow cells that converge on irrigation wells. Irrigation pumping is the largest annual discharge from the system, and flow is focused towards the depth of well screens at approximately 30 m. These processes result in a layered groundwater flow system beneath rice fields where rice-field water overlies pond inflow, which overlies centuries-old water that recharged the system prior to development (Figure 6.1b–d). Pump tests found a ratio of horizontal to vertical hydraulic conductivity within the aquifer of ~25. This large anisotropy enhances layering of ground water from different sources by focusing flow into horizontal paths (see supporting information, chapter 7).

Direct measurements of pan evaporation and water levels in seven ponds show that ponds lose, on average, ~1 cm/day of water during the dry season to the shallow aquifer (Harvey et al. 2006). Local villagers report that water loss from ponds declines over time, a behaviour that may result from the accumulation and clogging of pond sediments (Welch 1952). This process could explain why not all ponds in Bangladesh or West Bengal currently lose water at significant rates

(Harvey et al. 2006, Sengupta et al. 2008) and also implies that groundwater that is decades old could have originated from ponds of the same age that are no longer contributing much recharge.

In agreement with the physical evidence, the chemical signature of high-arsenic groundwater points towards ponds as the source of the contaminated water. The depth profiles in our observation wells of stable water isotopes and chloride, as well methane, which appears to behave conservatively, match profiles predicted by end-member mixing of concentrations measured in the different recharge sources, with pond recharge dominating the depth at which arsenic is elevated (Figure 6.1f–i, see chapter 7 for details regarding stable water isotopes). In fact, the chemical signature measured in the shallowest aquifer depths is matched by that measured in the rice field recharge, while the chemical signature measured at the depth of the arsenic peak is matched by that measured in the pond recharge. The chemical evidence supports both our understanding of the layered groundwater flow system and assertion that rice field recharge produces groundwater low in arsenic while pond recharge produces groundwater elevated in arsenic.

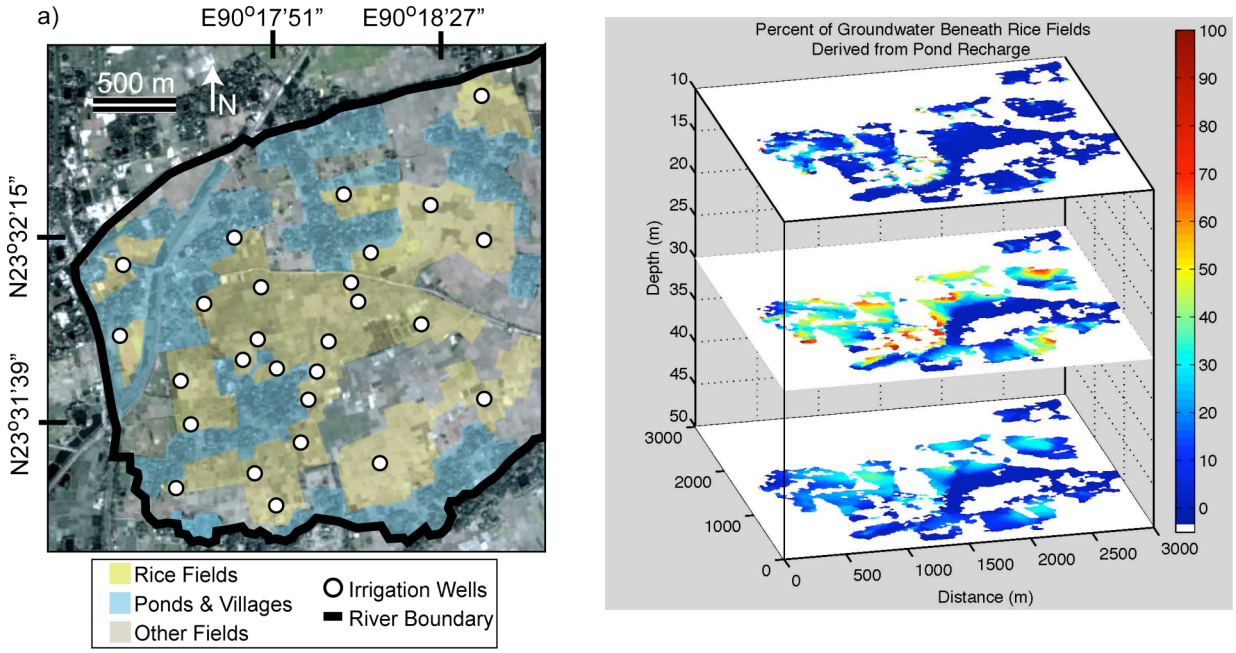

Figure 6.2 Three-dimensional groundwater flow and transport model.

a) Model domain.

b) The percent of groundwater derived from pond recharge at three different depths at grid points (5 m spacing) located beneath areas where rice fields contribute 100% of the recharge in the shallowest aquifer layer (see Methods, section 6.8). In the domain of interest, pond recharge peaks at the depth of elevated arsenic concentrations.

6.4. Reactivity of Pond and Rice-Field Recharge

Recharge from ponds contains biologically degradable organic carbon (BDOC) unlike the rice-field recharge that contains primarily recalcitrant organic carbon. BDOC is operationally defined as the fraction of organic carbon that is oxidized by microbes in the presence of oxygen (Servais et al. 1987) and is therefore a measure of how much of the total DOC may drive sediment transformations that mobilize arsenic. We measured BDOC in pore water extracted from sediments >0.5 m beneath two ponds (an old and young pond) and a rice field. Both water types contained 0.4 to 1.1 mM of recalcitrant DOC, but the recharge leaving the ponds also contained ~0.5 mM of BDOC (Figure 6.3 and chapter 7).

Even though rice fields are one of the largest sources of water to the aquifer, they do not appear to contribute recharge that can mobilize arsenic. Due to the low conductivity of the plough pan, most irrigation return-flow bypasses the anoxic and organic-rich shallow soil, and instead enters the subsurface through bunds, the un-ploughed, raised boundaries around the perimeter of fields (chapter 2 and Neumann et al. 2009). Much of the BDOC in this water is likely sorbed by the bund soil (Jardine et al. 1989) or oxidized before it enters the bund because the standing water in the field is supersaturated with oxygen when photosynthesis is high (Kirk 2004) (see supporting information, chapter 7). Rice fields appear to remove arsenic from the groundwater system (see supporting information, chapter 7). Arsenic concentrations in the irrigation water applied to rice fields are much higher (~5 μM) than the concentrations in recharge returning to the aquifer (~0.15 μM) (Figure 6.4b). Most of the irrigation arsenic remains in the rice field soils (Dittmar et al. 2007, Panaullah et al. 2009), and is removed from the fields when the monsoon floods recede (Roberts et al. 2009).

We hypothesize that microbial oxidation of the ~0.5 mM BDOC in pond recharge is responsible for the arsenic contamination found in the aquifer. A variety of previous laboratory incubation studies (Akai et al. 2004, Islam et al. 2004, Van Geen et al. 2004, Radloff et al. 2007) have found that the addition of labile organic carbon, or BDOC, mobilizes arsenic from Bengali aquifer sediments. Under a pond that loses ~1.5 cm/day of water to the subsurface, sampling lysimeters show that dissolved arsenic increases with depth; although, at the deepest sampling point, arsenic has not reached the peak concentration measured in the aquifer (Figure 6.4a).

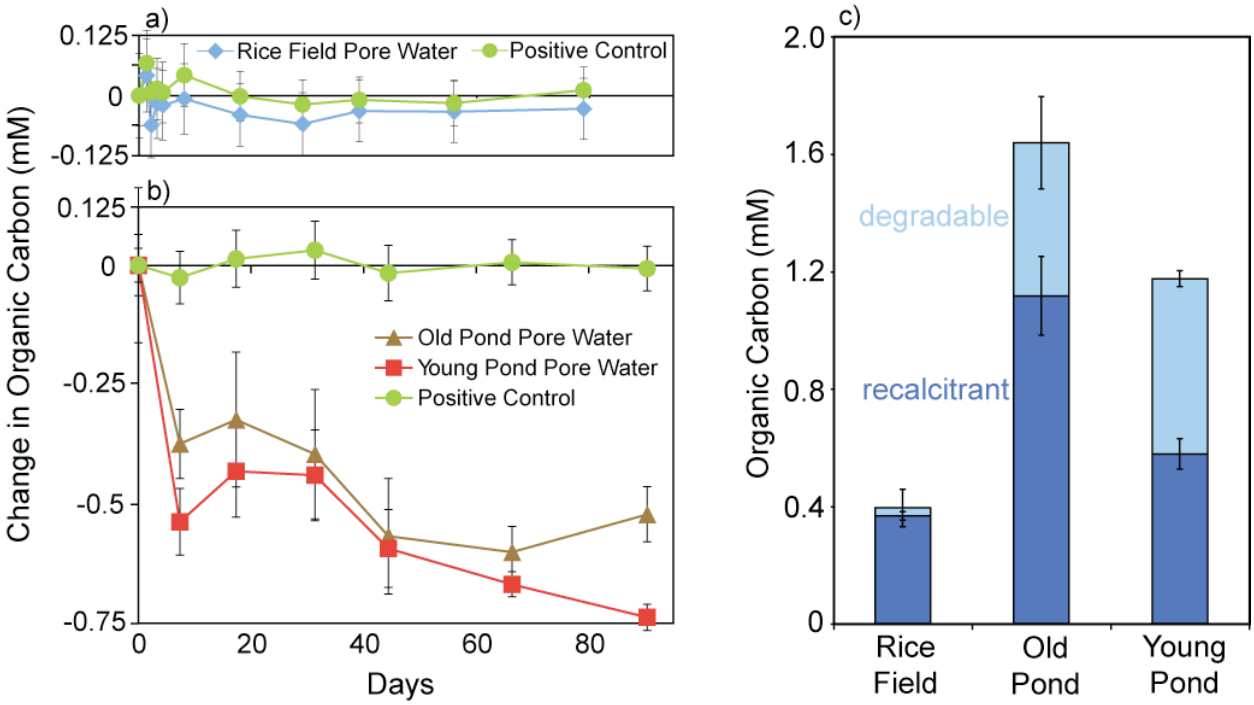

Figure 6.3 BDOC experiment.

a & b) Oxygen incubation of a) rice field pore water from a depth of 1.7 m in the bund and b) pond pore water from 0.5 m and 2.7 m below the bottom of a young and old pond, respectively. The positive control is Potassium Acid Phthalate. Error bars represent analytical uncertainty.

c) Recalcitrant organic carbon and BDOC for rice field and pond recharge. Error bars for recalcitrant carbon represent analytical uncertainty and for BDOC represent propagated error for the difference between initial and final concentrations.

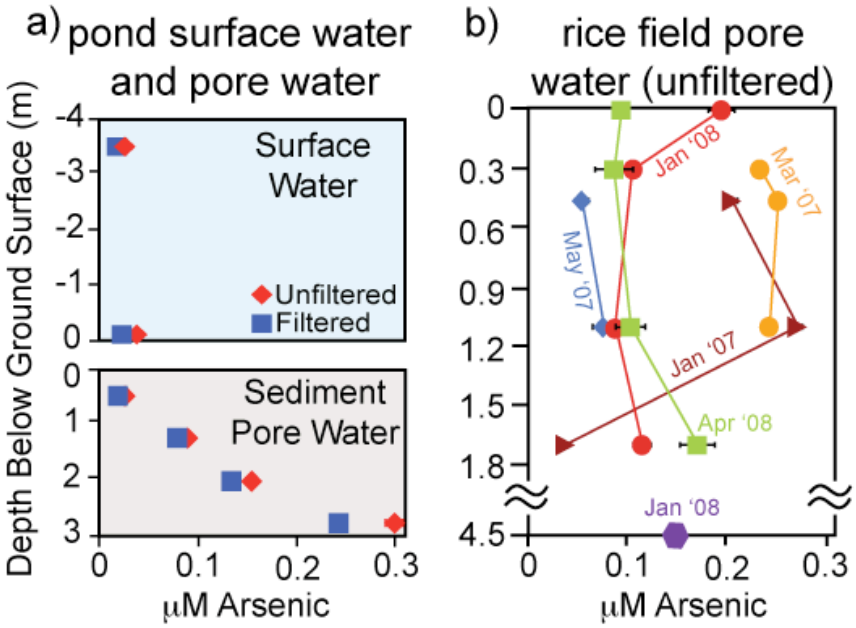

Figure 6.4 Arsenic concentrations beneath recharge sources.

Dissolved arsenic within a) the surface and pore water of a young (<50 years) pond and b) within the pore water of a rice field bund and a shallow aquifer well installed in the field. Error bars represent analytical uncertainty.

6.5. Arsenic Mobilization from Soils and Sediments

Several biogeochemical pathways may liberate arsenic as pond recharge carries BDOC into the aquifer, including magnetite reduction, arsenic desorption, biotite weathering and apatite dissolution; any set of these reactions may be occurring individually or simultaneously at a given location. The proposed pathways are consistent with our data and supported by PHREEQ-C inverse modeling (see supporting information, chapter 7). The PHREEQ-C modeling assumed thermodynamic equilibrium, which is reasonable given our 50-year travel time (Klump et al. 2006), and homogeneous aquifer geochemistry, which is supported by our previous sediment studies (Swartz et al. 2004).

Magnetite is the only phase containing Fe(III) detected in the aquifer sediment at our field site (Swartz et al. 2004, Polizzotto et al. 2006) and concentrations of potential aqueous electron acceptors, such as oxygen, nitrate and sulfate, are extremely low (Swartz et al. 2004). The small 150 μm authogenic cuboidal magnetite crystals observed in our sediments have the highest arsenic content of all the mineral fractions (Swartz et al. 2004). Oxidation of the 0.5 mM BDOC by magnetite would release 0.47 to 0.87 μM arsenic per pore volume and dissolution of all the magnetite would release 21 to 106 μM arsenic (see supporting information, chapter 7), much more than necessary to explain the peak arsenic concentration. Column and mineralogical studies have shown that the biogenic formation of mixed Fe(III)/Fe(II) phases often sequesters arsenic (As(V) and As(III)) (Coker et al. 2006, Kocar et al. 2006), but that full reduction of the mixed-iron phase results in arsenite (As(III)) mobilization (Tufano and Fendorf 2008). At the 30-m-aquifer depth, arsenic is predominately found as As(III) (Swartz et al. 2004), and based on the reducing nature of pond-sediment pore water (i.e., elevated methane concentrations, Figure 6.5), arsenic is likely also found as As(III) within the pond recharge water, although speciation in

the pore water was not explicitly measured. Because the magnetite was formed *in situ*, previous conditions must have favored magnetite formation. However, magnetite reduction is now thermodynamically favorable; the change in Gibbs free energy for the reduction of magnetite with glucose, a model compound for BDOC, is negative for both the pond recharge and the 30-m-deep-aquifer water (see supporting information, chapter 7).

Hydrogen concentrations, which are indicators of the predominant electron-accepting process (Lovley and Goodwin 1988, Chapelle et al. 1995), could provide the data needed to support or exclude magnetite as the primary electron acceptor for BDOC oxidation. In particular, these data could clarify the evolution of electron-accepting processes along a pond-recharge flow path as the BDOC travels from the pond into the aquifer. At the 30-m-aquifer depth, dissolved hydrogen concentrations (10nM, (Harvey et al. 2002)) are indicative of methane production, not iron reduction (Lovley and Goodwin 1988). Thus, it is unlikely that the proposed magnetite-reduction process occurs at this depth in the aquifer. It is possible magnetite reduction occurs at shallower depths within the aquifer and ceases once the BDOC is completely oxidized or magnetite is locally depleted, which could occur if the BDOC–magnetite reaction rate is greater than the BDOC transport rate through the aquifer.

As the pond recharge is transported to the 30 m-aquifer depth, phosphorus, calcium magnesium, and sodium increase (Figure 6.5b). Phosphate released from the reductive dissolution of magnetite or from microbial weathering of apatite for phosphate nutrient acquisition (Welch et al. 2002, Mailloux et al. 2009) can explain the increased phosphorus concentrations. Microbial weathering of Himalayan apatite has recently been demonstrated, and this process can liberate arsenic (Mailloux et al. 2009). Apatite dissolution can also explain the increased calcium concentrations and the tight correlation between arsenic and calcium at our

field site (Harvey et al. 2002). Increases in calcium, magnesium and sodium can be explained by the dissolution of carbonate minerals such as calcite, dolomite or nahcolite, which are all undersaturated in the pond recharge (see supporting information, chapter 7). Phosphate or carbonate released from any of these processes can compete with arsenic for sorption sites, leading to arsenic desorption (Smedley and Kinniburgh, 2002). It is also possible that the cation increase is a by-product of silicate weathering promoted by an initial decrease in pH as BDOC is oxidized to DIC. Hornblende, albite and biotite are all present in the aquifer sediments (Swartz et al. 2004) and other researchers have suggested that chemical weathering of silicates releases arsenic to the groundwater (Itai et al. 2008, Seddique et al. 2008).

We attribute the decrease in iron, manganese and silica (Fig 5b) to the precipitation of siderite, vivianite, SiO_2, and rhodocrosite, all minerals that are supersaturated in the 30m-deep aquifer water and are predicted to precipitate (see supporting information, chapter 7). In addition, Swartz et al.'s (2004) geochemical model of our site required the precipitation of siderite, vivianite, and amorphous SiO_2 to reproduce the dissolved concentrations of Fe(II), phosphate and silicate.

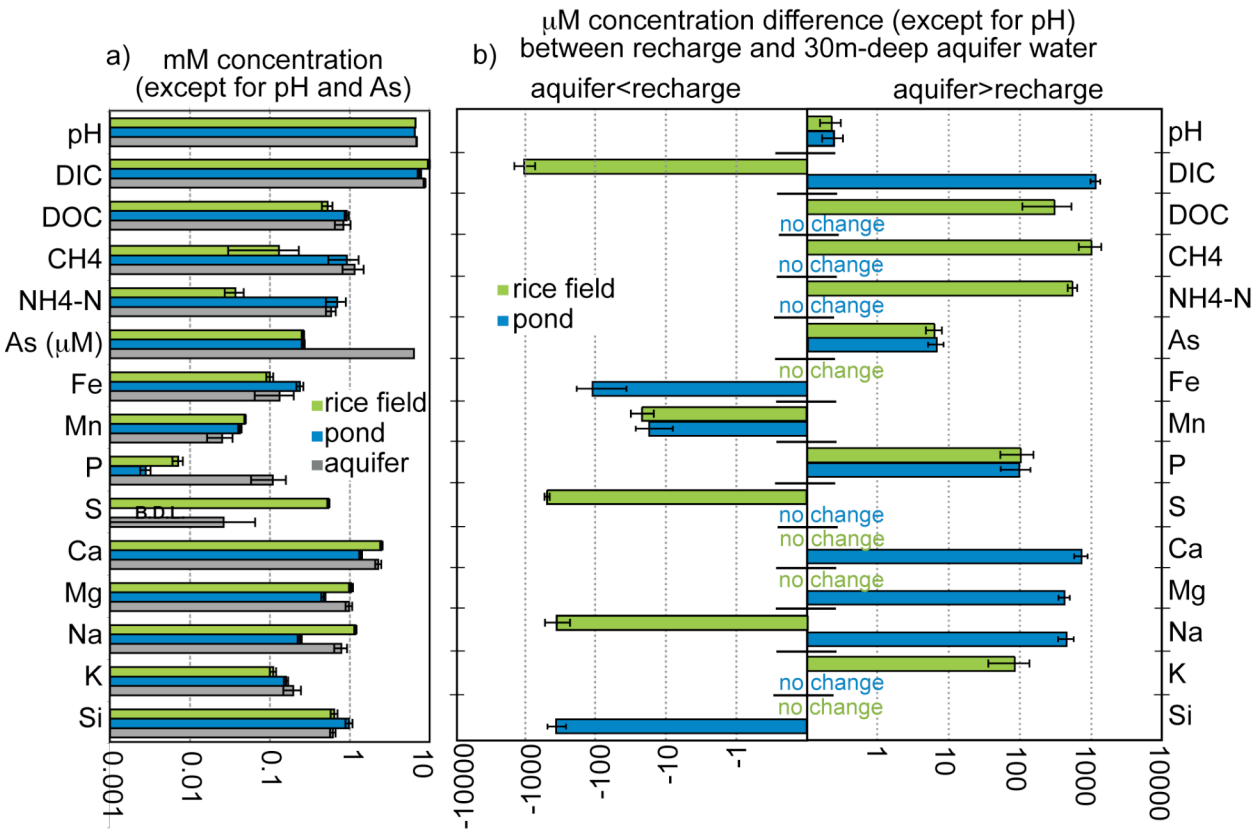

Figure 6.5 Chemical characteristics of recharge and aquifer water.

a) Solute concentrations (mM, except for pH and As) measured in pore water 1.07 m deep in a rice field bund (green), 2.7 m below the bottom of a young pond (blue), and 30 m deep within the aquifer (Swartz et al. 2004, Roberts et al. 2007) (grey). Pond and rice field error bars represent analytical uncertainty and aquifer error bars represent the standard deviation of all measurements taken at our site from 30 m-deep wells (Swartz et al. 2004, Roberts et al. 2007). Data are available in Table 7.2.

b) Concentration differences (mM, except for pH) between 30 m-deep aquifer water and both rice field (green) and pond (blue) recharge. Error bars represent the propagated error from panel (a). Comparison shows pond recharge can provide the high concentrations of ammonium and methane, and low concentrations of sulfur correlated with severe arsenic contamination throughout Bangladesh (BGS et al. 2001, Dowling et al. 2002, Harvey et al. 2002, Anawar et al. 2003, Stollenwerk et al. 2007, Itai et al. 2008, Mitamura et al. 2008), while the rice field recharge is depleted in ammonium and methane and elevated in sulfur.

6.6. Carbon Transformations and Carbon Dates

The hypothesis that the arsenic contaminated water originated as pond recharge is further supported through a combined analysis of the measured BDOC fraction and radiocarbon ages. At the depth of the arsenic peak, DIC has a young radiocarbon age, ~700 years, while dissolved organic carbon is old, 2000 to 4000 years (Harvey et al. 2002). This discrepancy in radiocarbon ages in the same water samples strongly limits the possible origins for carbon. First, the DIC could not have entirely originated from the DOC, or from the same organic carbon source as the DOC. Second, a large portion of the DIC at the arsenic peak must have been transported from the surface or overlying sediments. Third, a portion of the DOC must have been liberated from the sediment into younger groundwater.

Given these three constraints, the oxidation of BDOC from the surface offers a plausible explanation for the observed radiocarbon and δ^{13}C-DIC signature: the ~9 mM (Figure 6.5a) of DIC in contaminated groundwater with a radiocarbon age of ~700 years and δ^{13}C signature of -11 per mil (Figure 6.1j) can be explained as a mixture of ~7.5 mM modern (1750 to 1960) pond DIC (Figure 6.5a) with δ^{13}C of -10 per mil (Figure 6.1j), ~0.5 mM modern oxidized BDOC delivered by pond recharge (Figure 6.3) with δ^{13}C of -25 per mil (Clark and Fritz 1997), and ~1 mM of ~5000 years-old DIC dissolved from carbonate minerals with δ^{13}C of 0 per mil (Clark and Fritz 1997). The DOC at the arsenic peak can also be explained as young DOC from the surface mixed with old material dissolved from sediments. The radiocarbon age of the ~0.8 mM DOC at the arsenic peak is explained by the release of ~0.4 mM of old detrital organic carbon (~5000 years old) into groundwater containing ~0.4 mM of modern organic carbon. These concentration constraints suggest that a portion of the ~1 mM of young recalcitrant organic carbon entering the aquifer with the pond recharge (Figure 6.3b) exchanged with old organic

carbon on the aquifer sediments, which could occur if the young carbon was more hydrophobic than the old carbon (Kaiser and Zech 1998). The radiocarbon calculations imply that the pond recharge currently seen at the 30 m aquifer depth is 50 to 250 years old, in rough agreement with the 50-year-old tritium-helium-3 ages measured at this depth (Klump et al. 2006). Therefore, ponds excavated approximately 50 years ago are likely responsible for the contamination currently found at the 30 m aquifer depth, while recently excavated ponds currently recharging the aquifer could potentially be responsible for future contamination.

Neither methanogenesis nor methane oxidation appear to alter DIC and DOC levels within the aquifer. Methane concentrations do not noticeably increase as the pond recharge travels from the pond sediments to the 30-m aquifer depth (Figure 6.1i), although methanogenesis may be occurring at a low level. It is also unlikely that significant methane oxidation occurs because concentrations of the common electron acceptors for methanotrophy (oxygen, sulfate (Orphan et al. 2002), and possibly nitrate (Raghoebarsing et al. 2006)) were all found to be extremely low (μM concentrations) in the aquifer water (Harvey et al. 2002, Swartz et al. 2004).

6.7. Broader Impacts

Our data indicate that extensive excavation of ponds, concurrent with the development of groundwater-irrigated rice agriculture, has altered both the geochemical input to aquifers and the patterns of groundwater flow. Several other theories could potentially explain part of the arsenic pattern with depth. The increase in arsenic concentrations from the top of the aquifer to centre of the pond-recharge plume could be explained by longer exposure times of the groundwater to sediment (Stute et al. 2007) or decreased volumes of flushing with depth (McArthur et al. 2004, Stute et al. 2007, van Geen et al. 2008). However, these other theories are contradicted by the

decrease in arsenic concentrations from the plume centre downwards, and the close match between indicators of pond recharge and elevated arsenic concentrations (Figure 6.1f–i).

Predicting how concentrations will change at a particular location is challenging: new sources of recharge, ponds or rice fields, work to increase or decrease dissolved arsenic concentrations; shifting flow patterns could draw groundwater with either lower or higher concentrations towards a particular location; and increased flushing could reduce concentrations (McArthur et al. 2004, Stute et al. 2007, van Geen et al. 2008). Furthermore, arsenic levels may have been high at some locations for hundreds of years where oxides were reduced by either detrital organic carbon or recharge from natural wetlands, rivers or ponds rich in organic carbon. All of these complexities are compounded by transience of chemical concentrations. While groundwater potentials and velocities adjust quickly to changes, solute concentrations require at least as long as the travel time through flow paths before they reach new steady states. The groundwater residence time in aquifers under current conditions is decades to centuries (Harvey et al. 2002, Harvey et al. 2006, Klump et al. 2006), and over the last decades irrigation pumping has greatly altered flow patterns. Thus, the composition of much of the groundwater is likely still adjusting to anthropogenic changes that could act to increase or decrease arsenic concentrations.

Despite the complexity of these processes, our results have several implications for safe drinking water. Throughout Bangladesh, and in some other regions where arsenic contamination is likely (Manouchehr et al. 2008), our research suggests that the development of artificial ponds above wells should be avoided if it is possible, and that drinking water wells should not be placed downstream of recharge from existing ponds, wetlands, rivers or other permanently saturated water bodies potentially elevated in organic carbon. Our results also suggest that shallow wells beneath rice fields could offer a source of safe groundwater, particularly if

accumulated arsenic in the rice field is removed annually during flooding (Roberts et al. 2009). Such wells outside of villages would be inconvenient, and any program to install these would require further testing and long-term monitoring. Finally, our results support moving drinking water wells into deeper Pleistocene aquifers where arsenic concentrations are low, while leaving irrigation wells in the shallow aquifer (Michael and Voss 2008). The hydraulic barrier imposed by shallow irrigation pumping (Michael and Voss 2008) could prevent local recharge from reaching the deep aquifer. This solution requires testing and continual monitoring of the deeper wells (Van Geen et al. 2007), and does not prevent arsenic from entering the rice crop and the human diet (Meharg and Rahman 2003, Williams et al. 2006, Pal et al. 2009); but it could significantly decrease human consumption of arsenic by decreasing concentrations in drinking water.

6.8. Methods

Here we describe the methods used to characterize the groundwater flow system. Further details on these methods are given in Ashfaque (2007) and descriptions of chemical methods are given in the chapter 7. Seasonal water budgets and land-use patterns are presented in Harvey et al. (2006), hydrostratigraphy is described in Swartz et al. (2004), and rice field water budgets are given in Neumann et al. (2009) and chapter 2. In this study, hydraulic parameters were assessed with pump test data and model fits to hydraulic head. Sixty single-well pump tests were performed and analysis of the drawdown curves (see supporting information, chapter 7) shows that hydraulic conductivity varies little among wells, although specific storage is greater in the upper region of the aquifer. A multi-observation well pumping experiment was conducted to assess aquifer hydraulic properties at the 100m scale. After the rice season, an irrigation well was pumped and drawdowns were recorded in eleven observation wells (see supporting information, chapter 7). Aquifer parameters were estimated by fitting modeled heads to the observed heads at these eleven locations using the finite element software FEFLOW (Diersch 2002) coupled with the parameter estimation software PEST (Doherty 1994). The results are consistent with the single-well tests, but also indicate an anisotropy ratio of 25 for horizontal to vertical hydraulic conductivity. These parameter estimates also agree with those estimated by fitting the large-scale model described below to observed seasonal variations in heads (see supporting information, chapter 7).

A transient 3-dimensional numerical model constructed with FEFLOW(Diersch 2002) was used to trace recharge through the aquifer (Figure 6.1b–c and 6.2b). The ~9 km^2 domain was divided into 20 layers and discretized into 250,000 elements. The model was forced by seasonal shifts in river stages, irrigation rates, and rain and evaporation rates (Harvey et al. 2006).

Observed seasonal river stages were used as prescribed heads in the river channels. No-flow boundaries extended from the centre line of the river channels to the base of the aquifer to represent convergent flow into the rivers from both sides following monsoon flooding and recharge from the river to the aquifer during the onset of flooding. A no-flow boundary also extended across the east side of the domain and across the base of the aquifer, which rests on a 30-m-thick marine clay.

Because the model represents an area of square kilometers, it does not attempt to resolve the tightly woven mosaics of ponds and raised areas that results from the construction of villages. Villages are built above flood levels by excavating clay from pits that subsequently form ponds. Joint village/pond areas are represented with effective values that maintain the correct volume of water within the pond area while preserving the mass balance between pond drainage and flux into the aquifer. This is achieved by using the fraction of the village/pond area filled by ponds as the storage coefficient.

The flux applied to non-irrigated fields was calculated as the difference between rain and evapotranspiration. Evapotranspiration was set to pan-evaporation when the water table was at the surface, but decreased to zero as the water table fell to a one-meter depth. The flux applied to irrigated fields was the sum of the atmospheric flux (rain minus evaporation) and irrigation (volumetric rate withdrawn from the irrigation wells applied over the area of irrigated fields).

The contribution of different recharge sources was traced through the 3-D groundwater system by simulating advection and dispersion of conservative tracers introduced into each of the sources. First, the model was run to steady state under pre-development conditions, without irrigation or constructed ponds. Then, the model was run on a weakly time-step under current

conditions with seasonally-varying forcings for forty years, the approximate history of development.

The model represents flow conditions at scales greater than 20 m, not the small-scale at which variations in flow patterns may affect individual wells. The model does not differentiate individual ponds with different recharge rates (Harvey et al. 2006), incorporate bunds that control local infiltration rates within rice fields (Neumann et al. 2009 and chapter 2), nor represent the sharp interfaces between solutes transported along adjacent stream tubes. By not explicitly incorporating recharge through bunds, which form the perimeters of all rice fields (Neumann et al. 2009 and chapter 2), the model incorrectly predicts that pond water flows laterally immediately beneath some adjacent rice fields. This artifact was corrected in Figure 6.1b and 6.2b by using only the regions where 100% of the recharge contribution in the shallowest aquifer layer comes from rice fields. The large-scale structure of the model also leads to over-prediction of vertical mixing, although it accurately represents the peak depths of the different recharge sources. Model values of dispersivity were set higher than realistic to prevent numerical oscillations. This is a conventional approach for field-scale simulations of advective dispersive transport (Zheng and Bennett 2002). This artifact was corrected in the end-member mixing profile (Figure 6.1e). The locations of the model-determined (Figure 6.1c) recharge maxima for pond, rice field, and predevelopment water were retained, but the peak widths refined.

6.9. Acknowledgments

This work was supported by NSF EAR 0651678 and 0605515, and Center for Environmental Sensing and Modeling at the Singapore MIT Alliance for Research and Technology. We thank Matthew Polizzotto, Sarah Jane White, Jennifer Jay, Tiffany Lin, Linda

Roberts and Jessica Dittmar for help in the field; Allison St. Vincent, Farah Khan, Kajetan Zwieniecki, Stephan Hug, Uli Mayer, Olga Singurindy, Charuleka Varadharajan, Guangchao Li, Peter Jewett, Brian Jackson, Paul Zietz, Rodney Baker, Joshua Landis, and Janet Gabites for sample analysis help; Jenny Jay, Chu-Ching Lin, and the research groups of Philip Gschwend and Harold Hemond for intellectual support; Anis and Mitu at B.U.E.T. and the people of Bashailbhog village, especially Ripon Chowdhury, Sojib Chowdhury, Sha'alam, and Rasil for their instrumental support of our project.

6.10. Author Contributions

R.B.N. and C.F.H. wrote the manuscript; C.F.H. conceived and funded the project; A.B.M.B. and M.A.A. provided logistical support for the field work, including the arrangements for establishing the field site; K.N.A. oversaw the installation of all the aquifer wells, collected the arsenic data from the aquifer wells, developed the 3-D numerical model, performed field experiments to parameterize and constrain the model, and collected all of the d18O and d2H data prior to 2008; R.B.N. installed the rice field and pond lysimeters, collected the chemical data for the pond and rice field recharge, collected all d18O and d2H data from 2008, created the end-member mixing profiles, developed the PHREEQC inverse models, and conceived of and carried out the BDOC experiment; R.B.N. and J.K.S. collected the methane data for the aquifer wells, the rice field, and the pond; J.K.S. collected the 2007 carbon-13 data for the aquifer wells, the rice field and the pond.

6.11. References

Akai, J., K. Izumi, H. Fukuhara, H. Masuda, S. Nakano, T. Yoshimura, H. Ohfuji, H. M. Anawar, and K. Akai (2004), Mineralogical and geomicrobiological investigations on groundwater arsenic enrichment in Bangladesh, *Appl. Geochem., 19*, 215-230.

Anawar, H. M., J. Akai, K. Komaki, H. Terao, T. Yoshioka, T. Ishizuka, S. Safiullah, and K. Kato (2003), Geochemical occurrence of arsenic in groundwater of Bangladesh: sources and mobilization processes, *J. Geochem. Explor., 77*, 109-131.

Ashfaque, K. N. (2007), Effect of hydrological flow pattern on groundwater arsenic concentration in Bangladesh, Ph.D. Thesis, Massachusetts Institute of Technology: Cambridge, MA, pp. 286.

Benner, S. G., M. L. Polizzotto, B. D. Kocar, S. Ganguly, K. Phan, K. Ouch, M. Sampson, and S. Fendorf (2008), Groundwater flow in an arsenic-contaminated aquifer, Mekong Delta, Cambodia, *Appl. Geochem., 23*, 3072-3087.

BGS, DFID, and DPHE (2001), Arsenic contamination of groundwater in Bangladesh, *BGS Technical Report WC/00/19, Volume 1 & 2*, British Geological Survey, Keyworth.

Chapelle, F. H., P. B. McMahon, N. M. Dubrovsky, R. F. Fujii, E. T. Oaksford, and D. A. Vroblesky (1995), Deducing the distribution of terminal electron-accepting processes in hydrologically diverse groundwater systems, *Water Resour. Res., 31*, 359-371.

Clark, I. D., and P. Fritz (1997), *Environmental Isotopes in Hydrogeology,* Lewis Publishers, Boca Raton.

Coker, V. S., A. G. Gault, C. I. Pearce, v. G., N. D. Telling, J. M. Charnock, D. A. Polya, and J. R. Lloyd (2006), XAS and XMCD Evidence for Species-Dependent Partitioning of Arsenic During Microbial Reduction of Ferrihydrite to Magnetite, *Environ. Sci. Technol., 40*, 7745-7750.

Diersch, H. J. G. (2002), *FEFLOW finite element subsurface flow and transport simulation system, Release 5.0, User's Manual / Reference Manual / White papers,* WASY Ltd., Berlin.

Dittmar, J., A. Voegelin, L. Roberts, S. J. Hug, G. C. Saha, M. A. Ali, A. B. M. Badruzzaman, and R. Kretzschmar (2007), Spatial distribution and temporal variability of arsenic in irrigated rice field in Bangladesh: 2. Paddy soil, *Environ. Sci. Technol., 41*, 5967-5972.

Doherty, J. (1994), *PEST,* Watermark Computing, Corinda, Australia.

Dowling, C. B., R. J. Poreda, A. R. Basu, S. L. Peters, and P. K. Aggarwal (2002), Geochemical study of arsenic release mechanisms in the Bengal Basin groundwater, *Water Resour. Res., 38*,

Harvey, C. F., C. H. Swartz, A. B. M. Badruzzaman, N. Keon-Blute, W. Yu, M. A. Ali, J. Jay, R. Beckie, V. Niedan, D. Brabander, P. M. Oates, K. N. Ashfaque, S. Islam, H. F. Hemond, and M.

F. Ahmed (2002), Arsenic mobility and groundwater extraction in Bangladesh, *Science, 298*, 1602-1606.

Harvey, C. F., K. N. Ashfaque, W. Yu, A. B. M. Badruzzaman, M. A. Ali, P. M. Oates, H. A. Michael, R. B. Neumann, R. Beckie, S. Islam, and M. F. Ahmed (2006), Groundwater dynamics and arsenic contamination in Bangladesh, *Chem. Geol., 228*, 112-136.

Islam, F. S., A. G. Gault, C. Boothman, D. A. Polya, J. M. Charnock, D. Chatterjee, and J. R. Lloyd (2004), Role of metal-reducing bacteria in arsenic release from Bengal delta sediments, *Nature, 430*, 68-71.

Itai, T., H. Masuda, A. A. Seddique, M. Mitamura, T. Maruoka, X. Li, M. Kusakabe, B. K. Dipak, A. Farooqi, T. Yamanaka, S. Nakaya, J. Matsuda, and K. M. Ahmed (2008), Hydrological and geochemical constraints on the mechanism of formation of arsenic contaminated groundwater in Sonargaon, Bangladesh, *Appl. Geochem., 23*, 2236-2248.

Jardine, P. M., J. F. McCarthy, and N. L. Weber (1989), Mechanisms of Dissolved Organic Carbon Adsorption on Soil, *Soil Sci. Soc. Am. J., 53*, 1378-1385.

Kaiser, K., and W. Zech (1998), Rates of dissolved organic matter release and sorption in forest soils, *Soil Sci., 163*, 714-725.

Kirk, G. (2004), *The Biogeochemistry of Submerged Soils,* John Wiley & Sons, New Jersey.

Klump, S., R. Kipfer, O. A. Cirpka, C. F. Harvey, M. S. Brennwald, K. N. Ashfaque, A. B. M. Badruzzaman, S. J. Hug, and D. M. Imboden (2006), Groundwater dynamics and arsenic mobilization in Bangladesh assessed using noble gases and tritium, *Environ. Sci. Technol., 40*, 243-250.

Kocar, B. D., M. J. Herbel, K. J. Tufano, and S. Fendorf (2006), Contrasting effects of dissimilatory iron(III) and arsenic(V) reduction on arsenic retention and transport, *Environ. Sci. Technol., 40*, 6715-6721.

Lovley, D. R., and S. Goodwin (1988), Hydrogen concentrations as an indicator of the predominant terminal electron-accepting reactions in aquatic sediments, *Geochim. Cosmochim. Acta, 52*, 2993-3003.

Mailloux, B. J., E. Alexandrova, A. R. Keimowitz, K. Wovkulich, G. A. Freyer, M. Herron, J. F. Stolz, T. C. Kenna, T. Pichler, M. L. Polizzotto, H. Dong, M. Bishop, and P. S. K. Knappett (2009), Microbial Mineral Weathering for Nutrient Acquisition Releases Arsenic, *Appl. Environ. Microbiol., 75*, 2558-2565.

Manouchehr, Amini, A. C, Karim, Michael, Berg, Lenny, Winkel, H. J, Stephan, Eduard, Hoehn, Hong, Yang, and J. Annette, C. (2008), Statistical Modeling of Global Geogenic Arsenic Contamination in Groundwater, *Environ. Sci. Technol., 42*, 3669-3675.

McArthur, J. M., D. M. Banerjee, K. A. Hudson-Edwards, R. Mishra, R. Purohit, P. Ravenscroft, A. Cronin, R. J. Howarth, A. Chatterjee, T. Talukder, D. Lowry, S. Houghton, and D. K. Chadha

(2004), Natural organic matter in sedimentary basins and its relation to arsenic in anoxic ground water: the example of West Bengal and its worldwide implications, *Appl. Geochem., 19*, 1255-1293.

Meharg, A. A., and M. Rahman (2003), Arsenic contamination of Bangladesh paddy field soils: Implications for rice contribution to arsenic consumption, *Environ. Sci. Technol., 37*, 229-234.

Michael, H. A., and C. I. Voss (2008), Evaluation of the sustainability of deep groundwater as an arsenic-safe resource in the Bengal Basin, *Proc. Natl. Acad. Sci. U.S.A., 105*, 8531-8536.

Mitamura, M., H. Masuda, T. A. Itai, T. Minowa, T. Maruoka, K. M. Ahmed, A. A. Seddique, D. K. Biswas, S. Nakaya, K. Uesugi, and M. Kusakabe (2008), Geological structure of an arsenic-contaminated aquifer at Sonargaon, Bangladesh, *J. Geol., 116*, 288-302.

Neumann, R. B., M. L. Polizzotto, A. B. M. Badruzzaman, M. A. Ali, Z. Zhang, and C. F. Harvey (2009), The Hydrology of a Groundwater-Irrigated Rice Field in Bangladesh: Seasonal and Daily Mechanisms of Infiltration, *Water Resour. Res., 45*, doi:10.1029/2008WR007542.

Orphan, V. J., C. H. House, K. U. Hinrichs, K. D. McKeegan, and E. F. DeLong (2002), Multiple archaeal groups mediate methane oxidation in anoxic cold seep sediments, *Proc. Natl. Acad. Sci. U. S. A., 99*, 7663-7668.

Pal, A., U. K. Chowdhury, D. Mondal, B. Das, B. Nayak, A. Ghosh, S. Maity, and D. Chakraborti (2009), Arsenic Burden from Cooked Rice in the Populations of Arsenic Affected and Nonaffected Areas and Kolkata City in West-Bengal, India, *Environ. Sci. Technol., 43*, 3349-3355.

Panaullah, G., T. Alam, M. Hossain, R. Loeppert, J. Lauren, C. Meisner, Z. Ahmed, and J. Duxbury (2009), Arsenic toxicity to rice (Oryza sativa L.) in Bangladesh, *Plant Soil, 317*, 31-39.

Polizzotto, M. L., C. F. Harvey, G. Li, B. Badruzzman, A. Ali, M. Newville, S. Sutton, and S. Fendorf (2006), Solid-phases and desorption processes of arsenic within Bangladesh sediments, *Chem. Geol., 228*, 97-111.

Polizzotto, M. L., B. D. Kocar, S. G. Benner, M. Sampson, and S. Fendorf (2008), Near-surface wetland sediments as a source of arsenic release to ground water in Asia, *Nature, 454*, 505-508.

Radloff, K. A., Z. Cheng, M. W. Rahman, K. M. Ahmed, B. J. Mailloux, A. R. Juhl, P. Schlosser, and A. van Geen (2007), Mobilization of Arsenic During One-Year Incubations of Grey Aquifer Sands from Araihazar, Bangladesh, *Environ. Sci. Technol., 41*, 3639-3645.

Raghoebarsing, A. A., A. Pol, K. T. van de Pas-Schoonen, A. J. P. Smolders, K. F. Ettwig, W. I. C. Rijpstra, S. Schouten, J. S. S. Damste, H. J. M. Op den Camp, M. S. M. Jetten, and M. Strous (2006), A microbial consortium couples anaerobic methane oxidation to denitrification, *Nature, 440*, 918-921.

Roberts, L., S. J. Hug, J. Dittmar, A. Voegelin, R. Kretzschmar, B. Wehrli, O. A. Cirpka, G. C. Saha, M. A. Ali, and A. B. M. Badruzzaman (2009), Arsenic mobilization from paddy soils during monsoon flooding, *Nature Geosci.,* accepted.

Roberts, L., S. J. Hug, J. Dittmar, A. Voegelin, G. C. Saha, M. A. Ali, A. B. M. Badruzzaman, and R. Kretzschmar (2007), Spatial distribution and temporal variability of arsenic in irrigated rice fields in Bangladesh: 1. Irrigation water, *Environ. Sci. Technol., 41*, 5960-5966.

Seddique, A. A., H. Masuda, M. Mitamura, K. Shinoda, T. Yamanaka, T. Itai, T. Maruoka, K. Uesugi, K. M. Ahmed, and D. K. Biswas (2008), Arsenic release from biotite into a Holocene groundwater aquifer in Bangladesh, *Appl. Geochem., 23*, 2236-2248.

Sengupta, S., M. J. McArthur, A. Sarkar, J. M. Leng, P. Ravenscroft, J. R. Howarth, and M. D. Banerjee (2008), Do Ponds Cause Arsenic-Pollution of Groundwater in the Bengal Basin? An Answer from West Bengal, *Environ. Sci. Technol., 42*, 5156-5164.

Servais, P., G. Billen, and M. C. Hascoet (1987), Determination of the biodegradable fraction of dissolved organic matter in waters, *Water Res., 21*, 445-450.

Smedley, P. L., and D. G. Kinniburgh (2002), A review of the source, behaviour and distribution of arsenic in natural waters, *Appl. Geochem., 17*, 517-568.

Stollenwerk, K. G., G. N. Breit, A. H. Welch, J. C. Yount, J. W. Whitney, A. L. Foster, M. N. Uddin, R. K. Majumder, and N. Ahmed (2007), Arsenic attenuation by oxidized aquifer sediments in Bangladesh, *Sci. Total Environ., 379*, 133-150.

Stute, M., Y. Zheng, P. Schlosser, A. Horneman, R. K. Dhar, S. Datta, M. A. Hoque, A. A. Seddique, M. Shamsudduha, K. M. Ahmed, and A. Van Geen (2007), Hydrological control of As concentrations in Bangladesh groundwater, *Water Resour. Res., 43*, W09417, doi: 10.1029/2005WR004499.

Swartz, C. H., N. K. Blute, B. Badruzzman, A. Ali, D. Brabander, J. Jay, J. Besancon, S. Islam, H. F. Hemond, and C. F. Harvey (2004), Mobility of arsenic in a Bangladesh aquifer: Inferences from geochemical profiles, leaching data, and mineralogical characterization, *Geochim. Cosmochim. Acta, 68*, 4539-4557.

Tufano, K. J., and S. Fendorf (2008), Confounding impacts of iron reduction on arsenic retention, *Environ. Sci. Technol., 42*, 4777–4783.

Van Geen, A., Z. Q. Cheng, Q. Jia, A. A. Seddique, M. W. Rahman, M. M. Rahman, and K. M. Ahmed (2007), Monitoring 51 community wells in Araihazar, Bangladesh, for up to 5 years: Implications for arsenic mitigation, *J. Environ. Sci. Health Part A, 42*, 1729-1740.

van Geen, A., Y. Zheng, S. Goodbred, A. Horneman, Z. Aziz, Z. Cheng, M. Stute, B. Mailloux, B. Weinman, M. A. Hoque, A. A. Seddique, M. S. Hossain, S. H. Chowdhury, and K. M. Ahmed (2008), Flushing history as a hydrogeological control on the regional distribution of arsenic in shallow groundwater of the Bengal Basin, *Environ. Sci. Technol., 42*, 2283-2288.

Van Geen, A., J. Rose, S. Thoral, J. M. Garnier, Y. Zheng, and J. Y. Bottero (2004), Decoupling of As and Fe release to Bangladesh groundwater under reducing conditions. Part II: Evidence from sediment incubations, *Geochim. Cosmochim. Acta, 68*, 3475-3486.

Van Geen, A., Y. Zheng, R. Versteeg, M. Stute, A. Horneman, R. Dhar, M. Steckler, A. Gelman, C. Small, H. Ahsan, J. H. Graziano, I. Hussain, and K. M. Ahmed (2003), Spatial variability of arsenic in 6000 tube wells in a 25 km(2) area of Bangladesh, *Water Resour. Res., 39*, 1140, doi:10.1029/2002WR001617.

Welch, P. S. (1952), *Limnology,* McGraw-Hill Book Company, New York.

Welch, S. A., A. E. Taunton, and J. F. Banfield (2002), Effect of microorganisms and microbial metabolites on apatite dissolution, *Geomicrobiol. J., 19*, 343-367.

Williams, P. N., M. R. Islam, E. E. Adomako, A. Raab, S. A. Hossain, Y. G. Zhu, J. Feldmann, and A. A. Meharg (2006), Increase in rice grain arsenic for regions of Bangladesh irrigating paddies with elevated arsenic in groundwaters, *Environ. Sci. Technol., 40*, 4903-4908.

Zheng, C., and G. D. Bennett (2002), *Applied Contaminant Transport Modeling,* Wiley Interscience, New York.

Zheng, Y., A. van Geen, M. Stute, R. Dhar, Z. Mo, Z. Cheng, A. Horneman, I. Gavrieli, H. J. Simpson, R. Versteeg, M. Steckler, A. Grazioli-Venier, S. Goodbred, M. Shahnewaz, M. Shamsudduha, M. A. Hoque, and K. M. Ahmed (2005), Geochemical and hydrogeological contrasts between shallow and deeper aquifers in two villages of Araihazar, Bangladesh: Implications for deeper aquifers as drinking water sources, *Geochim. Cosmochim. Acta, 69*, 5203-5218.

7. Supporting Information for Chapter 6

7.1. Field and Laboratory Chemical Characterization Methods

7.1.1. Pond and rice field recharge chemistry

The chemistry of both the pond and rice field recharge was studied using Prenart Super Quartz lysimeters. All of the lysimeters used in this study were installed at the end of the dry season when a portion of the pond bottom was exposed and the rice field was dry and fallow. The lysimeters were left to equilibrate with the surrounding soil for eight months before they were sampled. The installation and sampling protocols for the lysimeters are described in section 4.3.3, along with the methods used to analyze the collected water.

7.1.2. Pond and rice field methane measurement

Methane in the pond and rice field recharge was measured using two different methods. The first method involved attaching evacuated glass tubes directly to the end of the lysimeter tubing. The vacuum in the evacuated glass tube was strong enough to pull a small amount of water from the lysimeter. The tube was transported back to MIT and 100μL of the gas phase contained in the tube was pulled into a glass syringe and injected into a gas chromatograph with a flame ionization detector (FID). The analysis run was calibrated by injecting different volumes (10 to 100μL) of 93% methane gas and 100μL of a 2% methane gas standard. It was assumed that the water in the tube was completely degassed due to a residual vacuum in the tube and the relatively small volume of collected water. Therefore, the dissolved gas concentration was determined knowing the concentration of methane in the gas phase, the volume of the gas phase and the volume of the water phase. Henry's law was not required. The volume of collected water was determined from the weight difference between the water-filled and dry tubes.

For the second method, water and gases from the pond and rice field lysimeters were collected into foil bags using the procedure described above. A portion of the gas phase in the foil bag was transferred into an evacuated 25 ml glass serum bottle by simultaneously puncturing the septum of the foil bag and the septum of the glass vial with a two-way needle. The flexible foil bag was at atmospheric pressure, which means that the gas collected within the serum bottle was also at atmospheric pressure. A field blank was collected by purging and filling a foil bag with argon and following the same transfer protocol. The septums of the serum bottles were covered in vacuum grease after the transfer. The air temperature was recorded along with the remaining volume of gas and water in the foil bag so that Henry's law could be used to determine the in-situ dissolved concentration of methane. The gas and water volumes were determined by pulling the remaining contents of the foil bag into a clear, graduated plastic syringe. The plunger of the syringe moved easily, ensuring that the gas within the syringe was at atmospheric pressure. The serum bottle was immediately mailed to the University of British Columbia and analyzed on a gas chromatograph with thermal conductivity detector using a two-point calibration.

7.1.3. Aquifer wells and arsenic

Aquifer wells were installed using the hand-flapper method, which is thoroughly described in Swartz et al. (2004). Water was sampled from the wells using a submersible Grundfos pump. Wells were purged prior to sampling. Purging lasted long enough to flush the well casing of stagnant water, and thus it depended on well depth. Arsenic samples were collected in plastic centrifuge tubes and acidified down to pH 1 with nitric acid. Samples were analyzed on a graphite furnace atomic absorption spectrophotometer at the Bangladesh University for Engineering and Technology.

7.1.4. Methane in aquifer wells

Methane from the aquifer was collected by pumping groundwater with a Grundfos pump into a submerged and inverted plastic graduated cylinder. The collected gas phase was transferred to SKC flex foil bags for transport back to MIT where it was analyzed on a FID gas chromatograph following the methods outlined in section 7.1.2. The volume of collected gas was measured in the graduated cylinder and the corresponding volume of pumped water was determined by measuring the flow rate and recording the time needed for collection. Henry's law was used to determine the in-situ concentration of dissolved methane.

7.1.5. δ18O and δ2H collection and analysis

Prior to 2008, pond, rice field, and river water samples were collected from the surface of the different water bodies, and aquifer samples were collected using the methods outlined in section 7.1.3. All samples were collected in plastic centrifuge tubes that were completely filled to minimize headspace and possible evaporation. In 2008, the pond water isotope data were collected by pulling water up from different depths in the pond through Teflon-lined Tygon tubing directly into plastic syringes. The water was immediately transferred into glass bottles. Water for the rice field isotopes were collected from the deepest lysimeter in the rice field and stored in glass bottles.

All samples were kept in an ice-filled cooler during sampling and transport back to the USA. Sample aliquots were then filtered with a 0.2 μm syringe filter and mailed to the University of British Columbia's (UBC) Stable Isotope Laboratory and run on a Delta Plus XL mass spectrometer. Blind duplicates were included within the sample batches and aliquots of a

few samples were sent to the UBC laboratory multiple different times as a quality check on the lab's analysis.

7.1.6. BDOC experiment

Samples for the BDOC measurement were collected into foil bags from pond and rice field lysimeters using the procedure explained above. Immediately after collection, the foil bag was transferred to an argon-filled glove bag. Inside the glove bag, a majority of the water in the foil bag was pulled into a plastic syringe and filtered with 0.2 μm syringe filter directly into a glass BOD bottle that was completely wrapped in foil. Any headspace remaining in the BOD bottle was filled with argon gas before the bottle was sealed. A wet paper towel was place around the bottle's glass stopper to ensure that the ground-glass joint remained wet and properly sealed. The BOD bottles were placed in an ice-filled cooler during sampling and transport back to the USA. Approximately 10ml of the water collected in the foil bag was kept and stored unfiltered. This water was used as the inoculum for the BDOC experiment.

The protocol outlined in Servais et al. (1987) was followed to determine the amount of BDOC in the water samples. The 100 to 300 ml of water stored in the BOD bottles was poured into foil-wrapped, 4 L glass bottles with screw lids. Roughly 5ml of the unfiltered water, or inoculum, were passed through a 1.2 μm sterile syringe filter directly into the 4 L bottles to remove any large particles. The bottles were then sealed with foil and lids, and placed on a stir plate with a glass stir bar. The bottles were sealed to ensure that the samples did not evaporate, and the large size of the bottles ensured that there was ample oxygen in the headspace for the organic carbon oxidation. The 4 L bottles were kept at room temperature and their water was periodically subsampled and preserved with sulfuric (Experiment 1) or phosphoric (Experiment

2) acid for non-purgable organic carbon (NPOC) analysis. The sulfuric acid did not oxidize the organic carbon, see section 5.5. The experiment was run until the NPOC in all of the samples stopped changing with time. The BDOC amount was assumed equal to the amount of NPOC lost during the experiment.

7.1.7. Carbon-13 Measurements in the Pond, Aquifer and Rice Field

Gas samples for δ^{13}C-DIC analyses were obtained from the aquifer following the protocol outlined above for the collection of methane samples (section 7.1.4). Collection differed only after the gas was sealed in the flex-foil bags. Samples for isotopic analysis were transferred from the flex-foil bags into 12 ml evacuated containers (Vacutainers) using a double-sided needle and the septa-port. The butyl-rubber stoppers were coated with vacuum grease and stored for later analysis. In the lab, 50 µl of gas from each sample vial were extracted in a gas-tight syringe and injected into a He-flushed 4 ml vial. The samples were run using a Delta Plus XL Isotope Ratio Mass Spectrometer equipped with a Gasbench II and a PAL-80 autosampler. Measurement errors based on internal and external standards were less than 0.5‰. Isotope values were corrected for the 6.5‰ equilibrium isotope fractionation between H_2CO_3 and HCO_3^-. This is necessary since the majority of inorganic carbon in the aquifer water is in the form of HCO_3^- (Swartz et al. 2004), and this sampling method only captured the small fraction of inorganic carbon in the form CO_2 or H_2CO_3 that outgassed with the methane into the inverted cylinder. Therefore, the actual isotopic composition of the bulk DIC in the aquifer water is approximately 6.5‰ heavier than the isotopic composition measured in our samples.

Samples of pond water and rice field surface water were collected using a stainless steel tube connected through airtight fittings to a septum-port. Water was drawn directly through a

double-sided syringe into 12 ml evacuated containers until the container was approximately ½ full (by eye). Two replicate samples were collected every 2.5 cm, continuing into the sediment until the porosity decreased beyond the capability of the evacuated container to draw water out. In the rice fields, depending on the timing relative to the irrigation cycle, it was often only possible to obtain water from one or two different sampling depths. Upon returning to the lab in the afternoon, the samples were preserved by the injection of 0.05 μl $HgBr_2$. Back in the USA, the contents of the containers were acidified by injection of 0.5 μl 100% H_3PO_4 and 500 μl of headspace gas were drawn out using a gas-tight syringe. The gas was then injected into a 4 ml He-flushed vial and the $\delta^{13}C$ quantified as above on a Delta Plus XL.

7.2. Groundwater Arsenic and Isotope Profiles at Other Sites

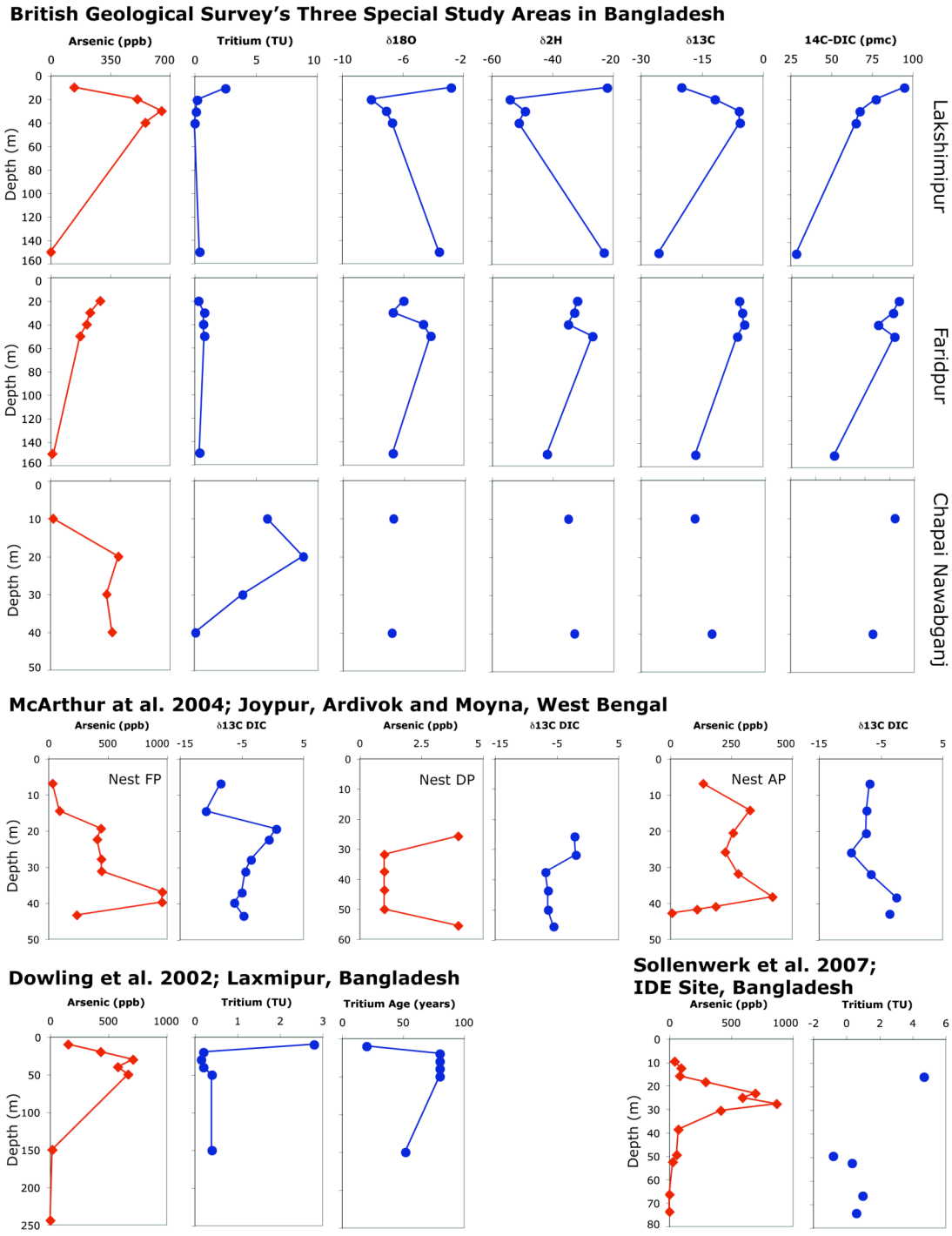

Figure 7.1 Arsenic and isotope data from field sites in Bangladesh and West Bengal.

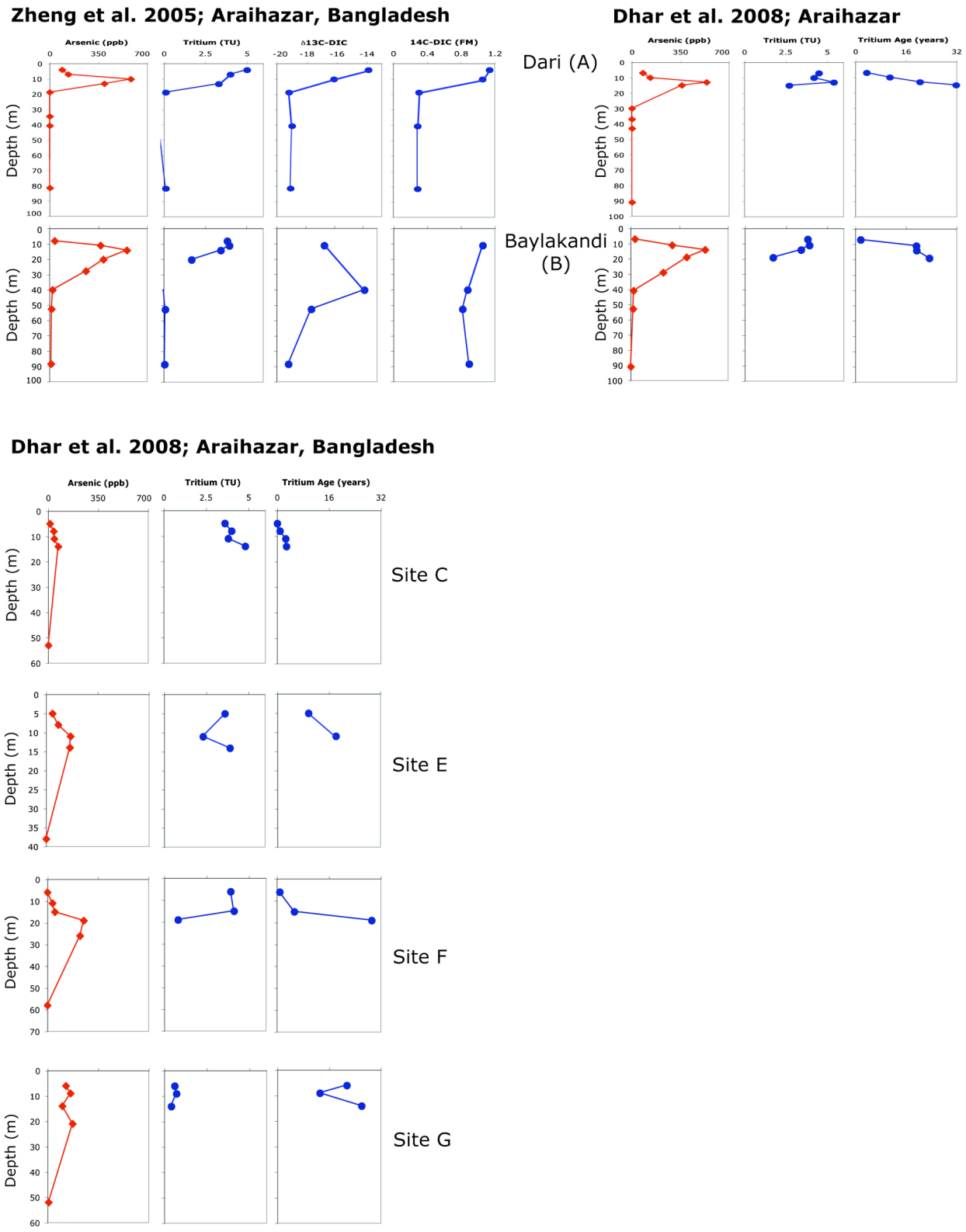

Figure 7.2 Arsenic and isotope data from Araihazar, Bangladesh.

Profiles of arsenic, tritium, ^{18}O, ^{2}H, ^{13}C-DIC and ^{14}C-DIC for sites with well nest in Bangladesh (Dhar et al., BGS et al. 2001, Dowling et al. 2002, Zheng et al. 2005, Stollenwerk et al. 2007) and West Bengal (McArthur et al. 2004) are shown above and analyzed in more detail below.

7.2.1. British Geological Survey's Three Special Study Areas

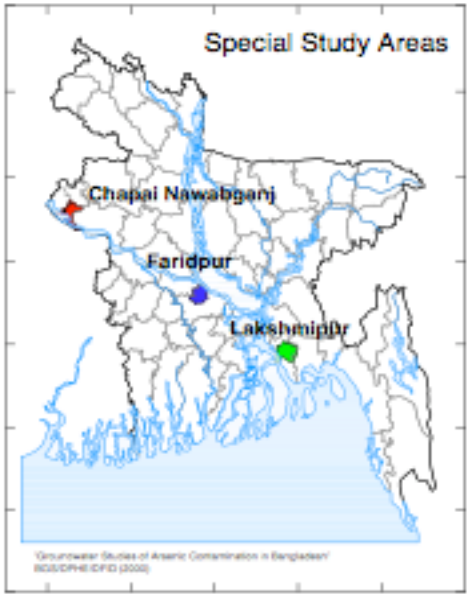

Figure 7.3 Locations of the British Geological Survey's three special study areas.
(Picture from BGS report.)

The arsenic, $\delta^{18}O$, $\delta^{2}H$ and $\delta^{13}C$ profiles at the Lakshimipur site exhibit the same behaviour as the profiles at our site (Figure 6.1a). Lakshimipur is in the southern part of the country while our site is roughly 30 km south of Dhaka and 7 km north of the Ganges River. At both locations, the arsenic peak corresponds with light $\delta^{18}O$ and $\delta^{2}H$ water and heavy $\delta^{13}C$-DIC water. This correspondence suggests that the arsenic-contaminated water at this field site originates in ponds or other natural water bodies that retain the $\delta^{18}O$ and $\delta^{2}H$ light water from the monsoon season and undergo methanogenesis making $\delta^{13}C$-DIC heavy. However, the radiocarbon age of the DIC at the arsenic peak is significantly older than what we measure at our

site. In fact, the DIC at Lakshimipur peak has the same radiocarbon age as the DOC at our site (~2000-3000 years old). These inorganic carbon ages suggest that arsenic mobilization in this area is associated with microbial respiration of old carbon, and could have occurred prior to the large-scale development of ponds an irrigation, perhaps due to input of organic carbon rivers or natural ponds or wetlands. The shape of the arsenic peak, however, does suggest some anthropogenic influence due to current irrigation pumping, which focuses water and arsenic at the depth of the irrigation wells.

At the two other special study areas, Faridpur and Chapai Nawabganj, there is not a well-defined arsenic peak from the chosen sample depths. In Faridpur, which is fairly close to our site, there are no measurements above 20 m that could define the top of the peak; in Chapai Nawabganj, which is further north, there are no measurements below 40 m to define the bottom of the peak. Even though an arsenic peak does not clearly exist at Faridpur, other data seem to suggest that arsenic is associated with light $\delta^{18}O$ and $\delta^{2}H$ water and heavy $\delta^{13}C$-DIC water, as we see at our site and at the Lakshimipur site. However, the data is sparse and does not demonstrate a strong pattern.

7.2.2. McArthur et al. 2004, West Bengal

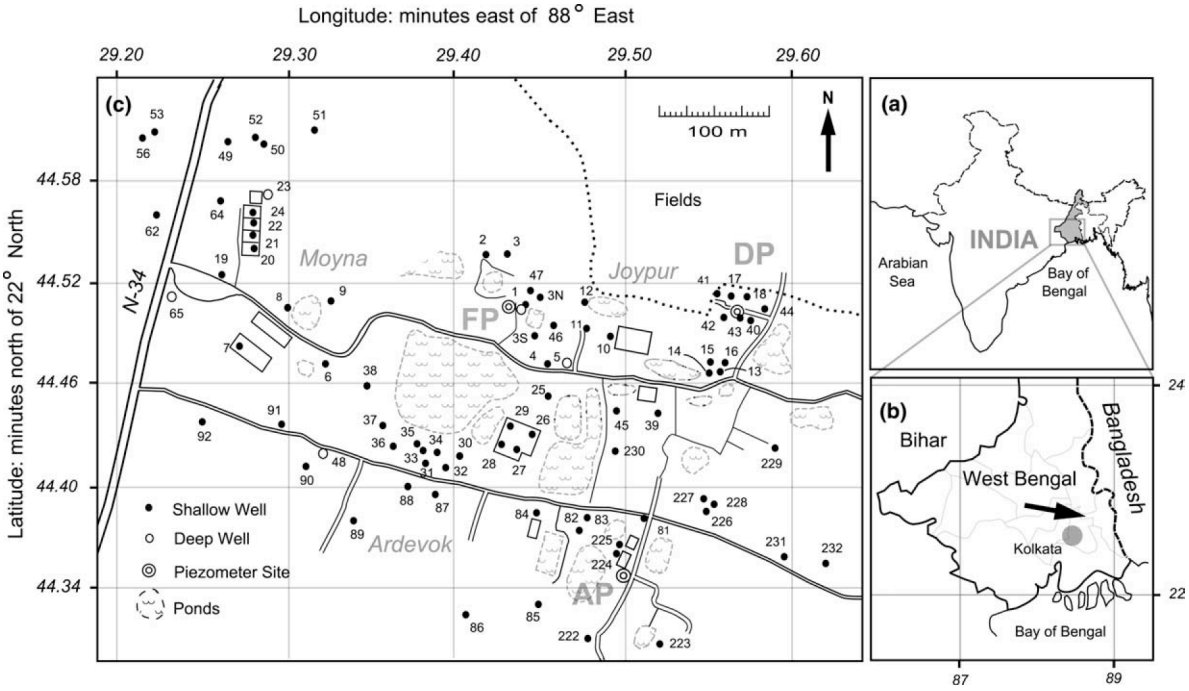

Figure 7.4 Location of McArthur et al. 2004 field site.
(Picture from McArthur et al. 2004.)

The arsenic profiles at McArthur et al.'s site in West Bengal do not have distinct peaks like we see at our site. It is possible that an arsenic peak is absent because groundwater flow paths do not converge at a specified depth due either to complex hydrogeologic architecture or the lack of wide-spread irrigation pumping. However, the higher arsenic concentrations seem to roughly correspond with heavier δ13C-DIC water, suggesting that the high arsenic concentrations correspond with methanogenesis, as seen at our site. However, there are no dates for the inorganic carbon at this site, so it is impossible to determine if the carbon responsible for arsenic mobilization and methanogenesis is young or old.

7.2.3. Dowling et al. 2002, Laxmipur

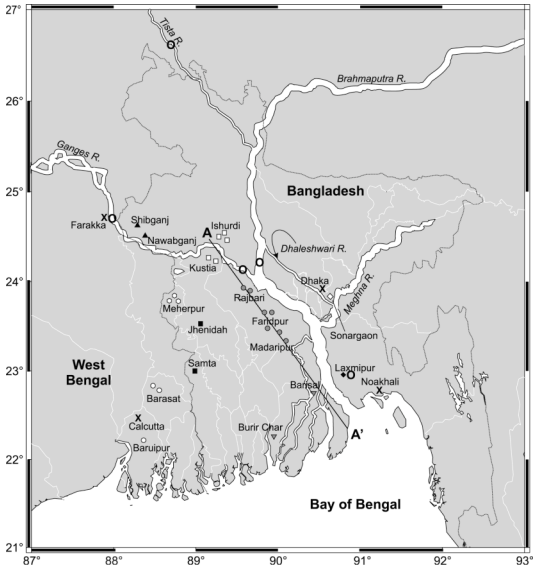

Figure 7.5 Location of Dowling et al. 2002 field site.
(Picture from Dowling et al. 2002.)

The arsenic and tritium profiles at Laxmipur collected by Dowling et al. closely resembles the profiles collected by the British Geological Survey at Lakshimipur. Although the two areas are spelled differently, they may actually represent different samples from the same place since they are both located in the southern part of the country on the east side of the Ganges river. If the two datasets were not collected from the same well nest, their similarity suggests that recharge patterns and subsurface conditions are fairly uniform within this region. Similar to our site, an arsenic peak clearly exists within the aquifer. The water at this peak has a triutm-helium-3 age of ~75 years. This young age suggests the arsenic is associated with water that recently entered the aquifer.

7.2.4. Stollenwerk et al. 2007, IDE Site

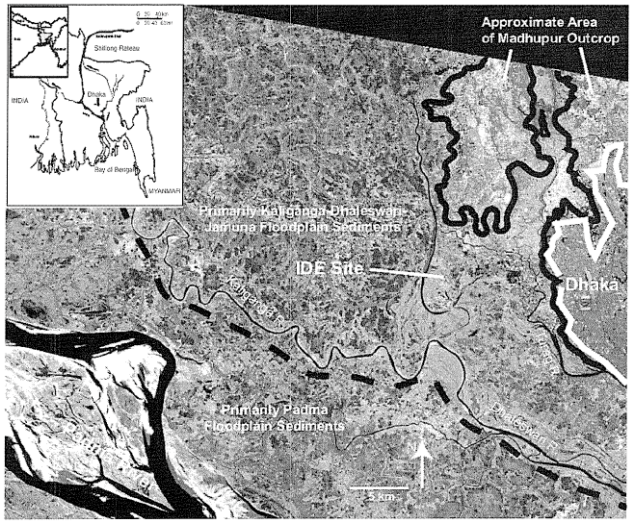

Figure 7.6 Location of Stollenwerk et al. 2007 site.
(Picture from Stollenwerk et al. 2007.)

The IDE site is located slightly northwest of our site, but within the same general area. The arsenic concentration profile matches the profiles measured at our site, with a peak occurring at a depth of roughly 30 m. It is likely that the same hydrologic and geochemical processes that control arsenic concentrations at our site control arsenic concentrations at the IDE site. Namely, irrigation pumping pulls surface water and young organic carbon down to the 30-m depth, mobilizing arsenic off of the soils and sediments.

7.2.5. Araihazar, Bangladesh (Zheng et al. 2005 and Dhar et al. 2008)

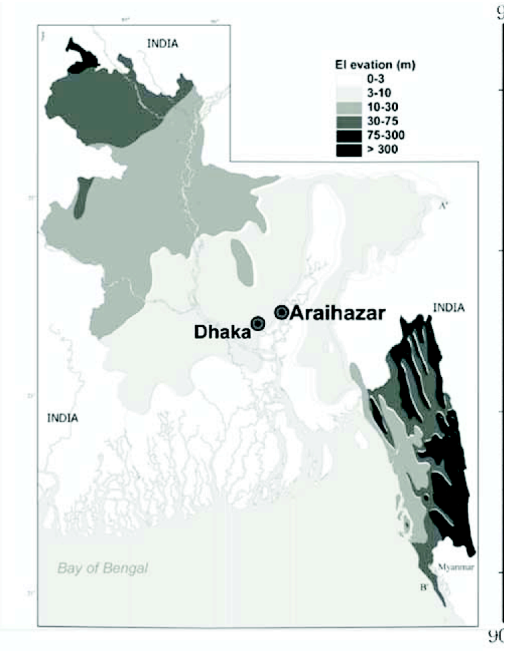

Figure 7.7 Location of Araihazar site.
(Picture from Zheng et al. 2005.)

Most of the well nests at the Araihazar site have an arsenic peak at a depth of 15 m, half as deep as the 30 m peak at our site. The peak is most distinct in well nests A and B, but exists at lower concentrations in all of the well nests, except for G. Most of the drinking water wells at this field site also extract from a depth around 15 m (Van Geen et al. 2003), suggesting that flow paths from an anoxic recharge source converge at this depth. The aquifer thickness at Araihazar is about half of that at our site. The younger tritium-helium age at the arsenic peak is likely due to the shallow nature of the peak – the water does not have to travel as far to reach these depths. Arsenic is also associated with modern and isotopically heavy dissolved inorganic carbon, suggesting that, similar to our site, modern organic carbon is driving arsenic mobilization and that this process is associated with methanogenesis. Thus, the data from this site appear similar to data from out site, but with depths of features reduced by about one-half.

7.3. Pond Information

7.3.1. Pond Growth Over Past 50 Years

Most of the ponds in Bangladesh are man-made. Since the landscape floods each year (see water level data in section 7.4), the villages and roads are built up above the level of the floods (Figure 7.8) by digging up soil from one location and transferring it to another location. The hole that remains in the ground becomes a pond that fills with floodwater during the monsoon season and then recharges the aquifer during the dry season (Figure 7.8). Since these ponds are largely the unintentional result of development projects, their number likely follows that of population growth, which has exploded over the past half-century (Figure 7.9). Ponds are also intentionally dug for the purpose of fish production, a practice that the country has actively promoted within the past half-decade (Kränzlin 2000).

Figure 7.8 Raised village surrounded by a pond at the Munshiganj field site.

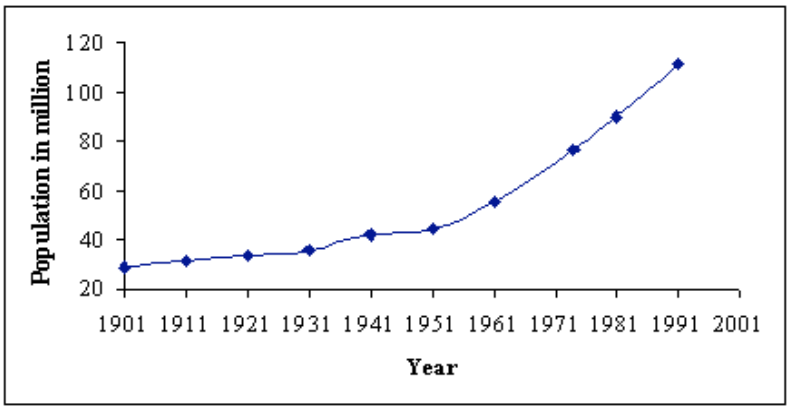

Figure 7.9 Population of Bangladesh during the last century.
Figure from the Food and Agricultural Organization of the United Nations (http://www.fao.org/docrep/007/ad104e/AD104E05.htm).

The increase in land area covered by ponds is supported by a pond study conducted in the 1970's (Huq and Islam 1977). The authors reported that in 1971, ponds covered 695 km^2 of the entire country of Bangladesh, and in their study area (Boyra Village) in 1977, ponds covered 0.0742 km^2. If we look at the whole country in 1971, ponds covered 695 km^2/133910 km^2 = 0.5% of the land area. The authors did not report the total area of Boyra village. Data from the government of Bangladesh (http://www.lgd.gov.bd/php/upprofile/upbasicdata.php?d=1802) shows that the Boyra Union in the Mymensingh Sadar Upazilla has an area of 12.76 km^2 and 6 villages. Assuming the villages are all roughly the same size, we can assume the village of Boyra is ~2 km^2. This means that in the early 1970's ponds covered ~0.0742 km^2/2 km^2 = 3.5% of Boyra's land area. If the authors actually studied the entire Boyra Union, rather than just Boyra village, the percent of coverage would decrease to ~0.0742 km^2/12.76 km^2 = 0.6 %, which matches the percentage of coverage calculated for the entire country. In our study area in ~2004,

we found that ponds covered ~11% of the area (Ashfaque 2007). If we assume that pond density is fairly uniform across the rural areas of Bangladesh, and we use the Boyra Village number as the 1970's reference point, then we conclude that pond area increased from roughly 3.5% in 1977 to 11% in 2004 – a 3-fold increase. If however we use the entire country number, then we conclude that pond area increased from roughly 0.5% in 1971 to 11% in 2004 – a 22-fold increase.

Furthermore, data collected by Kränzlin (2000) show that the total number of ponds in Bangladesh has increased over time (Figure 7.10). She attributes the increase to the growth and promotion of fish production in the country. Regardless of the motivation for pond development, the data illustrate that the number of ponds in Bangladesh has grown substantially within the past ~40 years, matching the growth in pond area.

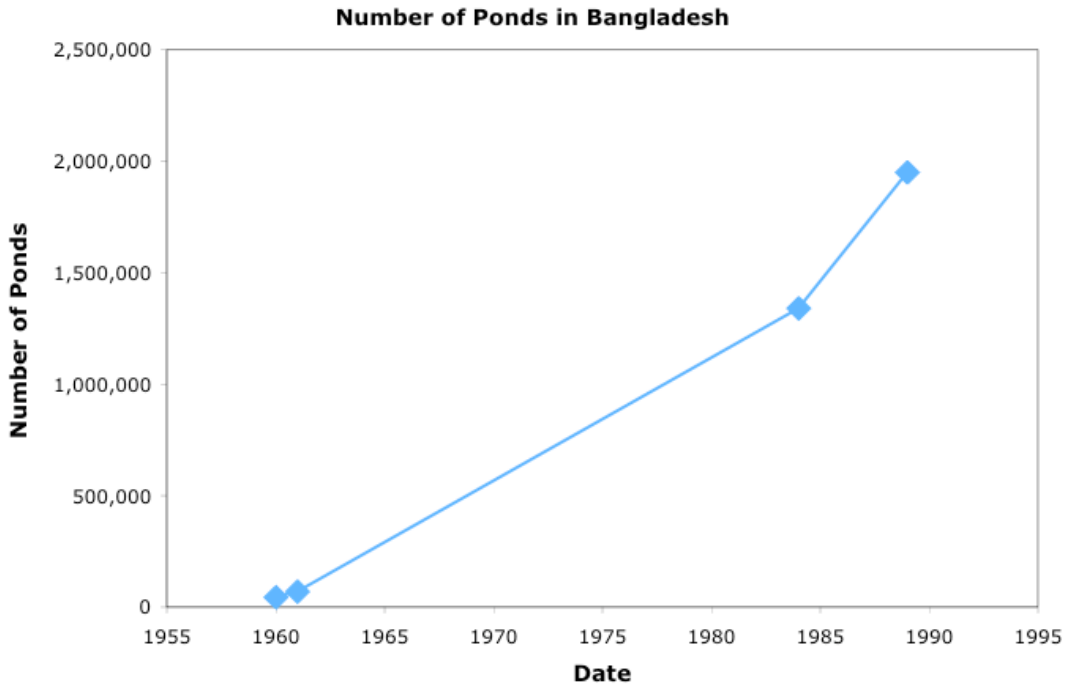

Figure 7.10 Number of ponds in Bangladesh from Kränzlin (2000)

7.3.2. Sediment Beneath Ponds

The ponds in Bangladesh are dug out of over-bank deposits that blanket the landscape. These are the same deposits on which rice fields are cultivated. Since it is difficult to collect samples from underneath ponds, our analysis of the over-bank deposit was conducted on soil cores collected from a dry rice field. The hydrologic and chemical character of the deeper sediments beneath ponds should match those of the deeper rice field soil. However, we expect the shallow sediment beneath ponds is composed of material that settled out of the pond surface water (Welch 1952), including plankton and other organic matter.

Hydraulic conductivity measurements on the rice field soil core showed that the over-bank deposit has a fairly uniform matrix conductivity of 0.02 cm/day or 2e-7 cm/sec (Figure 2.8). However, the hydrologic study conducted on the rice field from which the core was obtained showed that this matrix conductivity is smaller than the effective, field-scale conductivity that controls flow behaviour in the field. Rice field water flows through preferential flow channels that exist in the over-bank deposit, and these channels increase the effective conductivity of the deposit (see chapter 2).

Given measured head gradients between ponds and the shallow aquifer (Ashfaque 2007), we calculate that to sustain an infiltration rate of ~1 cm/day (the average loss rate for the ponds in our study area (Harvey et al. 2006)) the sediments beneath the pond need to have an effective hydraulic conductivity of ~1 cm/day (see Table 7.1). This required conductivity is larger than the matrix conductivity of the over-bank deposit measured in the rice field core (0.02 cm/day). This difference between matrix and effective conductivity is consistent with the rice-field study in chapter 2, and demonstrates that the ponds, like the rice fields, lose some water through preferential flow channels in the over-bank deposit.

Table 7.1 Head gradient and hydraulic conductivity in pond sediment.

	Avg. Pond Head at ~3 m Below Land Surface	Head in 15' (4.6 m) Deep Well	Head Gradient	K needed for infil. of 1 cm/day
March 1, 2003	3.7 m	1.89 m	(1.81 m)/(1.6 m)=1.1	0.9 cm/day
March 11, 2004	3.6 m	2.12 m	(1.48 m)/(1.6 m)=0.9	1.1 cm/day

Similarly, the arsenic content of the over-bank deposit beneath ponds is likely similar to that of the deeper rice field soils. (The shallow rice field soils have elevated arsenic concentrations due to arsenic in the irrigation water.) Dittmar et al. (2007) report that the deeper rice field soils contain roughly 10 mg/kg of arsenic, a higher concentration than that measured in the aquifer sediments (Swartz et al, 2004). However, it is possible that the over-bank deposits beneath the pond have lower arsenic contents due to the mobilization and transport of arsenic as pond recharge flows through these sediments.

7.3.3. Pond Water

Figure 7.11 shows the rate of decline for nine ponds in Munshiganj for a 2.5-year time period. The data demonstrate that the ponds gain water during the monsoon season and lose water during the dry season. The ponds gain more water than that due to rainfall during the monsoon season, suggesting that they fill with floodwater. They also lose water faster than the rate of evaporation during the dry season, showing that they recharge the subsurface. At the start of the dry season, the average pond depth in Munshiganj is 3 m (Ashfaque 2007). In January 2008, the studied young pond referenced in chapter 6 was 3.5 m deep, while the studied old pond was 1m deep. With an average loss rate of 1 cm/day (Harvey et al. 2006), the average depth of the Munshiganj ponds reaches 1.5 m at the end of the dry season, although this was not explicitly measured. In the old and young pond referenced in chapter 6, the decreased water levels at the end of the dry season exposed the pond banks, but the centre of the ponds remained covered with water. However, the pond owners do sometimes pump ponds dry in order to collect fish.

Consistent with the Munshiganj ponds, Hug and Islam (1977) reported that in Boyra Village in 1977 the average pond depth was 2.15 m at the start of the dry season and 1.13 m at the end of the dry season, five months later. This difference equates to a loss of ~0.68 cm/day.

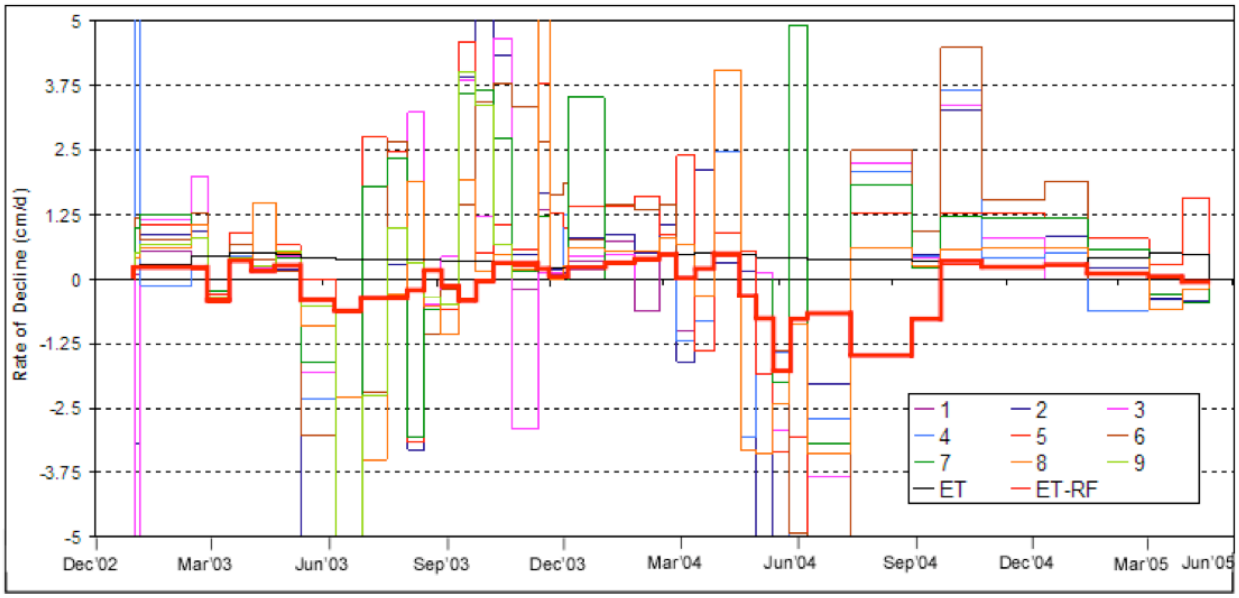

Figure 7.11 Rate of pond water level decline.

The rate of pond water level (PWL) decline for nine ponds, and the rate of pan evaporation and rainfall for the period of December 2002 to June 2005. Rates of PWL decline were calculated by dividing the difference in pond water levels by the duration between the two measurements. Positive differences indicate a decline.

7.3.4. Pond Chemical Profiles

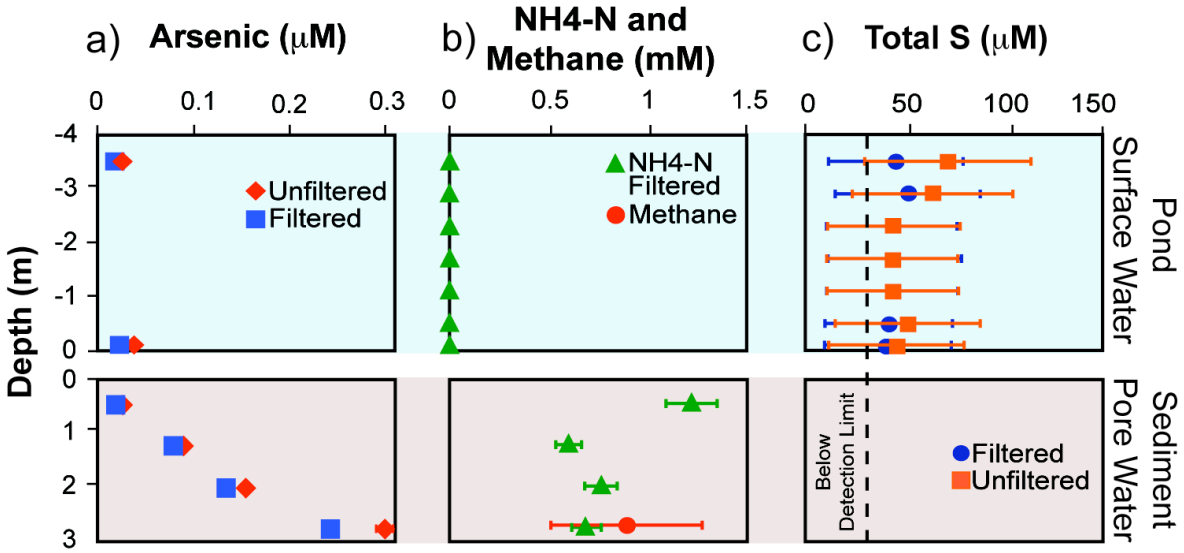

Figure 7.12 Chemical Profiles in a Young Pond.

The pond surface water has low levels of arsenic, methane and ammonium, but the concentrations of these solutes are significant in the pond sediments. In the pond sediment pore water, arsenic concentrations increase with depth and the high levels of ammonium and methane match those measured in the 30 m-deep aquifer water where arsenic is elevated (Harvey et al. 2002, Swartz et al. 2004, Harvey et al. 2006). In addition, the negligible concentrations of sulfur in the pore water of the pond sediments match the low sulfur concentrations measured in the 30-m-deep aquifer water. Thus, the concentrations within the pore water of the pond sediments help explain the tight correlation between arsenic, methane and ammonium and anti-correlation between arsenic and sulfur within the aquifer. Arsenic speciation was not determined due to the small volume of water collected from the lysimeters. However, due to the highly reducing conditions within the pond sediments, indicated by the elevated methane concentrations, we believe the arsenic within the pore water of the pond sediments is likely As(III).

7.4. Stable Water Isotope Data for Surface Waters

7.4.1. Munshiganj Data

The aquifer water that corresponds with the depth of maximum arsenic (~30 m) is isotopically lighter than the other water in the rest of the aquifer. Figure 7.13 shows that the water in this region is <-35 per mil for δ^2H and <-4.75 per mil for $\delta^{18}O$. Therefore, any source of surface water that is recharging the aquifer at this depth must have isotopic values that fall within this range.

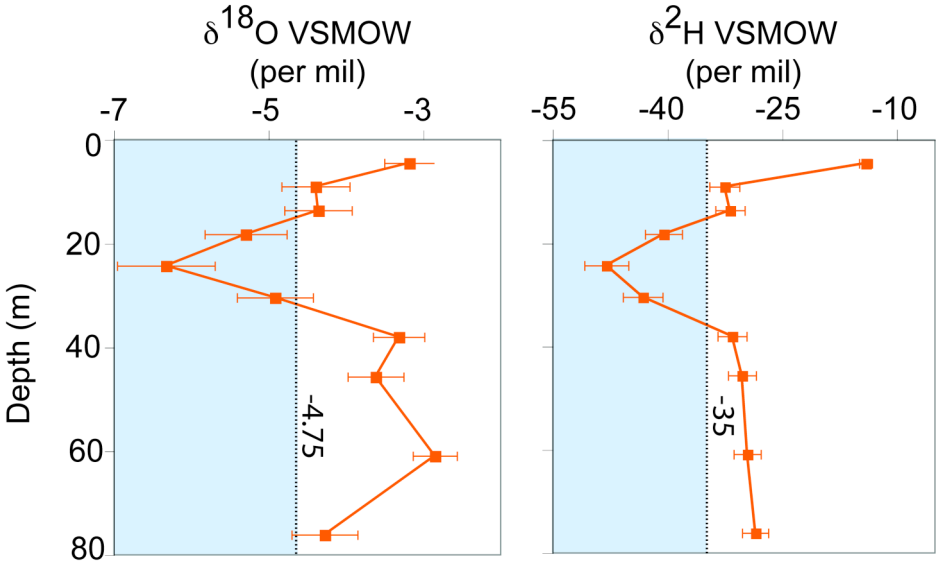

Figure 7.13 Aquifer isotope profiles.
Data were collected in 2005. The water at the depth where arsenic peaks is highlighted by the blue bar.

To properly interpret the surface water isotope data, we need to have an understanding of the seasonal hydrology in Bangladesh. Figure 7.14 shows the water levels, or hydraulic heads, measured throughout our study area in 2003 and 2004. The figure is modified from Harvey et al. (2006). When a surface water source has a greater hydraulic head than the aquifer, it is

recharging the aquifer. When the surface water source has a lower hydraulic head than the aquifer, the aquifer is discharging to that source. When the hydraulic heads are equal, there is no flow. The data show that during the monsoon season, the entire land area is flooded with water and there is no flow. At the start of the dry season, the aquifer discharges water to the rivers. It is not until March that the hydraulic gradient switches and the rivers begin to recharge the aquifer. The ponds continually recharge the aquifer during the dry season.

To determine which surface-water source is responsible for the isotopically light water detected at the depth where arsenic is elevated, we need to look at the isotopic signature of each source during the time when it is recharging the aquifer.

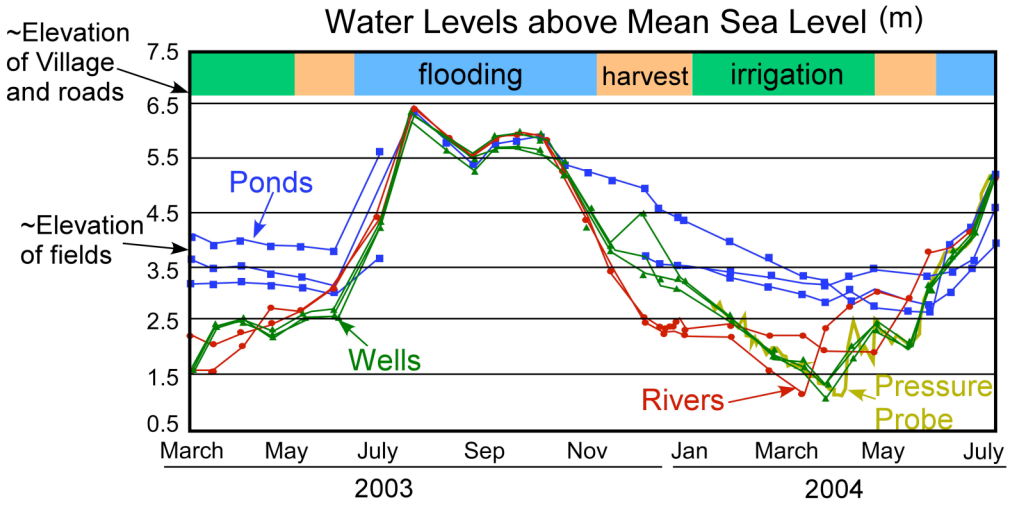

Figure 7.14 Water level measurements for Munshiganj study area.
Ponds data are blue, aquifer data are green, and river data are red. The elevation of the fields is the main elevation of the landscape. The villages and roads are built up above the flood level.

Rice field water, which is continually recharging the aquifer during the irrigation season, or dry season, is isotopically heavy both in January, which is the start of the irrigation season, and in March, which is the middle of the irrigation season (Figure 7.15). Rice field water cannot explain the isotopic signature of the arsenic-elevated water in the aquifer (Figure 7.13).

River water is isotopically light as the monsoon floods recede (November) and gets heavier as the dry season progresses (Figure 7.16). When the river is recharging the aquifer (March), the water is much heavier than that detected in the arsenic-elevated portion of the aquifer (Figure 7.13).

The isotopic composition of rain water for Bangladesh, taken from an online database (http://waterisotopes.org), is light during the monsoon season and heavy during the dry season (Figure 7.17). During the monsoon season, rain has the isotopic composition that matches the arsenic-elevated water in the aquifer (Figure 7.13). However, the rain is falling on a flooded land surface and there is no flow in or out of the aquifer. This water cannot recharge the aquifer. However, the rain does make the floodwaters isotopically light and this floodwater fills the ponds, explaining the light water measured in the ponds after the floods recede (Figure 7.18).

Ponds continually recharge the shallow aquifer once the monsoon floods recede. At the start of the dry season, the water in the ponds is isotopically light, matching the signature of the water in the arsenic contaminated portion of the aquifer (Figure 7.13). The ponds are the only surface-water source with light water during the period of time they are recharging the aquifer. However, pond water does get heavier over the course of the dry season due to evaporation. If the ponds are responsible for the arsenic-elevated water, why is this water not the average of the ponds' isotopic span? One explanation is that the ponds are not vertically well mixed. Our data show that oxygen, ORP, and isotopic values vary along the water column (Figure 7.19). The

surface of the pond is more oxic and isotopically lighter than the bottom of the pond, although the data are noisy. If, during the dry season, the pond remains poorly mixed in the vertical direction, then evaporation will continue to make the surface water of the pond heavy while the deeper water remains light. Unfortunately, prior to 2008, our sampling of pond water was biased towards the surface water of the pond. The isotopic spread that we measured in the ponds (Figure 7.18) is for the surface water, not the deep water.

The data in Figure 7.19 provide some empirical evidence of poor vertical mixing in the studied pond. We have not thoroughly explored the mechanisms that could be responsible for the potential lack of mixing. However, the data suggest that future research on ponds should include the entire water column and sediment rather than just the top surface water. The deeper pond water is more likely to recharge the aquifer than the water at the pond surface. However, the pond could lose water as seepage through the pond edges rather than the pond bottom, which would contribute water from the middle of the pond water column into the aquifer.

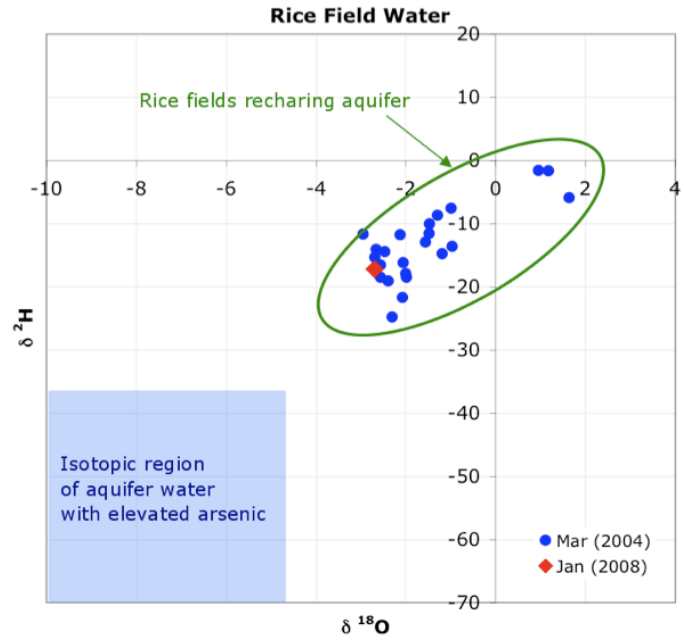

Figure 7.15 Isotopic composition of different rice fields.

Rice field recharge cannot explain the light isotopic signature of water at the arsenic peak.

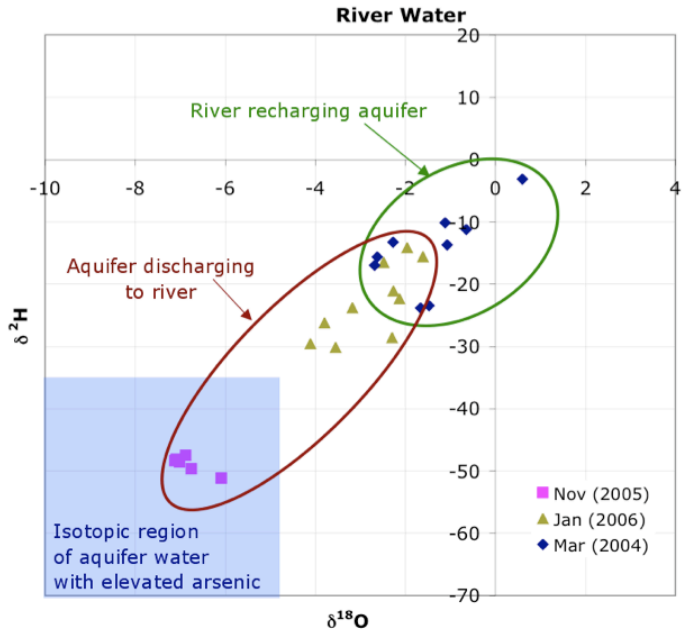

Figure 7.16 Isotopic measurements for the Ichimati river in Bangladesh.

When the river is recharging the aquifer, it has a heavy isotopic signature, and thus cannot explain the isotopically light water found at the arsenic peak.

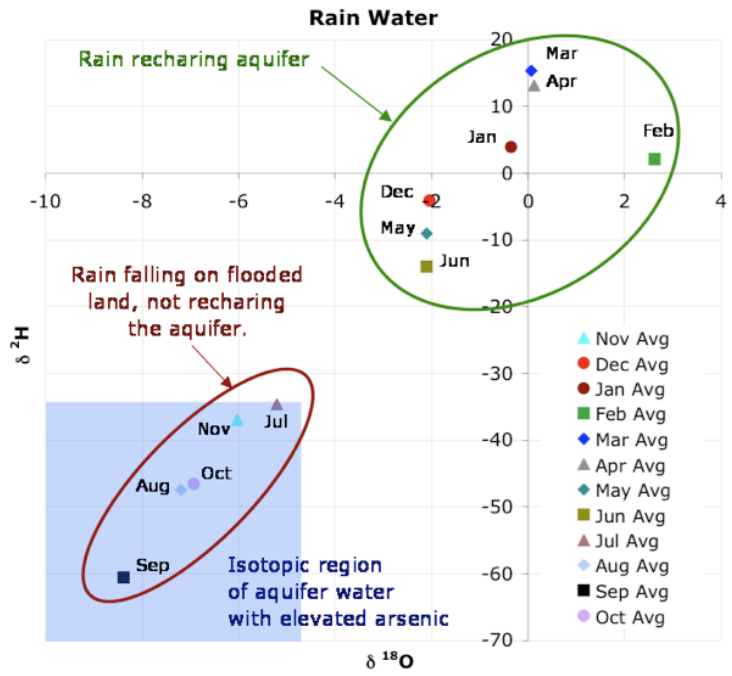

Figure 7.17 Isotopic composition of rain in Bangladesh.

Data taken from http://waterisotopes.org.Bangladesh. Rainwater has the light isotopic signature at the end of the monsoon season, when water in our study area is falling on an already flooded land surface. When the rainwater can infiltrate the subsurface, it has an isotopically heavy signature. Thus, direct rainwater cannot explain the water found at the arsenic peak.

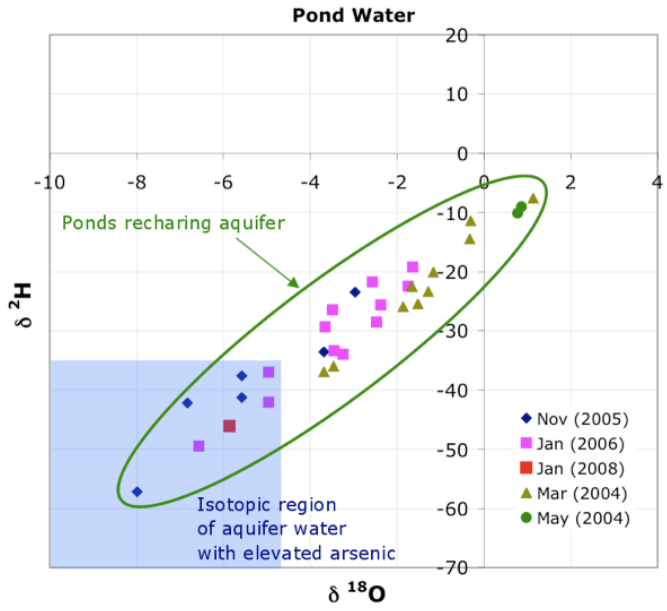

Figure 7.18 Isotopic composition of Munshiganj ponds.

The isotopic spread of ponds is large, but it is the only water source with isotopically light water when it is actively recharging the subsurface. Thus, it is the only surface-water source that can explain the isotopic signature of the water found at the arsenic peak. The water in the ponds is isotopically light because it originates from the isotopically-light rainwater and flood water from the monsoon season.

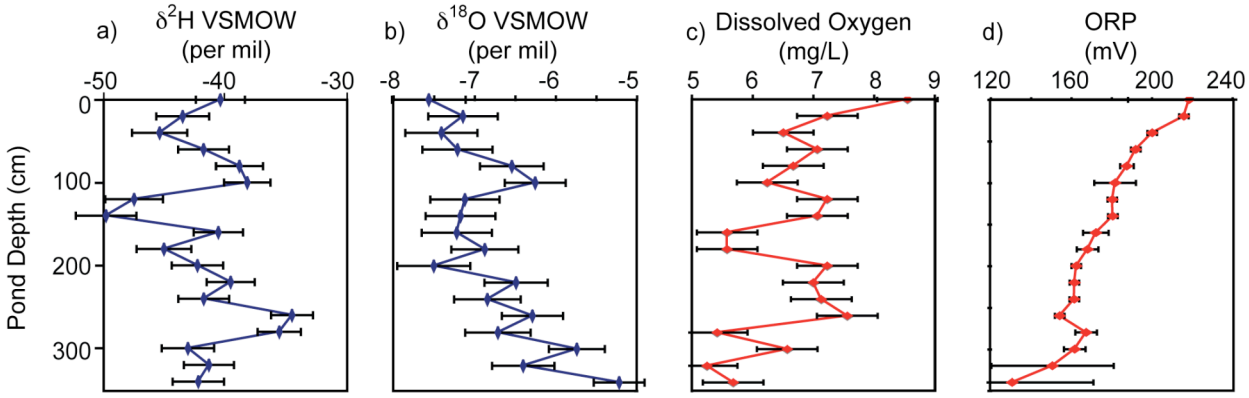

Figure 7.19 Isotopic, oxygen and ORP profiles in the surface water of a young pond in Munshiganj, January 2008.

Although they are noisy, the data suggest the pond is poorly mixed in the vertical direction.

7.4.2. Literature Data

Other research groups in Bangladesh and West Bengal have used isotopic measurement to argue that surface water bodies, primarily ponds, do not contribute water to the shallow aquifer (Stute et al. 2007, Sengupta et al. 2008). The primary argument is that the isotopic signature of the groundwater intersects the meteoric water line in a different location than the isotopic signature of pond water or other surface water (Figure 7.20).

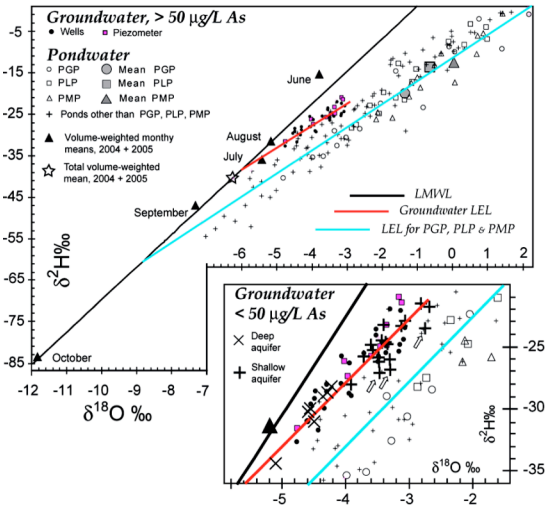

Sengupta et al. 2008

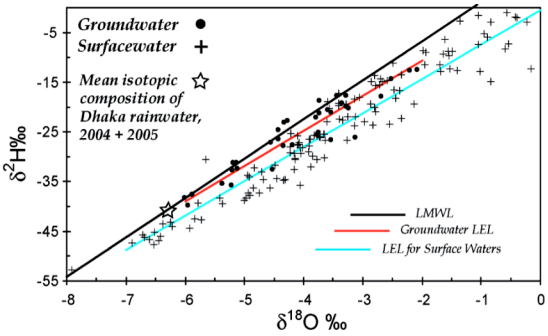

Stute et al. 2007

Figure 7.20 Groundwater and surface water isotopic data from West Bengal and Araihazar, Bangladesh.

The West Bengal data were collected by Sengupta et al. 2008, and the Araihazar data were collected by Stute et al. 2007.

Both datasets seem to suggest that ponds and other surface water bodies contain only rainwater from the very end of the monsoon season (September to October). It is not clear why the surface water, especially ponds, should contain only this type of water. If the landscape does not flood during the monsoon season and the ponds empty every dry season, the pond water, if it is well mixed, should represent the volume-weighted isotopic composition of rainfall. If instead

the well-mixed ponds do not empty every dry season, then the pond water should be slightly heavier than the volume-weighted isotopic composition of rainfall due to evaporation of the residual water. Finally, if the landscape floods, then the well-mixed ponds would include floodwater (river water and rainwater) from early in the monsoon season. We do not know the isotopic composition of the floodwater, but based on the river and rain data we collected (Figure 7.16 and Figure 7.17) it is likely heavier than the rainfall in September and October. Thus, the surface-water isotopic signature in Figure 7.20 does not represent what is expected for the region. It is possible that these data were collected from the very top surface of the different water bodies and that they water bodies are not well mixed, similar to our studied pond in Figure 7.19. These arguments motivate further study of the entire water column of surface-water bodies in Bangladesh and West Bengal.

7.5. Biodegradable Organic Carbon Experiment

Section 7.1.6 outlines BDOC experimental details and the protocols followed for sample collection. The rice field sample was collected from a depth of ~1.1 m below the field surface, the NP4 pond sample was collected from a depth of ~2.7 m below the bottom of pond P5 (a young pond), and the P1 pond sample was collected from a depth of ~0.5 m below the bottom of pond closest to the studied rice field (an old pond) (Harvey et al. 2006, Neumann et al. 2009). The samples were inculcated with unfiltered water collected from the same location. In the first experiment, a 5 mg/L standard (the positive control) and UV treated Milli-Q water (the negative control) were taken through the entire experimental procedure. The data show that the organic carbon concentration in the rice field did not change with time while the concentration in the pond recharge decreased by 4-8 mg/L or 0.3-0.7 mM (Figure 7.21 and Figure 7.22). This decrease is attributed to organic carbon that is biologically degradable, or labile.

The second BDOC experiment verified the lability of organic carbon in the pond recharge. A 5 mg/L standard and a UV-treated Milli-Q blank were used again as positive and negative controls, respectively, along with a UV-treated Milli-Q blank inoculated with pond recharge water (Figure 7.23 and Figure 7.24).

The experiments illustrated that the rice field sample lacked biologically available organic carbon that is needed to mobilize arsenic off of the soil and sediments, while the pond samples contained biologically available organic carbon and thus have the reducing power needed to mobilize arsenic. The experiment utilized unfiltered water as the inoculum, and therefore likely underrepresented the microbial community responsible for carbon mineralization within the subsurface, especially microbes associated with biofilms on the soils and sediments. However, the point of the experiment was not to replicate *in situ* chemical and biological

conditions, it was to test the lability of organic carbon by providing microbes within the water access to oxygen, the most energetically favorable electron acceptor. Oxygen is absent, or at extremely low levels, in the subsurface locations from which the water samples were obtained. Therefore, it is unlikely that the microbial community oxidizing the organic carbon within the experiment was the same community oxidizing organic carbon within the subsurface.

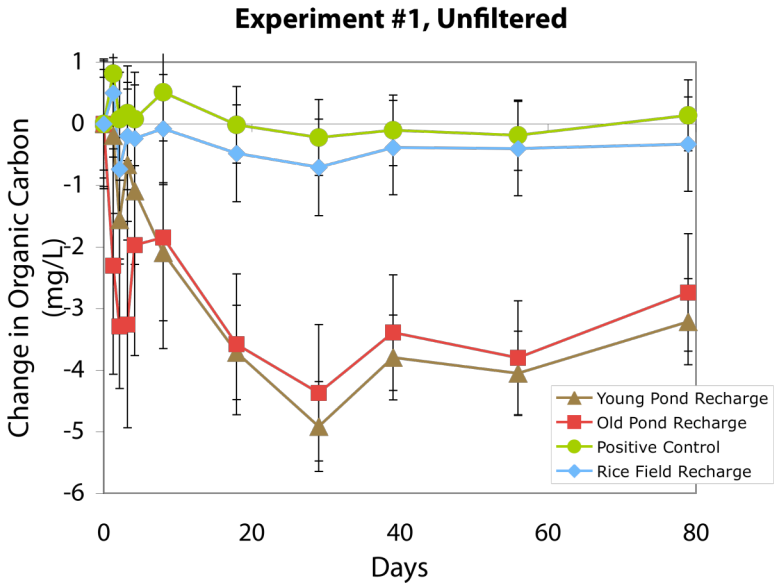

Figure 7.21 Organic carbon in different recharge sources during BDOC Experiment #1. Concentrations are unfiltered. The black error bars represent instrument error. The positive control is potassium acid phthalate.

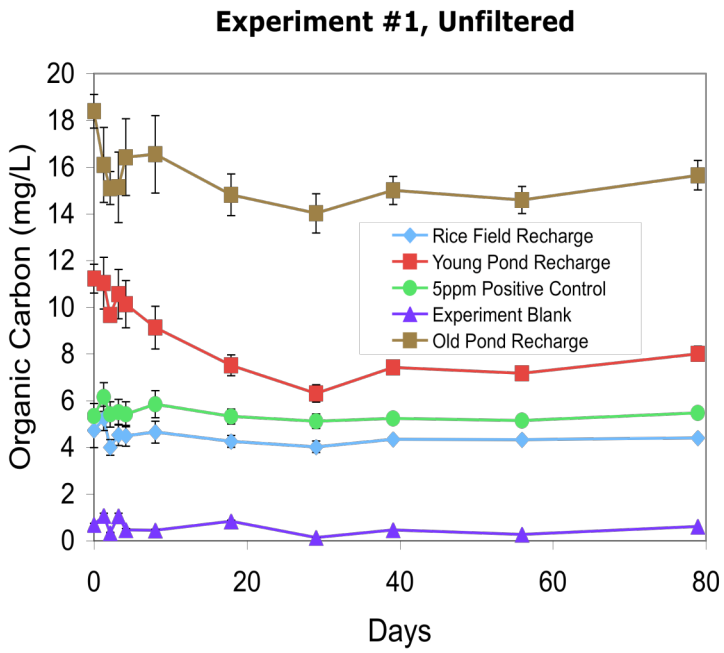

Figure 7.22 Change in organic carbon during BDOC Experiment #1.

Error bars represent the propagated error from Figure 7.21. The positive control is potassium acid phthalate.

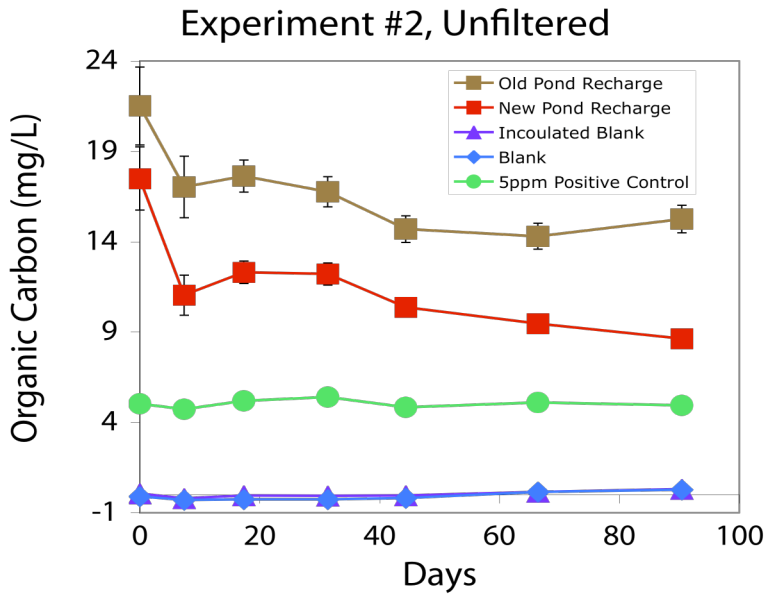

Figure 7.23 Organic carbon in different recharge sources during BDOC Experiment #2.

Error bars represent analytical uncertainty. The positive control is potassium acid phthalate.

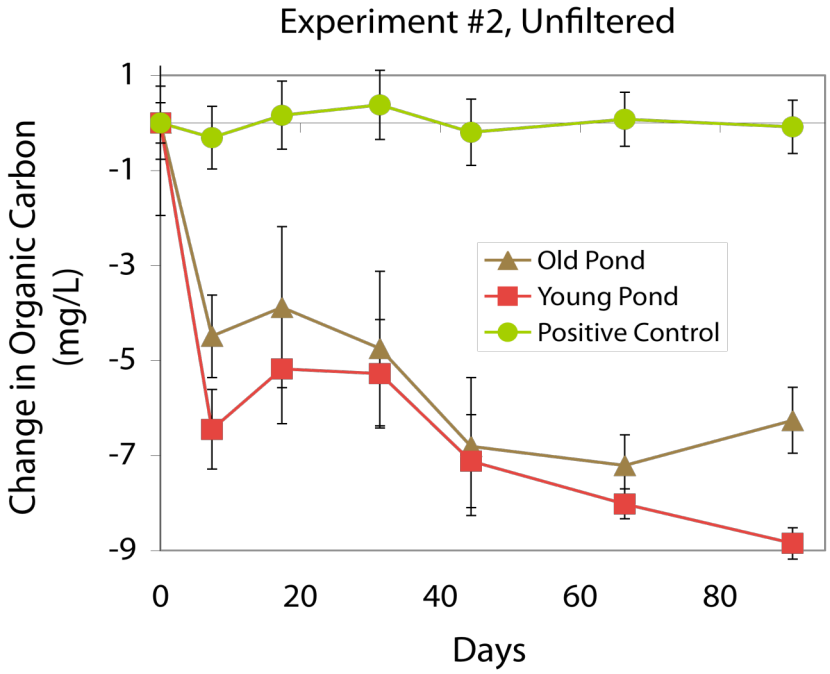

Figure 7.24 Change in organic carbon during BDOC Experiment #2.

Error bars represent the propagated error from Figure 7.23. The positive control is potassium acid phthalate.

7.6. Rice Field Information

7.6.1. Hydrology

(For more detailed information see chapter 2 and Neumann et al. (2009))

Agricultural studies describe two major features of rice fields that are important for their hydrology: the plough pan, which is a layer of low hydraulic conductivity that forms when the field is ploughed in water-saturated conditions, and the bund, or raised property boundary around the field that keeps irrigation water contained (Figure 7.25). Bunds act like drains for the field. Although bunds serve as dikes that contain surface water within the field, they also allow for water loss via downward infiltration. Because bunds follow property boundaries, the soil underneath them is usually not ploughed. Therefore the hydraulic conductivity of the bund is significantly greater than that of the rest of the field, which is underlined by the plough pan. In rice fields with established plough pans, the horizontal movement of surface water into bunds, and then vertically down through the bunds, often provides the largest loss of water from the fields (Walker and Rushton 1984, Tuong et al. 1994, Walker 1999, Huang et al. 2003).

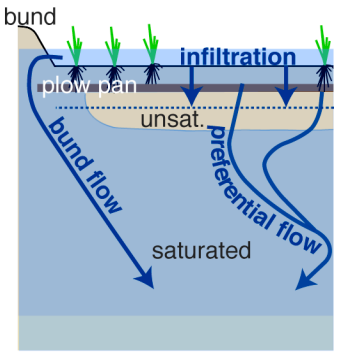

Figure 7.25 Flow patterns through a rice field.

Hydrologic studies of a rice field in Munshiganj confirm that most of the water from the surface of the rice field flowed into the bunds (Figure 7.26). Once the water entered the bunds, it flowed through the subsoil, and into the aquifer. In fact, water that did not flow through either

the bund or through cracks (preferential flow channels) in the field's subsoil did not recharge the aquifer. Tracer studies showed that the water that infiltrated vertically through the plough pan and remained in the soil matrix only reached a depth of roughly 50 cm over the course of the irrigation season (see chapter 2).

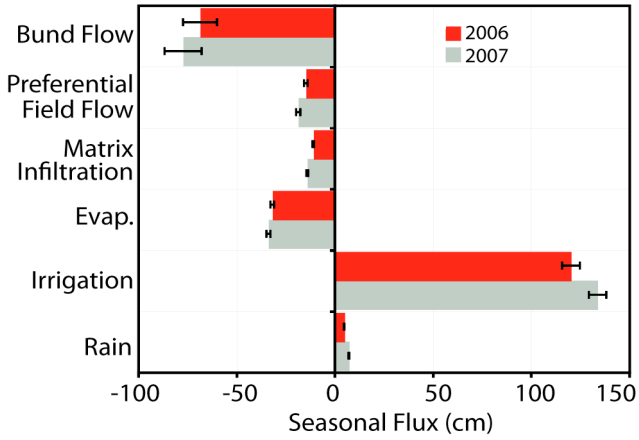

Figure 7.26 Seasonal water mass balance for the studied rice field.
Half of the water lost from the surface of the rice field flowed through the bunds, a fourth of the water was lost to evapotranspiration, an eighth was lost to preferential flow through the subsoil and an final eighth infiltrated through the soil matrix. Only bund flow and preferential flow were able to recharge the aquifer.

7.6.2. Chemistry

The dissolved oxygen concentration in the surface water of our studied rice field, which is the water that enters the bund and eventually recharges the aquifer, was continuously measured for multiple days, both in January and in April 2008, with an oxygen probe hooked up to a HOBO datalogger (Figure 7.27 and Figure 7.28). See section 4.3.4 for method details related to the HOBO logger probes. In January, when the rice plants were small, the field water was supersaturated with respect to oxygen during the day (when it was not raining) undersaturated with respect to oxygen during the night. This pattern is attributed to photosynthetic and

respiratory activities of floating algae (Kirk 2004). In April, when the rice plants were large, the water remained undersaturated with respect to oxygen both during the day and during the night. The plants likely shaded the water column and reduced daytime photosynthetic activity.

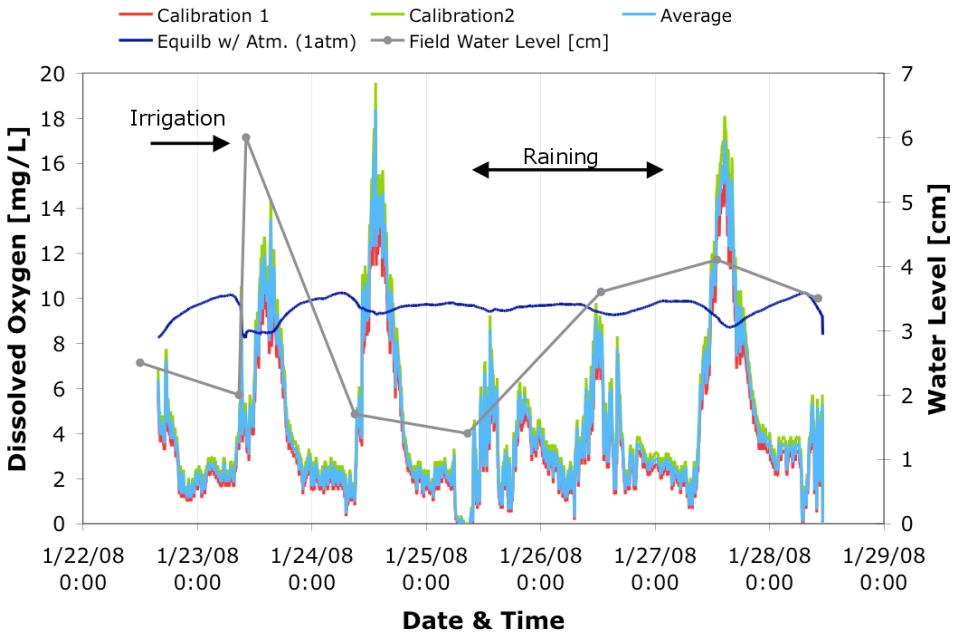

Figure 7.27 Dissolved oxygen and water levels in the rice field surface water, January 2008. Calibration 1 (red) for the oxygen probe is from before deployment and calibration 2 (green) is from after deployment. The dark blue line represents the oxygen concentration that would exist if the water were in equilibration with the atmosphere.

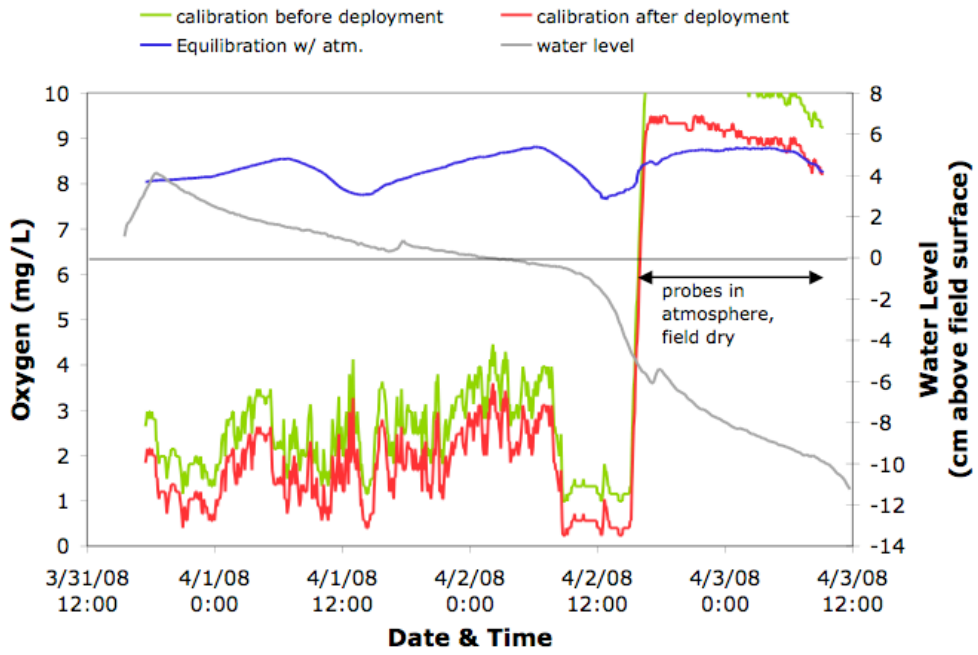

Figure 7.28 Dissolved oxygen and water levels in the rice field surface water, April 2008. Calibration 1 (green) for the oxygen probe is from before deployment and calibration 2 (red) is from after deployment. The dark blue line represents the oxygen concentration that would exist if the water were in equilibration with the atmosphere.

The rice field hydrology investigation showed that rice field recharge primarily travels through the bunds (the raised boundary around the field). Therefore, arsenic concentrations in the bund represent the arsenic content of the water that enters the aquifer. Figure 6.4 shows that, on average, bund water contains 12 μg/L (0.16 μM) of arsenic.

At our field site, the aquifer-derived irrigation water applied to the rice fields contains ~400 μg/L As. The low concentration of arsenic in the rice field recharge water (~12 μg/L) suggests that most of the arsenic applied to the rice field in the irrigation does not recycle back to the aquifer. An arsenic mass balance that utilizes the water mass balance results in Figure 7.26 shows that, indeed, the rice fields retain most of the irrigation arsenic (Figure 7.29). This arsenic is retained in the bund soil and surface soil of the fields.

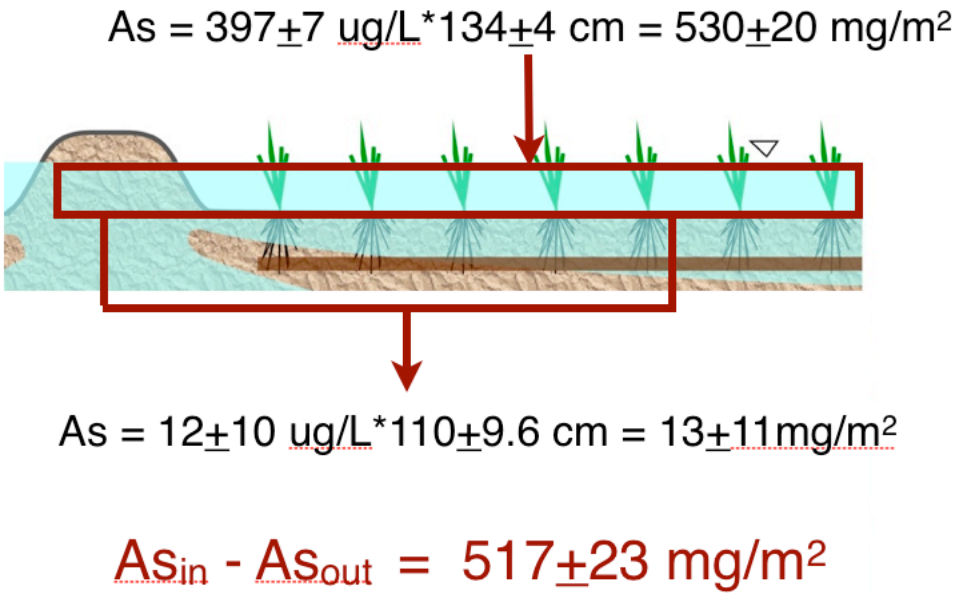

Figure 7.29 Arsenic mass balance for the rice field.

More arsenic is applied to the rice field with the groundwater-derived irrigation water than recycles back to the aquifer in the bund flow and preferential channel flow.

7.7. Concentrations in Aquifer Water (30m), Pond Recharge and Rice Field Recharge

Table 7.2 Aquifer and recharge chemistry data.

	Aquifer (30 m) *	Pond Rech. (unfiltered)†	Pond Rech. (filtered)†	Rice Rech. (unfiltered)§	Rice Rech. (filtered)§
pH	6.92 ± 0.07	6.53 ± 0.05	N/A	6.70 ± 0.05	N/A
DIC ** (mM)	8.67 ± 0.25	7.50 ± 0.38	N/A	9.8 ± 0.3	N/A
TOC (mM)	0.84 ± 0.19	Not measured	1.37 ± 0.15	Not measured	0.53 ± 0.08
BDOC (mM)	Not measured	Not measured	0.5 ± 0.1	Not measured	< 0.1
CH4 (mM)	1.16 ± 0.34	0.92 ± 0.38	N/A	0.13 ± 0.1	N/A
NH4-N (mM)	0.59 ± 0.08	Not measured	0.70 ± 0.19	Not measured	0.04 ± 0.01
As (μM)	6.36 ± 1.59	0.24 ± 0.01	0.30± 0.01	0.26 ± 0.01	0.24 ± 0.01
Fe (mM)	0.13 ± 0.07	0.24 ± 0.02	0.19 ± 0.02	0.10 ± 0.01	0.07 ± 0.02
Mn (μM)	25 ± 9	42 ± 2	42 ± 2	49 ± 1	49 ± 1
P (μM)	109 ± 51	2.8 ± 0.5	< 0.5	7.1 ± 0.9	0.3 ± 0.2
S (μM)	26 ± 39	< 2	< 2	541 ± 17	534 ± 17
Ca (mM)	2.29 ± 0.20	1.37 ± 0.06	1.37 ± 0.06	2.50 ± 0.08	2.50 ± 0.08
Mg (mM)	0.98 ± 0.09	0.47 ± 0.03	0.47 ± 0.03	1.04 ± 0.06	1.05 ± 0.06
Na (mM)	0.79 ± 0.14	0.24 ± 0.01	0.24 ± 0.01	1.18 ± 0.04	1.17 ± 0.04
K (mM)	0.20 ± 0.05	0.16 ± 0.01	0.16 ± 0.01	0.11 ± 0.01	0.11 ± 0.01
Cl (mM)	0.4±0.2	Not measured	0.17±0.01	Not measured	0.37±0.03

*Aquifer numbers are the average and standard deviation of data from the three 30 m wells in Swartz et al. (2004) and the one 30 m well in Roberts et al. (2007). Swartz et al. showed that filtered and unfiltered concentrations from the aquifer are identical.

†Pond recharge data taken from the deepest lysimeter within the pond sediment (2.7 m below the pond bottom). Samples collected January 2008.

§Rice field recharge data taken from the a lysimeter in the bund, or the raised boundary of the rice field (1.07 m below the field surface). Samples collected during the 2007 irrigation season.

** Dissolved inorganic carbon for the pond and rice field recharge was determined from alkalinity titrations and pH data. Alkalinity was assumed equal to bicarbonate.

7.8. PHREEQ-C Model

The measured composition of the pond recharge water from the deepest lysimeter and the 30m-deep aquifer water (Table 7.2) were utilized in a series of PHREEQ-C models to determine if our hypotheses about the transformations that are occurring along the pond recharge flow path are plausible. The PHREEQ-C results support the proposed processes rather than prove they actually occur.

7.8.1. BDOC Oxidation

First, it was assumed that 0.5 mM BDOC from the pond recharge is oxidized by 1 mM of magnetite. PHREEQ-C was utilized to determine the change in pH and alkalinity caused by this reaction. Relevant output from the PHREEQ-C model is shown below:

```
=============================================================
Database file:    /Applications/phreeqc-2.12.1/database/minteq.dat
-----------------------------------
TITLE             Magnetite Dissolution affect on pH and alkalinity

SOLUTION 1        pond water
```

pH	6.53
Fe(+2)	0.189
Ca	1.37
Mg	0.47
Na	0.24
K	0.16
C	7.5

REACTION 1

H2CO3	0.5
magnetite	1
1	millimoles

END

```
----------------------------------------
Beginning of batch-reaction calculations
----------------------------------------
Reaction          step 1
Using             solution 1              pond water
Using             reaction 1
```

Reaction 1

1.00E-03 moles of the following reaction have been added:

Reactant	Relative moles
H2CO3	0.5
magnetite	1

Element	Relative moles
C	0.5
Fe	3
H	1
O	5.5

Description of Solution

----

pH		7.61	Charge balance
Total alkalinity	(eq/kg)	8.69E-03	
Total CO2	(mol/kg)	8.00E-03	
Electrical balance	(eq)	-2.29E-04	
Percent error	100*(Cat-|An|)/(Cat+|An|)	-1.5	
Iterations		6	

End of simulation.

The model output shows that the reaction increases the pH of the solution from 6.53 to 7.61, increases the DIC concentration by 0.5 mM to 8 mM, and increases the Fe(II) concentration by 3 mM to 3.189 mM. In addition, we assume that this reaction releases ~1 mM of phosphorous due to apatite weathering or release from sorption sites. If apatite weathering occurs, then calcium is also released. We use this new solution composition as the starting point for the inverse models. A nice feature of the PHREEQ-C inverse model is that uncertainty can be assigned to both the initial and final solution compositions. We assign a large uncertainty to the iron, phosphorus and calcium concentrations in the initial solution composition.

7.8.2. Silicate Weathering

Relevant output from the inverse model exploring silicate weathering is shown below:

Database file: /Applications/phreeqc-2.12.1/database/minteq.dat

---

TITLE **Inverse modeling of pond water after magnetite reduction (Soln 1) and 30m aquifer water (Soln 2)**

SOLUTION 1 **pond water**

unit	mmol/L	
pH	7.61	
Fe(+2)	3.189	#+3 mM for magnetite reduction
Ca	2.37	#+1 mM for apatite dissol.
Mg	0.47	
Na	0.24	
K	0.16	
C	7.5	
P	1	#+1 mM for apatite dissol. & desorption
Mn(2)	0.042	
Si	0.98	

SOLUTION 2 **aquifer water**

unit	mmol/L
pH	6.92
Fe(+2)	0.132
Ca	2.29
Mg	0.98
Na	0.79
K	0.2
C	8.67
P	0.11
Mn(2)	0.025
Si	0.62

INVERSE_MODELING 1

solutions	1	2
uncertainty	0.1	
range		
phases		
Siderite	precip	
Vivianite	precip	
Rhodochrosite	precip	
Hydroxyapatite	precip	
Illite	precip	#weathering product
Calcite		
Hornblende	dissolve	

Albite	dissolve
Muscovite	dissolve
K-Feldspar	dissolve
Biotite	dissolve

balances #uncertainty %

	#soln 1	#soln 2
pH	0.05	0.07
Fe	0.5	0.52
Ca	1	0.09
Mg	0.06	0.1
Na	0.06	0.18
K	0.1	0.25
C	0.05	0.05
P	1	0.47
Mn	0.05	0.36
Si	0.1	0.08

PHASES

Biotite

KMg3AlSi3O10(OH)2 + 6H+ + 4H2O
= K+ + 3Mg+2 + Al(OH)4- + 3H4SiO4

log_k 0 #No log_k, Inverse modeling only

Hornblende

Na0.5Ca2Fe1.3Mg2.6Al1.1Al1.6Si6.4O22(OH)2 + 15H+ + 7H2O
= 0.5Na+ + 2Ca+2 + 2.6Mg+2 + 1.3Fe+2 + 2.7Al(OH)2+ + 6.4H4SiO4

log_k 0

Illite

K0.6Mg0.25Al2.3Si3.5O10(OH)2 + 11.2H2O
= 0.6K+ + 0.25Mg+2 + 2.3Al(OH)4- + 3.5H4SiO4 + 1.2H+

log_k -40.267
delta_h 54.684 kcal

K-Feldspar

KAlSi3O8 + 8H2O
= K+ + 3H4SiO4 + Al(OH)4-

log_k 0

END

Beginning of inverse modeling 1 calculations

Solution 1

	Input		Delta		Input+Delta
pH	7.61E+00	+	0.00E+00	=	7.61E+00
Al	0.00E+00	+	0.00E+00	=	0.00E+00
Alkalinity	8.17E-03	+	3.60E-04	=	8.53E-03
C(4)	7.51E-03	+	3.75E-04	=	7.88E-03
Ca	2.37E-03	+	-1.04E-03	=	1.33E-03

Fe(2)	3.19E-03	+	0.00E+00	=	3.19E-03
Fe(3)	0.00E+00	+	0.00E+00	=	0.00E+00
H(0)	0.00E+00	+	0.00E+00	=	0.00E+00
K	1.60E-04	+	0.00E+00	=	1.60E-04
Mg	4.70E-04	+	2.82E-05	=	4.99E-04
Mn(2)	4.20E-05	+	0.00E+00	=	4.20E-05
Mn(3)	0.00E+00	+	0.00E+00	=	0.00E+00
Mn(6)	0.00E+00	+	0.00E+00	=	0.00E+00
Mn(7)	0.00E+00	+	0.00E+00	=	0.00E+00
Na	2.40E-04	+	0.00E+00	=	2.40E-04
O(0)	0.00E+00	+	0.00E+00	=	0.00E+00
P	1.00E-03	+	1.00E-03	=	2.00E-03
Si	9.81E-04	+	-9.81E-05	=	8.83E-04

Solution 2

	Input		Delta		Input+Delta
pH	6.92E+00	+	7.00E-02	=	6.99E+00
Al	0.00E+00	+	0.00E+00	=	0.00E+00
Alkalinity	7.09E-03	+	-1.28E-04	=	6.96E-03
C(4)	8.68E-03	+	-4.34E-04	=	8.24E-03
Ca	2.29E-03	+	-2.06E-04	=	2.09E-03
Fe(2)	1.32E-04	+	-4.39E-05	=	8.82E-05
Fe(3)	0.00E+00	+	0.00E+00	=	0.00E+00
H(0)	0.00E+00	+	0.00E+00	=	0.00E+00
K	2.00E-04	+	5.00E-05	=	2.50E-04
Mg	9.81E-04	+	-9.81E-05	=	8.83E-04
Mn(2)	2.50E-05	+	0.00E+00	=	2.50E-05
Mn(3)	0.00E+00	+	0.00E+00	=	0.00E+00
Mn(6)	0.00E+00	+	0.00E+00	=	0.00E+00
Mn(7)	0.00E+00	+	0.00E+00	=	0.00E+00
Na	7.91E-04	+	-1.42E-04	=	6.48E-04
O(0)	0.00E+00	+	0.00E+00	=	0.00E+00
P	1.10E-04	+	-7.36E-06	=	1.03E-04
Si	6.21E-04	+	0.00E+00	=	6.21E-04

Phase mole transfers:

		Minimum	Maximum
Siderite	-3.28E-03	-4.71E-03	-1.55E-03
Rhodochrosite	-1.70E-05	-2.81E-05	-5.91E-06
Hydroxyapatite	-6.33E-04	-6.48E-04	-6.01E-04
Illite	-1.42E-03	-1.64E-03	-1.32E-03
Calcite	3.65E-03	1.99E-03	5.23E-03
Hornblende	1.33E-04	1.07E-04	1.67E-04
Albite	3.42E-04	3.10E-04	4.67E-04
Muscovite	8.08E-04	7.51E-04	9.54E-04
Biotite	1.31E-04	9.80E-05	1.57E-04

Model contains minimum number of phases

==========

```
Summary of inverse modeling:
                Number of models found:                 1
                Number of minimal models found:         1
-----------------
End of simulation
-----------------
```

With the given phases and uncertainty, PHREEQ-C was able to find one model that could explain the transformation of pond recharge (solution 1) into the water seen at the 30 m depth in the aquifer (solution 2) assuming silicate weathering provides the cation concentrations. The model required approximately 1 mM less calcium and 1 mM more phosphorous in solution 1 than was initially assumed. The model involved the dissolution of calcite and the weathering of hornblende, albite muscovite and biotite into illite. In addition, it requires the precipitation of siderite, rhodicrosite, and hydroxyapatite, all minerals that are supersaturated in the aquifer water (see section 7.11).

7.8.3. Carbonate Dissolution

Relevant output from the inverse model exploring carbonate dissolution is shown below:

Database file: /Applications/phreeqc-2.12.1/database/minteq.dat

---

TITLE **Inverse modeling of pond water after magnetite reduction (Soln 1) and 30m aquifer water (Soln 2)**

SOLUTION 1 **pond water**

unit	mmol/L	
pH	7.61	
Fe(+2)	3.189	#+3 mM for magnetite reduction
Ca	2.37	#+1 mM for apatite dissol.
Mg	0.47	
Na	0.24	
K	0.16	
C	7.5	
P	1	#+1 mM for apatite dissol. &desorption
Mn(2)	0.042	
Si	0.98	

SOLUTION 2 **aquifer water**

unit	mmol/L
pH	6.92
Fe(+2)	0.132
Ca	2.29
Mg	0.98
Na	0.79
K	0.2
C	8.67
P	0.11
Mn(2)	0.025
Si	0.62

INVERSE_MODELING 1

solutions 1 2
uncertainty 0.1
range
phases

Siderite	precip
Vivianite	precip
Rhodochrosite	precip
Hydroxyapatite	precip
Calcite	
Dolomite	dissolve
Magnetite	dissolve
Nahcolite	dissolve

quartz	

balances	#uncertainty % #soln 1	#soln 2
pH	0.05	0.07
Fe	0.5	0.52
Ca	1	0.09
Mg	0.06	0.1
Na	0.06	0.18
K	0.1	0.25
C	0.05	0.05
P	1	0.47
Mn	0.05	0.36
Si	0.05	0.05

END

Beginning of inverse modeling 1 calculations.

Solution 1

	Input		Delta		Input+Delta
pH	7.61E+00	+	0.00E+00	=	7.61E+00
Alkalinity	8.47E-03	+	0.00E+00	=	8.47E-03
C(-4)	0.00E+00	+	0.00E+00	=	0.00E+00
C(4)	7.51E-03	+	0.00E+00	=	7.51E-03
Ca	2.37E-03	+	-1.25E-03	=	1.12E-03
Fe(2)	3.19E-03	+	0.00E+00	=	3.19E-03
Fe(3)	0.00E+00	+	0.00E+00	=	0.00E+00
H(0)	0.00E+00	+	0.00E+00	=	0.00E+00
K	1.60E-04	+	0.00E+00	=	1.60E-04
Mg	4.70E-04	+	0.00E+00	=	4.70E-04
Mn(2)	4.20E-05	+	0.00E+00	=	4.20E-05
Mn(3)	0.00E+00	+	0.00E+00	=	0.00E+00
Mn(6)	0.00E+00	+	0.00E+00	=	0.00E+00
Mn(7)	0.00E+00	+	0.00E+00	=	0.00E+00
Na	2.40E-04	+	0.00E+00	=	2.40E-04
O(0)	0.00E+00	+	0.00E+00	=	0.00E+00
P	1.00E-03	+	5.78E-04	=	1.58E-03
Si	9.81E-04	+	0.00E+00	=	9.81E-04

Solution 2

	Input		Delta		Input+Delta
pH	6.92E+00	+	0.00E+00	=	6.92E+00
Alkalinity	7.10E-03	+	1.85E-04	=	7.29E-03
C(-4)	0.00E+00	+	0.00E+00	=	0.00E+00
C(4)	8.68E-03	+	2.28E-04	=	8.90E-03
Ca	2.29E-03	+	-2.06E-04	=	2.09E-03
Fe(2)	1.32E-04	+	0.00E+00	=	1.32E-04
Fe(3)	0.00E+00	+	0.00E+00	=	0.00E+00
H(0)	0.00E+00	+	0.00E+00	=	0.00E+00

K	2.00E-04	+	-4.00E-05	=	1.60E-04
Mg	9.81E-04	+	0.00E+00	=	9.81E-04
Mn(2)	2.50E-05	+	0.00E+00	=	2.50E-05
Mn(3)	0.00E+00	+	0.00E+00	=	0.00E+00
Mn(6)	0.00E+00	+	0.00E+00	=	0.00E+00
Mn(7)	0.00E+00	+	0.00E+00	=	0.00E+00
Na	7.91E-04	+	0.00E+00	=	7.91E-04
O(0)	0.00E+00	+	0.00E+00	=	0.00E+00
P	1.10E-04	+	0.00E+00	=	1.10E-04
Si	6.20E-04	+	0.00E+00	=	6.20E-04

Phase mole transfers:

		Minimum	Maximum	
Siderite	-3.06E-03	-4.61E-03	-1.40E-03	FeCO3
Rhodochrosite	-1.70E-05	-2.81E-05	-5.91E-06	MnCO3
Hydroxyapatite	-4.90E-04	-6.45E-04	-2.63E-04	Ca5(PO4)3OH
Calcite	2.90E-03	3.72E-04	5.13E-03	CaCO3
Dolomite	5.10E-04	3.84E-04	6.37E-04	CaMg(CO3)2
Nahcolite	5.50E-04	3.94E-04	7.07E-04	NaHCO3
Quartz	-3.60E-04	-4.40E-04	-2.80E-04	SiO2

Model contains minimum number of phases

==========

Solution 1

	Input		Delta		Input+Delta
pH	7.61E+00	+	0.00E+00	=	7.61E+00
Alkalinity	8.47E-03	+	0.00E+00	=	8.47E-03
C(-4)	0.00E+00	+	0.00E+00	=	0.00E+00
C(4)	7.51E-03	+	0.00E+00	=	7.51E-03
Ca	2.37E-03	+	-1.25E-03	=	1.12E-03
Fe(2)	3.19E-03	+	0.00E+00	=	3.19E-03
Fe(3)	0.00E+00	+	0.00E+00	=	0.00E+00
H(0)	0.00E+00	+	0.00E+00	=	0.00E+00
K	1.60E-04	+	0.00E+00	=	1.60E-04
Mg	4.70E-04	+	0.00E+00	=	4.70E-04
Mn(2)	4.20E-05	+	0.00E+00	=	4.20E-05
Mn(3)	0.00E+00	+	0.00E+00	=	0.00E+00
Mn(6)	0.00E+00	+	0.00E+00	=	0.00E+00
Mn(7)	0.00E+00	+	0.00E+00	=	0.00E+00
Na	2.40E-04	+	0.00E+00	=	2.40E-04
O(0)	0.00E+00	+	0.00E+00	=	0.00E+00
P	1.00E-03	+	5.78E-04	=	1.58E-03
Si	9.81E-04	+	0.00E+00	=	9.81E-04

Solution 2

	Input		Delta		Input+Delta
pH	6.92E+00	+	0.00E+00	=	6.92E+00
Alkalinity	7.10E-03	+	1.85E-04	=	7.29E-03
C(-4)	0.00E+00	+	0.00E+00	=	0.00E+00
C(4)	8.68E-03	+	2.28E-04	=	8.90E-03

Ca	2.29E-03	+	-2.06E-04	=	2.09E-03
Fe(2)	1.32E-04	+	0.00E+00	=	1.32E-04
Fe(3)	0.00E+00	+	0.00E+00	=	0.00E+00
H(0)	0.00E+00	+	0.00E+00	=	0.00E+00
K	2.00E-04	+	-4.00E-05	=	1.60E-04
Mg	9.81E-04	+	0.00E+00	=	9.81E-04
Mn(2)	2.50E-05	+	0.00E+00	=	2.50E-05
Mn(3)	0.00E+00	+	0.00E+00	=	0.00E+00
Mn(6)	0.00E+00	+	0.00E+00	=	0.00E+00
Mn(7)	0.00E+00	+	0.00E+00	=	0.00E+00
Na	7.91E-04	+	0.00E+00	=	7.91E-04
O(0)	0.00E+00	+	0.00E+00	=	0.00E+00
P	1.10E-04	+	0.00E+00	=	1.10E-04
Si	6.20E-04	+	0.00E+00	=	6.20E-04

Phase mole transfers:

		Minimum	Maximum	
Siderite	-3.06E-03	-4.61E-03	-1.40E-03	FeCO3
Rhodochrosite	-1.70E-05	-2.81E-05	-5.91E-06	MnCO3
Hydroxyapatite	-4.90E-04	-6.45E-04	-2.63E-04	Ca5(PO4)3OH
Calcite	3.41E-03	8.12E-04	5.51E-03	CaCO3
Magnetite	5.10E-04	3.84E-04	6.37E-04	MgCO3
Nahcolite	5.50E-04	3.94E-04	7.07E-04	NaHCO3
Quartz	-3.60E-04	-4.40E-04	-2.80E-04	SiO2

Model contains minimum number of phases

==========

Solution 1

	Input		Delta		Input+Delta
pH	7.61E+00	+	0.00E+00	=	7.61E+00
Alkalinity	8.47E-03	+	0.00E+00	=	8.47E-03
C(-4)	0.00E+00	+	0.00E+00	=	0.00E+00
C(4)	7.51E-03	+	0.00E+00	=	7.51E-03
Ca	2.37E-03	+	-7.33E-04	=	1.64E-03
Fe(2)	3.19E-03	+	-3.50E-04	=	2.84E-03
Fe(3)	0.00E+00	+	0.00E+00	=	0.00E+00
H(0)	0.00E+00	+	0.00E+00	=	0.00E+00
K	1.60E-04	+	0.00E+00	=	1.60E-04
Mg	4.70E-04	+	0.00E+00	=	4.70E-04
Mn(2)	4.20E-05	+	0.00E+00	=	4.20E-05
Mn(3)	0.00E+00	+	0.00E+00	=	0.00E+00
Mn(6)	0.00E+00	+	0.00E+00	=	0.00E+00
Mn(7)	0.00E+00	+	0.00E+00	=	0.00E+00
Na	2.40E-04	+	0.00E+00	=	2.40E-04
O(0)	0.00E+00	+	0.00E+00	=	0.00E+00
P	1.00E-03	+	9.16E-04	=	1.92E-03
Si	9.81E-04	+	0.00E+00	=	9.81E-04

Solution 2

	Input		Delta		Input+Delta

pH	6.92E+00	+	0.00E+00	=	6.92E+00
Alkalinity	7.10E-03	+	3.13E-04	=	7.41E-03
C(-4)	0.00E+00	+	0.00E+00	=	0.00E+00
C(4)	8.68E-03	+	3.85E-04	=	9.06E-03
Ca	2.29E-03	+	-1.43E-04	=	2.15E-03
Fe(2)	1.32E-04	+	0.00E+00	=	1.32E-04
Fe(3)	0.00E+00	+	0.00E+00	=	0.00E+00
H(0)	0.00E+00	+	0.00E+00	=	0.00E+00
K	2.00E-04	+	-4.00E-05	=	1.60E-04
Mg	9.81E-04	+	0.00E+00	=	9.81E-04
Mn(2)	2.50E-05	+	0.00E+00	=	2.50E-05
Mn(3)	0.00E+00	+	0.00E+00	=	0.00E+00
Mn(6)	0.00E+00	+	0.00E+00	=	0.00E+00
Mn(7)	0.00E+00	+	0.00E+00	=	0.00E+00
Na	7.91E-04	+	0.00E+00	=	7.91E-04
O(0)	0.00E+00	+	0.00E+00	=	0.00E+00
P	1.10E-04	+	0.00E+00	=	1.10E-04
Si	6.20E-04	+	0.00E+00	=	6.20E-04

Phase mole transfers:

		Minimum	Maximum	
Vivianite	-9.03E-04	-9.72E-04	-7.25E-04	Fe3(PO4)2:8H2O
Rhodochrosite	-1.70E-05	-2.81E-05	-5.91E-06	MnCO3
Dolomite	5.10E-04	3.84E-04	6.37E-04	CaMg(CO3)2
Nahcolite	5.50E-04	3.94E-04	7.07E-04	NaHCO3
Quartz	-3.61E-04	-4.41E-04	-2.80E-04	SiO2

Model contains minimum number of phases

==========

Solution 1

	Input		Delta		Input+Delta
pH	7.61E+00	+	0.00E+00	=	7.61E+00
Alkalinity	8.47E-03	+	1.24E-04	=	8.59E-03
C(-4)	0.00E+00	+	0.00E+00	=	0.00E+00
C(4)	7.51E-03	+	1.26E-04	=	7.63E-03
Ca	2.37E-03	+	-2.87E-04	=	2.09E-03
Fe(2)	3.19E-03	+	-9.27E-04	=	2.27E-03
Fe(3)	0.00E+00	+	0.00E+00	=	0.00E+00
H(0)	0.00E+00	+	0.00E+00	=	0.00E+00
K	1.60E-04	+	0.00E+00	=	1.60E-04
Mg	4.70E-04	+	0.00E+00	=	4.70E-04
Mn(2)	4.20E-05	+	0.00E+00	=	4.20E-05
Mn(3)	0.00E+00	+	0.00E+00	=	0.00E+00
Mn(6)	0.00E+00	+	0.00E+00	=	0.00E+00
Mn(7)	0.00E+00	+	0.00E+00	=	0.00E+00
Na	2.40E-04	+	0.00E+00	=	2.40E-04
O(0)	0.00E+00	+	0.00E+00	=	0.00E+00
P	1.00E-03	+	5.31E-04	=	1.53E-03
Si	9.81E-04	+	0.00E+00	=	9.81E-04

Solution 2

	Input		Delta		Input+Delta
pH	6.92E+00	+	5.78E-02	=	6.98E+00
Alkalinity	7.10E-03	+	1.85E-04	=	7.29E-03
C(-4)	0.00E+00	+	0.00E+00	=	0.00E+00
C(4)	8.68E-03	+	0.00E+00	=	8.68E-03
Ca	2.29E-03	+	-2.06E-04	=	2.09E-03
Fe(2)	1.32E-04	+	0.00E+00	=	1.32E-04
Fe(3)	0.00E+00	+	0.00E+00	=	0.00E+00
H(0)	0.00E+00	+	0.00E+00	=	0.00E+00
K	2.00E-04	+	-4.00E-05	=	1.60E-04
Mg	9.81E-04	+	0.00E+00	=	9.81E-04
Mn(2)	2.50E-05	+	0.00E+00	=	2.50E-05
Mn(3)	0.00E+00	+	0.00E+00	=	0.00E+00
Mn(6)	0.00E+00	+	0.00E+00	=	0.00E+00
Mn(7)	0.00E+00	+	0.00E+00	=	0.00E+00
Na	7.91E-04	+	0.00E+00	=	7.91E-04
O(0)	0.00E+00	+	0.00E+00	=	0.00E+00
P	1.10E-04	+	0.00E+00	=	1.10E-04
Si	6.20E-04	+	0.00E+00	=	6.20E-04

Phase mole transfers:

		Minimum	Maximum	
Vivianite	-7.11E-04	-8.62E-04	-6.27E-04	Fe3(PO4)2:8H2O
Rhodochrosite	-1.70E-05	-2.81E-05	-5.91E-06	MnCO3
Magnetite	5.10E-04	3.84E-04	6.37E-04	MgCO3
Nahcolite	5.50E-04	3.94E-04	7.07E-04	NaHCO3
Quartz	-3.61E-04	-4.41E-04	-2.80E-04	SiO2

Model contains minimum number of phases

==========

Summary of inverse modeling:

Number of models found: 10

Number of minimal models found: 4

End of simulation.

With the given phases and uncertainty, PHREEQ-C was able to find 10 models that could explain the transformation of pond recharge (solution 1) into the water seen at the 30 m depth in the aquifer (solution 2) assuming the carbonate dissolution provides the cation concentrations. For all ten models, less calcium (0.2 to 1 mM less) and more phosphorous (0.5 to 1 mM more) was required in solution 1 than was initially assumed. The four models that utilized a minimum

number of mineral phases had two solution sets. In one solution set, siderite, rhodicrosite, hydroxyapatite and quartz precipitated, while calcite, nahcolite and either dolomite or magnetite dissolved. In the other solution set, vivianite, rhodiscrosite and quartz precipitated while nahcolite and either dolomite of magnetite dissolved.

7.8.4. Summary

Both PHREEQ-C models (silicate weathering and carbonate dissolution) required that the BDOC oxidation and magnetite reduction release 1.5 to 2 mM of phosphorous. This phosphorous could be released either by desorption from magnetite or by apatite dissolution due to microbial weathering for nutrient acquisition (Welch et al. 2002, Mailloux et al. 2009). Calculations using extraction data from Swartz et al. (2004), which assume that all of the phosphorous released in the pH 2 extraction was sorbed onto magnetite (represented by all of the iron released in the oxalic acid extraction), suggest that oxidation of the BDOC and reduction of magnetite could release ~0.5 mM of phosphorous. In laboratory experiments with apatite, Welch et al. (2002) saw up to 0.5 mM of phosphorous released with the addition of 1 mM glucose (6mM of carbon). By the end of the experiment, the phosphorus released in the abiotic control had plateaued while the amount released by the microbes was linearly increasing. It is not clear how much phosphorous would have ultimately been released if the experiment were carried out longer. In incubation experiments on Bengali sediment (Van Geen et al. 2004, Radloff et al. 2007), on average, for every 1 mM of P released, 2.6 mM of Fe is released. This ratio suggests the BDOC oxidation by magnetite, which releases 3 mM of Fe, would release ~1.2 mM of phosphorous. The amount of phosphorus released in the incubations is within the range needed by the PHREEQ-C models.

7.9. Calculation of Arsenic Released from Magnetite Reduction

The amount of arsenic released with the reduction and dissolution of 1mM of magnetite and the oxidation of 0.5 mM of organic carbon, was determined using the extraction data from Swartz et al. (2004). We assumed that the oxalic acid extraction primarily targeted magnetite, since oxalic acid is known to dissolve magnetite (Canfield and Berner 1987, Canfield 1989). If sorption sites are empty (no sorbed arsenic), we simply consider the average amount of arsenic released to that of iron in the oxalic acid extraction, which is 156 μmol As/mol Fe (Swartz et al. 2004). Therefore, with three millimoles of iron released per liter of water from magnetite reduction, we calculate that 0.47 μM of arsenic is released. If sorption sites are full, then we also consider the amount of arsenic and iron released in the $MgCl_2$ and NaH_2PO_4 extractions. Inclusion of these two extractions increases the amount of arsenic released to 289.6 μmol As/mol Fe (Swartz et al. 2004), increasing the amount of arsenic released 0.87 μM.

We determined the amount of arsenic released from complete reduction of all the magnetite in the aquifer sediments two different ways. The first approach assumed that all of the magnetite in the aquifer was contained in the sediment fraction separated by Swartz et al. (2004) with a hand magnet, and that all of the arsenic in this fraction (10μg/g fraction) was associated with the magnetite. The abundance of this fraction (15%) was utilized along with a sediment bulk density of 2.65 g/cm^3 and a porosity of 0.3 to calculate that complete reduction of magnetite would release 7950 μg/L As or 106 μM As. The second approach utilized Swartz et al.'s (2004) extraction data. We assumed that the oxalic acid extraction dissolved all of the available magnetite. On average, this extraction released 294 ng As/g sediment. Utilizing a bulk sediment density of 2.65 g/cm^3 and a porosity of 0.3, we calculated that complete magnetite reduction would release 1558 ug/L As or 21 μM.

7.10. Gibbs Free Energy Calculations

All concentration data used in these calculations are presented in Table 7.2.

$12Fe_3O_4 + C_6H_{12}O_6 + 66H^+ \rightarrow 36Fe^{2+} + 6HCO_3^- + 36H2O$
ΔG^o = -1872.95 kJ/mol (Kostka and Nealson 1995)
$\Delta G = \Delta G^o + RTln(Q)$

Pond Recharge:
pH = 6.5
Fe = 0.24 mM (assumed all of the Fe is Fe(II))
HCO_3^-= 4.5 mM
BDOC = 0.5 mM
$\Delta G = \Delta G^o + RTln(10^{-130.3} * 10^{-14.1} * 10^{+429} * 10^{+3.3})$
= -1872.95 kJ/mol + 2.479 kJ/mol*ln($10^{+287.9}$)= -229.6 kJ/mol

30m-deep aquifer water:
pH = 6.92
Fe(II) = 0.132 mM
HCO_3^-= 6.89 mM
BDOC = 0.5mM (assumed based on BDOC experiment)
$\Delta G = \Delta G^o + RTln(10^{-136.6} * 10^{-12.97} * 10^{+456.7} * 10^{+3..3})$
= -1872.95 kJ/mol + 2.479 kJ/mol*ln($10^{+155.2}$) = -101.2 kJ/mol

7.11. Mineral Saturation Indices

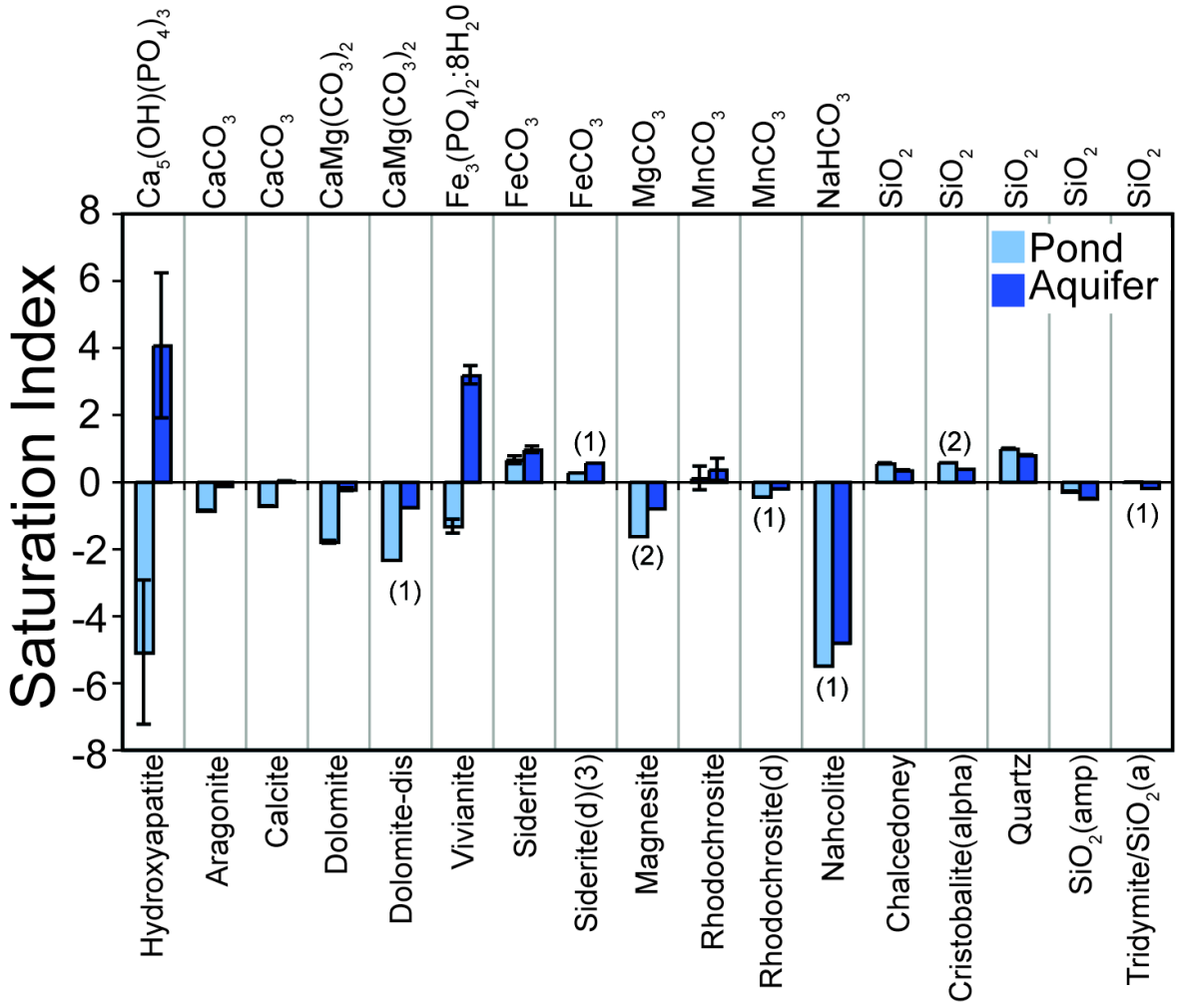

Figure 7.30 Saturation indices for the pond recharge and 30 m-deep aquifer water.

Saturation indices are calculated by the MINTEQ, PHREEQ-C and WATEQ4F databases. The error bars represent one standard deviation across the databases. The number in parentheses notes how many databases had information on this mineral. If no number is present then all three databases are represented.

7.12. References

Ashfaque, K. N. (2007), Effect of hydrological flow pattern on groundwater arsenic concentration in Bangladesh, Ph.D. Thesis, Massachusetts Institute of Technology: Cambridge, MA, pp. 286.

BGS, DFID, and DPHE (2001), Arsenic contamination of groundwater in Bangladesh, *BGS Technical Report WC/00/19, Volume 1 & 2*, British Geological Survey, Keyworth.

Canfield, D. E., and R. A. Berner (1987), Dissolution and pyritization of magnetite in anoxic marine sediments, *Geochim. Cosmochim. Acta, 51*, 645-659.

Canfield, D. E. (1989), Reactive iron in marine sediments, *Geochim. Cosmochim. Acta, 53*, 619-632.

Dhar, R. K., Y. Zheng, M. Stute, G. van, A., Z. Cheng, M. Shanewaz, M. Shamsudduha, M. A. Hoque, M. W. Rahman, and K. M. Ahmed (2008) Temporal variability of groundwater chemistry in shallow and deep aquifers of Araihazar, Bangladesh, *J. Contam. Hydrol., 99*, 97-111.

Diersch, H. J. G. (2002), *FEFLOW finite element subsurface flow and transport simulation system, Release 5.0, User's Manual / Reference Manual / White Papers*, WASY Ltd, Berlin.

Dittmar, J., A. Voegelin, L. Roberts, S. J. Hug, G. C. Saha, M. A. Ali, A. B. M. Badruzzaman, and R. Kretzschmar (2007), Spatial distribution and temporal variability of arsenic in irrigated rice field in Bangladesh: 2. Paddy soil, *Environ. Sci. Technol., 41*, 5967-5972.

Doherty, J. (1994), *PEST,* Watermark Computing, Corinda, Australia.

Dowling, C. B., R. J. Poreda, A. R. Basu, S. L. Peters, and P. K. Aggarwal (2002), Geochemical study of arsenic release mechanisms in the Bengal Basin groundwater, *Water Resour. Res., 38*,

Freeze, R. A., and J. A. Cherry (1979), *Groundwater,* Prentice Hall, Englewood Cliffs, NJ.

Goode, D. (1996), Direct simulation of groundwater age, *Water Resour. Res., 32*, 289-296.

Harvey, C. F., C. H. Swartz, A. B. M. Badruzzaman, N. Keon-Blute, W. Yu, M. A. Ali, J. Jay, R. Beckie, V. Niedan, D. Brabander, P. M. Oates, K. N. Ashfaque, S. Islam, H. F. Hemond, and M. F. Ahmed (2002), Arsenic mobility and groundwater extraction in Bangladesh, *Science, 298*, 1602-1606.

Harvey, C. F., K. N. Ashfaque, W. Yu, A. B. M. Badruzzaman, M. A. Ali, P. M. Oates, H. A. Michael, R. B. Neumann, R. Beckie, S. Islam, and M. F. Ahmed (2006), Groundwater dynamics and arsenic contamination in Bangladesh, *Chem. Geol., 228*, 112-136.

Hsieh, P. A. (1996), Deformation-induced changes in hydraulic head during ground-water withdrawal, *Ground Water, 34*, 1082-1089.

Huang, H. C., C. W. Liu, S. K. Chen, and J. S. Chen (2003), Analysis of percolation and seepage through paddy bunds, *J. Hydrol., 284*, 13-25.

Huq, M. F., and A. K. M. S. Islam (1977), A survey of man-made water areas in a village in Bangladesh to determine their productive capacity, current use and reasons for under-utilization, *Aquaculture, 12*, 75-88.

Kirk, G. (2004), *The Biogeochemistry of Submerged Soils,* John Wiley & Sons, New Jersey.

Klump, S., R. Kipfer, O. A. Cirpka, C. F. Harvey, M. S. Brennwald, K. N. Ashfaque, A. B. M. Badruzzaman, S. J. Hug, and D. M. Imboden (2006), Groundwater dynamics and arsenic mobilization in Bangladesh assessed using noble gases and tritium, *Environ. Sci. Technol., 40*, 243-250.

Kostka, J. E., and K. H. Nealson (1995), Dissolution and reduction of magnetite by bacteria, *Environ. Sci. Technol., 29*, 2535-2540.

Kränzlin, I. (2000), Pond management in rural Bangladesh: system changes, problems and prospects, and implication for sustainable development, Ph.D. Thesis, Basel University: Switzerland, pp. 213.

Mailloux, B. J., E. Alexandrova, A. R. Keimowitz, K. Wovkulich, G. A. Freyer, M. Herron, J. F. Stolz, T. C. Kenna, T. Pichler, M. L. Polizzotto, H. Dong, M. Bishop, and P. S. K. Knappett (2009), Microbial Mineral Weathering for Nutrient Acquisition Releases Arsenic, *Appl. Environ. Microbiol., 75*, 2558-2565.

McArthur, J. M., D. M. Banerjee, K. A. Hudson-Edwards, R. Mishra, R. Purohit, P. Ravenscroft, A. Cronin, R. J. Howarth, A. Chatterjee, T. Talukder, D. Lowry, S. Houghton, and D. K. Chadha (2004), Natural organic matter in sedimentary basins and its relation to arsenic in anoxic ground water: the example of West Bengal and its worldwide implications, *Appl. Geochem., 19*, 1255-1293.

Neumann, R. B., M. L. Polizzotto, A. B. M. Badruzzaman, M. A. Ali, Z. Zhang, and C. F. Harvey (2009), The Hydrology of a Groundwater-Irrigated Rice Field in Bangladesh: Seasonal and Daily Mechanisms of Infiltration, *Water Resour. Res., 45*, doi:10.1029/2008WR007542.

Radloff, K. A., Z. Cheng, M. W. Rahman, K. M. Ahmed, B. J. Mailloux, A. R. Juhl, P. Schlosser, and A. van Geen (2007), Mobilization of Arsenic During One-Year Incubations of Grey Aquifer Sands from Araihazar, Bangladesh, *Environ. Sci. Technol., 41*, 3639-3645.

Roberts, L., S. J. Hug, J. Dittmar, A. Voegelin, G. C. Saha, M. A. Ali, A. B. M. Badruzzaman, and R. Kretzschmar (2007), Spatial distribution and temporal variability of arsenic in irrigated rice fields in Bangladesh: 1. Irrigation water, *Environ. Sci. Technol., 41*, 5960-5966.

Sengupta, S., M. J. McArthur, A. Sarkar, J. M. Leng, P. Ravenscroft, J. R. Howarth, and M. D. Banerjee (2008), Do Ponds Cause Arsenic-Pollution of Groundwater in the Bengal Basin? An Answer from West Bengal, *Environ. Sci. Technol., 42,* 5156–5164.

Servais, P., G. Billen, and M. C. Hascoet (1987), Determination of the biodegradable fraction of dissolved organic matter in waters, *Water Res., 21*, 445-450.

Stollenwerk, K. G., G. N. Breit, A. H. Welch, J. C. Yount, J. W. Whitney, A. L. Foster, M. N. Uddin, R. K. Majumder, and N. Ahmed (2007), Arsenic attenuation by oxidized aquifer sediments in Bangladesh, *Sci. Total Environ., 379*, 133-150.

Stute, M., Y. Zheng, P. Schlosser, A. Horneman, R. K. Dhar, S. Datta, M. A. Hoque, A. A. Seddique, M. Shamsudduha, K. M. Ahmed, and A. Van Geen (2007), Hydrological control of As concentrations in Bangladesh groundwater, *Water Resour. Res., 43*, W09417, doi: 10.1029/2005WR004499.

Swartz, C. H., N. K. Blute, B. Badruzzaman, A. Ali, D. Brabander, J. Jay, J. Besancon, S. Islam, H. F. Hemond, and C. F. Harvey (2004), Mobility of arsenic in a Bangladesh aquifer: Inferences from geochemical profiles, leaching data, and mineralogical characterization, *Geochim. Cosmochim. Acta, 68*, 4539-4557.

Tuong, T. P., M. C. S. Wopereis, J. A. Marquez, and M. J. Kropff (1994), Mechanisms and Control of percolation losses in irrigated puddled rice fields, *Soil Sci. Soc. Am. J., 58*, 1794-1803.

Van Geen, A., J. Rose, S. Thoral, J. M. Garnier, Y. Zheng, and J. Y. Bottero (2004), Decoupling of As and Fe release to Bangladesh groundwater under reducing conditions. Part II: Evidence from sediment incubations, *Geochim. Cosmochim. Acta, 68*, 3475-3486.

Van Geen, A., Y. Zheng, R. Versteeg, M. Stute, A. Horneman, R. Dhar, M. Steckler, A. Gelman, C. Small, H. Ahsan, J. H. Graziano, I. Hussain, and K. M. Ahmed (2003), Spatial variability of arsenic in 6000 tube wells in a 25 km(2) area of Bangladesh, *Water Resour. Res., 39*, 1140, doi:10.1029/2002WR001617.

Walker, S. H. (1999), Causes of high water losses from irrigated rice fields: field measurements and results from analogue and digital models, *Agric. Water Manage., 40*, 123-127.

Walker, S. H., and K. R. Rushton (1984), Verification of Lateral Percolation Losses from Irrigated Rice Fields by a Numerical-Model, *J. Hydrol., 71*, 335-351.

Welch, P. S. (1952), *Limnology,* McGraw-Hill Book Company, New York.

Welch, S. A., A. E. Taunton, and J. F. Banfield (2002), Effect of Microorganisms and Microbial Metabolites on Apatite Dissolution, *Geomicrobiol. J., 19*, 343-367.

Zheng, C., and G. D. Bennett (2002), *Applied Contaminant Transport Modeling,* Wiley Interscience, New York.

Zheng, Y., A. van Geen, M. Stute, R. Dhar, Z. Mo, Z. Cheng, A. Horneman, I. Gavrieli, H. J. Simpson, R. Versteeg, M. Steckler, A. Grazioli-Venier, S. Goodbred, M. Shahnewaz, M. Shamsudduha, M. A. Hoque, and K. M. Ahmed (2005), Geochemical and hydrogeological contrasts between shallow and deeper aquifers in two villages of Araihazar, Bangladesh: Implications for deeper aquifers as drinking water sources, *Geochim. Cosmochim. Acta, 69*, 5203-5218.

8. Conclusions and Future Directions

8.1. Conclusions

The combined chemical and physical investigations demonstrated that the groundwater-irrigated rice fields in Bangladesh are removing arsenic from the aquifer while ponds are contributing biologically-available organic carbon that promotes microbial respiration and arsenic mobilization from the soils and sediments. Differences in flow behavior are largely responsible for the opposing roles that the two primary recharge sources play in the arsenic-contamination problem.

Although both water bodies are rich in organic carbon, the dynamic and spatially heterogeneous nature of the rice field flow patterns keeps the rice field recharge water free of the organic carbon needed to mobilize arsenic. The rice field plow pan acts as a barrier to flow and shunts ponded water from the surface of the field into the bunds; most of the water that recharges the aquifer flows through the bunds (chapter 2, see Figure 2.2 for a description of the field features). Bund flow occurs primarily after an irrigation event and ceases once the water level in the field reaches the surface muck (chapter 2). Therefore, bund flow is composed of irrigation water that has had a relatively small amount of time to interact with the organic-rich field surface. The short interaction time reduces the arsenic content of the irrigation water but does not allow for significant accumulation of organic carbon in the ponded water (chapter 4). Ultimately, the flow patterns keep the organic carbon and methanogenic conditions, for which rice fields are known, constrained to the surface muck. In fact, oxygen incubations of pore water collected from the bund illustrate that the rice field rechage lacks biologically available organic carbon (chapter 6), and thus lacks the reducing power needed to mobilize arsenic off the soils and sediments. This behavior, combined with the fact that rice fields are irrigated with arsenic contaminated water, means that rice fields remove arsenic from the aquifer. Most of the

irrigation arsenic applied to the fields does not recycle back to the aquifer; it is sequestered within the fields' surface soils and bunds (chapter 4). The high sorption capacity of these features is likely maintained by the fields' hydrology. The surface soils and bunds de-saturate between irrigation events and oxidize down to a depth of at least 2 m each year after the rice is harvested (chapter 2).

Conversely, ponds lose water to the subsurface at a constant rate during the dry season, which means any organic carbon in pond water also enters the subsurface. In addition, most ponds never completely dry out. At the end of the dry season, the banks of most ponds are exposed, but their centers remain covered with water (chapter 7). Thus, the pond sediments are continually saturated with water and solute concentrations within the pore water of the pond sediments are indicative of highly reducing conditions (e.g., elevated methane concentrations, chapter 6). Oxygen incubations show that a portion of the dissolved organic in the pond-sediment pore water is biologically available, which means that the pond recharge has the reducing power needed to mobilize arsenic off of the soils and sediments (chapter 6). Chemical tracers and groundwater modeling further show that in the aquifer, the pond recharge is focused at the same depth as the elevated levels of arsenic. Together, the data indicate that the biologically-available organic carbon in the pond recharge is promoting arsenic mobilization (chapter 6).

Due to the opposing behavior of the ponds and rice fields, the two primary recharge sources for the arsenic contaminated aquifer, it will be difficult to predict how groundwater arsenic concentrations will change in the future.

8.2. Management Suggestions

The rice field and pond investigations provided an understanding of many physical and chemical process in Bangladesh – and understanding that we can harness to develop scientifically-sound strategies for saving water and reducing arsenic exposure.

8.2.1. Rice Field Water

The rice field hydrology investigation (chapter 2) illustrated that most rice fields lose a majority of water through their bunds. The actual percentage of water lost down the bund depends on the perimeter-to-area ratio of the field; fields with lager perimeter-to-area ratios lose more water out their bunds than fields with smaller perimeter-to-area ratios (Figure 2.10). Water lost down the bund is wasted water in the sense that it does not contribute to the growth of the rice crop. It immediately re-enters the subsurface after it is pumped up from the aquifer. Table 3.8 presents estimates on the amount of money, water and greenhouse gas emissions that Bangladesh could save by eliminating bund loss.

An easy strategy for reducing bund loss includes plowing through and rebuilding the bunds each year. This strategy would develop a plow pan beneath the bunds, does not require the farmers to adopt any new behaviors or techniques. Each year the farmers rebuild bunds partially eroded by the monsoon floods (chapter 4) and they plow the entire rice field, minus the bunds (chapter 2). The proposed strategy simply requires the farmers to plow a slightly larger field area and to rebuild the entire bund rather than just part of the bund. However, the bunds follow property boundaries. Thus, to minimize property disputes, the bund location should be marked with stakes or other means before it is plowed.

Since bund flow requires ponded water in the field (Figure 2.7 and Figure 2.11), approaches that keep irrigation water within the surface muck, such as a trickle irrigation scheme, will also reduce bund loss. A true trickle irrigation scheme is problematic since it would likely require almost constant use of the irrigation pump and simultaneous siphoning of irrigation water into different fields. The farmers pay for the diesel fuel needed to irrigate their own fields, so this approach could lead to money disputes. However, a modified irrigation approach that involves applying only enough irrigation water to cover the surface muck but not enough to pond the water could work. This approach would avoid financial disagreements by maintaining distinct irrigation events of individual fields. Water level data from 2008 (Figure 5.1) show that irrigation generally occurs within two days of the field water level reaching the surface muck. Thus, the proposed approach would likely require the farmers to irrigate almost every other day.

Regardless of the approach, eliminating bund flow will significantly reduce the amount of rice field recharge entering the aquifer. The average perimeter-to-area ratio of the fields in our study area is 0.12 m/m^2, close to that of the intensively studied field (0.10 m/m^2). Eighty percent of recharge from the intensively studied field, which included bund flow and preferential flow through cracks in the subsoil, flowed through the bund (Figure 2.12), which suggests that more 80% of rice field recharge in our study area flows through bunds. Thus, eliminating bund flow could potentially reduce rice field recharge by more than 80%. Currently, rice fields contribute almost half of all the water that recharges the aquifer each year while ponds contribute roughly the other half (Harvey et al. 2006) (Figure 8.1). Eliminating bund flow would make ponds the primary recharge source for the aquifer. Under this scenario, if the reduction in irrigation-return flow is exactly offset by reduced pumping (Figure 8.1), the total amount of pond water entering the aquifer may not change. However, the flow patterns of pond recharge in the

aquifer will change (see Figure 6.1), which means that spatial patterns of arsenic concentrations in the aquifer will shift. Thus, the implementation of any water management strategies should correspond with a drinking-water monitoring program.

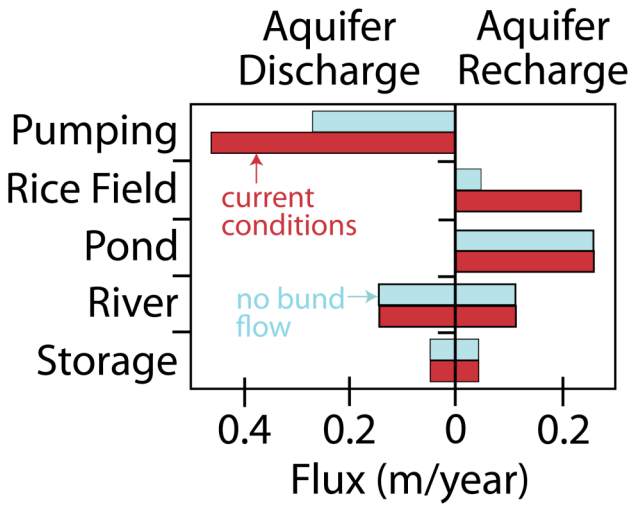

Figure 8.1 Aquifer discharge and recharge sources.
Data for "current conditions" are from Harvey et al. (2006). The "no bund flow" scenario assumes irrigation return flow is reduced by 80% and that this reduction results in an equivalent decrease in irrigation pumping. All other recharge and discharge sources were assumed unaffected by the change, although this assumption is untested.

8.2.2. Arsenic in the Rice Crop

Most fields, regardless of their perimeter-to-area ratios, sequester roughly the same amount of arsenic into their surface soils (Figure 5.18) and therefore have the same potential to contaminant the rice crop (see section 4.4.3). Most of the excess irrigation arsenic (per unit area) applied to fields with larger perimeter-to-area ratios flows into the bunds. Thus, the elimination of bund flow will not reduce the arsenic content of the surface soils or the rice crop; it will only reduce the arsenic content of bunds.

One option for reducing the arsenic content of the rice crop is to irrigate with arsenic-free water. This water could be obtained from surface water sources (i.e., ponds or rivers) or from the deep Pleistocene aquifer (Swartz et al. 2004). Both of these options are problematic. Current irrigation demands depend on groundwater and outstrip available surface water sources (Hossain et al. 2003), and, as discussed in section 8.2.3, irrigation pumping in the Pleistocene aquifer would likely pull pond recharge or arsenic contaminated water from the shallow aquifer down into the clean aquifer, contaminating the source. Therefore, solutions dealing with arsenic in the rice crop need to accommodate arsenic in the irrigation water.

Data in chapter 4 and work by Roberts et al. (Roberts et al. 2007) demonstrate that when irrigation water is added to a dry field, its arsenic content drops by roughly a factor of four within a few hours. This fact can be utilized to reduce the arsenic content of irrigation water before it is applied to the fields, by converting one of the rice fields adjacent to the irrigation well into an arsenic settling area (Figure 8.2). The irrigation water could flow through this converted field, interact with the soil, and reduce its arsenic content before entering the irrigation canal. This proposed solution has many potential pitfalls. First, someone must agree to convert his rice field, which produces food and generates money, into the settling area. Second, a portion of the irrigation water will be lost in the settling area due to evaporation, infiltration, and even bund flow if the bunds are not properly sealed. Finally, a significant amount of arsenic will accumulate in the soils of the settling area, and it not clear what faction of it will leave the system during the monsoon season. Furthermore, the soils do not have an infinite sorption capacity for arsenic, which means their ability to remediate the irrigation water may eventually diminish if they are not periodically flushed.

Reducing the uptake of arsenic by rice plants, even when the crop is not irrigated with arsenic-contaminated water, is an active research area (Stone 2008). Short of genetically altering the cultivar, solutions include growing the rice in aerobic rather than anaerobic conditions (Xu et al. 2008). This approach would require a fundamental change in the region's farming practices.

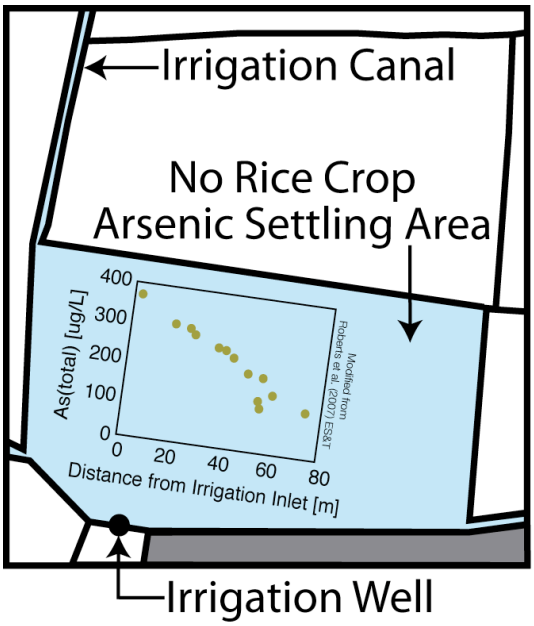

Figure 8.2 Proposed solution to reduce arsenic in irrigation water.
The solution creates an arsenic settling zone, utilizing the fact that arsenic concentrations in the surface water of the rice field decrease by roughly a factor of four as the irrigation water travels from the irrigation inlet to the far corner of the field (Roberts et al. 2007).

8.2.3. Arsenic in Drinking Water

Drinking arsenic-contaminated water provides a much larger arsenic exposure than eating contaminated rice (Meharg and Rahman 2003). Therefore, initial solutions should focus on providing a source of arsenic-free drinking water. Surface water is arsenic free, and, in the case of ponds, is readily available throughout most of the country. However, the surface water is microbially contaminated and the high transmission rate of water born diseases in Bangladesh

initially motivated the development of groundwater as a drinking water source within the country. Thus, the use of surface water would require the rural population to utilize household-level water treatment methods, such as filtration or chlorination. Arsenic can also be removed from water with an arsenic filter, such as the prize-winning SONO filter (Hussam and Munir 2007). The widespread use of these filters would allow for the continued use of existing drinking water wells. Both of these approaches, surface water use or arsenic filtration, require post processing of water by the end user. This water processing is inconvenient and it requires maintenance of the necessary equipment (e.g., filters). These are surmountable hurdles, but they must be fully considered if these solutions are pursued.

Based on the results of our investigations, two possibilities exist to provide the population with clean drinking water that does not require any treatment: deep drinking water wells that tap the arsenic-free Pleistocene aquifer or shallow wells underneath rice fields that tap irrigation-return flow. Both of these approaches place drinking water wells at locations within the aquifer that, under the current hydrologic system, do not receive pond recharge.

The installation of deep drinking water wells has been proposed and studied by other researchers. Using a basin-scale groundwater model, Michael and Voss (Michael and Voss 2008) determined that the deep wells remain isolated from nearby surface water inputs only if irrigation wells remain in the shallow, arsenic-contaminated aquifer. Irrigation pumping establishes a hydraulic barrier that keeps nearby surface water from traveling deeper into the aquifer. With this arrangement, drinking wells in the deep Pleistocene aquifer and irrigation wells in the shallow arsenic-contaminated aquifer, most of the drinking water wells tap water that is thousands of years old and originates at the far edges of the Bengal Basin. Van Geen et al. (Van Geen et al. 2007) have monitored solute concentrations in 51 deep drinking water wells for

a period of five years and found that all but 10 consistently met the World Health Organization's (WHO) arsenic drinking water standard of 10 μg/L. However, their analysis suggests that manganese may be a concern in the Pleistocene aquifer. Although manganese concentrations were lower in the Pleistocene aquifer than in most of the surrounding shallow wells, only 1/3 of the deep wells met the WHO manganese drinking water standard of 0.4 mg/L. These data suggest that a program of thorough and continual water-quality testing should accompany the installation of any deep drinking water wells.

As a solution to the arsenic-contamination problem in Bangladesh, the installation of shallow wells underneath rice fields needs further study. The solution is relatively inexpensive (~$100 dollars for a shallow well versus $1000 for a deep well), but has many potential problems. The wells' proximity to the surface would make them prone to microbial contamination and their location beneath groundwater-irrigated rice fields would make them vulnerable to any breakthrough of accumulated arsenic in the fields' soils and bunds. Furthermore, if efforts are made to reduce bund loss, rice field recharge will dramatically decrease. The impact that this reduced recharge would have on the groundwater flow system is unclear; pond recharge could potentially flow beneath the rice fields and contaminate shallow drinking water wells. Therefore, any effort to provide clean water from shallow wells must incorporate a thorough investigation of the possible outcomes and it should involve a water-quality monitoring program.

8.2.4. Land Management

The results of our investigations suggest that in regions prone to groundwater arsenic contamination (Manouchehr et al. 2008, Winkel et al. 2008), the development of man-made

ponds should be avoided if it is possible. In addition, drinking water wells should not be placed downstream of existing ponds, wetlands, rivers, or surface water bodies potentially elevated in organic carbon.

8.3. Future Work

Although the presented thesis work lead to some concrete conclusions regarding the arsenic contamination problem in Bangladesh, many unanswered questions and data gaps remain. In the following sections, these unanswered questions and data gaps are highlighted in hopes that they will generate follow-up studies and new thesis projects.

8.3.1. Rice Fields

8.3.1.1. Water Management Impacts

As previously mentioned, the elimination of bund loss (see section 8.2.1) would significantly decrease the amount of rice field water entering the aquifer. The impact that this reduced recharge would have on groundwater flow and arsenic patterns in the aquifer is unclear. These impacts could be investigated using a calibrated groundwater flow model, such as the one developed by Ashfaque (Ashfaque 2007). Ashfaque's model tracks recharge from different surface water sources within the aquifer. One could turn off irrigation-return flow in the model and track pond recharge to gain insight into how arsenic patterns in the aquifer may change if bund flow is eliminated.

8.3.1.2. Arsenic Fate

Data presented in chapter 4 demonstrated that much of the irrigation arsenic applied to rice fields is sequestered by the bunds, and they implied that the bunds lose this arsenic on an

annual basis, which lead to the hypothesis that solid-phase arsenic in the bund is lost to bund erosion during the monsoon season. It would be beneficial to test this hypothesis and quantify the amount of bund arsenic lost during the monsoon season by measuring the dimensions and arsenic content of multiple bunds both before and after the monsoon season. To thoroughly track the yearly accumulation and loss of solid-phase arsenic in the bund, this data collection effort could be coupled with bund-arsenic measurements from multiple time points during the year, including during the irrigation season and before and after the eroded bunds are rebuilt by the farmers.

The ultimate fate of the irrigation arsenic, including that sequestered within the bunds, is an interesting, though more difficult, question to pursue. As discussed in chapter 4, most of the irrigation arsenic is lost to the monsoon floodwaters (see Figure 4.6). However, it is not clear exactly where the floodwaters transport the arsenic. Most of it is likely flushed to the Bay of Bengal when the floodwaters recede (Roberts et al. 2009), but some of it, especially the portion eroded from the bunds, may settle back onto the landscape. One could potentially determine how much arsenic enters the Bay of Bengal by collecting sediment cores from the bay. The basin accrues sediment each year (Goodbred et al. 2003), so the sediments could provide a nice record of the arsenic efflux. The fate of the eroded arsenic, which has the potential to settle back on to the landscape, could be tracked by impregnating the bund and surface soils with a tracer. The tracer must be easily detected on the landscape since it will be widely dispersed during the monsoon season. For example, a tracer that can be detected with an instrument waved over the land surface, similar to a metal detector, may work. This tracer approach requires thought and, in the end, may be impractical.

Finally, it would be useful to study arsenic fate in a rice field located in a part of the country that does not experience monsoon flooding. In these rice fields, if they are irrigated with arsenic-contaminated groundwater, there is likely significant accumulation of arsenic within the soils and bunds. This study could determine how the accumulated arsenic impacts arsenic concentrations within rice plants and how likely it is to breakthrough and contaminate the shallow aquifer.

8.3.1.3. Unsatured Zone Composition

One outstanding question from chapter 2 is the composition of the unsaturated zone beneath the plow pan (see section 2.5.1). It is not clear if the gas phase contains atmosphere that entered the subsurface either through the bund or though the rice plants themselves (Van Bodegom et al. 2001), or if it contains reduced gases, like methane, which were generated by microbial activity within the subsurface. It is also possible that the composition of this zone changes as irrigation water is added and lost from the field. Methane could potentially accumulate during and immediately after an irrigation event when the unsaturated zone is isolated from the atmosphere (see Figure 2.5a). Any accumulated methane could then exchange with the atmosphere when the bund desaturates and creates a continuous gas phase connection between the atmosphere and the unsaturated zone (see Figure 2.5b). The composition of the unsaturated zone is scientifically interesting and has implications for both rice field biogeochemistry and methane emissions. In particular, if the gas phase contains methane, the rice fields could periodically burp methane into the atmosphere through their bunds.

8.3.2. Ponds

During this thesis project, not as much time was spent studying the ponds as studying the rice fields. Therefore, many opportunities exist for further pond investigations. In particular, due to their important role in the arsenic contamination problem, it would be useful to intensively study a larger number of ponds within both our study area and other areas throughout Bangladesh to determine what are typical and atypical behaviors.

8.3.2.1. Hydrology

Data collected on pond water levels suggest that ponds lose water to the subsurface at a constant rate during the dry season (Harvey et al. 2006). However, calculations presented in section 7.3.2 illustrate that some of this lost water likely flows through preferential channels within the subsurface beneath ponds, similar to water within rice fields (see Figure 2.6). It is also possible that some of the pond water flows out the sides of ponds rather than through the pond bottom. An improved understanding of pond hydrology is required to physically track pond recharge and explicitly determine how its solute composition evolves as it travels through the subsurface. Thus, a study of pond hydrology is warranted. This study could utilize many of the same techniques developed for the rice field hydrology investigation (see section 2.3), including pressure sensors and tracer tests.

8.3.2.2. Surface Water

The temperature, solute and isotopic composition of the entire surface water column of many ponds needs to be measured multiple times during the dry season. These data will clarify how pond water columns evolve, and they will prove or disprove the hypothesis that ponds remain poorly mixed during the dry season, allowing the surface water to evaporate and grow

isotopically heavy while the deeper water remains isotopically light (see section 7.4). If proved correct, the proposed lack of vertical mixing could explain the isotopic data sets collected for our field site as well as other field sites in Bangladesh and West Bengal (see section 7.4).

8.3.2.3. Pond Sediment and Sediment Pore Water

Many of the conclusions regarding pond biogeochemistry were drawn from measurements made on pore water collected from the sediments of two different ponds. Understanding the pore water composition is, in many ways, more important than understanding the surface water composition. The water recharging the aquifer from ponds necessarily travels through the pond sediments, and the concentrations of solutes within the pond sediments are dramatically different than that within the surface water (see Figure 7.12). However, many gaps exist within the current pore water data set. First, it would be beneficial to collect pore water samples from the sediments of many different ponds (e.g., old ponds and young ponds, big ponds and small ponds) to determine the typical concentrations of key solutes. Second, an understanding of speciation, especially iron and arsenic speciation, within the sediments would help chemically define the system. Finally, hydrogen concentrations could indicate the primary terminal electron acceptors for microbial respiration within the pond sediments (Lovley and Goodwin 1988), clarifying the evolution and state of the pond water before it enters the aquifer. In addition to hydrogen concentrations, a complete understanding of the interactions and chemical reactions occurring within the sediments requires knowledge of the mineral and chemical composition of the pond sediments, a significant piece of information missing from the current pond data set.

8.3.2.4. Large-Scale Experiment

Taken together, the data presented in chapter 6 implicates ponds as the recharge source responsible for arsenic mobilization. If funding exists, a large-scale experiment that explicitly tracks and monitors the evolution of pond recharge in the subsurface would powerfully illustrate the role that ponds play in the contamination problem and would provide the data needed to pinpoint the exact interactions and chemical reactions responsible for arsenic mobilization. Two simultaneous large-scale pond experiments, one that focuses on an existing pond and one that focuses on a freshly dug pond, would clarify if pond recharge promotes a continual release of arsenic from the soils and sediments, or if it promotes only an initial, transient release of arsenic immediately after the pond is dug.

The proposed experiments would require releasing a conservative tracer into the studied ponds and installing a larger number of wells to track the tracer and sample the pond plume as it migrates through the subsurface. Knowledge of pond discharge and groundwater flow patterns would be required to effectively track the pond water. The experiments would require many years of effort, as subsurface water moves slowly; the water found at the arsenic peak is roughly 50 years old (see chapter 6). However, the experiments would likely answer many questions about pond recharge and arsenic mobilization within a few years, well before the water reaches the arsenic peak.

8.3.3. Rivers

Rivers act as both a discharge and recharge source for the shallow aquifer (Harvey et al. 2006). Their role in the arsenic-contamination problem was not explicitly studied in this thesis project. It is possible that river recharge acts to mobilize arsenic. The smaller river tributaries,

in particular, are relatively stagnant and likely rich in organic carbon. However, it is also possible that rivers, especially the larger, more actively flowing rivers, act to minimize subsurface arsenic concentrations. Isotope data presented in section 7.4.1 illustrate that the rivers in our study area do not contribute water to the aquifer depth at which we see the elevated levels of arsenic. Furthermore, a recent Bangladeshi study found that the sediments of the Meghna river trap arsenic as arsenic-contaminated groundwater discharges into the river (Datta et al. 2009), and a Cambodian study found subsurface arsenic concentrations decreased when the Mekong river recharged the aquifer (Polizzotto et al. 2008).

A study of recharge from both a major river, like the Meghna, and one of its small tributaries, like the Ichimatti, could elucidate the role or roles that rivers plays in the contamination problem. It is hypothesized that recharge from the smaller tributaries behaves similarly to that of pond recharge and mobilizes arsenic, while recharge from the larger rivers acts to minimize subsurface concentrations.

8.3.4. Incubations

The oxygen incubation experiments presented in chapter 6 nicely demonstrated that the pond recharge water contained biologically degradable organic carbon while the rice field recharge water did not contain biologically degradable organic carbon. The experiment utilized water obtained from the pond sediments and from the rice field bund, and exposed this water to oxygen. It therefore exposed the microbes within the collected water to the most energetically favorable electron acceptor. The experiment tested only the biological availability of the organic carbon, it did not attempt to replicate the *in situ* chemical and biological conditions under which carbon mineralization occurs in the subsurface.

Incubation experiments that do attempt to replicate *in situ* conditions could provide valuable information about carbon oxidation and arsenic mobilization within the subsurface. Many incubation studies that involve aquifer sediment and artificial or sampled groundwater are published in the literature (Akai et al. 2004, Islam et al. 2004, Van Geen et al. 2004, Radloff et al. 2007). These studies show that the addition of labile organic carbon (e.g., lactate) to the aquifer sediments promotes arsenic mobilization. However, these experiments do not clarify what chemical interactions and transformation are responsible for arsenic mobilization, nor do they utilize *in situ* organic-carbon sources. Therefore, the opportunity exists to build upon both these previous incubation studies and the results of this thesis project by conducting anaerobic incubation experiments that utilize actual pond, rice field and river recharge water in conjunction with sediments obtained from different sources.

The proposed anaerobic incubation experiments (see Figure 8.3) would expose the subsurface microbial community to *in situ* redox conditions and natural organic matter in a controlled laboratory setting to test which recharge waters mobilize arsenic off of the selected sediments. Figure 8.3 illustrates that the proposed incubation combinations include pond sediments, rice field soils, and aquifer sediments from two different depths. Sediments at the two aquifer depths may behave dissimilarly since, in the aquifer, they are exposed to different recharge waters; the shallow depth (~5-m depth) sees primarily rice field recharge while the deep depth (~30-m depth) sees primarily pond recharge (Figure 6.1). Water and sediment samples from the incubations could be periodically sampled and analyzed to track the chemical evolution of the aqueous and solid phase. Solid phase characterization could include sequential extractions (Keon et al. 2001, La Force and Fendorf 2000) or x-ray florescence and adsorption techniques. These data would clarify if the proposed mobilization processes presented in section 6.5 are

correct. Unfortunately, collecting and preserving the *in situ* condition of the waters and sediments required for these experiments will be difficult.

If the incubations are successful, and fresh material can be obtained, it may be useful to take the experiments one step further and run the different recharge waters through columns of sediment material. This setup would attempt to mimic the *in situ* transport behavior, and elucidate how the recharge waters evolve as they are transported through the subsurface. Previous studies have shown that flow can control the types of reaction products formed from sediment-water interactions (Benner et al. 2002).

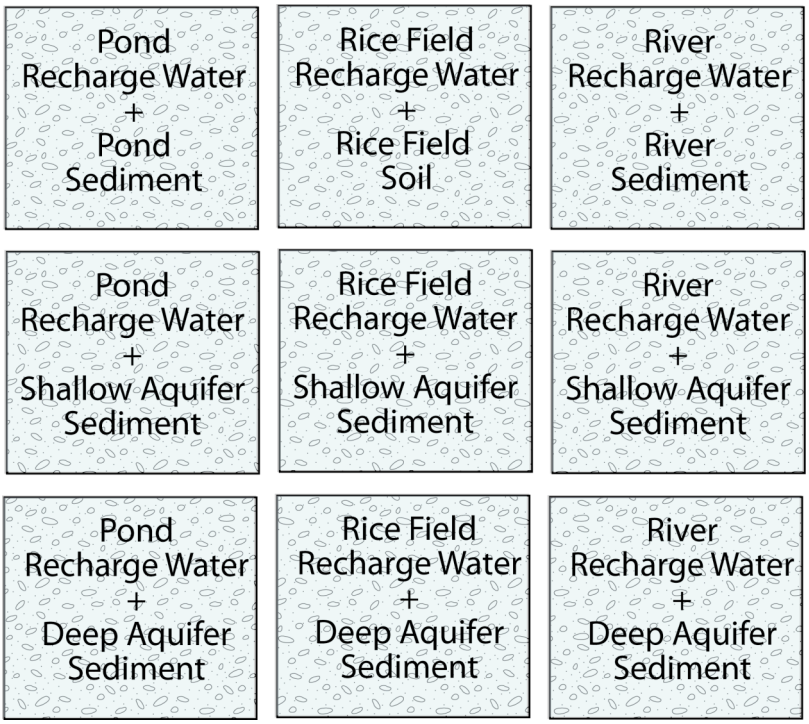

Figure 8.3 Series of proposed anaerobic incubation experiments.

Pond recharge water represents water obtained from pond sediments, rice field recharge represents water obtained from bunds, and river recharge represents water obtained from river sediments. Shallow aquifer sediment should be obtained from ~5-m depth and deep aquifer sediment should be obtained from the arsenic peak, ~30-m depth.

8.4. References

Akai, J., K. Izumi, H. Fukuhara, H. Masuda, S. Nakano, T. Yoshimura, H. Ohfuji, H. M. Anawar, and K. Akai (2004), Mineralogical and geomicrobiological investigations on groundwater arsenic enrichment in Bangladesh, *Appl. Geochem., 19*, 215-230.

Ashfaque, K. N. (2007), Effect of hydrological flow pattern on groundwater arsenic concentration in Bangladesh, Ph.D. Thesis, Massachusetts Institute of Technology: Cambridge, MA, pp. 286.

Benner, S. G., C. M. Hansel, B. W. Wielinga, T. M. Barber, and S. Fendorf (2002), Reductive dissolution and biomineralization of iron hydroxide under dynamic flow conditions, *Environ. Sci. Technol., 36*, 1705-1711.

Datta, S., B. Mailloux, H.-B. Jung, M. A. Hoque, M. Stute, K. M. Ahmed, and Y. Zheng (2009), Redox trapping of arsenic during groundwater discharge in sediments from the Meghna riverbank in Bangladesh, *Proc. Natl. Acad. Sci. U.S.A., 106*, 16930-16935.

Goodbred, S. L., S. A. Kuehl, M. S. Steckler, and M. H. Sarker (2003), Controls on facies distribution and stratigraphic preservation in the Ganges-Brahmaputra delta sequence, *Sediment. Geol., 155*, 301-316.

Harvey, C. F., K. N. Ashfaque, W. Yu, A. B. M. Badruzzaman, M. A. Ali, P. M. Oates, H. A. Michael, R. B. Neumann, R. Beckie, S. Islam, and M. F. Ahmed (2006), Groundwater dynamics and arsenic contamination in Bangladesh, *Chem. Geol., 228*, 112-136.

Hossain, M. D., D. Lewis, M. L. Bose, and A. Chowdhury (2003), Rice Research, Technological Progress, and Impact on the Poor: The Bangladesh Case (Summary Report), *EPTD Discussion Papers*, International Food Policy Research Institute, Washington, D.C.

Hussam, A., and A. K. M. Munir (2007), A simple and effective arsenic filter based on composite iron matrix: development and deployment studies for ground water of Bangladesh, *J. Environ. Sci. Health Part A., 42*, 1869-1878.

Islam, F. S., A. G. Gault, C. Boothman, D. A. Polya, J. M. Charnock, D. Chatterjee, and J. R. Lloyd (2004), Role of metal-reducing bacteria in arsenic release from Bengal delta sediments, *Nature, 430*, 68-71.

Keon, N. E., C. H. Swartz, D. J. Brabander, C. Harvey, and H. F. Hemond (2001), Validation of an arsenic sequential extraction method for evaluating mobility in sediments, *Environ. Sci. Technol., 35*, 2778-2784.

La Force, M. J., and S. Fendorf (2000), Solid-phase iron characterization during common selective sequential extractions, *Soil Sci. Soc. Am. J., 64*, 1608-1615.

Lovley, D. R., and S. Goodwin (1988), Hydrogen concentrations as an indicator of the predominant terminal electron-accepting reactions in aquatic sediments, *Geochim. Cosmochim. Acta, 52*, 2993-3003.

Manouchehr, Amini, A. C, Karim, Michael, Berg, Lenny, Winkel, H. J, Stephan, Eduard, Hoehn, Hong, Yang, and J. Annette, C. (2008), Statistical modeling of global geogenic arsenic contamination in groundwater, *Environ. Sci. Technol., 42*, 3669-3675.

Meharg, A. A., and M. Rahman (2003), Arsenic contamination of Bangladesh paddy field soils: Implications for rice contribution to arsenic consumption, *Environ. Sci. Technol., 37*, 229-234.

Michael, H. A., and C. I. Voss (2008), Evaluation of the sustainability of deep groundwater as an arsenic-safe resource in the Bengal Basin, *Proc. Natl. Acad. Sci. U.S.A., 105*, 8531-8536.

Polizzotto, M. L., B. D. Kocar, S. G. Benner, M. Sampson, and S. Fendorf (2008), Near-surface wetland sediments as a source of arsenic release to ground water in Asia, *Nature, 454*, 505-508.

Radloff, K. A., Z. Cheng, M. W. Rahman, K. M. Ahmed, B. J. Mailloux, A. R. Juhl, P. Schlosser, and A. van Geen (2007), Mobilization of Arsenic During One-Year Incubations of Grey Aquifer Sands from Araihazar, Bangladesh, *Environ. Sci. Technol., 41*, 3639-3645.

Roberts, L., S. J. Hug, J. Dittmar, A. Voegelin, R. Kretzschmar, B. Wehrli, O. A. Cirpka, G. C. Saha, M. A. Ali, and A. B. M. Badruzzaman (2009), Arsenic mobilization from paddy soils during monsoon flooding, *Nature Geosci., Accepted*,

Roberts, L., S. J. Hug, J. Dittmar, A. Voegelin, G. C. Saha, M. A. Ali, A. B. M. Badruzzaman, and R. Kretzschmar (2007), Spatial distribution and temporal variability of arsenic in irrigated rice fields in Bangladesh: 1. Irrigation water, *Environ. Sci. Technol., 41*, 5960-5966.

Stone, R. (2008), FOOD SAFETY: Arsenic and Paddy Rice: A Neglected Cancer Risk?, *Science, 321*, 184-185.

Swartz, C. H., N. K. Blute, B. Badruzzman, A. Ali, D. Brabander, J. Jay, J. Besancon, S. Islam, H. F. Hemond, and C. F. Harvey (2004), Mobility of arsenic in a Bangladesh aquifer: Inferences from geochemical profiles, leaching data, and mineralogical characterization, *Geochim. Cosmochim. Acta, 68*, 4539-4557.

Van Bodegom, P., J. Goudriaan, and P. Leffelaar (2001), A mechanistic model on methane oxidation in a rice rhizosphere, *Biogeochemistry, 55*, 145-177.

Van Geen, A., Z. Q. Cheng, Q. Jia, A. A. Seddique, M. W. Rahman, M. M. Rahman, and K. M. Ahmed (2007), Monitoring 51 community wells in Araihazar, Bangladesh, for up to 5 years: Implications for arsenic mitigation, *J. Environ. Sci. Health Part A, 42*, 1729-1740.

Van Geen, A., J. Rose, S. Thoral, J. M. Garnier, Y. Zheng, and J. Y. Bottero (2004), Decoupling of As and Fe release to Bangladesh groundwater under reducing conditions. Part II: Evidence from sediment incubations, *Geochim. Cosmochim. Acta, 68*, 3475-3486.

Winkel, L., M. Berg, M. Amini, S. J. Hug, and J. Annette, C. (2008), Predicting groundwater arsenic contamination in Southeast Asia from surface parameters, *Nature Geosci., 1*, 536-542.

Xu, X. Y., S. P. McGrath, A. A. Meharg, and F. J. Zhao (2008), Growing Rice Aerobically Markedly Decreases Arsenic Accumulation, *Environ. Sci. Technol., 42*, 5574-5579.